

PIGMENTED COLORANTS:
DEPENDENCE ON MEDIA AND TIME

A Thesis

Presented to the Faculty of the Graduate School
of Cornell University

in Partial Fulfillment of the Requirements for the Degree of
Master of Science

by

Jeffrey Blaine Budsberg

January 2007

© 2007 Jeffrey Blaine Budsberg

ALL RIGHTS RESERVED

ABSTRACT

We present a physically based model for predicting the visual appearance of artists' paint, which is dependent on both time and the material that binds the colorant to a surface.

In our study, we captured the reflectance spectra of a large number of paint samples at different intervals in time over the course of six months. These paint samples were handmade to ensure material quality, using various pigmented colorants and adhesive binding media. Converting our spectral data into different perceptually uniform color spaces, we show very significant perceptual differences in two domains: the appearance of paint changes over time; and the appearance of one pigmented colorant varies when dispersed in different materials.

Finally, we present an interactive viewer for predictive pigmented color mixture utilizing the paint reflectance spectra, Kubelka Munk theory and modern graphics hardware.

Biographical Sketch

The author was born in Houston, Texas on June 28, 1982 and resided there until completion of his high school degree at Cypress Falls High School. Jeff supplemented his high school curriculum with studies at the Glassell School of Art on weekends.

He moved to Ithaca, New York, to obtain his undergraduate degree in Fine Arts at Cornell University. During his undergraduate years, his interests and coursework were interdisciplinary, encompassing traditional arts, computer graphics, computer science and perceptual psychology. Jeff spent the spring semester of 2003 studying abroad in Rome and has a great passion for Italy. In the fall of 2004 he joined the Program of Computer Graphics at Cornell University as a Masters Student.

Acknowledgements

This work would not have been possible without the contributions and support from many individuals. First and foremost, I would like to thank my advisor Don Greenberg for his mentoring and enthusiasm. I am grateful for the opportunity that he has given me and I have had a wonderful experience in the Program of Computer Graphics. I also thank my minor advisor, Steve Marschner, for his help and commentary over the course of my research.

Several other faculty members and researchers provided important assistance. Early in my work, my conversations with Stan Taft proved instrumental as his research served as an inspiration for my own. Fabio Pellacini proved to be a great resource for hashing through ideas, as well as advising me on how to port my code to graphics hardware. James Ferwerda was a great aid in the discussion of color science and visual perception. I thank Steve Westin for assisting in the setup of the equipment in the light measurement laboratory and Victor Kord for lending his expertise on artists' materials. Bruce Walter and Kavita Bala were always available to help me whenever I popped into their offices.

There are many great students in the PCG whom I had the privilege of working with. Jon Moon and Piti Irawan were always upbeat and eager to help when I had tough graphics questions. I would always be joined after hours in the lab with

Milos Hasan—he was always ready for any Java-related questions I had. Nasheet Zaman would have comments and suggestions for everything I would toss her way. I thank Jeff Wang for everything. He has always been a great friend and goes out of his way to help others in any way. Jacky Bibliowicz was a good friend and very helpful when I first came to the PCG. I always enjoyed talking with Jeremiah Fairbank, as he came from my part of the campus.

There are many others in the lab that I wish to thank. Hurf has always provided amazing support with the many systems that I used and was positive even when I made mistakes. Martin always kept me up to date on the amazing equipment in the lab. Thank you Mary for taking care of us and for our very entertaining late night discussions on cooking and wildlife. Linda always kept track of everything I needed to do and fit me into Don’s schedule. I thank Peggy for cheerfully taking care of all of our administrative duties.

There is not space for all of the many wonderful people whom I have known during my time at Cornell. I thank the many friends that have entertained me away from my work, including Simon, Jon, Will and Nick.

I thank my family for their love and support. I thank Tiffany, the love of my life, for her love, comfort, encouragement, and strength.

This work would not have been possible without support from the Program of Computer Graphics, the Department of Architecture and the National Science Foundation ITR/AP 0205438.

Table of Contents

1	Introduction	1
2	Painting Background	9
2.1	Composition of a Painting	9
2.1.1	Support	10
2.1.2	Size	14
2.1.3	Ground	15
2.2	Composition of Paint	16
2.2.1	Pigment	18
2.2.2	Binding Media Influence	27
2.3	Binding Media Materials	38
2.3.1	Carbohydrate-Based	38
2.3.2	Protein-Based	39
2.3.3	Oils	41
2.3.4	Waxes	43
2.3.5	Synthetic Polymers	43
2.3.6	Catalytic Materials	44
3	Color Background	47
3.1	Light and Color	47
3.1.1	Visible Light Spectrum	48
3.1.2	Light Spectra	54
3.1.3	Human Visual System	56
3.1.4	Color Perception	63
3.1.5	Color Spaces	78
3.1.6	Overall Response	85
4	Previous Work	94
4.1	Introduction	94
4.2	Light transport in volumetric materials	94
4.2.1	Subsurface scattering theory	95
4.2.2	Path tracing	97
4.2.3	Diffusion approximation	99
4.2.4	Image-based measurement	103

4.2.5	Kubelka Munk theory	105
4.2.6	Time-varying appearance	113
4.3	Natural changes in pigmented materials	117
4.3.1	Fading of pigments	118
4.3.2	Kinetics of fading	125
4.3.3	Medium and substrate changes	129
4.3.4	Other effects	133
5	Preparation & Measurement	136
5.1	Sample creation	136
5.1.1	Importance of handmade samples	136
5.1.2	Pigments	141
5.1.3	Media	149
5.1.4	Substrate	152
5.1.5	Painting	156
5.2	Measurement	159
5.2.1	Spectrophotometer	159
5.2.2	Integrating sphere theory	162
5.2.3	Measurement	164
6	Experimental Results	166
6.1	Introduction	166
6.1.1	Effect of binding media	166
6.1.2	Effect of time	176
6.1.3	Applications	183
7	Interactive Viewing	187
7.1	Introduction	187
7.1.1	Conversion to Kubelka Munk	188
7.1.2	Rendering System	189
7.1.3	Implementation issues	194
8	Conclusion	196
A	Derivation of K-M theory	200
B	Supplemental sample analysis	209
	References	238

List of Tables

2.1	Average pigment particle size	23
2.2	Pigment specific gravity	26
2.3	Index of refraction for different media	31
2.4	Index of refraction for different pigments	36
5.1	Pigment data	145
5.2	Pigment data	146
6.1	Color conversions of Lapis Lazuli in different binding media	171
6.2	Perceptual differences between Lapis Lazuli in different binding media	172
6.3	Color conversions of Lapis Lazuli in Gouache over time	179
B.1	Color conversions of Cold Glauconite in different binding media . .	212
B.2	Perceptual differences between Cold Glauconite in different binding media	212
B.3	Color conversions of Cold Hematite Tint in different binding media	215
B.4	Perceptual differences between Cold Hematite Tint in different bind- ing media	215
B.5	Color conversions of Burnt Sienna in different binding media	218
B.6	Perceptual differences between Burnt Sienna in different binding media	218
B.7	Color conversions of Lampblack Tint in different binding media . .	221
B.8	Perceptual differences between Lampblack Tint in different binding media	221
B.9	Color conversions of Red Ochre Tint in different binding media . .	224
B.10	Perceptual differences between Red Ochre Tint in different binding media	224
B.11	Color conversions of Chrome Yellow in Distemper over time	227
B.12	Color conversions of Hematite Tint in Watercolor over time	227
B.13	Color conversions of Burnt Sienna Tint in Oil over time	232
B.14	Color conversions of Cold Glauconite in Watercolor over time . .	232
B.15	Color conversions of Red Ochre Tint in Casein over time	237

List of Figures

1.1	Sistine Chapel restoration	4
1.2	Color matching between fresco giornate	7
2.1	Composition of a painting's many layers	10
2.2	Cotton and linen canvas	11
2.3	Magnified cotton canvas	12
2.4	Stretching canvas over a wooden frame	13
2.5	Magnified primed canvas	16
2.6	Dispersion of pigment in a binding medium	17
2.7	A sample of pure pigments	19
2.8	Natural pigments of antiquity	20
2.9	Pictomicrographs of several pigments	21
2.10	Different grades of Malachite	25
2.11	Optical behavior at an interface	29
2.12	Critical angle	32
2.13	Optical behavior at multiple interfaces	33
2.14	Optical behavior with paint	34
2.15	The full optical behavior of a painting	37
2.16	The binding method of fresco painting	45
2.17	Cross section of a fresco painting	46
3.1	The visible spectrum	48
3.2	Hue, brightness and saturation	50
3.3	Newton's basic optics experiment	51
3.4	Subtractive color mixture in ink	52
3.5	Subtractive color primaries	53
3.6	Additive color primaries	54
3.7	Georges Seurat, <i>La Grande Jatte</i>	54
3.8	Emitted light spectra	55
3.9	Reflected light spectra	56
3.10	Cross section of the human eye	57
3.11	Cross section of the retina	60
3.12	Distribution of the retina's photoreceptors	61
3.13	Pictomicrographs of the human retina	62
3.14	Isoluminance	63

3.15	Photoreceptor absorption	65
3.16	RGB color space	65
3.17	RGB Color Matching Functions	66
3.18	XYZ Color Matching Functions	69
3.19	Calculation of CIE Tristimulus values	70
3.20	Metameric stimuli	71
3.21	CIE Chromaticity Diagram	73
3.22	Out of gamut colors	75
3.23	Chromaticity coordinates of varying pigment tints	77
3.24	Several different color spaces	79
3.25	The MacAdam ellipses	80
3.26	Munsell color system	81
3.27	Nonlinear color spaces	84
3.28	Receptor fields	86
3.29	Lateral inhibition	87
3.30	Mach bands	89
3.31	Work of Josef Albers	90
3.32	Edwin Land's Mondrian experiment	93
4.1	Phase functions	99
4.2	Dipole diffusion approximation	101
4.3	Dipole diffusion and path tracing results	102
4.4	Image-based object model results	104
4.5	Image-based material model results	105
4.6	Results using Kubelka-Munk theory	108
4.7	Canvas paint spectra	109
4.8	Kubelka Munk coefficients	109
4.9	Synthetic watercolor paints	110
4.10	Evaluation of Kubelka Munk pigment mixing	112
4.11	Theoretical copper patina growth	114
4.12	Simulated copper patina growth	115
4.13	Simulated marble weathering	116
4.14	Simulated spatially-varying appearance over time	117
4.15	Vermillion paint fading	119
4.16	Effect of ultraviolet filtering	120
4.17	Alizarin Crimson fading	123
4.18	Fading in respect to Munsell value and chroma	124
4.19	Fading depth versus pigment scattering	129
4.20	Binding media yellowing	131
4.21	Pigment-medium interface voids	133
4.22	The effect of ozone on paint	134
5.1	Misleading paint labels	140
5.2	Pigments used in our research	144

5.3	Canvas board materials	153
5.4	Reflectance spectra of multiple layers of gesso	154
5.5	Appearance of multiple layers of gesso	155
5.6	A typical painted sample	157
5.7	Possible pigment-binder problems	159
5.8	Optical setup for diffuse reflectance measurement	160
5.9	Diagram of a Czerny-Turner monochromator	161
6.1	Lapis Lazuli in different binding media after one day	168
6.2	Similarity comparison of Lapis Lazuli paint samples	173
6.3	Munsell plots of Lapis Lazuli in different binding media after one day	174
6.4	Variation of spectral reflectance curves of Lapis Lazuli in Gouache over time	178
6.5	Munsell plots of Lapis Lazuli in Gouache over time	182
6.6	Visual comparison of Lapis Lazuli in Gouache changing at each time interval	184
7.1	Our simulated canvas	190
7.2	Features of our interactive viewer	193
A.1	Flux density within a paint layer	201
A.2	The path of light between two homogeneous layers	207
B.1	Cold Glauconite in different binding media after one week	210
B.2	Munsell plots of Cold Glauconite in different binding media after one week	211
B.3	Cold Hematite Tint in different binding media freshly painted	213
B.4	Munsell plots of Cold Hematite Tint in different binding media freshly painted	214
B.5	Burnt Sienna in different binding media freshly painted	216
B.6	Munsell plots of Burnt Sienna in different binding media freshly painted	217
B.7	Lampblack Tint in different binding media after one month	219
B.8	Munsell plots of Lampblack Tint in different binding media after one month	220
B.9	Red Ochre Tint in different binding media after three months	222
B.10	Munsell plots of Red Ochre Tint in different binding media after three months	223
B.11	Variation of spectral reflectance curves of Chrome Yellow in Dis- temper over time	225
B.12	Munsell plots of Chrome Yellow in Distemper over time	226
B.13	Variation of spectral reflectance curves of Hematite Tint in Water- color over time	228
B.14	Munsell plots of Hematite Tint in Watercolor over time	229

B.15	Variation of spectral reflectance curves of Burnt Sienna Tint in Oil over time	230
B.16	Munsell plots of Burnt Sienna Tint in Oil over time	231
B.17	Variation of spectral reflectance curves of Cold Glaunconite in Wa- tercolor over time	233
B.18	Munsell plots of Cold Glaunconite in Watercolor over time	234
B.19	Variation of spectral reflectance curves of Red Ochre Tint in Casein over time	235
B.20	Munsell plots of Red Ochre Tint in Casein over time	236

Chapter 1

Introduction

Nothing endures but change

-Heraclitus

All materials have an inherent tendency to change in appearance and composition when exposed to the physical conditions of the outside environment. Normal atmospheric conditions alter their physical and chemical properties. Thus, materials respond dynamically as if they were alive; they sense and react according to their surroundings.

The rate of change depends on the innate characteristics of the material, the purity of the environment, and the level of exposure. For example, direct exposure to sunlight incites photochemical reactions within some materials, which can cause fading and discoloration. Water percolates through porous surfaces, carrying minerals that may discolor or deteriorate the object. High humidity and excess moisture promote mold, which leads to decay. Long-term oxygen exposure chemically alters the composition of organic materials. Foreign substances in the air deposit and accumulate on surfaces. Common airborne substances and chemicals

corrode the surfaces of materials. Fluctuating temperature and pressure conditions tend to cause materials to periodically expand and contract. As a result, the undue stresses promote warping and cracking in some materials. Other materials are sensitive to the oils and wear from human touch.

The phenomenon of natural material change is also subject to location. Marine environments contain higher levels of moisture and salt, while urban areas experience a higher concentration of abrasive chemicals due to industrial smog. Both are detrimental to the longevity of exposed materials.

This behavior is what drives museum curators and art historians to protect their collections vigorously, attempting to preserve the work for the next generation and beyond. Very regimented control is kept over all of the conditions in a museum, including the temperature, humidity and light levels. In many circumstances, paintings and textiles are protected with glass coated with ultraviolet filters to remove extraneous light. Patrons are urged not to use flash photography (if at all) to save expediting the adverse effects. Some institutions even have carbon filters to purify the air in which the artifacts reside. The most precious documents of the United States are enclosed in a special casing with only inert gas. All of these precautions (and more) are done to minimize any possible future deterioration of the collections.

Artwork that remains *in situ*, or in its original location, does not benefit from the protections available in a museum. Examples of such work include architectural decoration or paintings directly on the walls or ceilings of buildings. Such work has been subjected to harsh conditions over the years. Atmospheric conditions are generally unable to be controlled for these works, and moisture and temperature variations will inevitably deteriorate the materials. While all work

in situ experiences deposition of dust and erosion from airborne chemicals on the finished surface, historic work suffered from layers of candlelight soot. Today, at least the candles have been replaced, though electric lighting still poses a fading threat to the materials.

The preservation of artwork falls into categories. *Conservation* is to neutralize any adverse effects, therefore minimizing any progressive deterioration so that a work will remain intact for as long as possible. Preventative measures can help alleviate poor handling of materials and extend their lifespan. *Restoration* involves cosmetic treatment under expert care in order to return an object to its original appearance. Complete restoration is typically more controversial, as while it should be reversible, it often involves some irreversible change to the original work in order to achieve results.

Restoration of the artwork on the walls and ceiling of the Sistine Chapel in the Vatican City, Rome, was completed in 1990. This restoration was initially surrounded by a heated controversy in the art world, as some claimed it a breakthrough revelation, while others felt it ruined the masterpiece. A brown patina had developed over centuries, composed of candle smoke, soot, and repeated applications of poor quality varnish (*varnish* is a transparent coating used to enhance the optical properties of a work, as well as protect it from outside elements). It was argued that the patina harmonized the bright colors. Figure 1.1 illustrates the magnitude of change in restoring this piece of artwork.

While not a trivial task, trained restoration professionals can routinely achieve miraculous results from work that has suffered presumably irreversible damage. Typically, extensive damage (such as fire damage, watermarks, tears, and yellowing) can be repaired. Yet, this presents the question for art historians and conser-



Figure 1.1: Detail of the Azor-Sadoch lunette, Sistine Chapel, at various stages during the restoration process. Prior to the restoration, the work was hardly visible without the aid of electric lighting, and is now only naturally lit from the windows. Adapted from [Buo12].

vationists alike—when a work is to be restored, how does one know to what state it should be restored? Cleaning the surface of dirt and particles, as well as removing an old, yellowed coat of varnish will definitely improve the work. However, there is a deeper underlying problem—the materials that actually comprise the artwork change over time. The pigmented colorants (which provide the paint’s color), as well as the material that adheres the colorants to a work, are both susceptible to natural changes over time. A fresh mark of oil paint (or any other material) looks differently the next day, the next month, and the next century. Hence, while simply removing extraneous materials from the surface will get a *better* result, it will not necessarily reveal the *original* work. To do so would require the knowledge of how each individual material changed over the given time interval and accounting for each individual change. Therefore it is difficult to determine exactly how much a color has faded or shifted prior to the current state.

For the artist, the tendency of pigmented materials to change in appearance affects the manner of which an artwork is created. Since a dried brush mark on an artwork appears differently than that of wet paint of identical concentration and composition on a palette, color matching between sessions is very difficult. While in some artistic media this behavior is more easily controllable, this is a formidable problem in fresco painting. In fresco, one works with colorants that are completely imbedded into the masonry when dry. At this point, no further changes can be made to the work, save chipping off the artwork and beginning anew (more details on this and other methods of painting are covered in the next chapter). The permanence of this painting method is an advantage for one who undertakes mural painting, as fresco has longevity comparable to that of the architecture to which it is painted.

However, since mural artwork is typically large, only a portion of the painting can be completed in one day. The work is hence sectioned off into a “days work”, or a *giornata*. Giornate are planned such that they can be completed in under eight hours each. These giornate are typically arranged such that the seams correspond to the edges of objects in the preparatory drawing. For instance, in Figure 1.2, Masaccio’s fresco is sectioned into four giornate: Adam and Eve have their own respective sections, as well as the cherubim at the top, and the portal from Eden to Earth on the left.

The permanence of fresco painting does not leave room for error. In Masaccio’s work, one readily notices the divisions of the giornate, since the color of the ultramarine blue in the background sky does not exactly match up between sections. This is due to difficulty in color matching colored mixtures of paint between sessions. Massaccio was unable to match the colors since paint of the same composition looks much different dry than it does wet on an artist’s palette. Not only is this true for fresco painting, but for all other painting media, including oil, watercolor, and acrylic. Hence, when undertaking such a work, much careful planning is done as an attempt to avoid this color matching problem—large contiguous sections are divided into different giornate.

Today, the printing and film industry share a similar goal to that of art and conservation, as the components of the microscopic colorant particles in printing inks are very similar to that used in artists’ paint. Hence, the materials are similarly susceptible to the same effects that result from exposure to atmospheric conditions. The colored inks will fade from light or airborne chemicals, and the paper will deteriorate from its own acid content.

While inkjet printers are capable of producing realistic high-resolution images

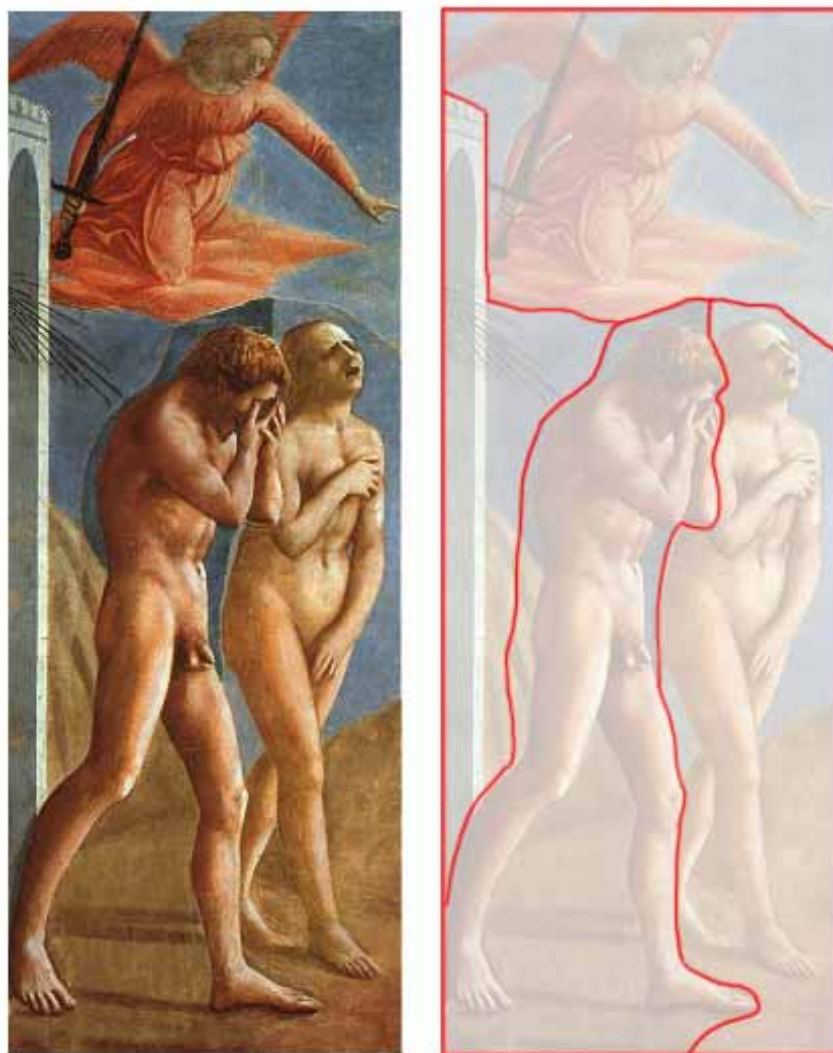


Figure 1.2: Left: difficulties in color matching between fresco giornate in Masaccio's Expulsion are evident, as colors in adjacent giornate do not always match. Right: divisions of the four giornate. Adapted from [Mas27].

at a very high quality (albeit limited color gamuts), their value would be greatly enhanced if they could be made more permanent. Therefore, when a typical user makes a print, what assurances are there that a once vibrant color print will appear equally as vivid long after it was printed? Ink manufacturers are able to control the initial materials (as artists do), but wish to minimize any future change in the colorant (as conservationists do). This problem is a very active research area for digital imaging and printing today.

In all of these cases, the goal is to find ways to predict the appearance of pigmented materials through time. In our research, we study paint appearance in perceptually uniform color spaces, showing very significant perceptual differences in two domains: the appearance of paint changes over time; and the appearance of one pigmented colorant varies when dispersed in different materials.

The thesis is organized in the following manner: Chapter 2 provides an overview of traditional artist materials and how microscopic events contribute to the overall appearance of the surface of a painting. Chapter 3 covers the relationship between light, paint, and our perception of color. Previous work related to simulating the overall appearance of translucent materials (such as paint) and research on natural changes in pigmented materials are detailed in Chapter 4. Chapter 5 describes our research process, including the preparation and measurement of the paint samples. The experimental results are presented in Chapter 6 and we introduce an interactive program to simulate the appearance of arbitrary paints in Chapter 7. Conclusions and applications are addressed in Chapter 8.

Chapter 2

Painting Background

I think you have to control the materials to an extent, but it's important to let the materials have a kind of power for themselves.

-Keith Haring

2.1 Composition of a Painting

In its basic form, a painting is a painted image on a surface. Commonly, a painting serves as a material object, viewed hanging against a wall. The resulting colors are from the deposition of paint strokes in a certain order onto a surface, usually via a brush. Unbeknownst to the viewer, there are many layers of preparation that one must impart to the surface before it is ready to be worked on. Within the painting, the skill of the artist dictates control over a viewer's experience of a work, since despite the visual and iconographic complexities that one associates with the work, it is still an image made from paint [TM00]. This fact is sometimes overlooked since digital reproductions of artwork distort our sense of scale, materials, and topology of the work. Therefore, a painting is more than just an image; it is a

heterogeneous sum of very different time-dependent superposed components that result in a visually complex, topological colored surface.

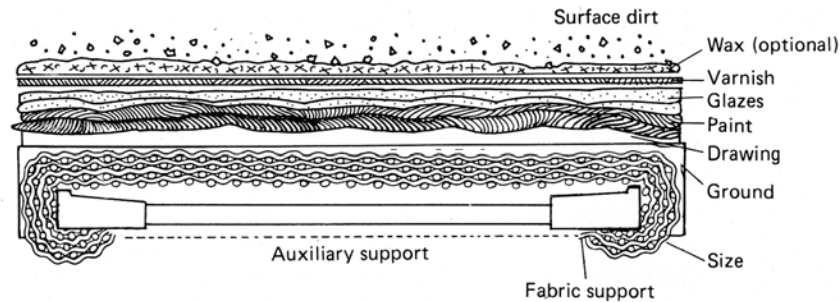


Figure 2.1: Diagrammatic view of a traditional painting's many layers. Adapted from [Got87].

2.1.1 Support

The surface to which paint is applied is called the *support*. It may be the most important structural element in a painting, as all other materials in a painting are attached to it. If the support fails at some point over time, the painting will probably not survive. Over the centuries, artists have used a whole range of supports, including stone, wood, and cloth, all of which impart different surface characteristics to works of art. If a support has a smoothly finished surface, the resulting painting will also typically exhibit a smooth surface, while a support with a pronounced texture will result in a work showing some of this texture.

In a painting, paint is deposited when a loaded brush comes into contact with irregularities in the surface. In very smooth grounds, absorbency acts as an alternative to coarseness or tooth, picking up paint from the brush as it is dragged across the surface. If a surface is overly absorbent, paint will be taken in from the brush too rapidly and satisfactory painting is hampered by too much drag. If a surface is completely nonabsorbent and smooth, such as a sheet of clean glass, a

loaded brush will find problems depositing a consistent mark, as the adhesion and deposition will be imperfect. Yet, substitute a sandblasted sheet of glass and the problem is alleviated, as the color will take to the surface more readily.

Proper supports should age gracefully and be sufficiently able to hold a wide variety of materials. Also, they need to be able to withstand the effects of atmospheric changes. For instance, under reasonable variable conditions of relative humidity and temperature, the support should expand, contract or warp as little as possible to preserve the integrity of the overlying paint film. A support can be of a flexible material, such as cloth, or of a rigid one, such as wood panel (or sheets of glass or metal). Masonry (such as walls or ceilings of buildings) has also served as historical supports for traditional artists.



Figure 2.2: Linen is distinguished from cotton canvas by its dull brownish green color and its usually pronounced irregular texture. Adapted from [Den05].

The term *canvas* is used in painting to describe any fabric that is used as a support. *Cotton duck* and *linen* are two distinct fabrics made from two different plant fibers. Cotton duck is a white fabric made from cotton fibers. It is an inexpensive, widely available, and a popular support for painting. Linen is a light-brown fabric made from the fibers of the flax plant, which is the same plant from

which linseed oil derives (the most commonly-used oil in oil painting). Linen is much more expensive and less commonly used in modern times.

It is universally considered that cotton is an inferior material to linen canvas. Cotton fibers are quite short and resistant to stretching. They suffer rapid degradation when subjected to atmospheric stresses, especially when the fabric is stretched tightly (as in painting). Individual linen fibers are considerably longer than those of cotton, thus the material is somewhat more durable and has a livelier feel when it is stretched over a frame. The higher volatility of cotton can result in cracking and damage to the paint layer. In addition, cotton fibers show a measurable color change after relatively little exposure to light. Despite these facts, many artists—unaware of the technical issues of archival painting—continue to use cotton duck canvas, mainly because it is so much less expensive. Overall, the best canvas is closely woven pure linen with the threads of warp and woof equal in weight and strength.



Figure 2.3: Left: magnified view of the interweaving threads of a cotton canvas. Right: further magnification shows the fibers comprising each thread. The average thread width for this canvas is approximately $575\mu\text{m}$ and the fibers are approximately $12\mu\text{m}$ in width

Flexible supports are stretched over a wooden frame (*stretcher*) to provide a suitable surface to work using tacks or staples. An artist does this carefully to

ensure uniform tension and stress, as seen in Figure 2.4. One must be careful not to over tighten the cloth, and thus save having undesirable problems. This includes canvas tears and the risk of the frame warping or breaking from stress. Therefore, the goal of stretching canvas is for the cloth to be just taut enough to readily spring back from a touch, since paintbrushes do not behave well on flimsy surfaces.



Figure 2.4: Stretching cotton canvas over a wooden frame via a staple gun. The surface to which paint will eventually be applied faces the ground. The crossbar in the middle of the frame provides added strength to the frame.

After the cloth is attached to the frame, the resulting flexible support is much lighter than a solid wooden panel and can be easily transported. A painting executed with good archival techniques will outlive its stretcher bars and its fabric support. Most people today are surprised to learn that both the canvas support of a painting and its stretcher bars have to be replaced periodically through time.

Flexible supports are much thinner than wood panels and therefore are more susceptible to atmospheric and mechanical damage. Constant movement resulting from fluctuations in temperature and humidity can contribute to physical deteri-

oration of a rigidly painted layer of paint. To counteract the instability of fabrics, not only can they be supported via stretchers, but are also sometimes mounted on rigid panels.

The nature of the support influences how we interpret the painting—soft supports impart soft surfaces, while rigid ones are very hard and smooth. Yet, the composition of the paint dictates which types of support are applicable for a given work. Canvas was originally developed as a support for oil-based paintings. This is because flexible supports demand pliable materials due to the natural evolution of the stretched canvas; oil paint responds well to canvas' natural evolution of shrinking and expanding. Paints that dry to thin, brittle films can only be used on very rigid supports. This is due to that fact that such paint would be very susceptible to cracking and flaking of flexible supports. However, an improperly primed wooden panel may also cause problems as well, since atmospheric moisture can cause warping in wood.

2.1.2 Size

Supports need further surface treatment before they can be used for painting. Untreated supports, flexible and rigid, are usually too absorbent to allow the controlled application of paint. After a canvas is stretched, the support is first prepared with an application of *size*. The historical preferred sizing material is a diluted solution of animal skin glue. The size prevents subsequent layers of the painting from being absorbed into the support, which would weaken the painting. Some paints are detrimental to the life of a support. Therefore, paint should never come into direct contact with the fibers or the canvas will *rot*, that is, eventually become weak, brittle, and crumbly.

A size is not a coating, it is a penetrating liquid employed to fill pores and to make surfaces suitable to receive coatings. It is used to seal and solidify the support, and acts as a guard against deterioration and mold. In the case of flexible supports, size shrinks the fabric to a taut, smooth membrane. Hence, on drying it should become somewhat tighter and free from folds and wrinkles.

2.1.3 Ground

The next intermediate layer between a support and subsequent paint films is a *ground*. Most supports will be unevenly absorbent, even if they have been correctly sized. A ground is to ensure that a particular kind of paint will perform with reasonable predictability.

Mark Gottsegen writes that grounds should meet a few basic requirements [Got87]. A ground should be white—some paint films grow more transparent with age and the respective colors will lose their relative relationships if the ground is not white. Also, since the ground is a structural element for the paint to grip, it should have a tooth and should be somewhat absorbent. This ensures proper paint deposition and adhesion as a brush moves across the surface. For flexible supports, the ground should not be too much affected by the continuous movement of the support. Brittle grounds and paint films should use more rigid supports.

The ground provides a better adherence of the subsequent paint layers. A ground is essentially a paint, made of materials compatible with the support material and the paint to be used. *Gesso*—a mixture of animal skin glue, chalk (calcium carbonate), and sometimes white *pigment* (powdered colorant)—has been used for centuries as a ground for wooden panels and canvas. Traditional gesso yields a highly reflective, opaque surface. Light that passes through the layers of the paint-

ing will hit the ground and reflect back toward the viewer creating a luminous surface.

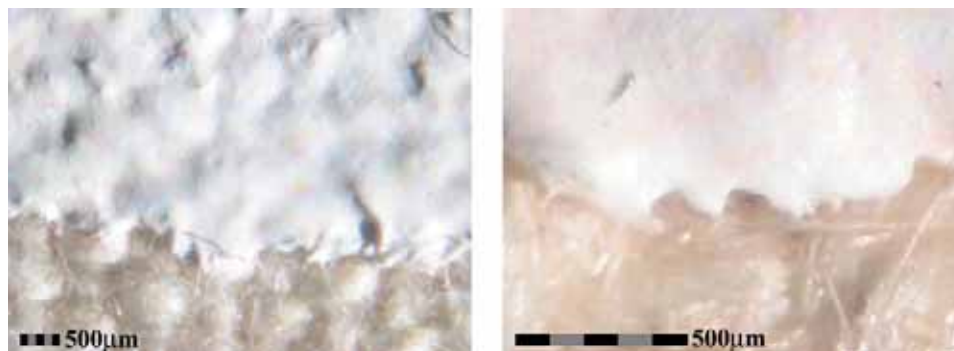


Figure 2.5: Two magnified views of cotton canvas, partially primed on the top of each image with three coats of acrylic gesso. Notice how the primed surface still maintains the original surface characteristics.

There is a common product available today at most art suppliers that is labeled “gesso”, but it is different from traditional gesso. Usually, it is actually a form of white pigment suspended in an acrylic polymer emulsion. While this “gesso” is a viable alternative (as it is freely available, ready to use, and reasonably priced), acrylic itself is a medium that has not been used in art for enough years for artists or conservationists to be certain of its stability or longevity. Hence, it is uncertain how it will affect overlying media as the work ages.

2.2 Composition of Paint

The most basic paint is comprised of powdered colors suspended in a liquid to help ease spreading. The nature of this liquid is crucial to the tactile and optical behavior of the paint. The component we perceive as hue in paint is known as *pigment*, or a fine colored powder of organic or inorganic material. The liquid that the pigment is dispersed in is the *binder*, which adheres the particles of pigment to

the surface of the support. In painting, the term *media* refers to the binder used in the piece of art.

Paint media, no matter how different from one another, share a common characteristic in the fact that they are manufactured in essentially the same way. The pigment must be dispersed as evenly as possible in the binding medium, as seen in Figure 2.6. Traditionally, the pigment and binder are first mixed into a stiff paste. The simple mixture does not constitute an adequate paint, as the particles need to then be ground on a flat plate of glass or stone with a muller. This is to uniformly distribute the particles in the solution. If the paint is to be saved for later use, the paint is then gathered with a palette knife and stored in tubes.

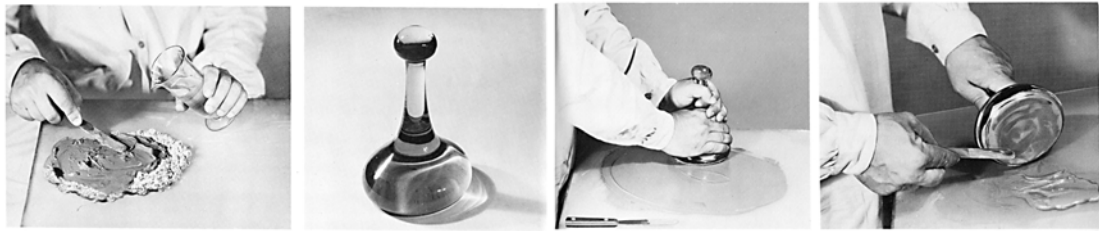


Figure 2.6: Ground Pigments are dispersed in a binding medium via strong friction with a muller. Adapted from [May80].

The choice of materials for a given project is dependent on the type of support the painter intends to use, the scale of the painting, its proposed environment, and the tactile and optical characteristics suitable to the artist's vision. While many artists have experimented in developing new techniques or adapting new materials to suit their pictorial needs, most have followed common practice or proved established procedures.

Historically, a traditional painter would personally, or with the help of assistants, make their own paints. Hands-on experience with paint preparation gave an artist a great understanding of materials and their properties. After the introduc-

tion of paint tubes in 1841 and the development of the paint industry in subsequent centuries, artists became separated from the paint manufacturing process. Unfortunately, most artists lost the motivation to understand the details of the trade. While artists became freer in the creative process—manufactured tubed paint allowed them to leave the studio to work—the diminishing knowledge of materials led to serious negative effects. The use of inadequate and incompatible materials, poorly tested paints, and the experimentation of paint formulas without knowledge of possible consequences led to disastrous effects on the longevity of paintings.

2.2.1 Pigment

There are two distinct types of colorants: *dyes* and *pigments*. Colored substances that dissolve in liquids and impart their colored effects to materials by staining or being absorbed are classified as dyes. Individual dye molecules are only five to ten times that size of a water molecule. The water molecules firmly attach to each dye molecule, allowing the result to swim freely in the water. Because of their small size, dyes dissolve in, bond with, or absorb into the material they come into contact with. These bonds are not easily undone and therefore the resulting color cannot be modified much after being applied to a surface. For most painterly works, the paint surface is reworked considerably; hence dyes are not suitable for most artistic work as they are very immediate colorants.

Instead, artists use pigments, or small insoluble colorant crystals. For example, a pigment that occurs naturally is the deep red colorant *Hematite*, comprised mostly of ferric oxide. In addition, the dyes that are used in painting must first be *laked*—bonded chemically to a transparent, inert metallic base which transform the dye into an insoluble pigment. For example, a historic laked dye is formed from the



Figure 2.7: A sample of pure pigments.

ground dried roots of the herbaceous *rubia tinctorium* of Greece and Asia Minor. The particles are laked with aluminum hydrate, forming the crimson red pigment *Madder Lake*.

Thanks to the developments in chemistry in recent history, painters today have hundreds of pure colors from which to choose. Historically, there were fewer pigments available to painters of Medieval Europe. With few exceptions, the same pigments are used in all types of paints. The difference in the various methods of painting—oil, watercolor, acrylic—lie in the material with which the pigments are applied and attached to the ground.

For a pigment to be suitable for use in an artists' paint, it must meet a number of requirements [Got87]. A pigment must be a fine, smooth powder that does not react to changes in normal atmospheric conditions. It should not react chemically with other paints or supplementary materials to which it is exposed—this includes the binder, vehicle, ground, or other pigments. While no pigment is perfect in all binders, a pigment should form a stable film with the binder. Defective pigment-binder mixtures usually show soon after paint manufacturing. *Flocculation* is when



Figure 2.8: Natural pigments of antiquity. Top row: yellow and red earth pigments; center row: vermilion, two shades of umber, and azurite; bottom row: two shades of green earth, malachite and lapis lazuli. Adapted from [Weh75].

a pigment rises to and projects from the surface of a dried paint film and thus can be powdered off. *Agglomeration* is when pigments coagulate into lumps and resist dispersion in the binder.

Painters usually visualize a paint color in terms of its *masstone*—the color appearance of a high concentration of only one pigment completely hiding the surface below. Hence, a pigment should be pure, without added inert ingredients that adversely affect its color or handling. A *tint* is the color appearance of any mixture of a pigment and a white pigment. This tends to lighten the color, make it less saturated, and sometimes shift the result to a slightly different hue.

The concentration of pigment to binding medium also has an effect on the resulting color. Higher concentrations of pigment to binder produce deeper, richer hues. However, there is a limit of how much a given media can be saturated with pigment; at some point it rejects absorbing more pigment and the solution's fluidity is adversely affected. This characteristic is also pigment dependent, as each material has a different absorption rate. This is sometimes referred to as the

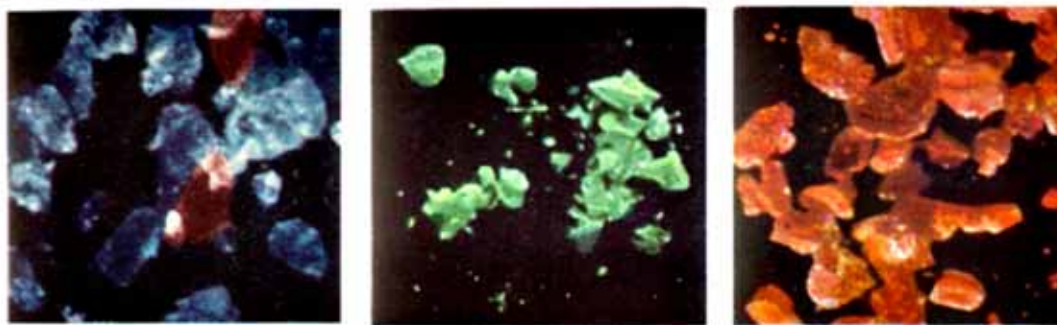


Figure 2.9: Pictomicrographs of pigments Egyptian blue, Malachite, and Vermilion. Adapted from [Weh75].

Pigment Volumetric Concentration (PVC):

$$PVC = \frac{\text{Pigment Volume}}{(\text{Pigment} + \text{Filler} + \text{Binder}) \text{ Volume}}$$

Further, color is meaningless without longevity. Thus, another important pigment attribute is *lightfastness*, the ability of the pigment to retain its color unchanged under prolonged exposure to normal conditions of light. This attribute is fundamentally determined by molecular structure, as some molecules degrade or change in continuous presence of light. *Permanence* refers to a pigment's chemical stability to any environmental factor, including light, heat, water, acids, alkalis, or mold. For example, ultramarine blue is extremely lightfast, but will fade on exposure to acids (possibly existing in the support or the air) [Mac05]. These effects are not uniform across all pigments. The most permanent of pigments are inorganic synthetics, and of those that deteriorate, the fastest fading materials are organic. Inorganic pigments that do change, however, do not fade but gray or darken.

While it may seem obvious that artists' paint demands pigments which resist marked change, independent testing and standardized labeling in the USA has only

become more common recently. The American Society for Testing and Materials (ASTM) developed testing procedures and standards for classifying a pigment's reaction to light in 1984. The *Standard Test Methods for Lightfastness of Colorants Used in Artists' Materials* approximate the color change that can be expected over time in pigments used in artists' paints in normal indoor exposure [D4384]. The ratings range from I *excellent* to V *very poor*. The tests only apply to certain binding materials and a rating for a pigment in one media does not necessarily equate to the same rating in another media. For example, pigments typically last longer inside the protective coatings of oil or acrylic than gum arabic (as in watercolor). For artists, paints should only be considered when they have a ASTM rating of I or II (*excellent* or *very good* lightfastness). Under these ratings, the pigment will remain unchanged for 50 to 100 years or more under exposure to light.

The most salient pigment attribute for painters is its color. There are many factors inherent in pigments that influence the color of a paint. Color is fundamentally created by the absorption of specific wavelengths of light by electrons oscillating across double chemical bonds in pigments [Mac05]. In addition, color is largely influenced by the particle size, shape and distribution of the pigment. Table 2.1 describes a representative distribution of modern artist's pigment grades; the smallest of pigments are much larger than a dye molecule, while the largest pigments can be seen by the naked eye.

There are many pigment properties determined by particle size, including light scattering properties that are important for artists. The fundamental attribute is the ratio of surface area to volume. Surface area A is of order $O(r^2)$, while volume V is of order $O(r^3)$ (where r is the radius of a particle). The ratio

Table 2.1: Average pigment particle size. Adapted from [Mac05].

Size	Material	Size	Material
1000 μm	= 1 mm = 10^{-3}m		pyrroles
100 μm	coarse historical pigments		naphthols
50 μm	smallest unmagnified particles visible	500nm	wavelength of green light
	cobalt violet		cadmium yellow
	manganese blue		titanium white
10 μm	cobalt green/turquoise		transparent red iron oxides
	cerulean blue		<i>translucent synth. organics</i>
	manganese violet		arylides
	black iron oxides		benzimidazolones
5 μm	viridian	100nm	dioxazines
	cobalt blue		zinc white
	violet/yellow iron oxides		prussian blue
1 μm	= 10^{-6}m		<i>transparent synth. organics</i>
	ultramarine blue		quinacridones
	red iron oxides	50nm	phthalocyanines
	cadmium red/orange		carbon black
	<i>opaque synthetic organics</i>	1nm	= 10^{-9}m
		0.3nm	water molecule

$$\frac{A}{V} = \frac{O(r^2)}{O(r^3)} = \frac{1}{O(r)} \quad (2.1)$$

illustrates that the particle size is inversely related to the surface area. As particles decrease in size, the surface area increases. This affects the *tinting strength* of pigments, the colorant power in relation to its mass. As particles get smaller, the tinting strength is increased and the quantity of pigment needed to produce a required color intensity is reduced. Tinting strength also indicates how much a pigment will dominate the color of a mixture with other pigments. Tinting strength is an important characteristic when determining relative costs of different colorants. For example, an artist purchasing a tube of a particular colorant may wish to know which brand is the best value. If an expensive brand contains more pigment per unit volume, it has a higher tinting strength, and hence may be a better bargain.

A larger surface area demands a higher ratio of liquid to pigment. Therefore, more finely divided pigments need more binder to maintain a similar paint consistency to that of larger particles.

As the particle size goes below about 10 times the wavelength of light (particle diameter λ (4000-7000nm)), scattering effects begin to become significant. Incident light is reflected multiple times before exiting the medium. At this level, the increase in tinting strength is sometimes offset by the increase in total surface scattering. High scattering is desirable in white paints, because more scattering means increased hiding power and opacity; so fewer coats are necessary to cover the surface.

Figure 2.10 illustrates how differently light behaves in response to varying particle size, given the same material. Finer ground pigments typically result in more

reflective or brighter hues due to the increased scattering. It is typical that the same mineral is processed in a range of different particle sizes to be used in different applications. Pigment sizes suitable for artists' work may be too coarse for commercial applications. Also, very fine pigments tend to be less lightfast than larger pigments of the same material. As a result, an artist may not want to use the same grade of mineral used elsewhere.



Figure 2.10: Different grades of Malachite affect the overall appearance of the same pigment. Left: medium grade with particle size between 20-100 μ m. Right: fine grade with an average particle size of 20 μ m. Adapted from [Pig05].

Note that all pigment particles tend to clump into aggregates, which may be 5 to 50 times the size of a single particle. Hence, in paint preparation, pigments must be ground carefully into a uniform solution.

Further, naïve painters experience pigments which tend to settle out of solution and need to be stirred each time the brush is charged with more paint. These pigments are classified as *sedimentary*—the pigment is either very dense or very heavy, or both. The mass of a pigment is not only dictated by particle size, but also the *specific gravity* of the pigment. Specific gravity is the ratio of the weight of the pigment to the weight of the water it displaces in solution. This ratio is constant regardless of particle size. It is of note that the specific gravity of synthetic

Table 2.2: Pigment specific gravity. Adapted from [Mac05].

gm/cm ³	Material	gm/cm ³	Material
1.4	arylide yellows	2.5	<i>aluminum hydrate</i>
1.5	quinacridone violet/rose	3.0	raw sienna/umber
1.6	naphthol reds	3.5	burnt sienna/umber
	phthalocyanine blues		viridian
	dioxazine violet	4.0	yellow iron oxide
1.7	benzimidazolone yellows		titanium white
1.8	lamp black		cobalt blue
	prussian blue	4.5	cadmium yellows/reds
2.1	phthalocyanine greens	5.0	red/black iron oxide
2.3	ultramarine blue/violet	5.5	zinc white

organic pigments can vary depending on the specific gravity of the substrate used in pigment laking. Table 2.2 lists a selection of pigment specific gravities, as well as a common laking substrate for comparison, aluminum hydrate.

Objects with a specific gravity less than $1.0 \frac{gm}{cm^3}$ float in water, while objects with much greater specific gravities weigh more than the water they displace, and thus will sink. For comparison, linseed oil (used in oil painting) has a specific gravity of $0.93 \frac{gm}{cm^3}$ [Box05], while fresh egg yolk (used in tempera painting), has a specific gravity of $1.09 \frac{gm}{cm^3}$ [Saa01]. Hence, due to different material properties, not all pigments behave equally in different media. To help disperse sedimentary pigments in solution, it is possible to add an inert material of medium grade.

Many historical colorants have been largely displaced by modern synthetic variants. Heating cobalt chloride and aluminum chloride together makes the pigment

Cobalt Blue. This chemical reaction produces particles of unusual fineness and uniformity. On the other hand, the natural pigment Azurite is prepared by crushing samples of the mineral extracted from copper ore deposits. During this process, aggregates of copper carbonate crystals are shattered into small, irregular shapes and sizes. Due to difficulties in extraction, the mineral may also contain *inclusions*, which are small amounts of other minerals (malachite, in this case). As a result, while exhibiting a similar hue, Azurite's reflectance properties will not compare to the purity of those found in Cobalt Blue.

The driving force of synthetic pigments mainly serves the dye and paint industries. They are formulated today to maximize their desirability—homogeneous in shape, size and composition—while at the same time improving color nuances, brightness and stability. For example, to increase the covering power of a pigment, particle sizes are reduced to the smallest possible (therefore increasing the possibility of poor lightfastness). Particles that are more consistent in shape and size also tend not to settle quickly and nor separate from their binder once inside a paint bottle or tube. While this increases the shelf life and thereby marketability of paint, commercial additives and processes sometimes reduce the color's effectiveness for artists' use.

2.2.2 Binding Media Influence

In the previous section, pigments have been discussed out of context. Pigments themselves do not have binding strength and therefore are never viewed directly on a painting. The material that adheres pigment particles to the ground is known as the *binding medium*. Many types of binders have been experimented with over the years, including plant gums, animal glues and drying oils. While pigments

provide the underlying color to a paint, the binder determines the primary optical and textural characteristics, as well as the working properties of the paint.

In addition, other substances may be added to further manipulate paint attributes. An artist may add a *vehicle* to dilute the pigment-binder mixture, allowing the paint to be spread more easily. This substance has no adhesive properties and evaporates after brush marks have been made. For instance, in oil paint, natural gum turpentine is often used as a vehicle. Other materials may be added to enhance the optical or textural characteristics of the paint surface. For years the strong, and bright colors in Venetian Renaissance paintings mystified art historians. It turns out that artists were experimental chemists that would mix unconventional ingredients. Ground particles of glass were added to the palette to enhance the reflective properties of the paint, which would make objects and figures in their paintings appear to glow [Goh05]. An artist can also alter the working properties of the paint, such as viscosity and handling. Many materials (wax, for example) are added to permit the sculpting of the topology of the surface. Further, one can even accelerate or deter drying or make the paint more or less fluid, if desired.

Our perception of color in a painting depends on the interactions between light and the layers of paint. In order to understand how the same pigment looks different when suspended in different media, we must first analyze the optics of paint films. When a ray of light hits a surface it is either *reflected* off the surface, *transmitted* through the material, or *absorbed* into the material.

The way light reacts to a surface is known as the *Bidirectional Reflectance Distribution Function (BRDF)* of the surface. This reflection can be as simple as being uniform in all directions, commonly called *diffuse*. Diffuse reflections are typically the result of rough surfaces, and are characterized as matte or dull in

appearance. Reflection can also mirror-like, or *specular*, as in metallic surfaces. Materials can also maintain a combination of both types of reflected light, as in glossy materials like plastic. In all cases, an incident light ray hits a surface and is reflected. The angle of which the ray is reflected is equal and opposite to the angle between the incident light ray and the normal (the ray perpendicular to the surface). It is the surface definition that determines the amount and direction of reflected light. Smooth surfaces have aligned normals, hence the reflection is mirror-like; rough surfaces have randomly-orientated normals and thus scatter the light.

In Figure 2.11, an incoming light ray \vec{i} is reflected as ray \vec{r} . At the point where the light strikes the surface, the *normal* \vec{n} defines the direction perpendicular to the surface. The incident ray is reflected such that the angle of incidence, θ_i , is equal to the angle of reflection, θ_r .

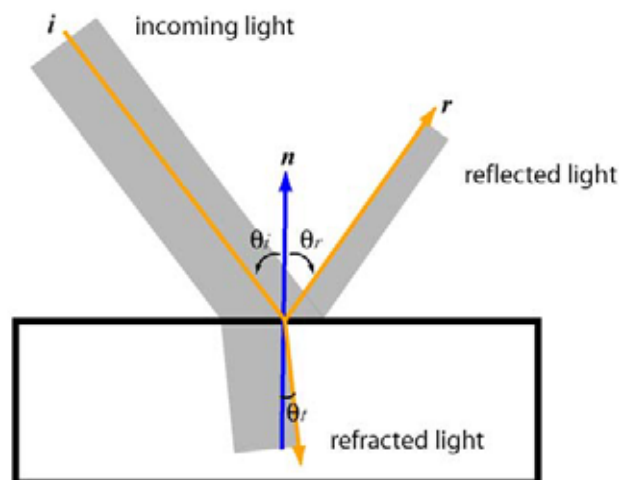


Figure 2.11: As light enters a medium, it is either reflected, transmitted, or absorbed.

We can never speak of the *speed of light* in the abstract, since it must always be in respect to some medium. The most common reference is a perfect vacuum,

though the speed of light in air is only slightly slower. When light travels unimpeded through a vacuum, it travels at a rate of about $c \approx 2.998 \times 10^8 \frac{m}{s}$. When light travels through a medium denser than a vacuum, its velocity v decreases to a value less than c . The ratio of the speed of light in a vacuum to the velocity of light in another medium is the *index of refraction* η for that material:

$$\eta(\lambda) = \frac{c}{v_\lambda} \quad (2.2)$$

where

- v_λ is the velocity of light of wavelength λ in the medium
- c is the speed of light in a vacuum

Note that the index of refraction is a function of the wavelength of light. *Wavelength* λ is the distance between repeating units of a wave pattern, while *frequency* f is the rate of which repeating elements in a wave travel. For a wave pattern, the velocity v is given by

$$v = f\lambda \quad (2.3)$$

For light, the velocity is constant ($v = c$). Visible light is not pure, but comprised of many different wavelengths, each traveling at different frequencies. For example, the frequency of blue light (short wavelengths) is higher than red light (long wavelengths). However, in practice it is sometimes typical to use a single wavelength to simplify calculations. A midrange wavelength of light, 589nm, is commonly used to represent the visible spectrum—the prominent yellow-red band of the Sodium D-line emission [Col06].

The surface where two media come into contact is called an *interface*; we see a change of the speed of light at any interface between two materials of different

Table 2.3: Index of refraction η for binding media, vehicles, and others. Adapted from [TM00].

Material	η	Material	η
<i>Binders</i>		<i>Vehicles</i>	
Gum arabic 10%	1.334	Water	1.330
Casein	1.338	Spirits of turpentine	1.47
Egg yolk	1.346	Glycerol	1.47-1.48
Hide glue 10%	1.348	Dammar varnish	1.539
Mowiol	1.410	<i>Others</i>	
Molten beeswax 74°C	1.438-1.442	Air	1.0008
Walnut oil	1.477	Glass	1.517
Linseed oil	1.478	Ruby	1.760
Acrylic resin	1.49	Diamond	2.418

densities. One ramification of this change of speed is that the light appears to bend when passing through the interface. The amount of this bending, or *refraction*, is determined by the indices of refraction of the materials on the opposing sides of the interface. The most basic law describing how light refracts is known Snell's law:

$$\eta_i \sin(\theta_i) = \eta_t \sin(\theta_t) \quad (2.4)$$

where

θ_i is the angle between the incident ray and the normal at the interface

θ_t is the angle between the transmitted ray and the reversed interface normal

η_i is the index of refraction for the incident medium

η_t is the index of refraction for the medium into which the light is transmitted

In general, when light travels from a dense medium to a less-dense medium, the transmitted rays bend further away from the surface normal than the incident ray ($\theta_i < \theta_t$). An implication of this statement is that at some angle, called the *critical angle*, the light is bent such that the transmitted rays are perpendicular to the surface normal. This behavior is illustrated in Figure 2.12.

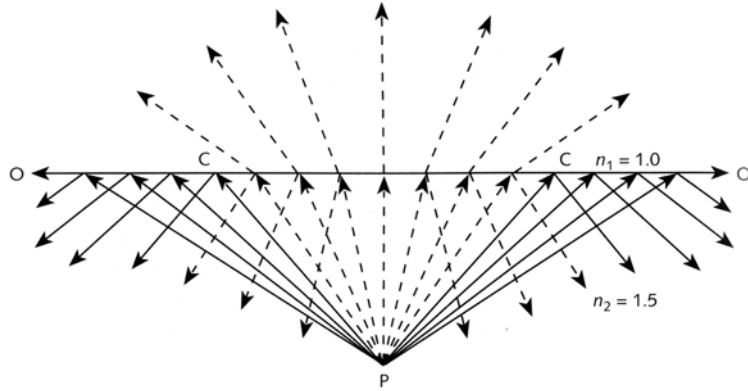


Figure 2.12: Rays originating from point P inside a material of refractive index $\eta_2 = 1.5$ are bent when entering a less-dense medium, such as air ($\eta_1 = 1$). Since the rays are bent away from the normal, some of the light is reflected back into the material. The ray striking C is at an angle of 42° and travels to point O . The critical angle is 42° in this case, since rays with a larger incident angle will be completely reflected back into the dense medium. Adapted from [JF01]

Essentially, at some angle the incoming rays will be bent in a way such that they travel parallel to the surface of the medium. This phenomenon is called *total internal reflection*. From Snell's law (Equation 2.4), we find the critical angle ϕ_c may be found from:

$$\begin{aligned} \eta_i \sin(\phi_c) &= \eta_t \sin\left(\frac{\pi}{2}\right) \\ \sin(\phi_c) &= \frac{\eta_t}{\eta_i}. \end{aligned} \quad (2.5)$$

In other words, the critical angle is the smallest angle of incidence, in the denser material, for which is totally internally reflected.

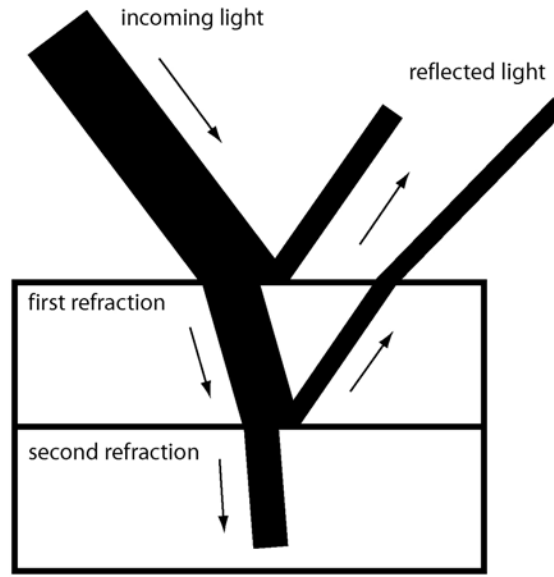


Figure 2.13: Light passing through two substances of different indices of refraction, where $\eta_{air} < \eta_1 < \eta_2$.

A ray can also be traced through multiple interfaces, as in Figure 2.13, provided its energy has not been completely absorbed. Hypothetically, if a ray traverses an interface where both substances had the same refractive index, no refraction would take place and the ray would maintain its original direction. However, in the case depicted above, the refractive indices increase as the incident light travels between each material. As a result, the ray undergoes multiple refractions (this behavior is typical in paintings). Light that was refracted at the first interface and reflected back at the second interface will pick up some of the colorant from that interface before exiting into the air.

The phenomenon where transmitted light rays scatter inside a material before either being absorbed or leaving at another position is called *subsurface scattering*. It is a very important visual element for many reasons. The soft diffusion of light within a material is important to many translucent materials, such as marble, skin, milk and wood. This characteristic is evident when viewing one of these

materials while lit from behind. Light will bleed on the sides and through areas of thin volume, while a material without subsurface scattering would not exhibit such subtle detail. This effect will also soften the shadowed areas of the material since light traverses across the shadow boundaries from reflections underneath the material. Also, as the scattered light traverses the material, light rays pick up coloration before exiting. In skin, light scatters in the many layers of the epidermis and the dermis, as well as capillaries, before exiting and reaching your eye. This way, the sudden flush of one's face is readily noticed by others, even though the expanding blood vessels are relatively far underneath the skin.

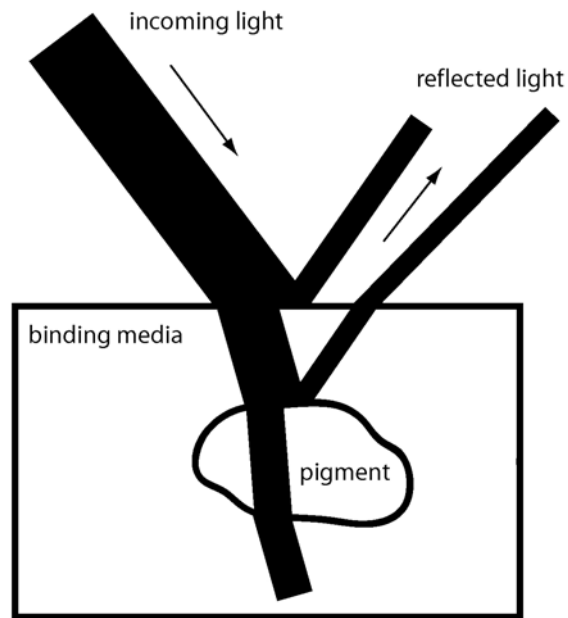


Figure 2.14: Light interacts with both the media and pigments in paint.

Paint also exhibits this complex translucent behavior, where light diffuses through multiple interfaces. Figure 2.14 shows the behavior of light as it enters a single layer of paint, where a pigment acts as a second interface for the ray. Light first refracted by the binding media, picks up color upon reflecting off the pigment particle and exits the surface of the paint film. The resulting color exhibits optical

properties of both the pigment and binder. As seen previously in Figure 2.9, the shape, size, and orientation of each particle varies greatly within each pigment. This has a great effect on the directions of reflection and refraction of light.

Each interface incites changes in the speed of light, while picking up color of materials it encounters along the way. In addition, the distinction between pigment particle and binding medium is an interface just like any other, and thus can also reflect and refract light. Many indices of refraction for common pigments can be found in Table 2.4.

Also, many collections of pigments contain inclusions and impurities, which have their own respective optical properties, affecting the overall appearance. Lapis Lazuli (natural ultramarine blue) is mined from copper ore, which often contains pyrite. It is often too expensive to completely purify mined materials that serve as pigments. As a result, the extraneous minerals reflect wavelengths from different parts of the visible spectrum than that of the pure pigment.

Figure 2.15 combines many effects that have been discussed, illustrating the complex optical behavior of a layer of paint on a ground. The outer surface definition and texture of the paint film has an effect on the first scattering event. Light that is transmitted at this interface interacts with both the media and pigments until it is either absorbed or it exits the outer film. In addition to the physical properties of the media and pigment, the concentration of pigments to binder has a great effect on the amount of paint required for an opaque paint film. This thickness is important, because it determines how much light reaches either the underlying layers of paint, or the painting's ground. Furthermore, a thick layer of a dense medium will displace refracted rays further from original ray than will a thin layer of the same material.

Table 2.4: Index of refraction η for different pigments. Adapted from [O’H04].

Color	Pigment	η	Color	Pigment	η
Blue	Azurite	1.73-1.84	Green	Dioptase	1.64-1.71
	Indigo	1.49-1.52		Glaucosite	1.62
	Smalt	1.49-1.52		Malachite	1.65-1.90
	Lapis Lazuli	1.50		Verdigris	1.53-1.56
Red	Red Ochre	2.26-2.398	Yellow	Chrome yellow	2.260-2.398
	Cinnabar	2.81-3.15		Gold Ochre	2.260-2.398
	Hematite	2.78-3.01		Jarosite	1.71-1.82
	Caput mortem	2.78-3.01		Orpiment	2.40-3.02
	Vermilion	2.82-3.15	Chalk (whiting)	1.51-1.65	
Brown	Goethite	2.08-2.40	White	Titanium dioxide	2.72
	Burnt sienna	1.85		White lead	1.94-2.09
	Raw sienna	1.87-2.17		Zinc oxide	2.00-2.02
	Burnt umber	2.20-2.30	Black	Black oxide	2.42
	Raw umber	1.87-2.17		Lamp black	2.42

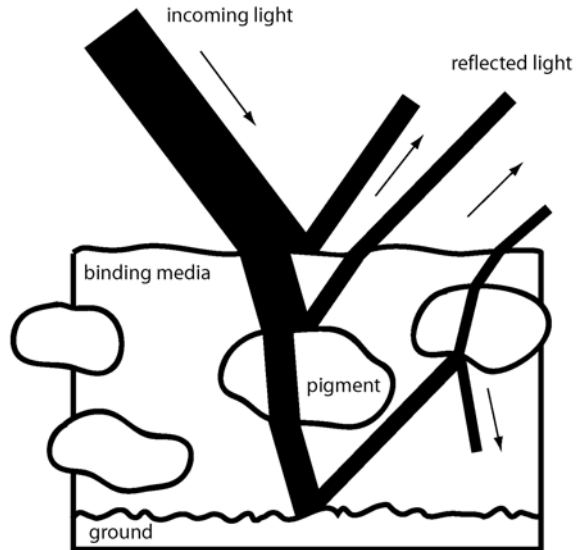


Figure 2.15: A schematic view of complex light behavior in a layer of paint on the surface of a painting.

The importance of the ground is evident. Physically, it acts as a tooth for the paint to attach to the surface of the painting. Optically, it reflects rays that were transmitted into the media back toward the viewer. For the most luminous colors, an ideal ground would not absorb or transmit any light, but be completely reflective. Hence, any coloration of the ground will tend to decrease the amount of reflection and possibly affect the hue. Further, the more translucent the overlying coating of paint, the more the brightness of the resulting painting is affected by the ground.

Many artists execute their artwork using many superimposed translucent layers, which add subtle, yet sophisticated details of color. The application of a thin concentration of pigment to binder is called a *glaze*. However, while a painting may have layers of identical material, there will still be interfaces where light will be affected. This is due to differences in each layer's material composition, as well as material changes over time. For instance, oil paint takes nine months to a year

to completely congeal. Hence, these chemical changes in the binding media affect the phase velocity of the light in the medium, which in turn affects the index of refraction.

2.3 Binding Media Materials

Historically, traditional binding materials are all natural substances. Some require no processing, while others have to be extracted from their source by some means. In modern times, compounds synthesized in the laboratory have supplemented natural occurring materials. This chapter classifies natural binders by their respective organic compounds, leaving synthetic and other binders to their own categories. This method of classification is convenient because it groups materials of similar composition together. Much of this section is aided by the work of Taft and Mayer [TM00].

2.3.1 Carbohydrate-Based

Carbohydrates are compounds that contain carbon, hydrogen and oxygen. The basic building blocks of carbohydrates are simple sugars, of which glucose (one of the most abundant organic compounds on the earth) and fructose (found in honey and fruit juices) are prominent examples. These simple sugars, known as *monosaccharides*, bond together to form large conglomerates known as *polysaccharides*. Common examples are starch and cellulose; both are created from a multitude of glucose molecules.

Examples of paint binders utilizing polysaccharides are honey and plant gums. Honey is not a widely utilized binder, though found to be used in the past. The substance is easily soluble in water and readily re-dissolved after the sticky sub-

stance has dried. This behavior is desirable when an artist wants to rework an area that was completed previously. However, the resulting paint film is not very permanent nor durable, as it is sensitive to moisture and quite brittle.

A great number of plant gums were used in different times as binders. The most common is the material *gum arabic*, which comes from a particular variety of the *acacia*. *Acacia* was one of the few trees that grew in ancient Egypt and served as a binder in that period. Gums have similar behavior to that of honey; it is reworkable and the dried film results in a matte surface. Gum arabic is the primary ingredient for *watercolor* painting. Other watercolor additives that are sometimes included are a *plasticizer*, usually glycerin, to soften the dried gum arabic and help it re-dissolve; and a *preservative*, to suppress the growth of mold and bacteria.

The method of mixing watercolor paints with an opaque white pigment is traditionally referred to as *gouache*. *Gouache* is an opaque watercolor paint, and creates a flawless, flat color area. Watercolors are layered in glazes, while *gouache* is applied more directly, since applications of *gouache* will completely hide the layers underneath. Whereas, the white of the paper provides the light for watercolors (those who practice watercolor typically do not use white), the brilliance of *gouache* comes from the pigment. The perfection of the *gouache* surface appeals to illustration and commercial artists. Projects on both binders can be completed quickly, as gum arabic dries rapidly.

2.3.2 Protein-Based

Proteins are compounds that consist mainly of carbon, oxygen, hydrogen and nitrogen. Similar to carbohydrates, proteins are also comprised of building blocks. There are approximately two-dozen naturally occurring amino acids known, which

bond together to form proteins. Examples of important proteins include keratin (found in skin, wool and feathers), hemoglobin and silk.

In the context of traditional binding materials, glue refers specifically to a substance derived from boiling skins or connective tissues of certain mammals or fish. The adhesive is the protein collagen, which is a major structural ingredient in mammals and fish. Skin glue is made from the extracted gelatin from boiled raw hides, and is sold in powder form or as plates.

The protein has the unusual property of being soluble in hot water, but gels as the solution cools to room temperature. If substance is left, the water will completely evaporate and the substance will harden. Hence, a painter using this media must work while the glue is hot. Glue paint is made fresh daily, as reheated glue loses some of its binding strength. The method of painting with a solution of gelatin and water is called *distemper*. A common artists' glue paint is extracted from rabbit skin, which yields a very strong, matte, and colorful paint film. The most attractive quality of the glue paints is its beautiful reflection of light due to the grains of pigment that are lying on the top of the paint layer. Of all the binding media, glue is almost certainly the one mostly widely utilized around the world, though from different animal sources.

An *emulsion* is a stable mixture of an aqueous liquid with a oily, fatty, waxy or resinous substance. The yolks of hen's eggs contain albumen (a gummy substance), a nondrying oil, and lecithin (an efficient, stabilizing lipoid). Yolk is approximately one-third protein, the rest containing oil droplets in water. Albumen belongs to a class of proteins that have the property of being coagulated by heat, as demonstrated by a cooked egg. The same effect occurs when it is spread out in a thin film and exposed to daylight. *Tempera* painting refers to a binder of egg yolk.

Tempera paint is not stored, but made fresh daily, and dries quickly to an unusually luminous and brilliant film. The dried paint film is insoluble to the extent that it is water-resistant under normal conditions. Tempera is sometimes used in conjunction with other painting media. Its quick-drying behavior is well-suited for underpainting, since an artist can block out compositions very quickly. Also, some pigments react chemically with select media and hence tempera is used in alternating layers of such media.

Milk is another example of an emulsion, as it contains suspended droplets of water-insoluble butterfat. The solution is approximately one-fourth protein, and also contains water, oil and milk sugar. *Casein* is a binder formed from the solids of skim milk. It is manufactured by allowing skim milk to sour, separating the curd from the whey, and washing and drying it. The crude curd from milk has been employed as a binding medium since the earliest records. However, homemade casein will contain impurities, and modern commercial casein is a much more viable alternative for painting. Casein is an aqueous paint, but insoluble and weatherproof when dry. The resulting paint film is a very strong matte surface, with slightly more luster than gouache, and is typically used as an opaque color.

2.3.3 Oils

Oils are derivatives of a large class of diverse natural compounds known as lipids. The majority of oils are *nondrying* or *semidrying* in nature; if spread out in a thin film and exposed to air, they will either remain liquid or become only somewhat solid. Some oils are *drying oils*, whereas through chemical reactions and oxidation, they form solid films when exposed to air. The dried oil film differs in physical and chemical composition from its liquid counterpart. It cannot be brought back

to its original state by any means.

The major drying oils are linseed, walnut and poppy-seed. Linseed and walnut oil are the most common; the former is pressed from the seeds of the flax plant and the latter from the seeds of walnut trees. Unlike binding media covered previously, oil paint is not soluble in water. Natural solvents serve as the vehicle for oil paint, such as the spirits of gum turpentine. Oil paint is long considered as the most versatile medium for paint, as many materials may be used as additives in oil to produce a diverse range of optical and handling properties.

Oil is relatively slow drying. While the surface of the film may be dry to the touch in the first few days, the substance takes much longer to completely congeal (sometimes over a year). This is an advantage to the painter as a number of effects can be produced by working *wet-into-wet*, or mixing one layer into another before the underlying film dries. Applying layers of different consistencies can achieve effects not attainable in other media. In oil one can also glaze a transparent film over another as in watercolor, producing a distinct color. Unsatisfactory work is also easily scraped off with a palette knife and repainted, instead of overpainting as in other media.

Drying oils do not dry at the same rate. Painters would naturally seek faster drying oils, but the same reactions that lead to drying result in yellowing. Unfortunately, faster drying oils yellow more than slower counterparts, dirtying whites, turning blue passages greenish, and so forth.

The paint film that results from oil paint is very durable, water and moisture resistant, and much more flexible than the aqueous paints. Oil paint can be applied to both rigid and flexible supports. It retains flexibility in the dry state, holding up against expansion and contraction due to fluctuation in atmospheric conditions.

2.3.4 Waxes

Historically, the most important wax for artistic purposes is beeswax. Chemically, beeswax contains some free fatty acids, hydrocarbons, and esters formed from alcohols and fatty acids. Similar to drying oils, beeswax can be dissolved in natural solvents. *Encaustic*, or the method of painting with wax, originates from ancient Greece.

Heat is used to liquefy the media, and the paint is applied hot with a brush or palette knife (encaustic literally means “burned in”). Hence, the wax does not dry, yet congeals as it cools. In modern usage, the beeswax is often combined with resin or turpentine to increase the fluidity of the paint. A wide range of textures is possible by varying the consistency of the paint. Applying external heat to the artwork makes some additional effects. An artist may heat behind the support to keep the surface warm while brush marks are made or apply heat to the paint surface to *burn in* (fuse and adhere) existing layers. Encaustic paintings have a unique lustrous, rich, and translucent surface.

Due to the cumbersome nature of its equipment, it was displaced by other media (tempera and oil) in the Medieval and Renaissance periods. However, encaustic has seen resurgence in modern times due to the abundance of tools to manipulate the media, including hot plates, electric tools and heat lamps. Also, since wax readily dissolves in turpentine, it is sometimes used as an additive in oil paint for its textural and optical properties.

2.3.5 Synthetic Polymers

Rivaling oil in its versatility is a modern paint formulated from a synthetic polymer referred to as *acrylic polymer emulsion*, or commonly known as simply *acrylic*.

While it has been used since the 1930s, widespread use followed commercial manufacture in the 1950s. Artists are drawn to its quick-drying behavior (a matter of minutes) and tough, flexible film suitable for almost any surface. Also, the media uses water as a vehicle, eliminating the toxic fumes from oil's solvents in the studio. This simplifies cleanup of brushes and thinning of the paint as well.

One of the most compelling qualities of acrylic paint is its uncanny resemblance to almost any other media, via manipulating the substance with various additives. It can be thinned and used in light washes on paper as in watercolor, or thickened and applied to large panels of canvas as in oil. It does not require the same support preparation as other media and can be applied to unprimed surfaces, as it is resistant to moisture upon drying. Similar to oil, additives can alter the finish, viscosity, texture, and drying properties of acrylic paint.

However, there are drawbacks to this new medium. The acrylic polymer emulsion used as a binder is not as transparent as some other painting media, resulting in a slightly less luminous surface. Another disadvantage is that acrylic cannot hold as much pigment as other binders, which results in a slight hue reduction. In regards to art conservation, not enough research has been done to examine the longevity of acrylic polymer emulsion as a suitable binder, in comparison to historical binders.

2.3.6 Catalytic Materials

There exists another form of painting that does not conform to our usual definition of paint. In this case, the pigment is spread onto the surface of a wall without the presence of a binder. The adhesion of particles to the support is the result of a chemical process between the plaster of the wall and the air. Hence, the

plaster serves as ground, support and binder. This ancient method of painting on masonry walls is deemed *fresco* (Italian for fresh), appropriate since a pigment-water solution is applied to damp plaster.

The plaster is a mixture of slaked lime (calcium oxide in solution with water, forming calcium hydroxide), and an aggregate (sand, marble dust, or a volcanic ash called *pozzolana*). The wall surface is built up of layers of different formulations of lime, water and aggregate as shown in Figure 2.16. Each successive layer has a greater percentage of lime, gradually increasing the binding strength of the plaster. Layering insures even, slow drying, which reduces the likelihood of cracking.

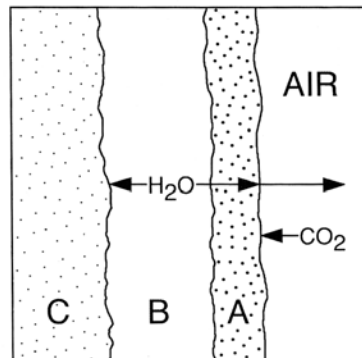


Figure 2.16: As layers of a fresco dry, water migrates through the surface layer or *intonacco* (A), and *arriccio* (B) toward the masonry wall (C) while the rest evaporates into the air at the surface. As carbon dioxide is drawn into the plaster, pigments are locked into the surface. Adapted from [TM00].

Each layer is kept damp until after the succeeding layer is applied, and the colors are applied to the final layer before it dries, usually within about eight hours. As the composite of layers dries, water migrates out of the plaster layers. The carbon dioxide from the air transforms the calcium hydroxide in the lime into calcium carbonate. During this process, platelets of calcium carbonate lock the particles of pigment into the plaster. This process acts as the equivalent of an

organic binder found in more conventional paints.



Figure 2.17: Cross sections of two ancient fresco fragments, showing coarse aggregates below the paint layer. Adapted from [Weh75].

Fresco serves well as a medium for mural painting due to its permanence, for it maintains the same longevity as the architecture. However, the difficulties for the painter reside primarily in the fact that the work must be executed quickly and directly. Extensive preparatory work must be done in advance, usually in the form of sketches. Large-scale *cartoons*, or full-sized drawings, are made to work out the composition beforehand. As covered previously, most fresco paintings are large in scale; hence the intonacco is sectioned into giornate that are more manageable. Each giornata must be completed in under approximately eight hours, after which the plaster has dried too much and pigment refuses to adhere. The painting cannot be revived after the plaster has set, and alterations can only be made by chipping away the plaster and starting anew. For small alterations, sometimes paint is applied *secco* (Italian for dry), on top of the dried plaster with tempera or distemper. Secco is also used for pigments chemically incompatible with lime (pigments containing copper, for example).

Chapter 3

Color Background

Color is my day-long obsession, joy and torment.

-Claude Monet

3.1 Light and Color

The human visual system consists of three major components: *eyes*, which capture light and convert it into neural messages; *visual pathways*, which modify and transmit those messages from the eye to the brain; and *visual centers of the brain*, which interpret the messages in ways useful for guiding behavior [SB02]. Hence, the study of color science is broken down into three areas: *physical*, quantifying the physical energy which reaches the eye; *perceptual*, determining the perceptual responses of the human visual system; and *interpretive*, determining the overall impression. All of these components are crucially involved in seeing.

3.1.1 Visible Light Spectrum

Light is but just one form of electromagnetic radiation, similar to infrared, ultraviolet, and x-rays. All of these forms of energy are formed by the oscillation of electrically charged material. Electromagnetic radiation travels very rapidly (approximately 186,000 miles per second) and tends to travel in straight lines. The light energy is arranged along a spectrum according to the distance between oscillations, or *wavelength* (λ), measured in *nanometers* (*nm*). High rates of oscillation mean the radiation travels a short distance per cycle—meaning a short wavelength.

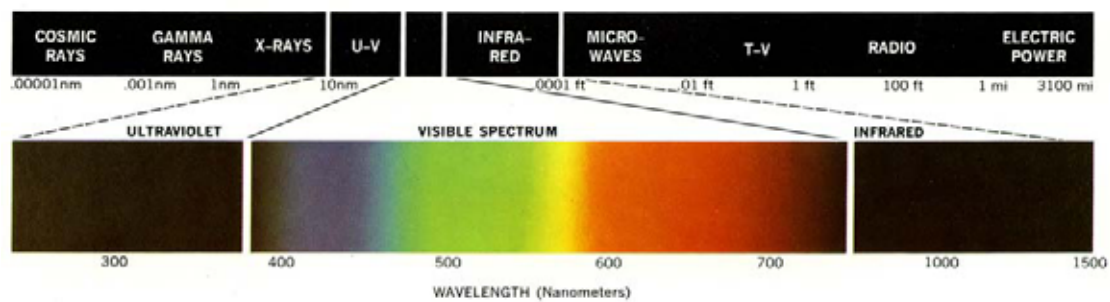


Figure 3.1: A section of the electromagnetic energy spectrum showing the range of wavelengths comprising the visible spectrum. Adapted from [GW77].

Figure 3.1 underscores an important point: the visible light that we depend on for sight only occupies a very small portion of the electromagnetic spectrum. The human eye is especially tailored for our environment. The light we see is useful as a medium of information about the world because it interacts (reflects and absorbs) with objects in a manner that gives us information about the surfaces and structure of objects. However, the color sensations we experience are not only of individual wavelengths, but of the summation of the entire visible spectrum. An object is “green” if most of the reflected light from the object is around 500nm. However, *some* light will also be reflected at *all* other visible wavelengths (380-700nm)

Most of the sunlight's energy in the short wavelength (ultraviolet) range is absorbed by molecules in the earth's atmosphere. Energy with longer wavelengths than visible light tends to penetrate objects, rather than be reflected by them. Hence, why microwaves are useful in cooking and infrared cameras can sense an object's heat.

The visible spectrum of light is comprised of an infinite set of different colors. If color samples are placed side by side, most people can distinguish a huge number of different colors, with one estimate placing that number at 2.3 million [PA98]. In the study of perception, the term *color* actually refers to three different qualities. *Hue* refers to a particular color within the visible spectrum as defined by its dominant wavelength, or the central tendency of its combined wavelengths. For example, light with a central tendency within $565 - 590nm$ will appear yellow. *Brightness* is the perception elicited by the luminance of a hue. *Saturation* is the intensity of a specific hue. Full saturation lends to a vivid color, while less saturated colors appear more muted and gray. Colors must be described in all three of these varying dimensions, and the relationship between hue, saturation and brightness is visualized in Figure 3.2.

Any discussion of color perception is not complete without the contributions of Isaac Newton, who revolutionized how we think about color vision. What one perceives as white light is not simply one wavelength of light, but actually a combination of all different wavelengths of light. This was observed long before Newton, as the scattered spectra from chandeliers and diamond jewelry had been seen for centuries. Newton's lasting contribution stemmed from his unique exploration of splitting up and reconstituting the spectral components of light to form colors. In a simple, but elegant experiment (Figure 3.3), Newton directed a beam of sun-

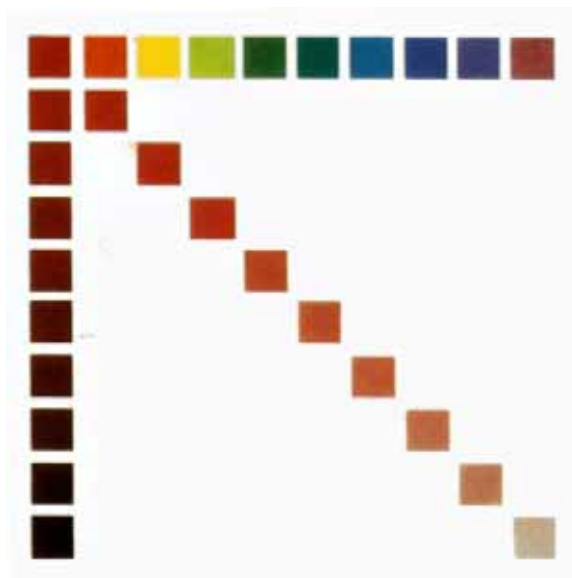


Figure 3.2: Hue, brightness and saturation. Different hues run horizontally; the brightness of a single red hue is adjusted along the vertical axis; saturation of the red hue is varied along the diagonal. Adapted from [SB02].

light from a small aperture to a prism, where the light fanned out into a rainbow of colors. Lights of shorter wavelengths (blue and violet) are refracted the most. Newton then used a convex lens to collect the refracted components and pass them through another prism. However, he would first selectively block out portions of this modified spectrum, which would allow him to distinguish between *pure* and *composite light* (light made up of several different components). To Newton, these observations suggested that the white light from the sun was not pure, but made up of several different colors. We now know that light from the sun contains a multitude of energy from different regions of the electromagnetic spectrum, and is the sum of many different wavelengths of light.

Color can be mixed in two drastically different ways, each method using its own set of component primaries. Everyone knows from art class that various shades of green are made when you mix blue and yellow paint together. This is called

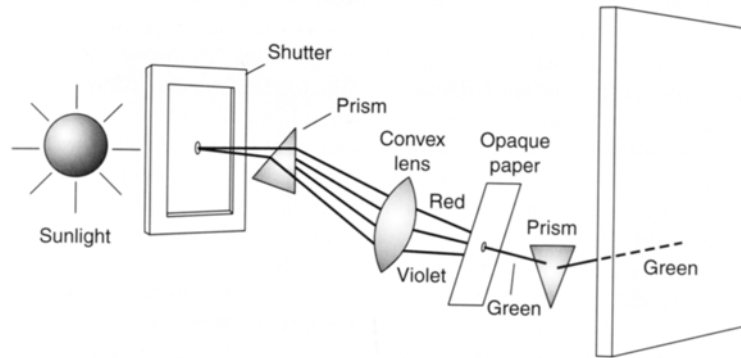


Figure 3.3: Setup for Newton’s basic experiment. In this case, after white light was decomposed, the resulting green light is selectively allowed to pass through the second aperture and the second prism, yet the light remains green. Hence, Newton would deem the green light pure. Adapted from [SB02].

subtractive color mixing, since the primaries absorb (or subtract) a portion of the incident light, keeping that portion from your eye. The light that is not absorbed is reflected and visible to the eye. For instance, inks are a common example of a subtractive colorant. If white light strikes ink that absorbs all spectra except long wavelengths, it will appear red. Multiple inks superposed will absorb the other’s reflecting spectra. The resulting color from the ink mixture will be comprised only of reflected light that is not absorbed by any of the inks. Thus, the combination of several subtractive colorants yields a mixture whose total reflectance is the product of the constituents:

$$C = \prod_i C_i$$

Hence, *multiplicative mixing* would be a more appropriate name, but the term subtractive color has stuck. The term subtractive mixing possibly originates from the different components absorbing the other’s contributing spectra.

To illustrate the system, consider the curve in panel A of Figure 3.4 which shows the reflectance spectrum of a typical blue ink. A graph of spectral reflectance

measures how much light is reflected at each wavelength over the visible spectrum. Notice how the ink tends to reflect more light in the short-wavelength portion of the spectrum. This is expected, as the respective colors at those wavelengths are from violets and blues to blue-greens. The blue ink also absorbs much of the orange and red regions of the spectrum, as the reflectivity in these regions is low.

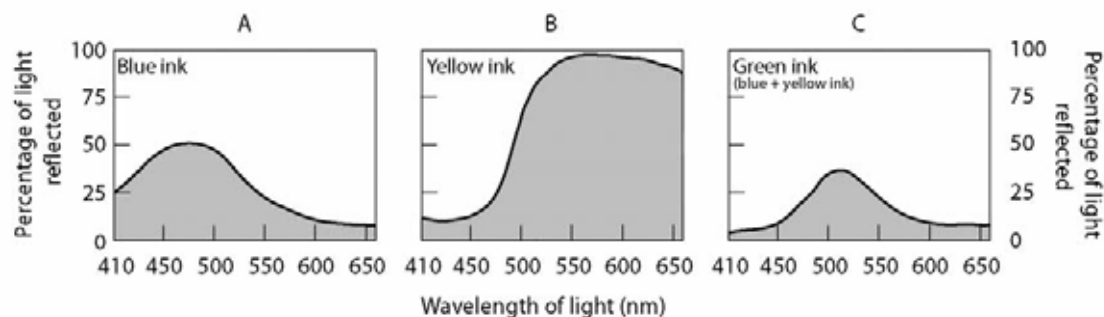


Figure 3.4: An example of subtractive color mixture. Adapted from [SB02].

Panel B shows the reflectance spectrum for a yellow ink, which tends to reflect wavelengths longer than 500nm and absorbs light in the violet and blue regions. When these two inks are mixed together, the resulting ink reflects only where both inks reflect appreciable amounts of light. The remaining area is in the middle of the spectrum, or green (which is what we expect).

Combining the three primary subtractive colors: cyan, magenta and yellow, one obtains a gamut of available colors. The absence of all of these colors leaves white, while the full presence of all three combines to make black. Other than dyes, other materials behave as subtractive colorants, such as inks, colored filters and photographic emulsions.

Color can also be produced via *additive color* mixing. Though it is rare in nature, additive color is essential in display monitors such as television and computer screens. The system involves light emitted directly from an illuminant (not

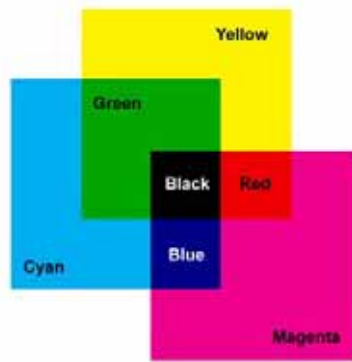


Figure 3.5: Subtractive color mixing of cyan, yellow and magenta primaries from pure white light. Adapted from [GM97].

reflected as in subtractive color). To create a given color, different combinations of the red, green and blue color primaries are added together. Given several colored lights described by RGB intensities $C_i = (R_i, G_i, B_i)$, illuminating the same white surface, the resulting color will be

$$C = \sum_i C_i$$

The light intensities are simply added together. For instance, red light $(1,0,0)$ and green light $(0,1,0)$ form yellow light $(1,1,0)$, as seen in Figure 3.6. Full intensity of all three primaries forms white light $(1,1,1)$, while the complete absence of light is black $(0,0,0)$.

Additive color can be executed by superimposing each illuminant (the equivalent of perfectly aligning the images from three differently colored projectors). However, current display technology borrows concepts from nineteenth-century impressionist painters, such as Georges Seurat and Paul Signac. The two were profoundly influenced by the French chemist Michel Chevreul and his ideas of simultaneous contrast and optical color mixing. The artists developed the style of *pointillism*, where only pure hues of the artist’s palette are used, but the brush marks are applied in dots that were close enough together to be blended by the

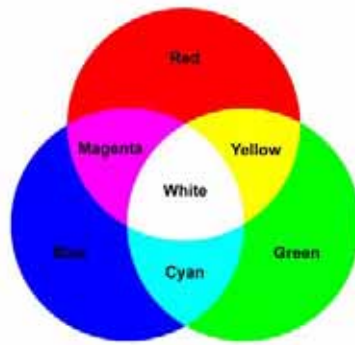


Figure 3.6: Additive color mixing of equal intensities of red, green and blue primaries. Adapted from [GM97].

viewer's eye. Similarly, digital displays contain millions of tiny red, green and blue dots, or *pixels*, on a screen, each of which can be displayed with varying intensities. The eye fuses the colored dots and thus perceives an entire gamut of colors.



Figure 3.7: Left: Georges Seurat, *La Grande Jatte*. Pointillism as the precursor to additive color mixing in digital displays. Middle: detail showing the visual texture resulting from the layering of small brush strokes of paint. Right: pictomicrograph of the paint surface showing the layering of brush marks of color. From a distance, these marks mix optically to form a unique color area [Seu86].

3.1.2 Light Spectra

Previously, it has been show that daylight is a composite light. In fact, the distribution of sunlight's energy over the electromagnetic spectrum consists of relatively

equal amounts at all visible wavelengths, as seen in Figure 3.8. Contrast this with the distribution of energy from a fluorescent light bulb, where there are relatively large peaks in the lower and central wavelengths (blue and green, respectively). This is why photographs taken inside under fluorescent light often have the characteristic of being slightly more greenish-blue than pictures taken in natural lighting.

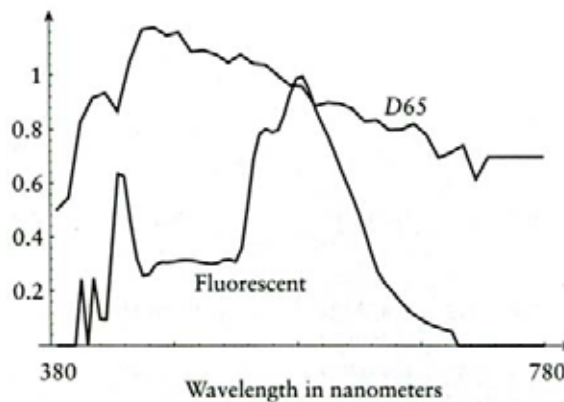


Figure 3.8: Intensity of the D_{65} illuminant (typical average daylight) and fluorescent light over the visible spectrum. Adapted from [G95b].

In order to quantify the physical energy of the spectral distributions of emissive light sources, one must integrate the illuminant's energy over all wavelengths. In discrete math, the energy reaching the eye at all wavelengths from emitted light, $P = \sum_{\lambda} E(\lambda)$, where $E(\lambda)$ is the emitted light energy at each wavelength.

Light does not only reach the eye via emitted light, but also from reflections. The perception of light reflected from the surface is dependent on both the reflectance properties of the material and the given light source. Therefore, changes in lighting will affect the perceived appearance of an object. Artists attempt to work under similar lighting conditions to that of the environment where the art will be exhibited, save encountering problems in hue shifting.

Physically, the energy reaching the eye at all wavelengths from reflected light, $P = \sum_{\lambda} E(\lambda)R(\lambda)$, where $R(\lambda)$ is the reflected light energy at each wavelength.

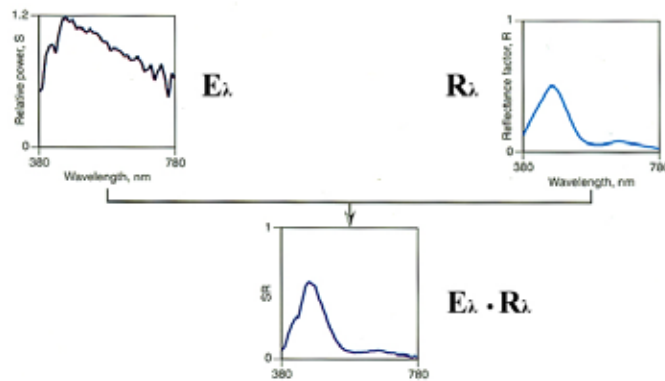


Figure 3.9: The physical amount of energy from a surface is dependent of the emitted light source E and the reflectance R of the material. Adapted from [Ber00].

Figure 3.9 illustrates the spectra of a reflected light stimulus—resulting from the combination of an emitted light and a material’s reflectance.

Similarly, to quantify a material’s transmitted light energy over all wavelengths, $P = \sum_\lambda E(\lambda)T(\lambda)$, where $T(\lambda)$ is the transmitted light energy at each wavelength.

3.1.3 Human Visual System

In understanding the human visual system, many compare the human eye to a traditional camera. Both are optical devices designed to record visual images onto light-sensitive material (film, in the case of a camera; photoreceptors, in the case of our eyes). Both have controls for adjusting the amount of light that enters the device, whether they are mechanical or biological. However, eyes are much more powerful than just recording static data to film. They continuously recode information and transmit signals to the brain for interpretation and reaction.

When looking at another individual’s eyes, one only sees a small portion of the outer surface (approximately one-sixth). The human eye is approximately 24 millimeters, or slightly smaller than a ping pong ball [SB02]. Most of the eye is

protectively tucked away in the eye socket. The basic layout of the eye is three concentric layers, two fluid-filled interior chambers, and the devices for capturing light at the front of the eye. The outer two layers protect and nourish the eyeball (*fibrous* and *vascular tunics*, respectively), while the *retina* (the innermost layer) initiates the neural messages bound for the brain. What we see as the white portion of one's eyes is the *sclera*, which is part of the outermost, fibrous coat. It's tightly packed fibers give the sclera its toughness, protecting and holding the pressure-filled shape together. At the very front of the eye, the outer coat loses its coloring and becomes transparent. The surface bulges into a slight hemisphere, and is called the *cornea*. The cornea's transparency is critical for vision, as light must enter the eye unimpeded. This is possible because the cornea has a very orderly arrangement of fiber and no internal blood supply of its own. Thus, it must draw nourishment from the clear fluid in the *anterior chamber*. The cornea is very sensitive to touch and any foreign bodies coming into contact produces a number of protective mechanisms (including tears and lid-closure) to maintain its transparency.

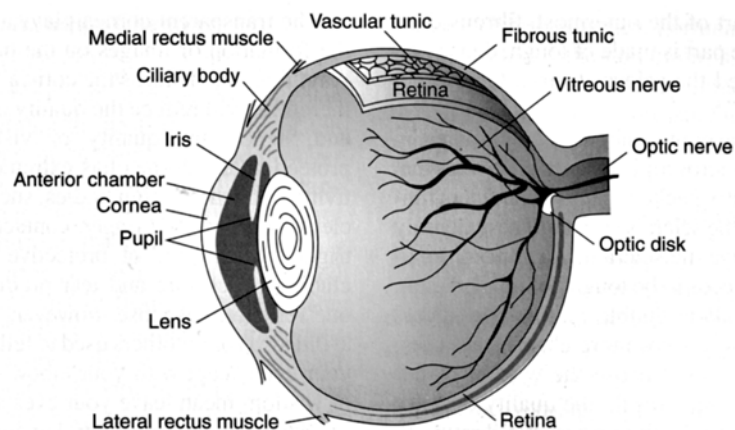


Figure 3.10: Cross section of the human eye, showing major layers and structures. View is from above the left eye. Adapted from [SB02].

The vascular tunic lies on the wall of the eyeball for the rear two thirds, consisting of a heavily pigmented, spongy structure called the *choroid*. It contains a vast network of blood vessels and capillaries that provide oxygen and nourish a very important class of cells in the retina, the *photoreceptors*, that turn light into neural signals. The choroid's dark pigmentation also helps absorb light not captured by the photoreceptors, save stray light from diminishing the quality of the image that reaches the eye. Incidentally, this is the same reason the inside of a camera is painted flat black—the paint absorbs scattered light and protects the sharpness of images on the film. Toward the front of the eye, this middle, choroidal layer breaks away from the outer layer and runs roughly parallel to the front of the eye. This section of the middle layer forms a slender spongy structure called the *ciliary body* which produces *aqueous humor*, the watery fluid that fills the cavities in the eye. This fluid performs important maintenance to the eye, including supplying oxygen and nutrients to the cornea and lens and carrying waste away. The fluid also maintains the constant pressure in the eye. If there is too little fluid, the eye becomes deformed and light does not focus correctly on the back of the eye. If there is too much pressure for too long, vision can be impaired permanently—the condition called *glaucoma*.

As it curls inward, the ciliary body gives way to the *iris*, that circular tissue that gives your eye its characteristic color. The iris actually contains two layers, an outer layer containing pigment and an inner layer containing blood vessels. If the outer layer is heavily pigmented, the iris appears brown. If it is lightly pigmented, the inner layer is partially visible through the outer one and the iris takes on a lighter color. The *pupil*, or black region in the eye is not an object, but actually a gap within two sets of muscles in the iris. The inner set runs in a circle around

the iris. When this band of muscles contracts, the pupil gets smaller. The second set of muscles run radially from the edge of the first set of muscles. When this set contracts, the eye dilates and the gap widens. These muscles determine the amount of light that reaches the back of the eye.

The size of the pupil is dependent on the availability of light in the surroundings. The size of the pupil is inversely proportional to the amount of available light. Hence, your pupil opens more in low-light situations. In young adults, the pupil's diameter varies over a range of 4:1, which fluctuates the amount of light from 16:1 [SB02]. To understand why large pupils are not always used, we once again turn to photography. The *aperture*, or opening, of a camera restricts the diameter of the cone of light which reaches the film. A device called the *diaphragm* controls the opening and can be modified in a similar manner to the iris. Reducing the aperture size increases the *depth of field*, or the range of objects in focus in an image. While sharp images are desirable, they require small apertures, resulting in the need for much more light.

A very important optical element in the eye is the *crystalline lens*, which resides right behind the iris. The covering of the lens is an elastic capsule, which varies the optical power of the lens by molding the shape. By shifting one's focus between near and far objects, you are consciously adjusting the shape of the lens. This fine tuning of the focus of image on the back of the eye is known as *accommodation*. A condition of the hardening of the fibers in the lens is called *sclerosis*, which diminishes one's ability to accommodate objects of varying distances. Similar to the cornea, the lens is also susceptible to transparency issues. Reduced transparency in the lens is called a *cataract*.

The innermost of the eye's three layers, the *retina*, is where light from the

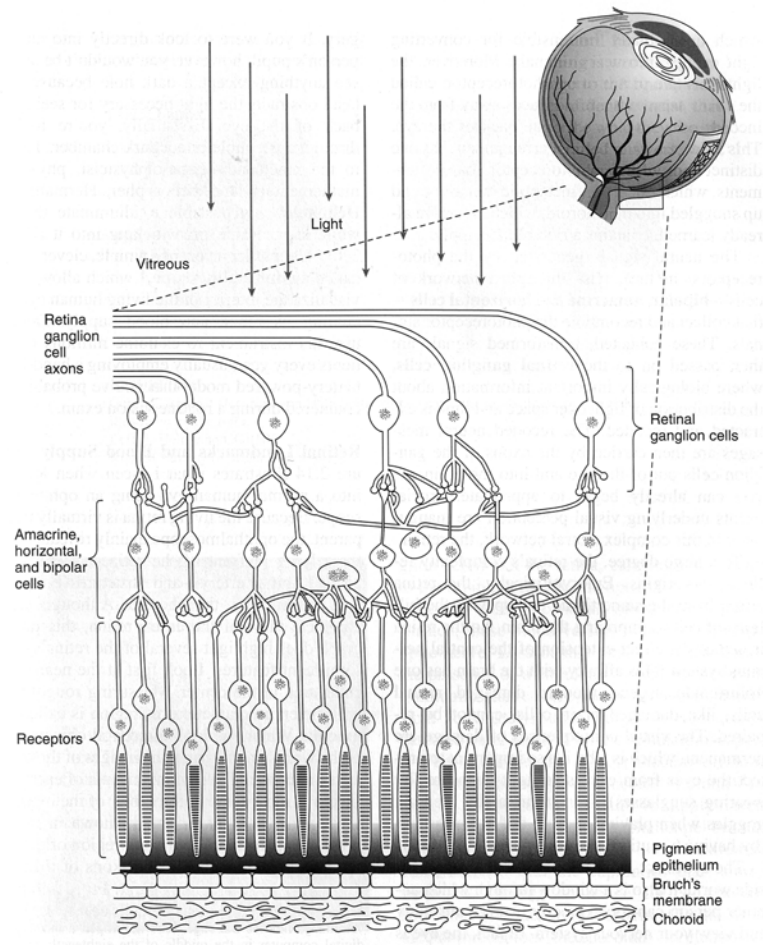


Figure 3.11: Cross section of the retina. The small box in the inset at the base of the eyeball shows the region of the eye represented in the enlarged drawing. Adapted from [SB02].

world is received. It is very thin but has a complex, layered organization as seen in Figure 3.11. The *photoreceptors*, which are actually responsible for converting light energy into neural signals, unusually face away from the incoming light. This is due to the high metabolic demands of the receptors, which are implanted in the nutrient-rich choroidal layer. The neural signals are passed through a complex network of cells that collect and recombine the signals, before reaching the retinal *ganglion cells*. Here, important information about the distribution of light over space and time is extracted and encoded. Individual light measurements are transformed into visually important information about the contrast, color, edges, and textures. The compression is done very efficiently, as the human eye contains an estimated 1.25 million retinal ganglion cells, compared to roughly 100 million receptors in the eye [SB02]. The recoded neural messages are then carried by axons via the optic nerve to the lateral geniculate nucleus and the visual cortex in the brain for further processing.

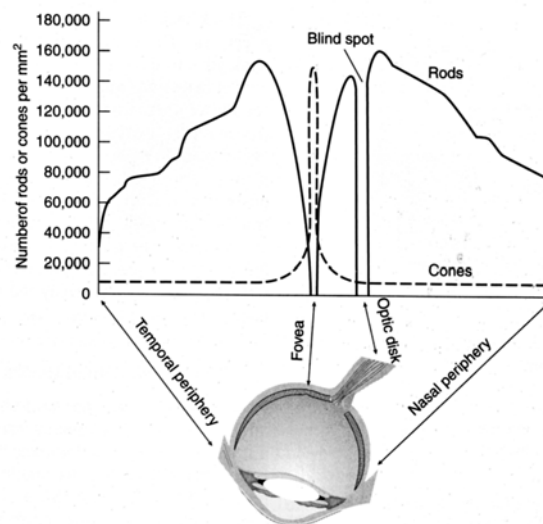


Figure 3.12: Distribution of rods and cones over the extent of the retina of the right eye, as seen from above. Note the complete absence of rods within the fovea, where cones abound. Adapted from [SB02].

Not all areas have the same sensitivity and resolution to light. As light passes through the retina, some of it is absorbed or scattered before it reaches the photoreceptors. In the central portion of the retina, the *fovea*, some of the overlying structures are pushed to the margins. This allows more light to reach this area unimpeded, resulting in a much higher spatial resolution than in the periphery of the eye.

In addition, the human eye contains two classes of photoreceptors: *rods* and *cones*, their names derived from their respective shapes. Rods and cones are not uniformly distributed throughout the fovea, as seen in Figure 3.12. Cones predominate in central vision, while rods are abundant in the periphery. In the very center, not only do only cones dominate, but they are even thinner and more heavily packed than they are elsewhere. Notice the interruption of the plot in the figure where there is a complete absence of receptors. Technically, this “blind spot” is the *optic disk*, where the nerve cells of the eye form the optic nerve carrying the visual information to the brain. Surprisingly, we almost never notice the large gap that the optic disks create on our retinas.

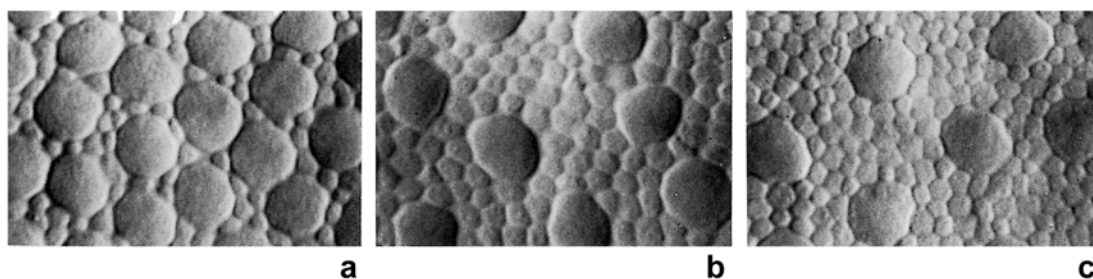


Figure 3.13: Pictomicrographs of the nasal side of the human retina at different distances from the center. The large cells are cones and the small ones are rods. The photos are each about $44\mu\text{m}$ in width. (a) 1.35 mm from the center of the retina. (b) 5mm from the center of the retina. (c) 8mm from the center of the retina. Adapted from [G95a].

Since the density of the 100 million photoreceptors varies spatially on the retina,

the optical image we receive is not sampled uniformly by the photoreceptors. By analogy, it would be as if the light-sensitive silver nitrate crystals on film were unevenly spread across the surface. This importance sampling would result in sharp areas where there is a lot of data, as well as blurred areas where there is less data (since it must be interpolated). In addition to the reduced network of structures in the fovea, the increased density of receptors permits very high acuity in the fovea. One notices how visual resolution diminishes drastically as one attempts to read fine text from the eye's periphery.

3.1.4 Color Perception

Color provides a unique source of information for picking out an object from its background. In Figure 3.14, notice the green patch on red sleeve of the girl's sweater in the picture on the left. The patch literally disappears in the achromatic version of the picture. This is due to the intensity of light reflected from the patch on the shoulder being essentially identical to the intensity elsewhere on the sleeve. The patch is said to be *isoluminant* with its background. Without color vision, the patch goes undetected.



Figure 3.14: Color and black & white photographs of a girl with a green patch on a red sleeve demonstrating isoluminance. Adapted from [SB02].

Besides aiding our ability to detect the presence of objects, color also helps

identify and distinguish between various objects in the environment. Subtle shades of red determine whether an apple or tomato is ripe to eat. Farmers use color to identify infertile soil and to determine when their crops are ready for harvest. Doctors routinely rely on color to make diagnoses: blood that is pale red indicates anemia, and yellowish skin suggests a possible skin disorder [SB02].

Light registers its presence on the retina by interacting with special light-sensitive molecules contained within the photoreceptors. However, not all wavelengths of light are equally effective in producing a response. Rods give their biggest response when stimulated with approximately 500nm, which under daylight conditions appears bluish-green, as illustrated in Figure 3.15. The spectral sensitivity of cones is more complicated, as there are three distinct classes of cones. One class is responsive to short wavelengths of light, maximally responsive to light of about 440nm. Another class responds to medium wavelengths of light, centered around approximately 530nm. The third type of cone responds best to long wavelengths of light, with a peak response at 560nm. For reference, under daylight conditions, short, medium and long wavelength-sensitive cones respond best to violet, green, and yellow, respectively. In actuality, there is a lot of overlap in the spectral sensitivities of the three types of cones. Also of note, the curves in Figure 3.15 separate electromagnetic radiation that we can and cannot see, since photoreceptors only respond to certain wavelengths of light.

Through his experiments, Grassman discovered [Gra53] the trichromatic nature of our vision—almost the entire range of perceivable colors can be completely described using just three light sources, instead of the entire visible range in the electromagnetic spectrum (380-700nm). A tristimulus color space can be defined, for instance, by a triplet of numbers that represent the intensities of three colored

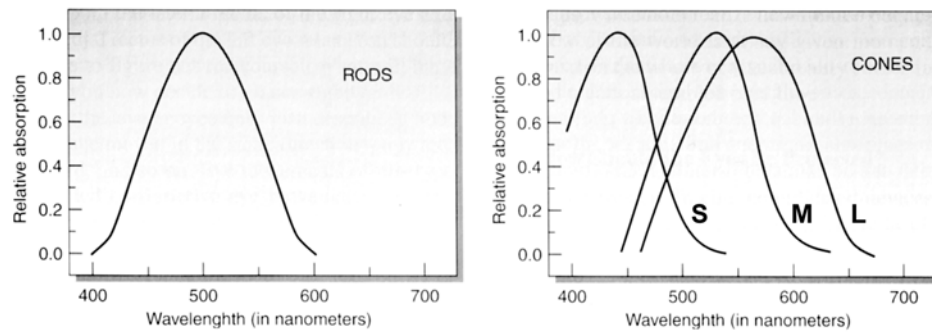


Figure 3.15: These graphs show how the amount of light by photoreceptors varies with the wavelength of the light. Adapted from [SB02].

lights. Let \hat{r} , \hat{g} , and \hat{b} , be the spectral energy curves associated with the three lights. These lights can be of any color (red, green, and blue, for example), as long as they are perceived differently to the viewer and are not combinations of each other. Hence, each light will excite the short S , medium M , and long L wavelength-sensitive cones to differing degrees.

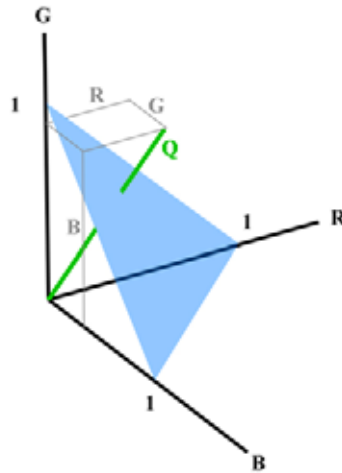


Figure 3.16: RGB color space. Q is the color vector, and its RGB components of Q are in gray. The blue triangle illustrates the unit plane.

Given these lights, we can create new colored spectra by combining them in varying intensities. Since emitted lights are an additive color system, the final spectrum of the new color will be $R\hat{r} + G\hat{g} + B\hat{b}$, where R , G , and B are scalars

that range between zero and full intensity. By varying the amount of each of the three light sources, many colors can be reproduced. Zero intensity for all three values yields black, while equal full intensity (usually one) results in white. Figure 3.16 illustrates the RGB color space, where each light source is a basis vector. The color in question can be described as a vector, whose magnitude defines the intensity of the color. Feasible colors in the range of this space are defined as $\hat{Q} \mid 0 \leq \{R, G, B\} \leq 1$. Colors outside of this range can not be matched by the three light sources.

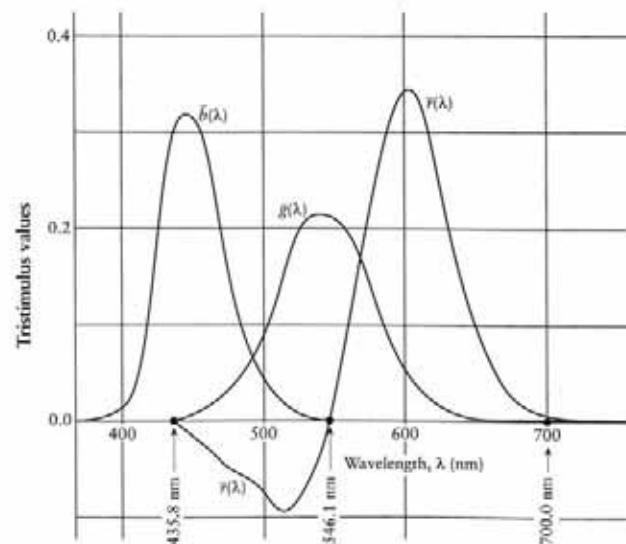


Figure 3.17: RGB Color Matching Functions. The negative portion of $\bar{r}(\lambda)$ describes the area of the visible spectrum which the three primaries are unable to match. Adapted from [G95a].

A natural question to ask is, given a particular test color, what values of R , G , and B are required to generate the same response from a viewer? This is known as the color-matching problem. If one proceeds with this experiment using each wavelength in the visible spectrum as the test color, a set of color matching functions can be obtained. Since everyone's response is slightly different, the procedure

is repeated many times for different subjects and averaged, resulting in a set of *standard observer* color matching curves for the particular set of color primaries (Figure 3.17). Given standard matching functions $\bar{r}(\lambda)$, $\bar{g}(\lambda)$, $\bar{b}(\lambda)$, which describe how much light is required to match a particular reference stimulus $P(\lambda)$, we can compute R , G , and B :

$$\begin{aligned} R &= \int_0^\infty P(\lambda)\bar{r}(\lambda)d\lambda \\ G &= \int_0^\infty P(\lambda)\bar{g}(\lambda)d\lambda \\ B &= \int_0^\infty P(\lambda)\bar{b}(\lambda)d\lambda \end{aligned} \tag{3.1}$$

Unfortunately, when using combinations of only three light sources there are always colors that cannot be reproduced exactly. This situation might occur, for instance, when trying to match an intense yellow light using red, green and blue primaries. Remember in additive color, full intensities of green and red will yield yellow. However, if the yellow test lamp is too vivid, full intensity green and red will not be able to match it exactly. In this case, if enough blue is added to the yellow test lamp to desaturate it, the red and green lights can match it. Mathematically speaking, we used a negative amount of blue light to match the vivid yellow test lamp: $Y - B\hat{b} = R\hat{r} + G\hat{g}$. While this limits the system, digital displays are not necessarily compromised in this situation, as there are a number of ways to gracefully display a plausible suitable color instead. However, these out of gamut colors do create inconveniences in performing color calculations.

To eliminate the inconveniences associated with negative values in tristimulus color spaces, the CIE (Comission Internationale de l'Éclairage) in 1931 defined a set of tristimulus color primaries X , Y , and Z which encompass all of the visible

spectrum. This insures that the respective color matching functions $\bar{x}(\lambda)$, $\bar{y}(\lambda)$, and $\bar{z}(\lambda)$ are all non-negative. The drawback of having a system in which all visible colors can be represented is that the primaries are virtual and no longer correspond to physical colors. The color coordinates of a stimulus $P(\lambda)$ in XYZ color space (also known as $CIEXYZ$) are:

$$\begin{aligned} X &= \int_0^\infty P(\lambda)\bar{x}(\lambda)d(\lambda) \\ Y &= \int_0^\infty P(\lambda)\bar{y}(\lambda)d(\lambda) \\ Z &= \int_0^\infty P(\lambda)\bar{z}(\lambda)d(\lambda) \end{aligned} \tag{3.2}$$

where X , Y , and Z are the tristimulus values; \bar{x} , \bar{y} , and \bar{z} are the color-matching functions of the 2^o Observer; and k is a normalizing factor. By convention, the scalar factor k generally is determined such that $Y = 100$ when the object is a perfect white:

$$k = \frac{100}{\int_0^\infty E(\lambda)\bar{y}(\lambda)d(\lambda)}$$

where $E(\lambda)$ is the spectrum of the white light illuminating the scene.

If, the stimulus is that of reflected light $R(\lambda)$, the equation substitutes $P(\lambda) = E(\lambda)R(\lambda)$. The CIE chose the \bar{y} color matching function to be identical to the human luminance efficiency function, which mean that Y encodes the luminance of a color. The scale factor, k , is defined such that for an ideal diffuse reflector (the brightest white), Y will have a value of exactly 100. While the range 0-100 is convenient for humans, computer programs scale XYZ to lie on the range $[0,1]$.

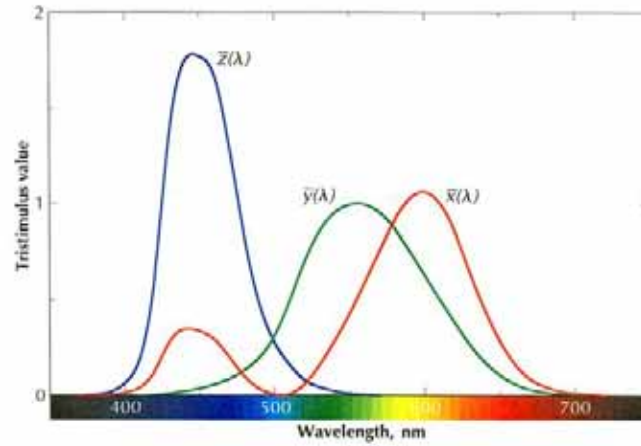


Figure 3.18: XYZ Color Matching Functions. Notice that all of the spectra are positive, therefore the three primaries can match any visible color. Adapted from [GM97].

A natural way to discretize Equation 3.2 is to define a discrete sequence of wavelengths, $\lambda_i = \lambda_0 + i\Delta\lambda$ for $0 \leq i \leq n - 1$. A simple Riemann sum is used to approximate the integral:

$$\begin{aligned}
 X &= k \sum_{i=0}^{n-1} P(\lambda_i) \bar{x}(\lambda_i) \\
 Y &= k \sum_{i=0}^{n-1} P(\lambda_i) \bar{y}(\lambda_i) \\
 Z &= k \sum_{i=0}^{n-1} P(\lambda_i) \bar{z}(\lambda_i)
 \end{aligned} \tag{3.3}$$

where

$$k = \frac{100}{\sum_{i=0}^{n-1} E(\lambda_i) \bar{y}(\lambda_i)}$$

Though the Riemann sum is the simplest method of discretizing integrals, there are other methods such as Simpson's rule or Gaussian quadrature. A graphical

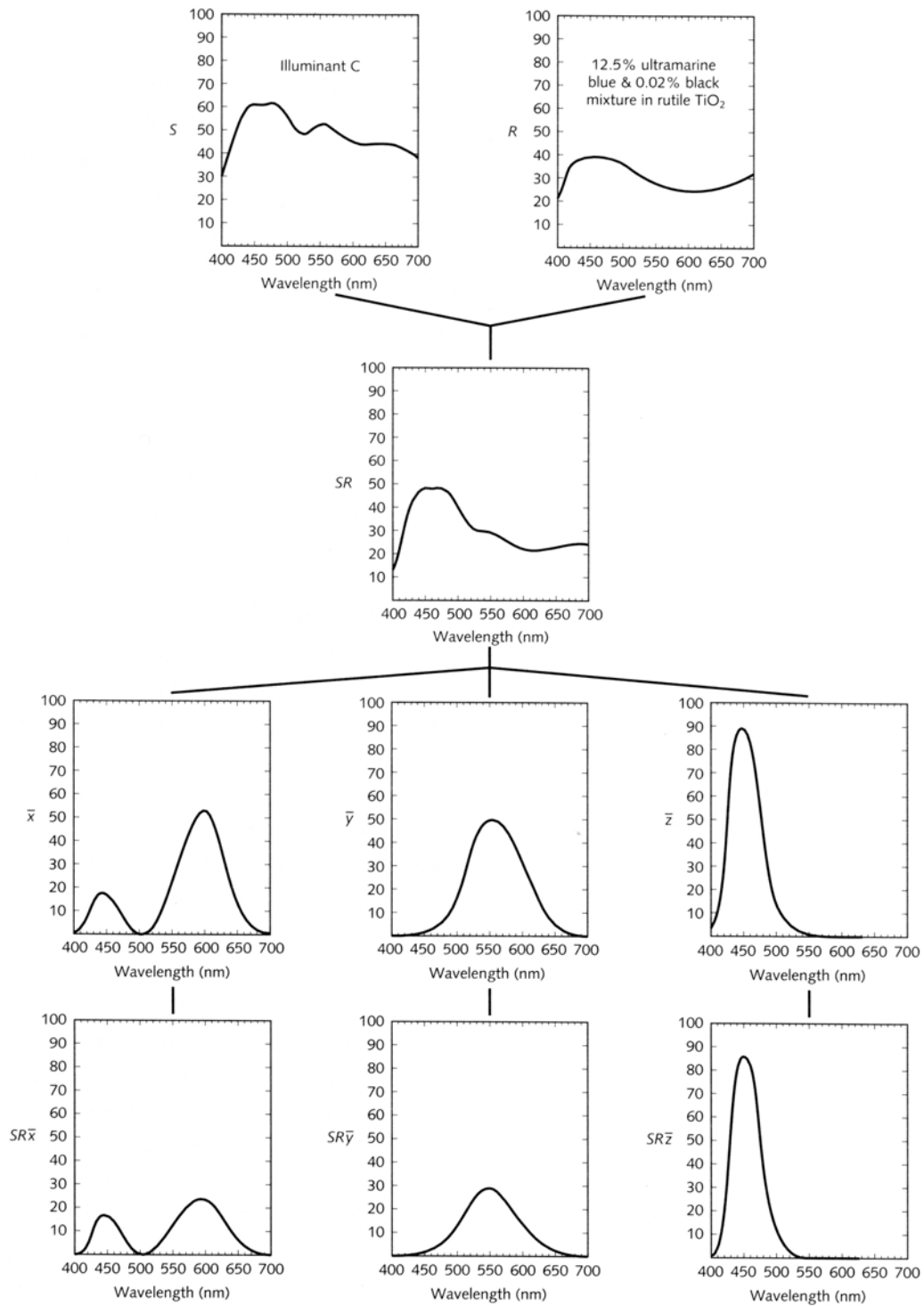


Figure 3.19: Graphical representation of the calculation of CIE Tristimulus values X , Y , and Z for a stimulus. Adapted from [JF01].

representation of converting a reflected light stimulus to XYZ primaries via color matching functions is seen in Figure 3.19.

It is important to note that spectral reflectances contain more information than do the tristimulus values. Then, it is possible for two materials with reflectances $R_1(\lambda) \neq R_2(\lambda)$ to have the same color (have identical XYZ values) under light source $H_1(\lambda)$. However, these two materials will not match under a different light source $H_2(\lambda)$. Two materials that look identical under one lighting condition, but not another are known as *metamers*. An example of metameric stimuli are illustrated in Figure 3.20.

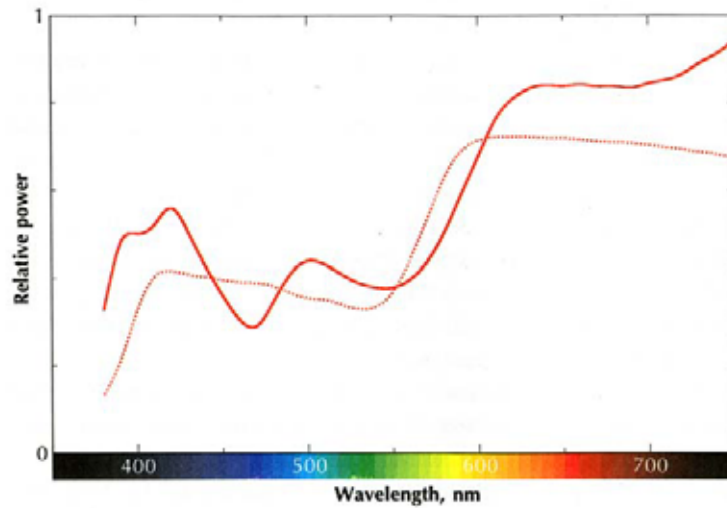


Figure 3.20: An example pair of metameric stimuli. The two stimuli produce equivalent stimulations of the eye’s photoreceptors when viewed under identical lighting conditions, but they have different spectral distributions. Adapted from [GM97].

Another important tool for color analysis is the *Chromaticity Diagram*. Chromaticity coordinates provide hue and saturation information independent of luminance. The XYZ chromaticities are given by:

$$\begin{aligned}
x &= \frac{X}{(X + Y + Z)} \\
y &= \frac{Y}{(X + Y + Z)} \\
z &= \frac{Z}{(X + Y + Z)}
\end{aligned} \tag{3.4}$$

Since by definition, $x + y + z = 1$, there are actually only two independent variables necessary to specify the color. The chromaticity diagram represents this by plotting the first two coordinates (x, y) . By plotting the chromaticities of spectral delta functions $\delta(\lambda_0 - \lambda)$ for $380\text{nm} < \lambda_0 < 700\text{nm}$, one obtains the horseshoe-shaped spectral locus shown in Figure 3.21. The spectral locus contains the purest, most saturated colors possible (the numbers along the outside of the locus correspond to pure wavelengths of color), while the interior contains less saturated colors. Points exterior to the locus are not visible to the human eye.

Given two tristimulus color spaces defined in terms of color matching functions, one set of color primaries can be matched by the other set:

$$\begin{aligned}
R' &= a_{11}R + a_{12}G + a_{13}B \\
G' &= a_{21}R + a_{22}G + a_{23}B \\
B' &= a_{31}R + a_{32}G + a_{33}B
\end{aligned} \tag{3.5}$$

Hence, there exists a simple 3x3 transformation matrix that will convert between the two spaces. For instance, there is a matrix that will convert from XYZ to RGB coordinates. This transformation is necessary to display XYZ colors on a monitor (remember that XYZ are imaginary light sources). Given the chromaticity coordinates of an RGB system $(x_r, y_r), (x_g, y_g), (x_b, y_b)$, and its reference white (w_x, w_y) , the conversion matrix M can be computed. To convert any XYZ

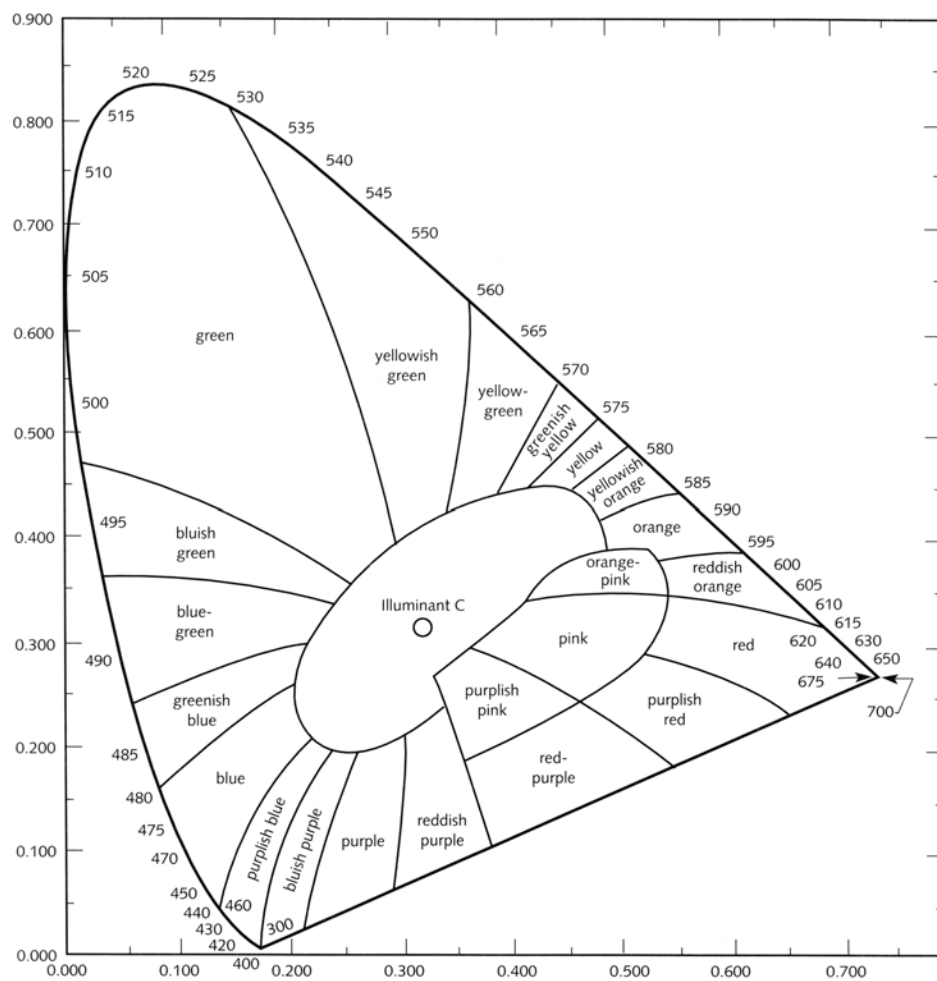


Figure 3.21: Hue names associated with the CIE Chromaticity Diagram.
Adapted from [JF01].

color into the appropriate *RGB* color or vice versa, post multiply by the conversion matrix M or its inverse:

$$[RGB] = [XYZ][M] \quad (3.6)$$

$$[XYZ] = [RGB][M]^{-1} \quad (3.7)$$

However, the resulting *RGB* color from the transformation may be invalid if the color is not within the gamut of colors supported by the *RGB* primaries. There are two types of out-of-gamut colors: those that have a chromaticity that cannot be matched by the primaries and those that experience luminance overflow. The first set of colors, when mapped to a set of primary phosphors, gives *RGB* values of less than zero. The second set, yields *RGB* values greater than one, as the magnitude of the color in one or more channels may greater than the maximum luminance of the display.

The problem of displaying such out-of-gamut colors is an important issue for painting, since many commonly used real-world pigments fall outside the gamut of existing color monitors.

Most gamut-matching methods seem to fall into two general categories: *global* and *local* approaches. A local approach examines each pixel, or color, in an image individually and adjusts only those that are out of gamut. A global approach applies information gathered from the entire image when considering how to modify every pixel in the image, even those within the gamut.

Figure 3.22 describes an example of a visible color Q which is unable to be realized by the *RGB* primaries. The chromaticity diagram makes it immediately clear why mixtures of three visible light sources can never reproduce all visible colors. It is geometrically impossible for a triangle *inscribed* within the spectral locus to simultaneously *circumscribe* it. In this case, we have: $Q - R\hat{r} = G\hat{g} + B\hat{b}$.

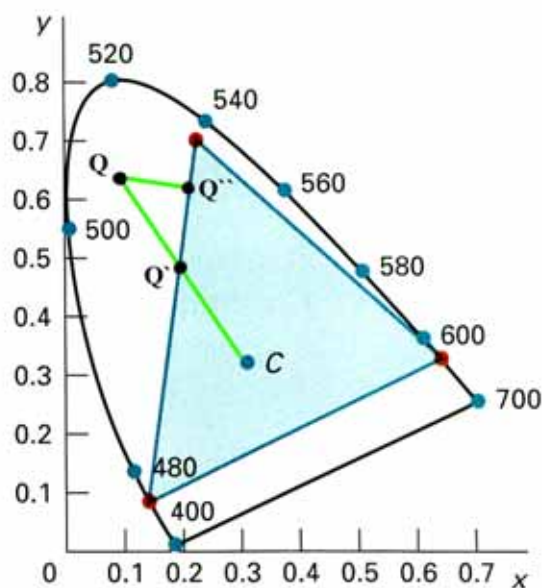


Figure 3.22: To display out of gamut color Q in RGB space, one can clip to the nearest neighbor in the gamut Q'' or decrease the saturation until the gamut is reached Q' .

A simple local method would to clamp values in the range $[0, 1]$. One could do this by locating the nearest neighbor that is reproducible via orthogonal projection and display that value Q'' . Here, the hue has been changed considerably. An alternative would to decrease the saturation of the original color until it could be reproduced via the primaries. In our figure, this is the equivalent of finding the intersection Q' of the line made by Q and the white point C with the edge of the gamut. This method maintains the hue, but at the cost of reduced luminance. Either case transforms Q to a color which can be represented. Yet, simple methods such as these generally perform poorly, as they create noticeable discontinuities in smooth regions of color.

In contrast, global gamut matching techniques consider all of the colors in an image when making color changes. Such methods maintain the relative relationships between colors. One global method finds the smallest a and largest b color

components in the image (the smallest and largest RGB values) and displays each pixel i as:

$$\left(\frac{R_i - a}{b - a}, \frac{G_i - a}{b - a}, \frac{B_i - a}{b - a} \right) \quad (3.8)$$

This compresses the input range such that the image now spans the gamut of the color primaries. Essentially, the largest color component is scaled to the maximum intensity and the smallest component to zero intensity. All other components are scaled to fit in the new range. If the largest color component is much greater than the maximum displayable intensity, the procedure in Equation 3.8 will drastically decrease the intensity of the entire image (since all colors are scaled by the largest component). In global gamut mapping techniques, all of the colors in an image are affected. The end result can be quite perceptually different from the original image, and the process is much more computationally expensive than local techniques.

A problem with these methods arises with painting (and other subtractive mixing systems), as the CIE chromaticity diagram is based on additive mixtures. Varying the concentrations of two additive colorants will yield colors with chromaticity coordinates connected via a straight line. Different amounts of red (1,0,0) and white (1,1,1) make various pinks $C = (1, \alpha, \alpha) | \alpha \in (0, 1)$.

However, pigmented mixtures (and other subtractive colorants) do not typically yield straight lines on the chromaticity diagram. Figure 3.23 illustrates this behavior as the chromaticities of paint mixtures of colored pigments and white are plotted. While some paths are close to being straight lines on the chromaticity diagram, others exhibit loops and turns as individual pigments are mixed with varied ratios of white pigment.

The reasons why some lines loop while others approach straight lines are be-

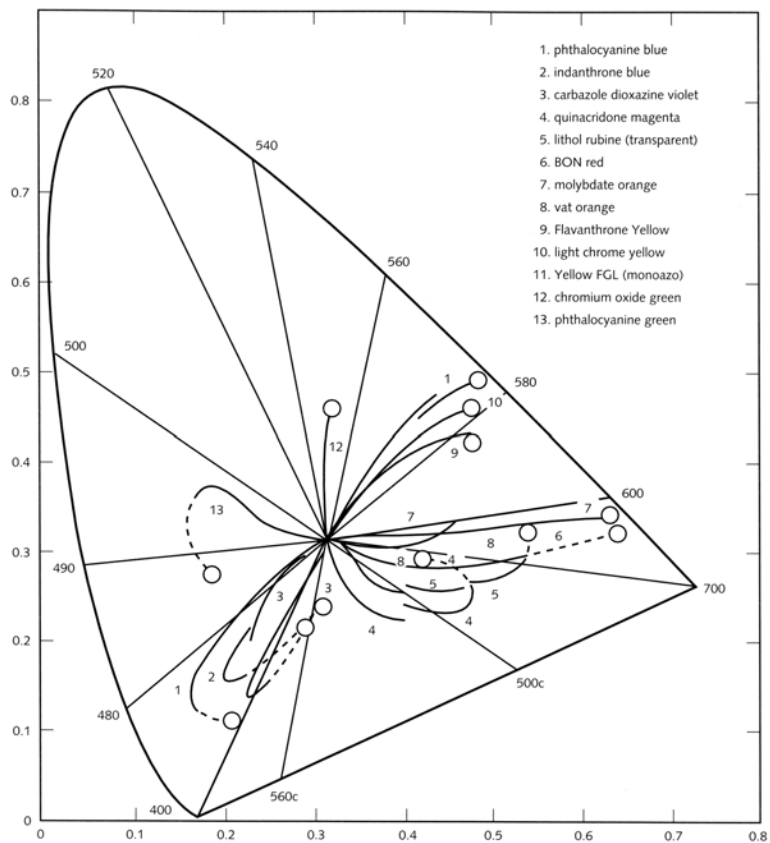


Figure 3.23: Loci of the chromaticity coordinates of common pigments mixed with varying amounts of white (rutile TiO_2). Discontinuities are due to changes in pigments volume concentration and dotted segments are interpolated. Adapted from [JF01]

haviors of subtractive mixing and its dependence on the absorption and scattering characteristics of the pigments used in the mixture. This cannot be captured by any linear transformation, illustrating why it is difficult to capture the behavior of real-world colorants on digital displays. Transformations such as complete gamut scaling and linear projection will result in undesired hue and saturation shifts with subtractive colorants.

3.1.5 Color Spaces

The XYZ color space is not a very intuitive space. While Y was designed to represent the brightness of a color, it is difficult to interpret the meaning of the values of X and Z . Many other abstract color spaces have been developed primarily as user interfaces to aide in color selection. Geometric solids represent the available colors in each space's gamut, as seen in Figure 3.24. The RGB color cube ((a) in the figure), is not much better than XYZ for color calculations. It is difficult to find any one color, and once located, it is difficult to adjust that color. Classic examples of both problems are to ask a viewer to find brown, and then once found, make a lighter shade of brown.

The next four color spaces are quite similar to each other. Each has a lightness axis that runs the vertical length of each solid. Each space also represents saturation by the distance from the vertical axis and hue via the angle around the axis. A simple conversion can be made to convert colors from RGB into any of the spaces.

The HSV (hue, saturation, value) hexicone is shown in Figure 3.24(b). The central axis carries the gray values from black at the bottom to white at the top. The six vertices that comprise the hexagon are the same as in the RGB cube:

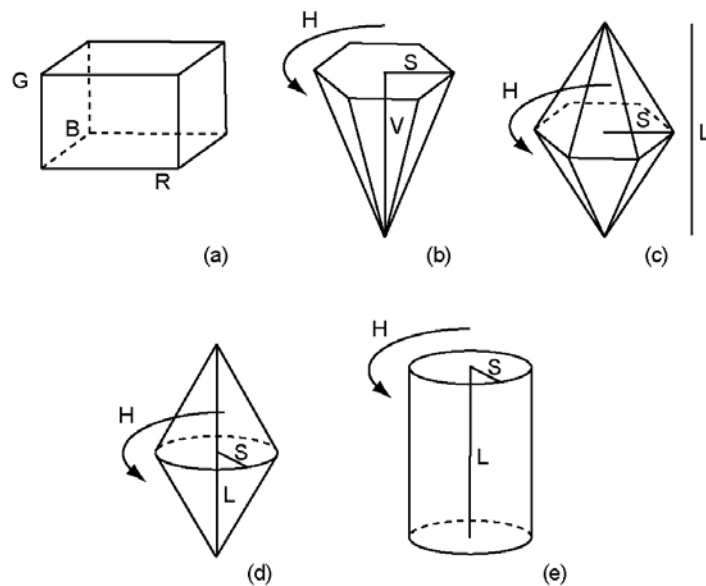


Figure 3.24: Several different color spaces.

red, green, blue and their combinations: yellow (from red and green), cyan (green and blue), magenta (blue and red). The *HSL* (hue, saturation, lightness) double hexicone is shown in Figure 3.24(c). Its difference from the previous space is that the level of maximum saturation is at $L = 0.5$, instead of $L = 1.0$. The *HSL* double cone (d) is similar to the *HSL* double hexicone, except the cross section is circular, rather than hexagonal. The *HSL* cylinder (e) is like the *HSL* cone (d), except that the complete radius is available at all points along the L axis.

While the previous color spaces provide an intuitive interpretation of the axes, an ideal color space would be perceptually linear. In such a color space, the perceptual difference between any two colors is represented by the distance between them. These spaces are useful when only a finite number of colors can be represented and wish to cover the entire gamut in the most effective way. To maximize the use of a space, we would like equal increments to result in color steps that were

of perceptually equal sizes. Unfortunately, this is not the case in XYZ space.

Figure 3.25 shows the nonlinearity of the Chromaticity diagram. In psychophysics, the smallest difference in a specified modality of sensory input that is detectable by a human being is known as a *just noticeable difference (jnd)*. The average user's jnd's are used to compare sets of colors in an attempt to distinguish the threshold of visual color differences. The region on a chromaticity diagram which contains all colors which are indistinguishable, to the average human eye, from the color at the center of the ellipse is known as a *MacAdam ellipse*.

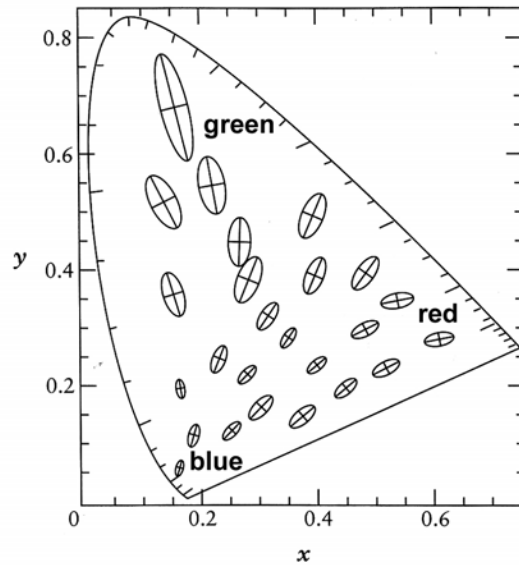


Figure 3.25: The MacAdam ellipses. Adapted from [G95a].

The important observation is that the MacAdam ellipses are not the same size nor in the same orientation. Thus, a particular magnitude of shift in color space may be undetectable at one point, but the same shift applied to a different color would be quite visible. For example, our acuity in distinguishing between nearby green colors is much poorer than in nearby reds, and poorer still than in the blue range of the XYZ chromaticity diagram.

The *Munsell color system*, a particular implementation of *HSV*, is based on these notions of color perception and is widely used in art as well as many other industries. This color space is defined by a physical collection of samples. Neighboring color swatches in the model are said to be perceptually equidistant from one another, based on averages of numerous studies involving jnd's. The system is a cylindrical coordinate system: a color wheel plus an irregular 2D grid around the core. The notation for a given color is specified as *HV/C* (hue, value/chroma). *Hue* is characterized by 100 equally spaced hues around the perimeter. *Value* varies along the vertical axis from black (0) to white (10). *Chroma*, increases from no saturation (0) on the center line outward to full saturation (10 to 18, depending on the hue).

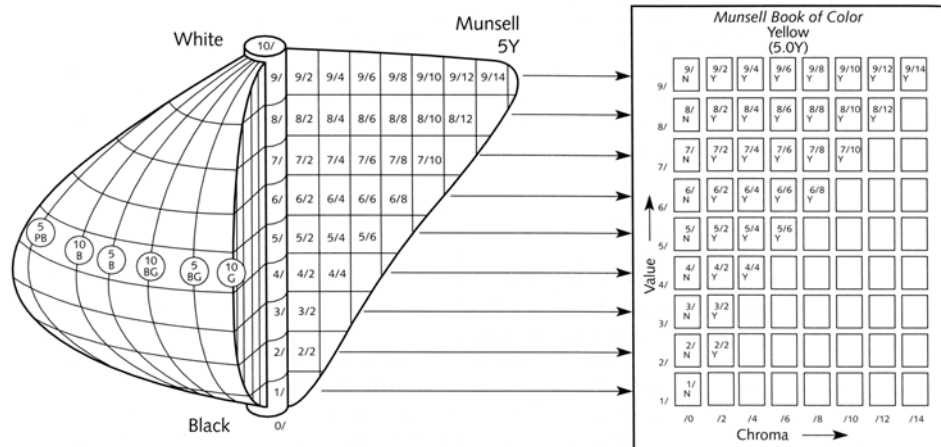


Figure 3.26: Cutaway of the Munsell color solid and the corresponding constant hue page, 5Y. Adapted from [JF01].

There are many reasons for the popularity and usefulness of the Munsell system. It is exemplified by real color chips in the *Munsell Book of Color* [Mun], which is a carefully controlled illustration of the system; it is an open-ended system in the chroma dimension so that new, vivid colorants and new sources of color can be accommodated; and has been defined in terms of the 1931 CIE illuminant *C*,

enabling one to transform between the two spaces.

Instead of physical collections of samples, a number of attempts have been made define a perceptually uniform color space mathematically. The most notable are the $L^*u^*v^*$ and $L^*a^*b^*$ color spaces, both nonlinear mathematical transformations from XYZ space. Each space is designed with respect to a reference white color (X_n, Y_n, Z_n) , usually one of the CIE standard illuminants, scaled such that $Y_n = 100$. Both spaces use the same definition of L^* :

$$L^* = \begin{cases} 116 \left(\frac{Y}{Y_n} \right)^{\frac{1}{3}} - 16 & , \frac{Y}{Y_n} \geq .008856 \\ 903.3 \left(\frac{Y}{Y_n} \right) & , \text{otherwise} \end{cases} \quad (3.9)$$

Note that $L^* = 100$ for the reference white when $Y = Y_n$. In fact, L^* may be used to consider the lightness of the color.

For the $L^*u^*v^*$ color space, the other components for the conversion between XYZ and $L^*u^*v^*$ are given by:

$$\begin{aligned} u^* &= 13L^*(u' - u'_n) \\ v^* &= 13L^*(v' - v'_n) \end{aligned} \quad (3.10)$$

where

$$\begin{aligned} u' &= \frac{4X}{X + 15Y + 3Z} \\ v' &= \frac{9Y}{X + 15Y + 3Z} \\ u'_n &= \frac{4X_n}{X + 15Y + 3Z} \\ v'_n &= \frac{9Y_n}{X + 15Y + 3Z} \end{aligned}$$

The $L^*a^*b^*$ space is another perceptually based color system that is frequently used. The value for L^* is the same as in Equation 3.9. The other variables are given by:

$$\begin{aligned} a^* &= 500L^* \left[f\left(\frac{X}{X_n}\right) - f\left(\frac{Y}{Y_n}\right) \right] \\ b^* &= 200L^* \left[f\left(\frac{Y}{Y_n}\right) - f\left(\frac{Z}{Z_n}\right) \right] \end{aligned} \quad (3.11)$$

where

$$f(r) = \begin{cases} r^{\frac{1}{3}} & , r \geq .008856 \\ 7.787r + \frac{16}{116} & , \text{otherwise} \end{cases}$$

Just as L^* corresponds to the luminance channel in the visual system, a^* corresponds to the red-green channel and b^* to the blue-yellow channel. This closely models how our visual system encodes data from the real world. The *Opponent color theory* [Her78] states that colors are detected by recording differences between cone responses. Processing is done in the cells that gather the information from the photoreceptors in the eye, accentuating the differences among the responses. The three opponement channels are: red versus green, yellow versus blue, and black versus white. Responses to one color in a channel inhibit the other and are mutually exclusive. This is why an object never appears *both* red and green.

The responses of the cones in the human visual system significantly overlap and must be analyzed in unison to reduce redundancy. The achromatic, or luminance, channel is the combination of the responses from the medium (M) and long (L) wavelength cones (M+L). The yellow-blue channel is the difference of the short (S) wavelength cone responses and the medium and long wavelength cone responses (S-(M+L)). The red-green channel is the difference between the medium and long wavelength cone responses (M-L). This processing results in a great decrease in

bandwidth as converted signals are sent to the lateral geniculate nucleus and visual cortex for further processing.

Figure 3.27 shows a plot of both the $L^*u^*v^*$ and $L^*a^*b^*$ color spaces. The solid in the center is the region occupied by the colors reflected by the CIE Illuminant D_{65} .

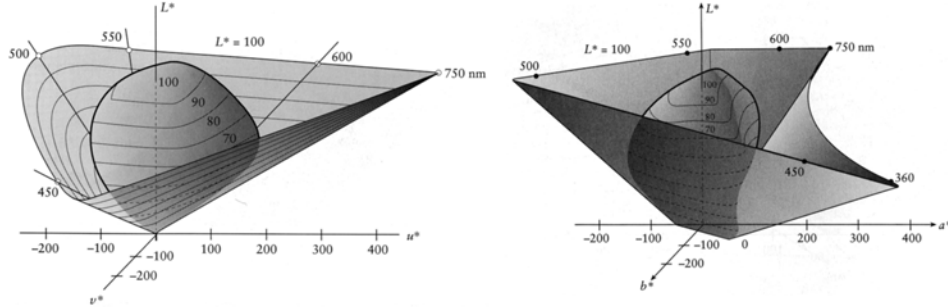


Figure 3.27: Nonlinear color spaces; left: $L^*u^*v^*$ and right: $L^*a^*b^*$. Adapted from [G95a].

By design, the Euclidean distance between any two colors, A and B, in either perceptual color space may be computed from the magnitude of the vector between the colors:

$$\begin{aligned}
 E_{uv}^* &= \sqrt{(L_A^* - L_B^*)^2 + (u_A^* - u_B^*)^2 + (v_A^* - v_B^*)^2} \\
 E_{ab}^* &= \sqrt{(L_A^* - L_B^*)^2 + (a_A^* - a_B^*)^2 + (b_A^* - b_B^*)^2}
 \end{aligned}
 \tag{3.12}$$

The important feature of these spaces is that two pairs of colors with the same distance metric between them are almost perceptually different by the same amount. While neither of the two spaces is perceptually completely uniform, they are close. Work continues on developing more uniform spaces.

3.1.6 Overall Response

One can easily quantify a light source's spectral intensity and the reflectivity of a material through careful measurements. Through experimentation, the average human's perceptual response for each type of photoreceptor can also be determined. Together, this should determine the overall response of a typical viewer for a given stimulus. However, this is not the case, as the human brain is very subjective and does not evaluate a color in isolation. The surrounding environment has a great deal of influence on a color.

Previously, the opponent nature of human vision was discussed. The human eye detects differences between neural impulses and magnifies them. This process takes place after the photoreceptors have elicited a response from the stimulus. Retinal ganglion cells collect neural impulses from photoreceptors and condenses them by approximately 80 times [SB02], preserving the important features of the original signals. Ganglion cells each have a *receptor field* on the retina, a patch within which a cell's activity may be influenced. Light outside of this region has no effect on the cell. The receptor field roughly takes the shape of two concentric circles. One region within the field responds to an increase in light, while the other responds to a decrease in light. We will refer to these regions as 'on' and 'off' responses, respectively.

Imagine the center of a receptor field has an on response, while the ring is an off response, as in Figure 3.28(a). If the cell undergoes uniform illumination, the cell only gives a weak response. This is because such a stimulus produces opposite effects in the center and surrounding area—the center is excited, while the ring inhibits the response. This interaction is called *lateral inhibition*, which is the antagonistic neural interaction between adjacent photoreceptors in the retina.

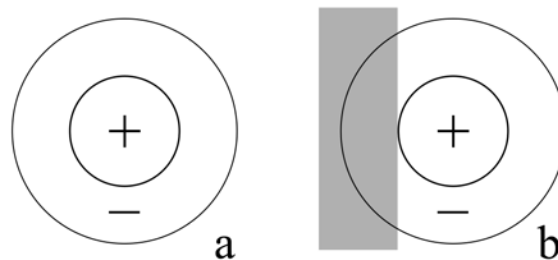


Figure 3.28: Retinal ganglion receptor fields exhibiting lateral inhibition. Receptor *a* has a completely uniform light response, while *b* is partially covered in shadow.

Given the same type receptor field, imagine that the uniform light is interrupted by a shadow that covers part of the outside ring, the edge of which lies tangent to the inner circle (as in Figure 3.28(b)). The inner region still receives the same amount of light, while a good portion of the outer ring receives a lower level of light, reducing the negative effect. The net result is a much stronger response from the cell than in the previous situation.

The antagonistic arrangement of center and surround allows the retinal ganglion cell to perform large amount of filtering. Lateral inhibition has allowed the cell to condense multiple neural responses into a single light/dark boundary detection. Some ganglion cells are arranged as presented here, and others have receptor fields reversed—the off response is in the center, while the ring has an on response. The actual response of the receptor field is actually a smooth function with negative lobes, as seen for an on-center ganglion cell in Figure 3.29.

The sizes also vary with retina location, as ganglion cells in the periphery can be up to 50 times their counterparts in the foveal region. This also supports the fact that we have higher spatial resolution in the fovea as the smaller foveal ganglion receptor fields collect and aggregate less signals and therefore have finer accuracy. In addition, there are different kinds of ganglion cells that have varying contrast

sensitivities, as well as spatial and temporal resolutions.

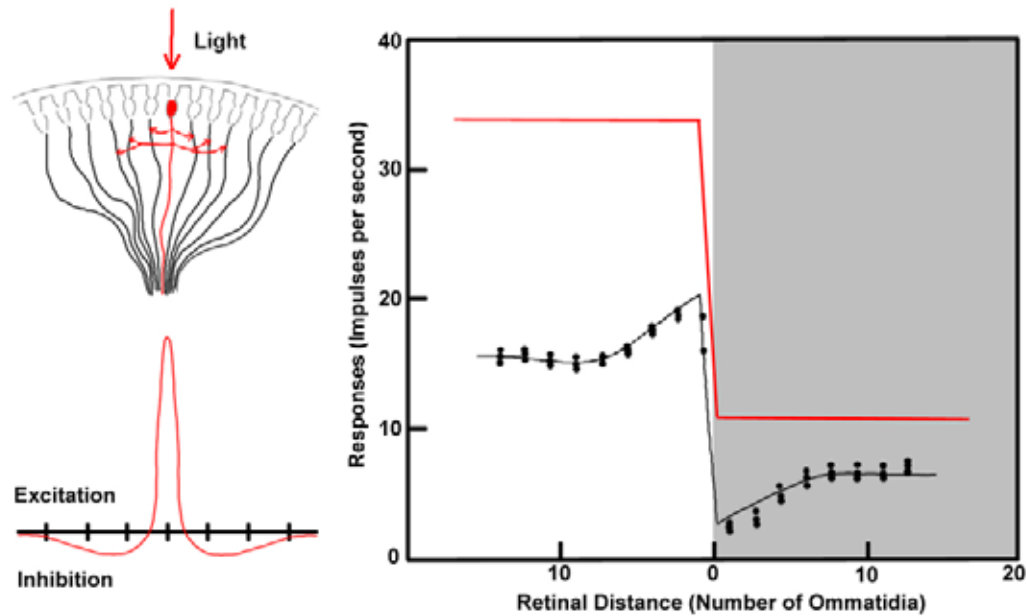


Figure 3.29: Lateral inhibition. Adapted from [Rat72].

An important consequence of lateral inhibition is that humans are very adept at edge detection. Figure 3.29 describes a situation where a stimulus is bright on the left side and darker on the right. The red line shows what the retinal response would be in lateral inhibition did not exist; the light portion is brighter and has a high reflectivity, while the darker portion reflects less light. However, while the actual luminance across each region is uniform, the observed lightness of each region is not. Near the boundary of the stimuli, the lighter region seems to get brighter as it nears the darker region and the darker region seems to get darker as it nears the lighter region.

To understand the phenomena, we will elaborate on different situations. The black points on the graph (and the best fit line) illustrate the observed brightness curve, obtained by psychophysical measurements. Starting from the left, there is constant bright illumination. Here, we have a situation similar to the first

example shown in Figure 3.28. Under constant stimulation, the opponent nature of ganglion receptor fields will produce a weakened response. The off-regions of the cells are inhibiting the response and we perceive the stimulus as being darker than it actually is. As we move closer to the edge, more off-region portions of receptor fields are receiving less light. Therefore more off-region receptor fields are receiving their desired response, while the on-receptors are still receiving their desired bright response. Hence, the total amount of excitation is increasing as we move toward the edge. The maximum response is right at the edge of the light and dark regions. The result is that we perceive the light area getting slightly brighter close to the edge. A similar effect occurs for the dark area, as it is perceived as slightly darker near the edge.

Ratliff was the first to physically measure these differences in intensity and perceived brightness. He measured the nerve impulses produced by steady illumination of a single receptor in the eye of the horseshoe crab *Limulus*. The nerve fibers from the receptor are separated by microdissection and connected to an electrode from an amplifier and a recorder. However, Ernst Mach explored the connection between reflected light intensity and the resulting sensation beforehand. He hypothesized the antagonistic influences in the retina, as his experiments with intensity and perception of light did not correspond. The pattern in Figure 3.30 is similar to one of which Mach developed. The apparent lightness within each bar varies even though the intensity of light reflected is constant. Most people describe the edges of each bar having slight bands. Hence the term *Mach bands*, which are the illusionary spatial gradations in perceived lightness that occurs without corresponding gradations in the actual distribution of light.

Mach bands emphasize the important distinction between intensity and light-



Figure 3.30: Mach bands.

ness. *Intensity* is an objective, physical variable, and can be measured with a light meter. *Lightness* is subjective, perceptual variable, whose measurement require a biological visual system. Although intensity changes in a stepwise fashion, lightness does not.

Related is the work of Josef Albers, who was also one of the first modern artists to investigate the psychological effects of color and space and to question the nature of perception. He studied color experimentally, through a series of practical exercises and as a teacher had important influence on generations of young artists. Like Mach, Albers discovered that a color is very rarely seen by itself, devoid of its surroundings. Hence, the overall impression of a color depends on the colors that surround and interact with it. Figure 3.31 illustrate some of Albers' work in perception.

The figure on the left depicts two white squares, each centered in different patches of a brick pattern. The only difference in the two images is that the grout

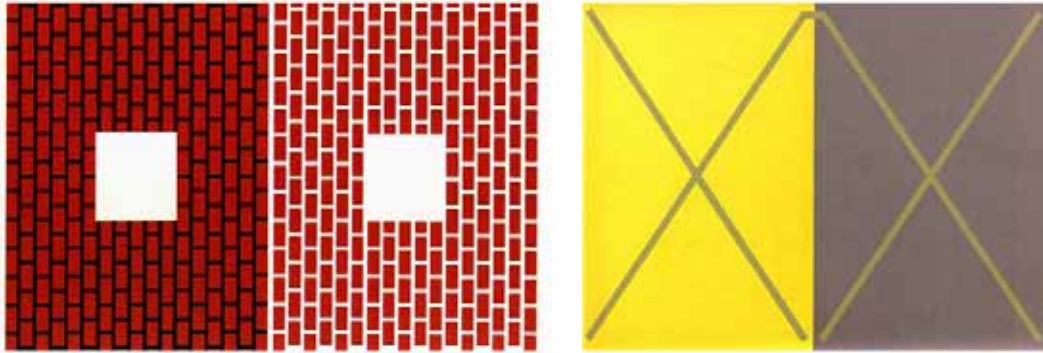


Figure 3.31: The work of Josef Albers. Adapted from [Alb71]

of the brick on the left is black. The grout on the right, the background, and both square are all exactly the same color. However, while color combinations are subjective, here one typically perceives the square on the left to be more intense or brighter than the one on the right. Hence, one color appears as two, given the different surrounds.

In the experiment on the right of Figure 3.31, Albers provides a similar exercise. Yellow and purple boxes are aligned next to each other, while two large crosses cover each box. The cross in the yellow surround appears purple, while the other appears more yellowish. However, while a very strong illusion, the crosses are of exactly the same color gray as seen by the small bridge at the top connecting the two crosses. This demonstrates that lateral inhibition does not only occur in the luminance channel, but in the color channels as well.

Albers' research led to many other experiments, many of which dealt with *simultaneous* contrast, or the tendency for contrasting colors to emphasize their differences when placed together. He stressed in his teachings that knowing how colors interact allows for better designs and avoid unintentional effects.

It is also possible that different physical intensities can yield the same lightness.

This routinely happens when you view an object under different lighting conditions. For instance, the spectral distribution of indoor tungsten lights is different to that of natural sunlight. Yet, a sheet of notebook paper in each is still perceived as white. The tendency of an object's color to remain unchanged despite changes in the light spectrum is called *color constancy*. To achieve color constancy, the visual system must separate the surface's reflection properties from the spectral distribution of the emitted light. One way this is done is the visual system adjusts its sensitivity to the overall level of illumination, called *light adaptation*. One has experienced this by entering a very dark room, such as a movie theater—the eyes gradually adjust to much lower light levels after a few minutes. Colored afterimages, which are often experienced after long exposures to the same stimulus, are attributed as an effect of adaptation. In this case, different regions of the eye have adapted to different colors, not an overall luminance change.

Yet, adaptation is not a complete explanation for color constancy. Color contrast among objects and their surroundings is also important. Since contrast does not change much when the illumination changes, the visual system exploits the ratios between colors in a scene. This is evident in the work of Edwin Land in his Retinex Theory of Color Vision [Lan77]. In Land's experiment, he created a painting with a collection of rectangular shapes of varying hues in the manner of Mondrian, a famous abstract painter. For each of five trials, he illuminated a different colored shape such that it exhibited an identical energy flux to the other four colors. Hence, all of the energy reaching the viewer's eye from the five shapes is identical. The viewer then matched each shape's color with the closest Munsell color chip, illuminated under the same source. Even though the five samples all sent the same physical color sensation to the eye, the viewer had different color

sensations for each trial and picked a different Munsell color chip for each. The results are seen in Figure 3.32.

Here, under lighting conditions that match the physical sensations of different colors, the red still looks red, and the yellow still appears as yellow in their respective surroundings. Clearly, the human visual system relies on more than just a single color sensation. The environment has a great effect on the overall appearance of a color, as simultaneous contrast maintains the relative relationships between the colors. Hence, vision is more than just physical energy and perceptual responses, but is subjective and is affected by one's interpretation.

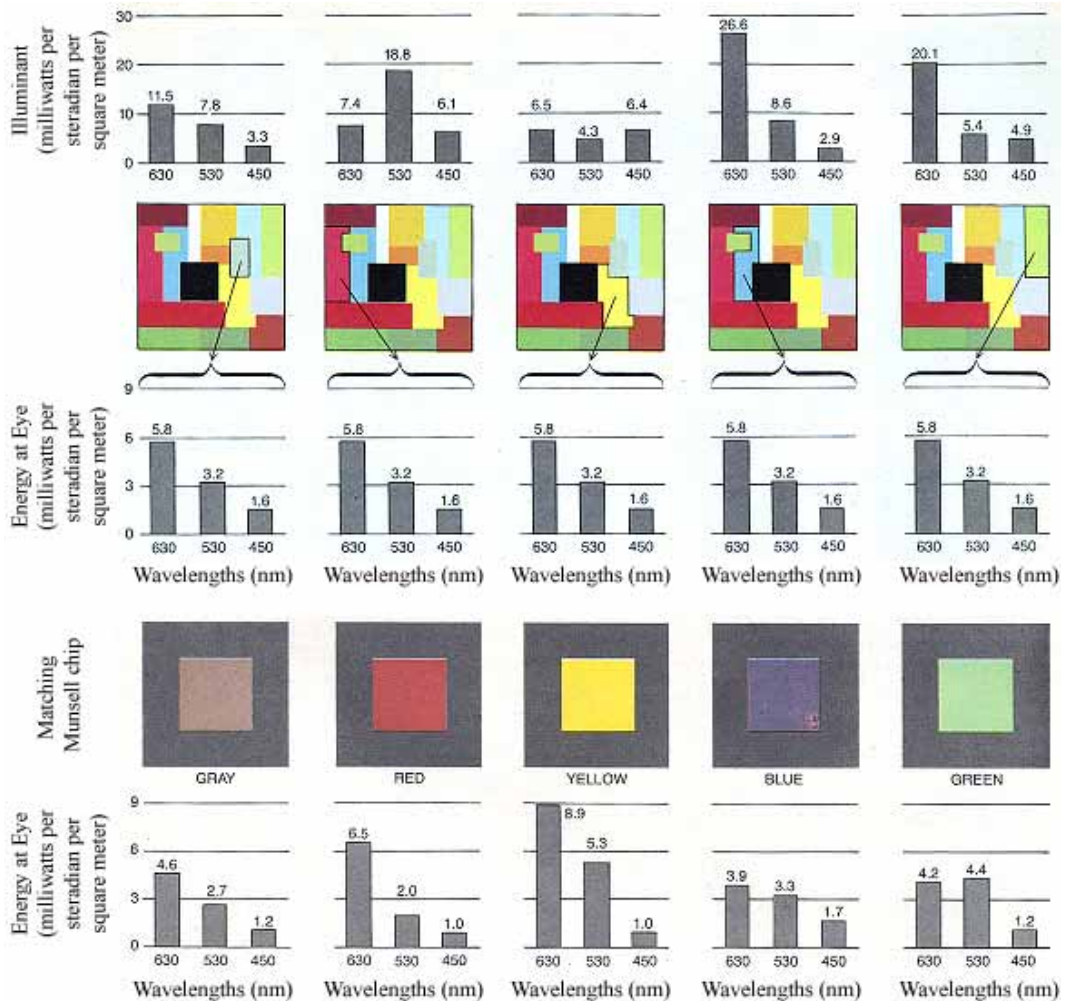


Figure 3.32: Edwin Land's Mondrian experiment. The five trials comprise the columns of the image. The arrows in the second row indicate the color shape selected for each trial. The amounts of each narrow-band illuminant needed to provide the exact same color sensation to the viewer are in the top row. The sensations that reach the eye are all identical, as seen in the third row. The Munsell color chips chosen by the viewer are seen in the fourth row, as well as their respective energies that reach the eye in the fifth row. Adapted from [Lan77]

Chapter 4

Previous Work

There is no subject, however complex, which – if studied with patience and intelligence – will not become more complex.

-Unknown

4.1 Introduction

This chapter is divided into two sections. The first primarily discusses modeling the complex behavior of paint and other volumetric materials in the computer graphics literature. The latter section discusses the study of naturally occurring changes in pigmented materials and how this alters one's perception of the surface appearance. In conjunction, these two disciplines can be used to effectively predict the behavior of pigmented solutions over time.

4.2 Light transport in volumetric materials

Accurately modeling the scattering of light by materials is fundamental for realistic image synthesis. Simple models to approximate the appearance of materials

have been developed since the 1970s and are built into graphics hardware today. While these models are adequate in simulating some materials, they are typically unable to capture the subtle effects that distinguish most materials. As a result, more sophisticated models have been developed over the years to simulate light reflections.

4.2.1 Subsurface scattering theory

When the flow of light hits an object, the energy is partly transmitted or absorbed into the material and partly scattered back into the environment. The amount scattered light and its directional distribution depend on the material's surface properties. In Chapter 2, it was noted that the *bidirectional reflectance distribution function (BRDF)* describes a material's response to incoming light as it is reflected toward a viewer. The BRDF f_o is defined as the exitant radiance in a direction per incident radiance from a direction per unit projected solid angle. That is,

$$f_o(\vec{\omega}_i, \vec{\omega}_o) = \frac{L_o}{L_i} / \mu(\Omega_i) \quad (4.1)$$

The reflected radiance L_o in direction $\vec{\omega}_o$ is then

$$L_o(\vec{\omega}_o) = \int_{H^2} f_o(\vec{\omega}_i, \vec{\omega}_o) L_i(\vec{\omega}_i) d\mu(\vec{\omega}_i) \quad (4.2)$$

However, the BRDF is only an approximation to the more general *bidirectional subsurface scattering distribution function (BSSRDF)*. In the case of the BRDF, it is assumed that light striking a surface location is reflected at that same location. While this may be the case for many materials (as in metals), light arriving at the surface of most materials enters and then scatters inside before leaving at a

different location. Subsurface scattering effects that the BRDF cannot capture include color bleeding within materials and the diffusion of light across shadow boundaries and silhouettes. This behavior is described by the BSSDRF S , which relates the outgoing radiance, $L_o(x_o, \vec{\omega}_o)$ at the point x_o in the direction $\vec{\omega}_o$, to the incident flux, $\Phi_i(x_i, \vec{\omega}_i)$ at the point x_i , from direction $\vec{\omega}_i$ [NRH⁺77]:

$$S(x_i, \vec{\omega}_i; x_o, \vec{\omega}_o) = \frac{dL_o(x_o, \vec{\omega}_o)}{d\Phi_i(x_i, \vec{\omega}_i)} \quad (4.3)$$

The amount of radiance leaving point x_o in direction $\vec{\omega}_o$ is then

$$L_o(x_o, \vec{\omega}_o) = \int_A \int_{\Omega} S(x_i, \vec{\omega}_i; x_o, \vec{\omega}_o) L_i(x_i, \vec{\omega}_i) (n_i \cdot \vec{\omega}_i) d\vec{\omega}_i dA(x_i) \quad (4.4)$$

where the term $S(x_i, \vec{\omega}_i; x_o, \vec{\omega}_o)$ is the BSSRDF. This function is an eight-dimension function and costly to evaluate numerically.

All paintings fall into this category of translucent materials, as subsurface scattering dictates the appearance of paint to a great extent. As seen in Chapter 2, light scatters multiple times within the binding media, interacting with the pigment particles before exiting to the environment. Hence, a viewer's perception of the material depends not only on the surface characteristics of the paint, but also on the light interactions within the paint. Therefore, BSSRDF's are very important in the realistic simulation of paint. There are several approaches to dealing with the complexity induced by this multiple scattering. These implementations are all various approximations to the BSSRDF.

4.2.2 Path tracing

One approach to handling subsurface scattering is to directly simulate the microscopic light events at the molecular level. In the *Monte Carlo* approach, one traces paths of many light photons through a volumetric material and develops a probabilistic model of the distribution of light energy. As a path of light enters the material and experiences a scattering event, the ray is scattered and transmitted. Since integrating over the entire sphere at each scattering event is too costly, 'random' samples are taken. If the material is *isotropic* (the scattering is independent of direction), the appearance does not depend on the angle between the viewing direction and the incoming light. If the scattering is *anisotropic* (dependent on direction), the method behaves better with nonuniform sampling and respective weighting. In general, for both cases in Monte Carlo algorithms, as the number of random samples increases, the summation of those values converges toward the integral. This method is used frequently in computer graphics due to its convergence rate and ease of operation.

It is typically assumed that (*phase*) *scattering functions* (the function that describes how the light behaves at the scattering event) describe scattering of a homogeneous distribution of particles suspended in a medium. Usually, the particles are of equal size (or distributed in some reasonable way). Also, while the index of refraction of both the particle and medium both influence the scattering of light, particle size exhibits more of an effect on the phase function.

When the particles are much larger than the wavelength of light (particle diameter $\gg (380 - 700nm)$), the geometric particle objects dominate the reflectance. When the particle size approaches that of the wavelength of light, scattering events become much more evident. In this situation, the complex theory of *Mie scattering*

describes the scattering and absorption of light at each scattering event (accounting for the size, shape and density of every particle, as well as the and relative indices of refraction). The Mie scattering functions are very numerically expensive to compute. Therefore, efficient approximations have been presented from the optical literature for sparse or dense particle densities (called *hazy* and *murky*, respectively) [NMN87]:

$$\begin{aligned} P_{hazyMie}(\cos \alpha) &= 1 + 9 \left(\frac{1 + \cos \alpha}{2} \right)^8 \\ P_{murkyMie}(\cos \alpha) &= 1 + 50 \left(\frac{1 + \cos \alpha}{2} \right)^{32} \end{aligned} \quad (4.5)$$

where α is the angle between the incident and outgoing directions. Another popular approximation to the Mie functions in the *Henyeey-Greenstein* phase function [Bli82]:

$$P_{henyeyGreenstein}(\cos \alpha, g) = \frac{1 - g^2}{(1 + g^2 - 2g \cos \alpha)^{3/2}} \quad (4.6)$$

The function takes an asymmetry parameter g (the mean cosine of the phase function), which varies from strong retro-reflection ($g < 0$) to strong forward scattering ($g > 0$). Isotropic scattering is achieved when $g = 0$.

Kozakov presented a successful method of calculating the characteristics of paint based on Monte Carlo methods [Koz04]. In the work, a statistical model of a paint coating was developed involving interaction between photons, particles, and the binding medium, as well as the photon path length between collisions. The model accounts for a single pigment and medium (titanium white in alkyd enamel) and actual paint reflectance data was measured and utilized in the work.

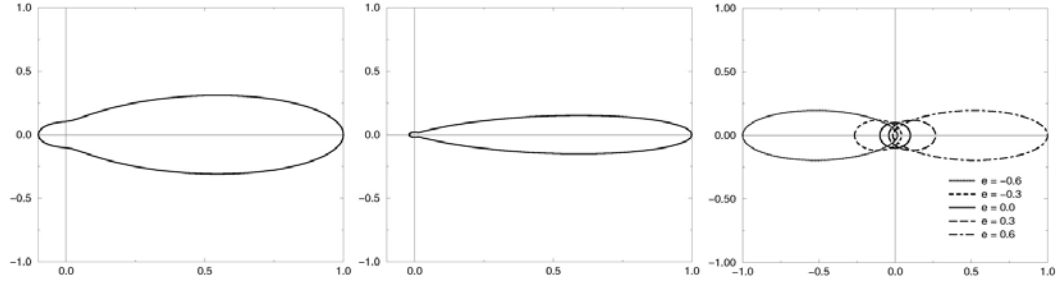


Figure 4.1: Common phase functions for particles whose diameters are approximately the size of the wavelength of light. For each, the incident light ray is from the left; each scattering event is at the intersection of the axes. Left: The hazy Mie function; middle: the murky Mie function; right: the Henyey-Greenstein function. Adapted from [G95b]

The results include accurate prediction of overall paint reflectance, absorption, and covering power as compared to measurements of actual samples.

Approaches similar to this, while capable of simulating all of the effects of sub-surface scattering, are still computationally very expensive. This is due to the fact that techniques based on path tracing are particularly inefficient for highly scattering materials (such as milk, skin or paint), in which the light scatters multiple (often several hundred) times before exiting the material. Moreover, the sampling nature of Monte Carlo often results in noise, which is not satisfactory for the subtleties in spatially varying pigmented materials. Ultimately, while this approach will eventually converge to the desired solution, this level of detail is somewhat too complex for calculating information about pigmented solutions.

4.2.3 Diffusion approximation

Another approach to handling the appearance of pigmented materials is to use an analytic technique. Jensen notes that light distribution in highly scattering media tends to be isotropic since each scattering event blurs the light [JMLH01]. Hence, single scattering (where incident light only scatters once before exiting)

only accounts for a small percentage of total outgoing radiance in these materials. In this context, the relationship between the incoming and outgoing directions can be removed, simplifying the BSSRDF to a four-dimensional function $R_d(x_i, x_o)$ known as the *diffuse BSSRDF*.

Diffusion theory can provide a good approximation for multiple scattering in highly scattering media without having to resort on costly Monte Carlo simulations. The diffusion equation has a simple solution in the case of a single isotropic point light source in an infinite medium:

$$\phi(x) = \frac{\Phi}{4\pi D} \frac{e^{-\sigma_{tr}f(x)}}{r(x)} \quad (4.7)$$

where

$\phi(x)$ is the radiant flux

Φ is the power of the point light source

$D = \frac{1}{3\sigma'_t}$ is the diffusion constant

σ_a is the absorption coefficient

g is the mean cosine of the phase function

$\sigma'_t = \sigma'_s + \sigma_a$ is the reduced extinction coefficient

$\sigma'_s = \sigma_s(1 - g)$ is the reduced scattering coefficient

$r(x)$ is the distance to the point source

$\sigma_{tr} = \sqrt{3\sigma_a\sigma'_t}$ is the effective transport coefficient

A more accurate approximation is the *dipole diffusion approximation*. In this model, the volumetric source distribution is modeled using two point sources, as illustrated in Figure 4.2. The first one, the positive real light source, is located at

distance z_r beneath the surface. The second one, the negative virtual light source is located above the surface at a distance $z_v = z_r + 4AD$.

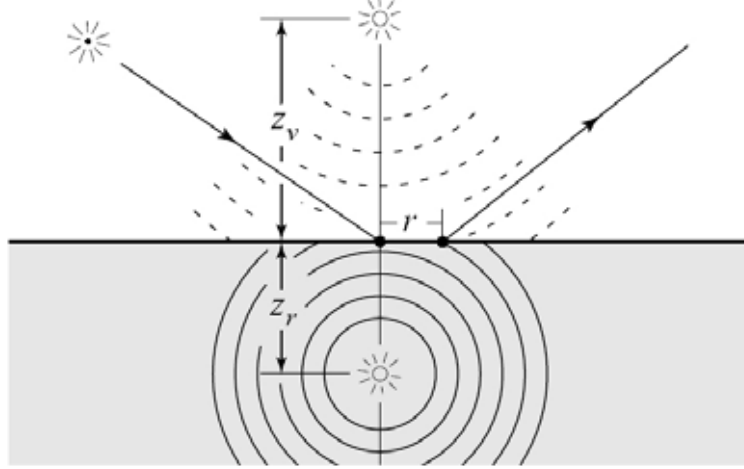


Figure 4.2: An incoming ray is transformed into a dipole source for the diffusion approximation. Adapted from [JMLH01]

Using this approximation, the diffuse reflectance at point x_o due to illumination at point x_i is

$$R_d(x_i, x_o) = \frac{\alpha}{4\pi} \left(z_r(1 + \sigma s_r) \frac{e^{-\sigma s_r}}{s_r^3} + z_v(1 + \sigma s_v) \frac{e^{-\sigma s_v}}{s_v^3} \right) \quad (4.8)$$

where

$$z_r = \frac{1}{\sigma'_t} \text{ and } z_v = z_r + 4AD$$

$$s_r = \|x_r - x_o\|, \text{ with } x_r = x_i - z_r \cdot N_i$$

$$s_v = \|x_v - x_o\|, \text{ with } x_v = x_i - z_v \cdot N_i$$

$$A = \frac{1 + F_{dr}}{1 - F_{dr}}$$

$$F_{dr} = \frac{1.440}{\eta^2} + \frac{0.710}{\eta} + 0.668 + 0.0636\eta$$

$$D = \frac{1}{3\sigma'_t} \text{ and } \sigma = \sqrt{3\sigma_a\sigma'_t}$$

$$\sigma'_t = \sigma_a + \sigma'_s \text{ and } \alpha' = \frac{\sigma'_s}{\sigma'_t}$$

σ'_s is the reduced scattering coefficient

σ_a is the absorption coefficient

η is the relative refraction index

The full model presented by Jensen et al. consists of two terms: a single scattering component, which through path tracing yields the exact solution for light that is bounced only once within a material; and a multiple bounce component, the dipole point source diffusion approximation to account for multiple scattering. Results from this work are illustrated in Figure 4.3. The diffusion approximation of the BSSRDF in this model provides good visual quality and has been successful in capturing the effects of participating media in a variety of materials, including milk, marble and skin. It matches the appearance of the Monte Carlo simulation, yet is significantly faster.



Figure 4.3: A simulation of subsurface scattering in a marble bust. The bust is illuminated from behind and rendered using: left, the BRDF approximation (in 2 minutes); middle, the BSSRDF approximation (in 5 minutes); right, a full Monte Carlo simulation (in 1250 minutes). Adapted from [JMLH01].

4.2.4 Image-based measurement

Further, physically correct parameters can be determined for volumetric materials by image-based measurement. Lensch et al. captured an object’s response to illumination using a high dynamic range camera from multiple points [LGB⁺03]. In this work, the highly scattering homogeneous materials are represented by the four-dimensional diffuse BSSRDF.

The algorithm is subdivided into two parts. The first is a large preprocessing step to compute and store the impulse response to incident light for each surface point under subsurface scattering. The responses are divided into local and global effects. Local effects are modeled as a per-texel filter kernel that is applied as a texture map representing the incident illumination. The global response is stored as vertex-to-vertex throughput factors for the object’s triangle mesh. During the rendering stage, two responses are combined using the current light situation to form the final image.

The work builds on subsurface scattering research, as it is unique in attempting to handle interactive image synthesis. The advantage is that the model is able to handle rendering of translucent materials at roughly interactive rates (approximately 5 frames per second), while including dynamic camera movement and changes in illumination.

Goesele et al. extended this work by presented a technique (denoted as the DISCO acquisition technique) that can derive the necessary input data for real translucent materials with spatially-varying properties [GLL⁺04]. This work is the first to acquire the subsurface light transport behavior for arbitrary heterogeneous materials.

The model utilizes the previous method of interactive rendering of highly-



Figure 4.4: A model of an alabaster horse sculpture acquired by the DISCO method. Differences in the material are clearly visible when the model is lit from behind. Adapted from [LGB⁺03].

scattering homogeneous media [LGB⁺03] and also incorporates an imaged-based method to capture spatially-varying details [LKG⁺01]. In this approach, local inconsistencies that occur naturally in materials are recovered (such as cracks, volumetrically-varying properties, hollow objects, etc). The model is quite successful, save the very high time demands (acquisition takes between 8-20 hours). Results from the model are illustrated in Figure 4.4.

Tong et al. identified that while the previous model is successful in image-based rendering of real-world objects, it is not applicable to arbitrary geometries [TWL⁺05]. Hence, similar approaches are deemed *object models* as the subsurface scattering properties are coupled to a specific geometry. In contrast, a *material model* can be applied to any geometry using further approximations and additional computation.

Recently, Peers et al. addressed the problem of acquiring and compactly representing the heterogeneous subsurface scattering functions, as the datasets repre-

representing the spatially varying component are impractically large [PvBM⁺06]. Their material model is represented by a number of terms contributing to the incoming and outgoing radiance. The subsurface scattering core is approximated as homogeneous and divided out of the kernel. This leaves only the discontinuities resulting from heterogeneities in the material—these residuals are compactly represented with a matrix factorization. The successful model can be applied to any arbitrary geometry and results are illustrated in Figure 4.5.

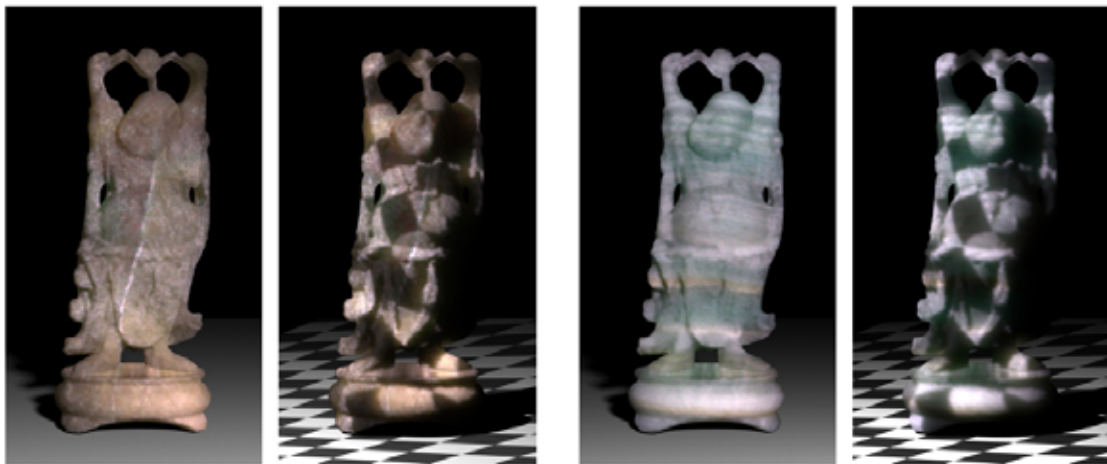


Figure 4.5: The Stanford Buddha model rendered using the material models for layered white onyx and cracked crystal onyx. Both materials are shown under uniform and textured illumination. Adapted from [PvBM⁺06].

4.2.5 Kubelka Munk theory

While the previous methods are all very successful in simulating materials that exhibit subsurface scattering effects, they do not work well for paints. Paint is a heterogeneous mixture of varying pigment concentrations (and at times other materials) dispersed in a binding solution, applied in multiple layers of varying thicknesses on a support. These algorithms either cannot capture these dynamic

effects or are too computationally expensive to do so interactively.

As contrasted to the previous approaches, we can work at the macroscopic level and simply model the aggregate behavior of the paint with respect to incident light. This approach was taken by German scientists Paul Kubelka and Franz Munk, who developed a simple set of differential equations to describe the transport of light in pigmented materials [KM31]. The model is very effective for pigmented materials, is not very complicated and is very efficient. The original paper in 1931 is based on the assumption of a homogeneous material of a medium that is infinite in extent. The model describes the material properties of a pigmented material in terms of only two wavelength-dependent parameters: an absorption constant, $K(\lambda)$, and a scattering constant, $S(\lambda)$:

$$R_{\infty} = \frac{1}{1 + \frac{K}{S} + \sqrt{\left(1 + \frac{K}{S}\right)^2 - 1}} \quad (4.9)$$

Equation 4.9 represents the solution to the most basic Kubelka-Munk differential equations as they were originally presented [KM31]. The diffuse reflectance, R_{∞} , of a paint sample of complete hiding (a paint of a thickness such that the substrate cannot be seen underneath) is a function of the absorption and scattering coefficients. Note that the dependence on wavelength is omitted for clarity and the equation is computed over the visible spectrum. The derivation of the solutions of Kubelka and Munk's differential equations and other improvements to the theory over the years are described in Appendix A.

The resulting solutions to the differential equations have found wide scientific utility in areas as diverse as the study of paint, paper, textiles, and skin, as well as art conservation and planetary science. In computer graphics, the equations have been used in a variety of rendering contexts for materials that exhibit subsurface

scattering and absorption properties. The following research demonstrates the usefulness of K-M theory to simulate the appearance of pigmented materials.

Haase and Mayer introduced the Kubelka-Munk model to computer graphics, using the K-M equations for rendering and color mixing in both interactive and offline applications [HM92]. The work included a simple airbrush tool, where users could work with real-world pigmented paints, instead of arbitrary *RGB* colors.

The program stored and updated the current K and S values for every pixel in the image, using a custom four-wavelengths representation based on Meyer's previous work [Mey88]. The four-wavelength encoding was based on integrating against the human visual response functions in *ACC* color space. The interpolation of the wavelengths used to compute tristimulus values from spectral data was done using Gaussian quadrature. Computing reflectance values for K and S values over the entire visible spectrum is very computationally expensive, and therefore limiting the wavelength information is necessary for the purposes of real-time interaction. Since the reflectance spectral curves are reasonably smooth functions, the errors caused by this minimal sampling are minimized.

The results of this theory are illustrated in Figure 4.6. A real photograph painted with varying concentrations of two red paints and a white paint is simulated using *RGB* values and Kubelka-Munk theory. The spectral reflectances of the paints are shown in Figure 4.7 and the dependencies of the absorption and scattering coefficients are shown in Figure 4.8.

Curtis et al. used the Kubelka-Munk equations for optically compositing thin glazes of paint in their watercolor simulation [CAS⁺97]. The model uses a three wavelength *RGB* representation for the K and S coefficients. The K and S values were not determined experimentally, but specified interactively. This method of

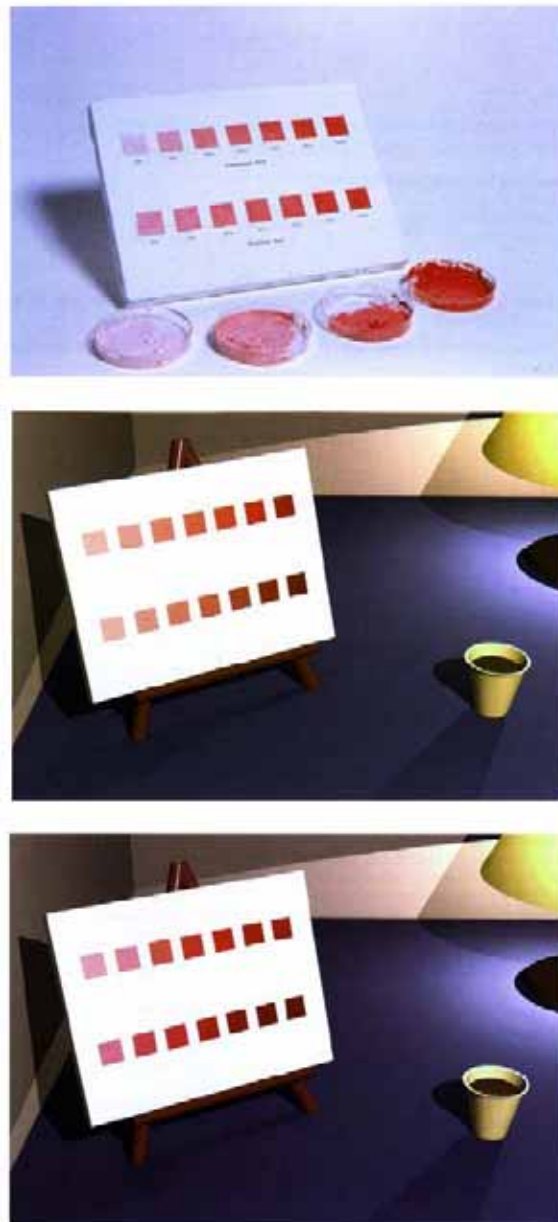


Figure 4.6: Results using Kubelka-Munk theory. Top: A photograph of a real canvas painted with mixtures of Cadmium red (top painted row on canvas) and Naphthol red. The tint concentrations from left to right, were 2, 5, 10, 20, 40, 80, and 100% of dry weight by pigment. Middle: A simulation of the painted canvas using RGB values to mix the reds with white. Bottom: A simulation of the canvas using the Kubelka-Munk theory. Adapted from [HM92]

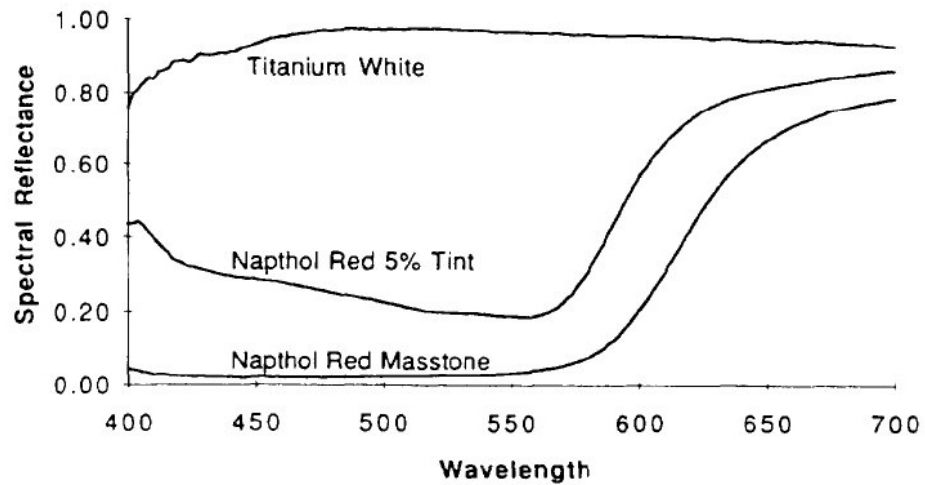


Figure 4.7: A selection of reflectance spectra of the paints used in Figure 4.6. Adapted from [HM92]

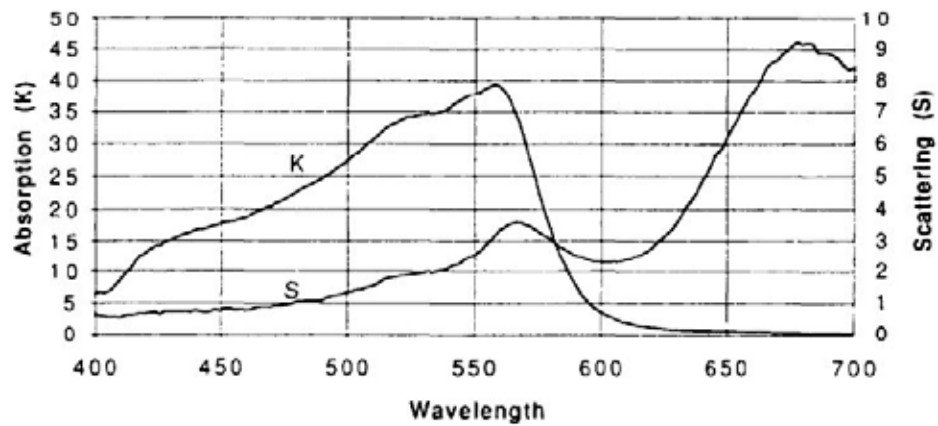


Figure 4.8: Kubelka Munk absorption K and scattering S values corresponding to the naphthol red pigment shown in Figure 4.6. Adapted from [HM92]

specifying pigments works adequately for creating a wide range of plausible paints, without the careful measurements needed for true K-M theory.

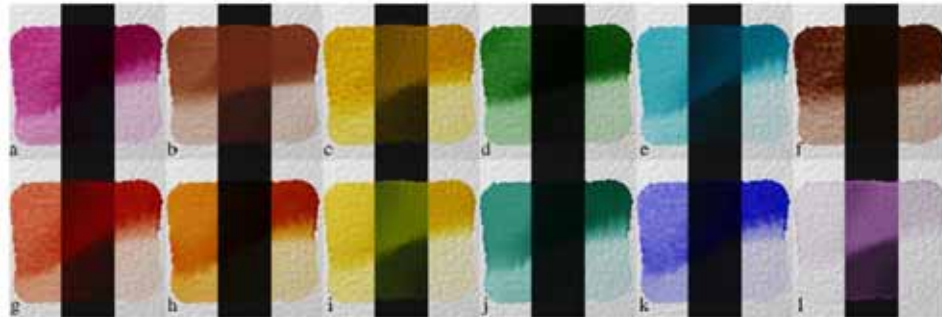


Figure 4.9: Various synthetic pigments determined interactively from Curtis et al. The swatches are painted over a black stripe to distinguish the more opaque pigments from transparent ones. Adapted from [CAS⁺97].

The optical compositing equations are used to determine the overall reflectance of the layers and reasonable results are achieved. Although the watercolor renderer runs too slowly for interactive painting, the work demonstrated that compositing many glazes of pigments using the K-M model was feasible in real-time. The model used simpler rendering and a lower resolution during user interaction, and then added more detail and more accurate colors as a post-processing step.

Rudolf et al. used the same form as Curtis et al. in their wax crayon simulation [RMN03]. Crayons were treated as a translucent pigmented material (this is different from real world crayons, as they contain other impurities). The model used three wavelengths for the K-M coefficients and the crayon colors were similarly not derived from real-world measured materials. The model was also not fast enough for real-time rendering, but still served as a good preview-and-render system (strokes took 0.3-2 seconds to render on a high end workstation of the time of the paper).

However, there are issues with these implementations of Kubelka-Munk theory.

Johnson and Fairchild point out that under some lighting conditions, *any* trichromatic color space as the *RGB* or *ACC* will give incorrect results [JF99]. Such a problem exists when one tries to color match under one lighting condition, only to appear differently in another lighting situation due to metamerism. As a result, there is no way for a three-component color representation to capture this effect. Johnson and Fairchild argue that for color-sensitive applications, full-spectral color representations are necessary. Also, none of the previous implementations were truly real-time, interactive systems.

Recently, William Baxter presented a model (denoted as IMPaSTo) as an attempt to address previous Kubelka-Munk issues [BWL04]. Accurate compositing and rendering of pigmented mixtures is done similarly to previous work in graphics with K-M theory.

The absorption and scattering coefficients were determined from many real-world oil paints. Multiple tints of different concentrations were made for each of the 11 pigments, for a total of 71 measurements (including samples only including the pure pigments). 101 reflectance values were obtained from each paint sample over the visible spectrum, and K-M absorption and scattering coefficients were calculated at each wavelength.

The following equation was used to relate the reflectance of a mixture, $R_{\infty,i}$, to the absorption K_j and scattering S_j of each constituent pigment and their relative concentrations, c_{ij} .

$$\left(\frac{K}{S}\right)_{mixture,i} = \frac{\sum_j K_j c_{ij}}{\sum_j S_j c_{ij}} = \frac{(1 - R_{\infty,i})^2}{2R_{\infty,i}} \quad (4.10)$$

For pigments not involved with a particular mixture, $c_{ij} = 0$.

While Johnson and Fairchild showed that full spectral data provides better

color representation, it is not feasible to store full-spectrum K and S samples on a per-pixel basis or compute it interactively. Most naturally occurring spectra are fairly smooth functions and hence are approximated by polynomials of moderate degree. After selecting a light spectra, the model chooses eight sample wavelengths and weights. A better implementation would focus more weight on the response matching functions, as some of the outlying sample wavelengths do not maximize their effectiveness in Baxter’s model. A Gaussian quadrature integration scheme is used to compute the final conversion of per-wavelength K-M diffuse reflectances to RGB for display.

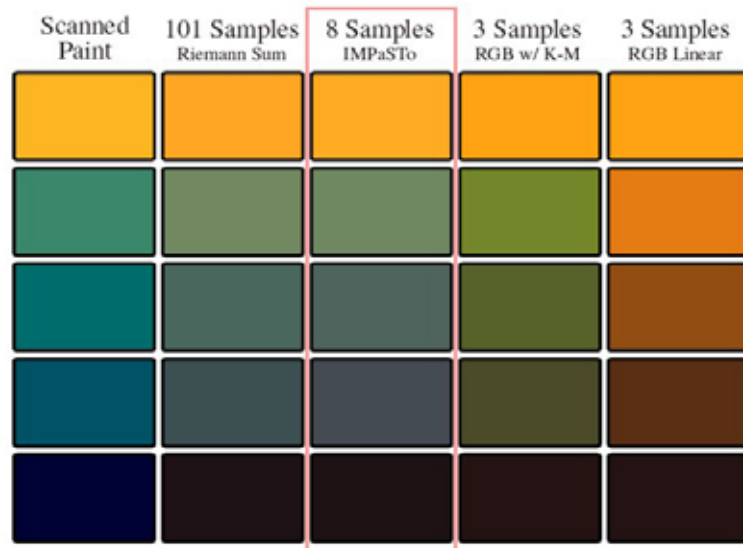


Figure 4.10: The left column shows graded mixtures of Yellow Ochre and Prussian Blue under a 5600K light. The right four columns show computer simulations of the mixtures using different techniques. As one can see, linear RGB incorrectly predicts brown. While IMPaSTo does not match the scanned colors exactly, it is important to note that the 8-sample Gaussian quadrature is almost identical to using 101 samples. Thus, given more accurate data as input, the samples could be matched very closely. Adapted from [BWL04].

Unlike previous K-M implementations, this work offers true real-time rendering. The model is realized using programmable fragment shaders on graphics hardware.

Fragment programs determine the diffuse reflectance of any one layer of paint, then calculate the final composited reflectance using the eight chosen wavelengths. Eight make a good fit with graphics hardware, as it enables the data to be stored in either two textures or in one floating-point texture packed in half precision floating point format.

Only wet paint is stored as pigmented data; as paint dries it is added to the base canvas' reflectance. The model only allows for one wet layer of paint, which is not necessarily the case in real world paints. A tiling system is utilized to reduce the demand for re-rendering the entire painting every frame, as only the portion of the work which is modified needs to be updated (allowing for a substantial increase in speed). Also, storing a painting as spectral data allows it to be re-lit by any full-spectrum illuminant.

Similar to previous implementations, since the K-M calculations only yield diffuse reflectance, the lighting computation is completed using per-pixel dot-product bump mapping and Blinn-Phong specular highlights. Results from the rendering model are illustrated in Figure 4.10. Ultimately, this work shows that Kubelka Munk theory can provide very plausible physical approximations to pigmented materials in real-time, which are quite satisfactory for many applications.

4.2.6 Time-varying appearance

In all of the previous work, the material properties were all assumed to be constant over time. In contrast, Dorsey and Hanrahan presented a model attempting to model how materials change over time as they are subjected to atmospheric conditions [DH96]. The model incorporates information about a material's structure, its interaction with light, and the physical processes that will affect it over

time. A metallic surface patina is represented as a series of layers (unlike the actual material), each describing one of the metal's dynamic properties (such as 'coat', 'erode', and 'polish'). A schematic diagram of these processes is illustrated in Figure 4.11. The layered operators are procedurally manipulated via observed heuristics of time-dependent deposition and erosion. Kubelka-Munk theory is used to composite the multiple layers of metal's dynamic properties in order to predict the appearance of metallic patinas.

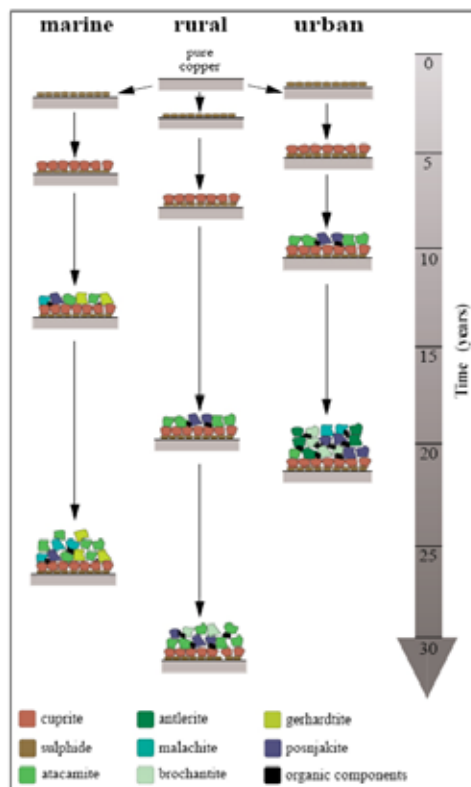


Figure 4.11: A schematic diagram of the process involved in the growth of copper patinas in marine, rural and urban atmospheres. Adapted from [DH96].

The work achieved excellent visual representations of the phenomena, as seen in Figure 4.12. However, it is not a physically based model as no direct measurements were taken of the materials. In their paper, the copper reflectance spectra were



Figure 4.12: A sequence of images showing the aging of a statuette, illustrating the buildup of the underlying smooth copper sulphide tarnish and the rough green patina. Adapted from [DH96].

matched to physical samples and photographs and the K-M absorption K and scattering S coefficients were calculated from the estimated reflectances. Also, since K-M theory only calculates diffuse reflectance, glossy and specular reflections were approximated to complete the approximation to the BRDF.

Dorsey et al. further explored the weathering phenomena with stone [DEJ⁺99]. In the simulation, changes are not only made to the appearance of stone over time, but to the underlying 3D model as well (Dorsey's previous work was limited to 2D surface effects, using a stack of layered operators). As stone weathers, the majority of the changes occur near the surface of the material. First, a digitized mesh representing the geometry of an object was converted into voxels. Then, the model was parameterized with surface-aligned volumes (denoted *slabs*) containing a narrow region of the outer portion of the model. Each of these slabs underwent the authors' weathering model, which employed a series of effects within the porous stone material. These included the flow of moisture, the transport, dissolution, and re-crystallization of minerals, and erosion of the material. The base composition of the stone material was a procedurally generated, volumetric texture. Input to

the system consisted of wetness and deposit maps computed with visibility to the different sources.

Many of the subtle effects occur below the surface of the material. Therefore, to render the heterogeneous volumetric material, a subsurface Monte Carlo technique was used with an approximation of the Henyey-Greenstein phase function. Results from the model are very plausible, as seen in Figure 4.13. In all, the model qualitatively exhibits observed stone weathering effectively, although the model was not substantiated by measurement. The authors state that an exact model is not feasible as the scientific knowledge for stone weathering is incomplete.



Figure 4.13: Simulated marble weathering of *Diana the Huntress* showing minor erosion of the statue and yellowing due to dissolved iron. Adapted from [DEJ⁺99].

Recently, Gu et al. presented a model which also factors space and time-varying effects [GTR⁺06]. An overall temporal curve controls different spatial locations evolving at different rates. The work measured data from a number of natural processes, including burning, drying, ripening, decay and corrosion. Time-varying textures were acquired with images from multiple light sources and viewpoints over a hemisphere. This had to be done rapidly to avoid discrepancies in the capture of the data. This procedure allowed for a true fit to a TSV-BRDF (time and spatially

varying BRDF) and rendering with arbitrary lighting and viewing.



Figure 4.14: Sequences of images demonstrating the model from Gu et al. **Top:** A teapot rusting. **Bottom:** The bowl uses the burning wood dataset and a drying cloth lines the table. Adapted from [GTR⁺06].

Of the 26 natural processes studied, the behavior of some materials was experimentally accelerated due to time restrictions. Burning was incited by a heat gun and corrosion of metals via chemical solutions. The model is quite effective in representing a number of materials. However, the single temporal characteristic curve does not hold for materials where multiple time-varying processes occur (the authors note this behavior in the decaying apple slice studied, though paint also has this behavior as seen in the next section). Results for this model are illustrated in Figure 4.14.

4.3 Natural changes in pigmented materials

Much research has been done in the preservation of artwork at conservation institutes to ensure that today’s treasures are passed down to the next generation. Some pigments change in appearance after only a few weeks, while others do not show change for tens of years, or more. Knowledge of the rate of colorant fading

or darkening enables the museum personnel to develop the best conditions for the preservation of the objects while still allowing for them to be displayed.

4.3.1 Fading of pigments

For proper care of a work over its duration, a great extent depends on the identification of the materials used in its creation. A noninvasive technique is *spectrophotometry*, which measures the light reflected or transmitted at each wavelength in the visible spectrum. As covered previously, a graph of the reflected light at each wavelength of a material is spectral curve. The shape of this curve can be helpful in identifying the colorants and media used in a work.

In studying the rate of change for a specific pigment, accelerated-aging tests are often carried out. These methods simulate a material experiencing long exposure to daylight by a very intense ultraviolet light exposure over a much shorter period of time. Samples are often immersed in ultraviolet light from a source enclosed in a carbon arc, which has a spectral energy distribution is close to that of natural sunlight.

Feller states that these accelerated-aging tests are carried out for three major purposes [Fel94]: to establish in a conveniently short time the relative ranking of materials with respect to their chemical stability or physical durability; to predict long-term serviceability of a material under expected conditions of use; and to speed up and study the chemical reactions which elicit the degradation.

These techniques are used to study colorant changes, although one should remember that these conditions do not exactly represent real world behavior. For example, these tests are not representative of outdoor aging, as they do not include other important factors such as the presence of moisture, temperature and

pressure changes, or other atmospheric effects.

Some pigments darken, as seen with Vermillion (the red form of mercuric sulfide) in Figure 4.15. In the unexposed sample, Vermillion's characteristic red appearance is dictated by the high reflectance in the long-wavelength range of the visible spectrum. As the sample is exposed to an Atlas xenon arc Fade-Ometer, one readily notices that the reflectance maxima in the long wavelength region decreases with age due to the darkening.

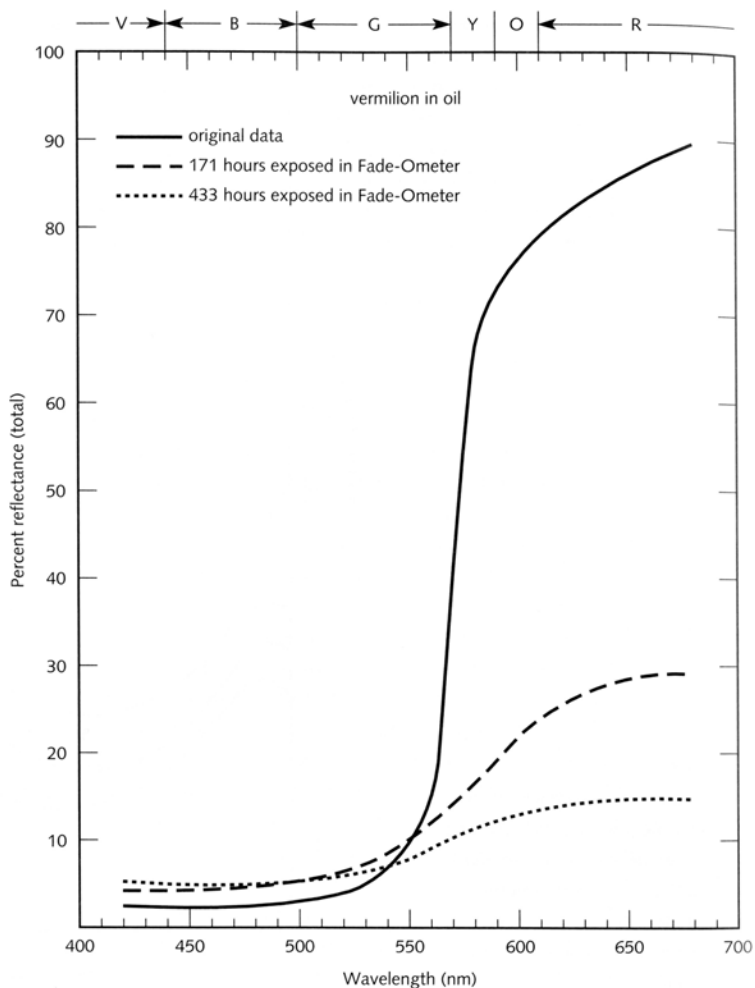


Figure 4.15: Reflectance of Vermillion before and after exposure in the Fade-Ometer. Adapted from [JF01].

For extra protection from these effects, museum curators sometimes install glass

in front of a displayed work. Feller contrasts the reflectance curves of two exposed samples of Emerald Green (copper acetate–copper arsenate) in oil (Figure 4.16). While both samples are mounted behind a glass panel, one panel also has an ultraviolet filter restricting the passage of potentially hazardous wavelengths of light from reaching a work of art.

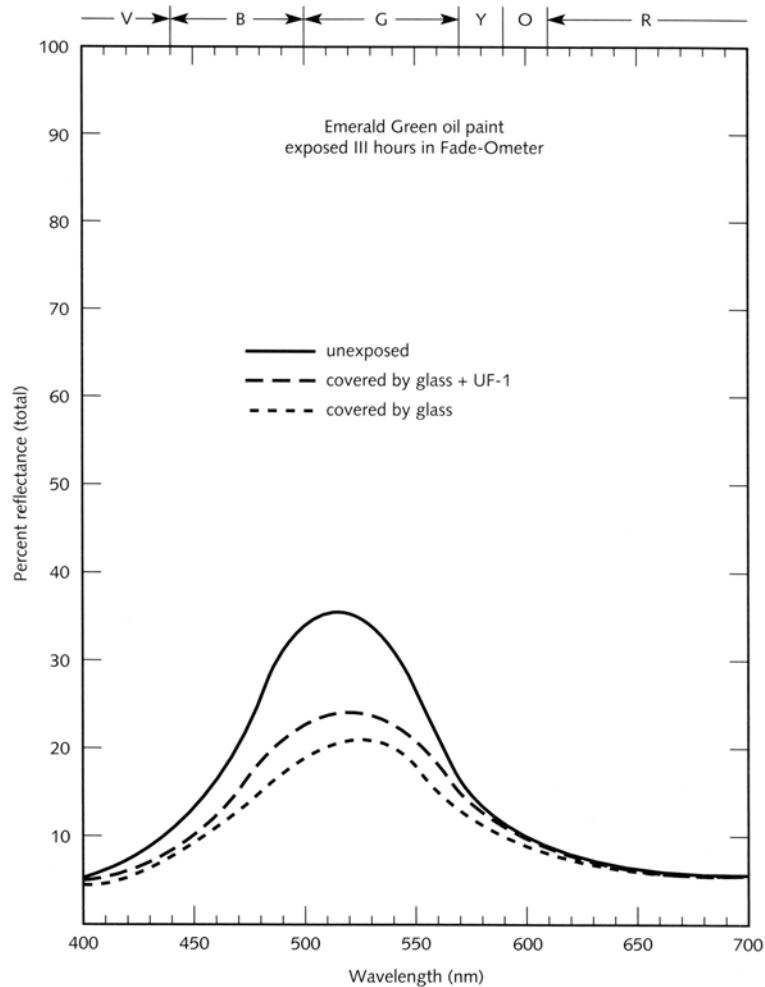


Figure 4.16: Reflectance of Emerald green before and after exposure in the Fade-Ometer under glass, with and without an ultraviolet filter (Plexiglass UF-1). Adapted from [Fel68].

The figure displays the typical spectral reflectance for a green material—a moderate amount of light is reflected from the central portion of the visible spectrum,

while all other light is mostly absorbed. Note that the darkening of the paint is less for the exposure under the ultraviolet filter. In order for *photochemical deterioration* (chemical reactions induced by electromagnetic energy) to occur, radiant energy must be absorbed, activating the molecules. Typically, the energy of photons in the long wavelength (low frequency) range of the electromagnetic spectrum (infrared range and higher) is not sufficient to induce chemical reactions. Yet, as frequencies increase, photons carry more energy. Ultraviolet light, with a higher frequency (and much more energy) than that of the visible spectrum, is capable of inducing significant photochemical changes in the pigment particles.

The *Grotthus-Draper Law* states that only radiation that is absorbed by a substance may cause a chemical reaction—light must be taken in by a material in order for the energy from the light to act upon it [Fel94]. Yet, not every frequency of light elicits a change in the material. Photochemical changes are dependent on the molecular structure of the pigment particles. Sir William Bragg used the analogy to tuning forks, which are set in vibration when sound waves of the appropriate frequency pass through them [Bra59]. Correspondingly, electromagnetic energy tends to be absorbed in molecules when they are in tune with a particular frequency of incident light.

If a red and a blue pigment were equally susceptible to photochemical deterioration, the blue pigment would deteriorate much faster. This is due to the increased energy in the lower wavelength range of the visible spectrum (compared to higher wavelengths). However, since pigments are made of different materials, they absorb different portions of the electromagnetic spectrum to differing degrees. Hence, blue pigments do not necessarily deteriorate faster than red pigments.

Figure 4.17 illustrates Alizarin Crimson red fading to a colorless form due to

light exposure. This effect is especially noticeable in the model's left sleeve. The sequence of images shows a portrait exposed to increasing levels of accelerated illumination. Five concentrations of Alizarin Crimson red were applied in glazes to depict the sleeves of the woman's portrait. The scale on the left of each image corresponds to the five alizarin concentrations used in the painting.

The painting was exposed to light from a xenon lamp for a series of exposure times. After each time period, the painting was removed for measurement of the concentration of alizarin remaining in the glazes. The work was also photographed at each stage. The full exposure is approximately equivalent to a hundred years on a museum wall well illuminated by diffuse daylight. While the images only reflect a subjective comparison to the original paintings due to gamut restrictions, the changes in the deterioration of the Alizarin Crimson are readily seen.

The reflectances of the five concentrations of Alizarin Crimson were measured and converted to the Munsell color space. The changes in each glaze can be seen in Figure 4.18 as the plot describes each hue (for paint samples 1-5) in respect to their Munsell chroma and value. The Munsell coordinates for each original paint are plotted as white dots and the exposed sample reflectances as black dots. Each original paint sample is grouped with its corresponding samples of increasing exposure via a blue ellipse.

As expected, the exposed sample reflectances grew further from each original sample as time passed. The Munsell value increased on all samples over time (the equivalent of the hue growing closer to white). The chroma is more complicated, however. The initially darker glazes (denoted 1,2, and 3 on the graph), increased in chroma as the fading proceeded (the maximum chroma was achieved by the middle concentration (3)). In contrast, the lighter glazes (4 and 5) decreased in chroma

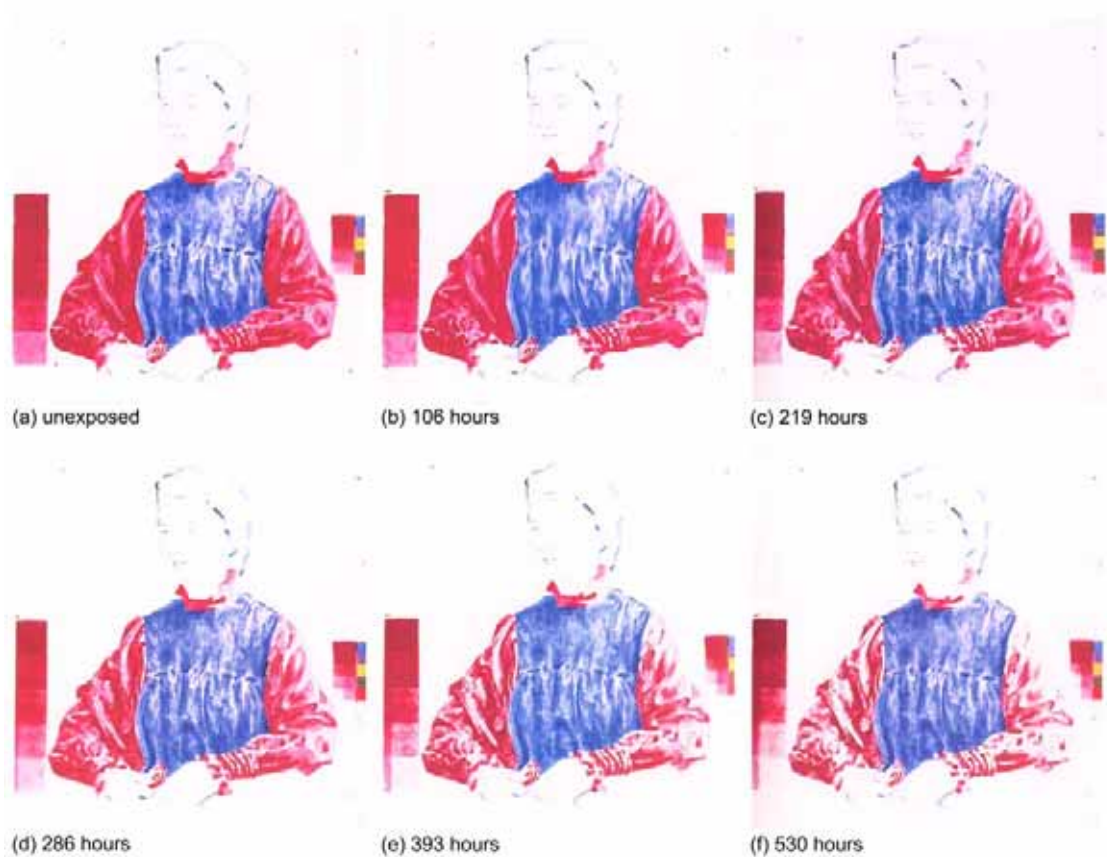


Figure 4.17: The sequence of images shows the fading of different concentrations of alizarin crimson over timed exposure to ultraviolet light. The full exposure is approximately equivalent to a hundred years on a museum wall well illuminated by diffuse daylight. Adapted from [JF01].

over time. Perceptually, these hues have much greater differences than the darker ones, as seen by the magnitude of the distances between points. Typically, it is this last type of change that we recognize as fading. That darker colors actually increase in chroma, or saturation, thus appearing to get brighter as they get lighter, is not often understood to be the result of fading.

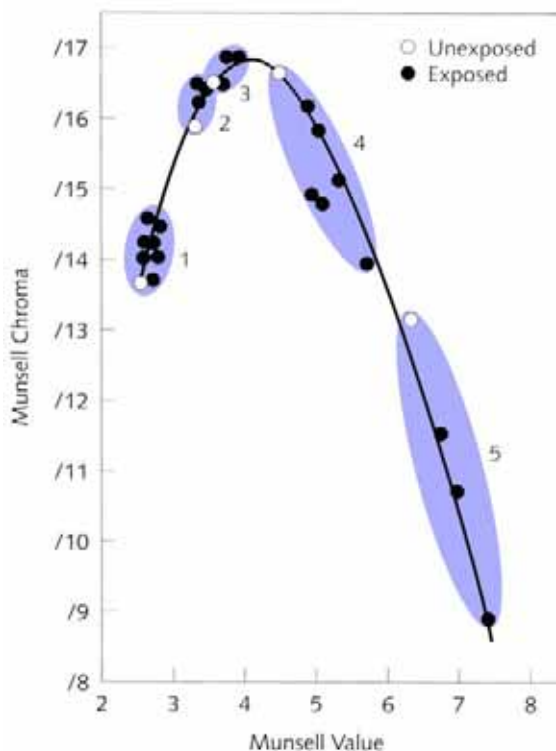


Figure 4.18: Fading of the five Alizarin Crimson hues used in Figure 4.17 in respect to Munsell value and chroma. As the samples age, the exposed samples (black dots) tend to shift from their original appearance (white dots). Adapted from [JF01].

A consequence of this drastic loss of pigmented colorant is that the resulting artwork sometimes experiences *pentimento*—where an underlying image in a painting shows through when overlying layers of paint have become transparent with age. Also, paint mixtures that include a fugitive pigment may undergo a hue shift, as the more resilient material’s colorant will dominate as the mixture ages.

Accelerated-aging in the manner that has been presented is the conventional approach to assessing a fading risk—pigment materials are identified from reflectance data and a rough measure of the lightfastness is established through independent tests of similar materials under analogous lighting conditions. The painting itself is typically not aged. Hence, analysts are faced with the enormous challenge to correctly identify colorants and their associated materials (binder, additives, etc) with the precision necessary to identify light sensitivity. Yet, the result is still an estimate of lightfastness. Discrepancies could arise from the possible misidentification of materials, the origin and specification of the studied materials, as well as other well-established factors in further fading: particle size, pigment concentration, and prior fading history.

Whitmore et al. presented an accurate method for predicting the lightfastness of pigmented materials that *comprise* rather than *approximate* the material [WPB99]. In this work, accelerated-aging tests are done on tiny (0.4mm diameter) areas of an object while simultaneously monitoring the color change of the material—both of which are accomplished using fiber-optic light guides. The method is terminated when a noticeable but definite color change has been produced. Although the bleached spot is very small, the results compare well to more conventional aging accelerated tests and show promise as a tool to recognizing light-sensitive materials.

4.3.2 Kinetics of fading

Pigments are based on chemical compounds and should obey laws of chemical reactions in the course of their deterioration—the rate that a chemical process takes place at any moment is related to the concentrations of the constituent substances.

The rate of change of the concentration of a substance over time is proportional to the concentration C raised to some power n :

$$\frac{dC}{dt} = kC^n \quad (4.11)$$

If the exponent is $n = [0, 3] \mid n \in \mathbb{Z}$, the reaction is said to be zero, first, or second order, respectively—these are the most commonly encountered modes of chemical change.

The combination of optical properties and reaction kinetics allow for the prediction of colorant loss in a fading glaze. Johnston-Feller et al. used Kubelka Munk color matching techniques to determine the concentrations of pigments present at any given stage in fading [JFFBC84]. The work demonstrated that the fading process for many pigments can be described on the basis of first-order kinetics as a function of time. From Equation 4.11, we have

$$-\frac{dC}{dt} = k_1 C \quad (4.12)$$

$$\ln C = \ln C_0 - k_1 t \quad (4.13)$$

where C_0 is the initial concentration and C is the concentration remaining after time t . Via Kubelka Munk theory, the percentage of colorant remaining after an elapsed period of time can also be expressed as

$$C = 100\% \left[\frac{(K/S)_e}{(K/S)_o} \right] \quad (4.14)$$

where

$(K/S)_o$ are the coefficients derived from the original sample's reflectance

$(K/S)_e$ are the coefficients derived from the aged, exposed sample's reflectance

Note that the sample can be a mixture of pigments, in which case Duncan's K-M linear pigmented mixing from Equation A.16 would be substituted with respective weighting.

In order to analyze the data in terms of hue shift in a color-matching program, Johnston suggests calibration with at least a three color pigment basis plus white, and the use of Duncan's pigmented mixing equation. One selects the hues of the pigments to ensure coverage over the entire gamut of colors (typically this selection mimics the opponent color channels, choosing white, black, red or green, and yellow or blue). In this way, widely varying temporal changes (such as fading, darkening, and hue changes) can all be detected and recorded effectively [JFFBC84]. By means of Munsell notation and color difference calculations, the work found that orderly changes in concentration related to a nonlinear change in the perceived color of a paint.

Whitmore and Bailie presented a model predicting and verifying experimentally the loss from fading from two perspectives: in terms of colorant loss from photochemical reaction and the resulting perceptual color changes [WB97]. The work determined that colorant loss takes place at three distinct stages. The darkest (or most concentrated) glazes lose colorant at the maximum (linear) rate, yet the color change is slight because there is little spectral change. Usually, 'fading' for these glazes includes a shift in hue, followed by an increase in chroma. This is due to reflectance changes away from the absorption peak.

As colorant is further lost, the absorbed wavelengths are less highly absorbent, hence the colorant loss slows. However, the magnitude of the perceptual color change increases (this is what is known as typical fading, with the chroma decreasing and value increasing). Glazes having an intermediate reflectance (20 – 80%

over white grounds) suffer the greatest rate of color change. Finally, the fading will appear to slow, but only after most of the glaze has been lost (absorbing very little light). Note that the first two stages of fading are easily recognized from the Munsell plots of the alizarin crimson glazes in Figure 4.17.

The model predicts that only absorption determines the fading rate. The fact that the colorant concentration does not affect the colorant loss rate (pale tints do not lose their colorant faster than that of darker colors) has been previously observed [GED64, JFFBC84]. However, while prior fading should not affect the loss rate, this was not the case experimentally. Whitmore and Bailie noted that older colorants seem more resistant than fresh ones to further fading (given the same concentrations). The authors list possible discrepancies: the pigment may either react to form products that influence further fading, or originally have been a mixture of components with different individual fading rates (different particle sizes, previous fading of one of the constituents, etc).

Pigments scatter incident light, which in turn, increases the depth of which photochemical processes occur. Johnston-Feller showed that the depth of fading in paints from accelerated aging is decreased as the concentration of white pigment decreases in a tint. (Figure 4.19). White pigments scatter light deeper into the paint, and hence fading occurs deeper within the paint if there is more white present.

Yet, the behavior of fading taking place only in the upper portion of the paint sample is important for analysts attempting to classify materials in a work. If the surface has faded substantially, it is possible to view relatively unfaded material underneath via cross-sections, revealing many of the original colorants [Fel94].

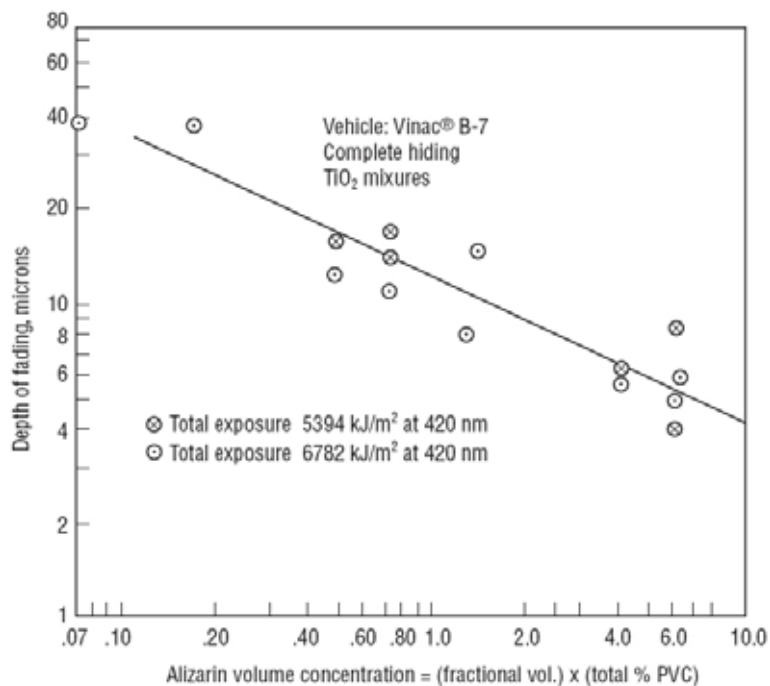


Figure 4.19: Depth of fading in Alizarin Lake/Titanium Dioxide white paint. The depth of fading is proportional to the amount of white pigment in the paint. Adapted from [Joh86].

4.3.3 Medium and substrate changes

Many paints vary in stability when exposed to light, heat, high humidity, or extreme values of pH. A pigment will behave differently when dispersed in different media. Therefore, it is important that the stability be described in relation to the binding medium.

The primary interest for the long term stability of organic materials is thermally or photochemically induced *oxidation*. Some materials cure by oxidation, or when oxygen enters the substance and cross-links the constituent molecules. These reactions tend to leave materials weak and brittle, possibly affecting the color. Oxidation affects canvas supports (fabrics lose tensile strength), as well as organic paint binders (paint surface erosion). In thick samples, the surface layer

protects the deeper remaining colorant, restricting access to oxygen. [Fel94].

In general, following exposure, binding media, papers, and textiles are susceptible to yellowing and sometimes a slight darkening due to these chemical changes. In some materials, such as linseed oil, bleaching may occur. Changes in the absorption involving yellowing will mostly affect the short-wavelength portion of the visible spectrum (blues and violets), and these changes can have a drastic effect on the overall color balance of a work [Lau26].

Johnston studied this behavior with unsaturated plastic panels containing pigmented colorant, which were exposed outdoors in Florida [Joh67]. After six months of exposure, the panel had changed noticeably. A common measure of the magnitude of change is to compare colors that have been converted in a perceptually uniform color space (such as $L^*a^*b^*$). By design, the magnitude of the distance between any two colors in a perceptually uniform space, ΔE , determines how alike the colors are. This distance (or measure of perceptual similarity) is given by the Euclidean distance formula via Equation 3.12. The measured change that Johnston recorded in the panels was a ΔE of 1.5 $L^*a^*b^*$ units. There is a common misconception that $\Delta E = 1.0$ represents a just noticeable difference. Instead, a ΔE of one represents on the average, about *three-times* the value of a just noticeable difference [JF01]. Thus, the recorded change in the panels were *several times* more than the minimal perceivable amount of change.

The panel was pigmented with a greenish Cobalt Blue (5%) and Titanium Dioxide (95%). Johnston states that the spectral reflectance curves (illustrated in Figure 4.20) show that the concentration of the blue pigment, as illustrated by the absorption maximum at approximately 610-640nm, had not changed at all. All of the change occurred in the short-wavelength region due to the yellowing of the

material in which the pigment was dispersed.

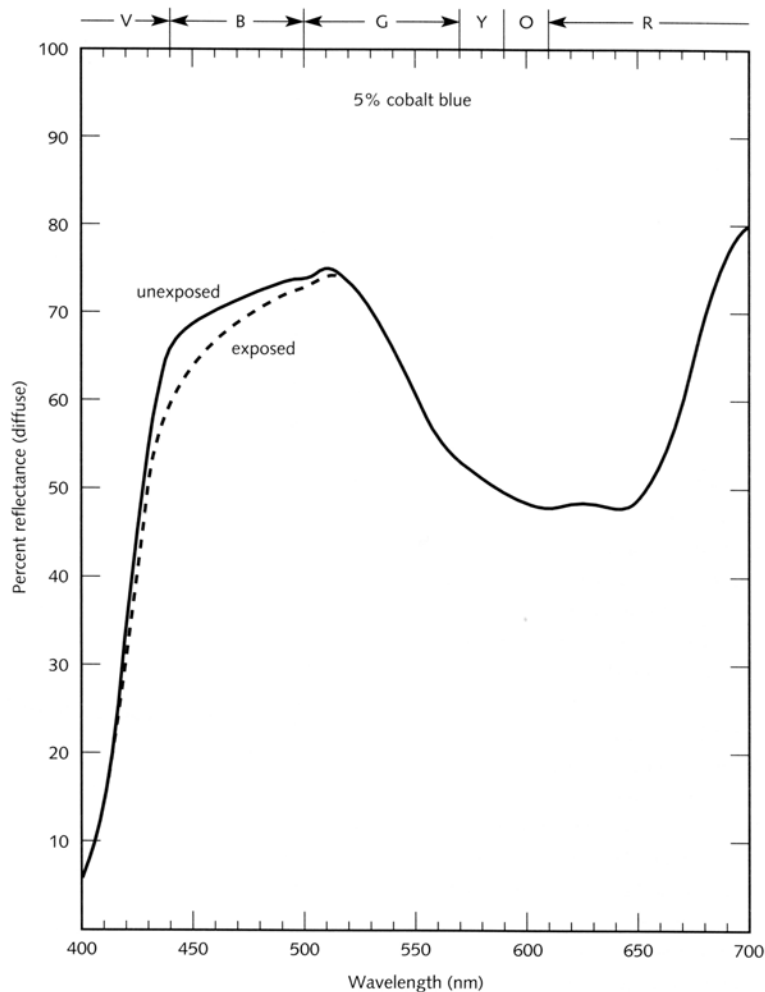


Figure 4.20: Curves of a colored plastic made with Cobalt Blue and Titanium Dioxide before and after exposure outdoors in Florida for six months. The perceived change in this instance is due to yellowing of the medium, rather than changes in the pigment. Adapted from [JF01].

An interesting and useful diagnostic tool for museum conservators concerned with color-balance deterioration due to yellowing was introduced by LaFontaine [LaF86]. It was proposed to view a work through a light source filtered to provide more blue light and less yellow light, in order to help restore the reflected light distribution as if the yellowing of the medium had not occurred. In this method, the amount of correction can be adjusted via a dimmer on the filtered auxiliary

light source. This method is used widely by conservators and curators in viewing work that is suspect to yellowing deterioration of either the paint medium, textiles or paper.

Fading, darkening and perceived changes in color can result from reasons other than deterioration of the pigment or oxidation. Changes in the surface reflection at the paint-air interface may seem to indicate changes in colorant concentration. The gloss in high-gloss materials may decrease, thereby giving the appearance of fading. Gloss loss can be attributed to blooming, dirt and soot, or *microcracking*, arising from certain combinations of temperature, relative humidity and other climatic conditions. Matte finish samples may increase in glossiness (due to oils from fingerprints, burnishing or varnish), resulting in a perceived darkening of color. All of these types of changes are typically uniform over all wavelengths, while pigment changes are more likely to be only in selective ranges of the electromagnetic spectrum.

Spectrally uniform changes in reflectance can also be the result of changes at the pigment-medium interface. For example, if the suspending medium shrinks over time, microscopic voids surrounding the pigment particles may form. While Titanium Dioxide and Carbon Black dispersed in a stable plastic medium typically do not exhibit fading, the material in Figure 4.21 appears to have done so. Examination of the micrograph reveals existing voids around pigment clumps in many regions. These voids contain neither pigment nor media. They have a much lower refractive index than the surrounding materials, and thus scatter light very effectively. Consequently, this lightens the overall sample, which a viewer might perceive as pigment fading.

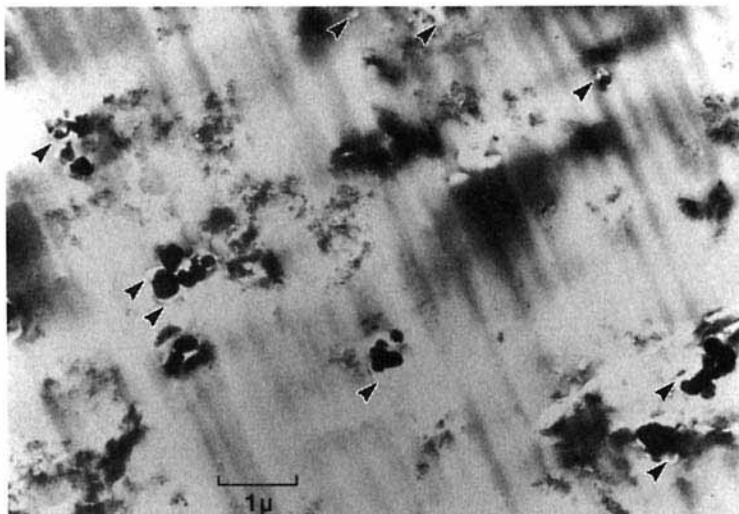


Figure 4.21: Transmission electron micrograph of a plastic pigmented with Titanium Dioxide (large black particles) and Carbon Black (clouds of fine black dots). The arrows point to voids that surround the pigment clusters. Adapted from [JF01].

4.3.4 Other effects

Studies carried out in recent years have shown that several categories of artists' colorants fade, many of them substantially, when exposed to common urban atmospheric pollutants. In these studies, air in a contained system was first purified with a carbon filter. Then, parts per billion (ppb) levels of the selected air pollutant were introduced to the purified air. A paint sample was exposed to the system for a given amount of time in the dark to measure the effect of the airborne chemical on the appearance of the paint.

Many chemical pollutants have been studied due to their possible impact on colorants in museum collections, since the substances are abundant in ambient and indoor air. The substances that have been studied include ozone [SC83, WCD87], nitrogen dioxide [WC89], nitric acid [SCG⁺92, GSC92], and peroxyacetyl nitrate [IGG93a]. These substances are all oxidants produced in photo-

chemical smog and have been identified as major pollutants in many urban areas of the world. Other studies of chemicals on artists' materials include the effects of formaldehyde [IGG92] and sulfur dioxide [IGG93b].

The significance of airborne chemicals can be readily seen from a few examples. Shaver and Cass found that several artists' pigments when applied to paper will fade in the absence of light when exposed to ozone at the concentrations found in photochemical smog [SC83]. The system exposed pigments with little protection from a heavy binder—watercolor on paper. The painted strips were cut in half: one subjected to the harsh ozone conditions, while the other placed as the unexposed control. The duration of the experiment lasted 95 days in 0.40 ppm ozone in the absence of light. Several of the pigments tested faded considerably during the experiment. The resulting reflectance spectra for the Alizarin crimson test and control samples are illustrated in Figure 4.22.

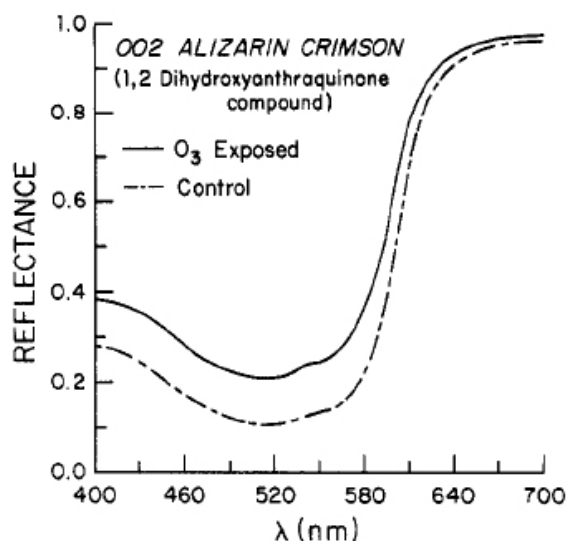


Figure 4.22: The effect of ozone on paint. Reflectance spectra of Alizarin crimson in a watercolor binder with and without exposure to 0.40 ppm of ozone O_3 for 95 days. Adapted from [SC83].

The ozone-exposed sample reflects more light across the spectrum, which per-

ceptually appears as adding white to the sample, giving a faded appearance. Several other pigments experienced similar results, though not all pigments underwent changes during the experiment. In unprotected atmospheres (without the use of activated carbon filters) it would take three (outdoor) to six (indoor) years to accumulate a dose (concentration times magnitude) of ozone exposure from the atmospheric ozone concentrations measured and reported in the work. Pigment size is also a major factor influencing the surface area exposed to the air, which may influence the rate of reaction with the chemical.

Similarly, nitrogen dioxide is a common air pollutant formed in the atmosphere from the nitric oxide emissions from fuel combustible sources. Whitmore and Cass found more than half of the natural organic pigment colorants studied had a significant color change $\Delta E > 2$ from exposure to 0.50 ppm NO_2 in air for 12 weeks [WC89]. A dose of this magnitude would be experienced inside an unprotected museum in a few years (2-6 years) in an urban setting. The procedure for the experiment was similar to that of the ozone exposure, mentioned previously.

All of these chemical effects are cumulative and irreversible. In relation to the duration of a piece of artwork, these pigment changes occur rather quickly. Care must be taken to protect artwork from such harsh conditions.

All in all, the appearance of color of pigmented materials is not constant and can be the result of a number of different factors. Through the use of spectrophotometers, one can accurately measure these changes over time. Through the use of mathematical predictive color mixing systems, such as Kubelka Munk theory, further changes can be predicted. Hopefully, this knowledge will minimize the risk of further deterioration of artwork for future generations. Equally enticing is the use of the data to travel back in time to see a painting in its original brilliance.

Chapter 5

Preparation & Measurement

5.1 Sample creation

To study the nonlinear relationship of paint appearance with varying pigments and binding media over time, a number of paint samples were created. Pure pigments were dispersed in a number of different binding media and each applied to a primed piece of canvas. Great care was taken to make sure the samples were of the highest quality. The diffuse reflectance of each sample was measured over the visible spectrum at different intervals in time.

5.1.1 Importance of handmade samples

Historically, painters knew their pigments intimately, as they would hand select materials from reliable sources and mix their paints by hand. After the introduction of commercial paint manufacturing, artists were separated from this process and bought tube colors without knowledge of their origin. Further obscuring the origin of their pigments, paint manufacturers sold their colors under confusing and sometimes misleading proprietary names. The practice of documenting the exact

ingredients used in a batch of paint has only become more commonplace recently, and still it is not widely practiced.

In addition, commercially manufactured paint contains not only pigment and binder, but often other substances to reduce manufacturing costs, adjust visual and handling characteristics, and increase the shelf life of a paint. A specific hue may be diluted with an *extender* or *filler* to reduce costs. Typically, this practice is done more frequently in student grade paints, and as a result, they have a greater percentage of fillers than professional artist grade paints. Also, fillers tend to accompany rare and expensive pigments to maximize hue volume. Dextrin is a common filler for aqueous media, used to bulk out paint without noticeably affecting the color. Fine grades of inert powders often serve to bulk out colorants in paint—calcium carbonate, chalk, whiting, ground marble, and limestone are all common fillers. While some fillers may not adversely affect the optical properties of pigments much, too much filler can degrade color appearance, producing a whitish, thin or bland color. However, in some cases fillers are beneficial. In an attempt to balance the high tinting strength of some pigments, filler is added to dilute the pigments' strength to a comparable degree to that of others. As a result, high tinting strength pigments will not overpower mixtures on a palette.

Other substances are purposefully used to modify the appearance of a hue in commercial paint. Some commercial brands add highly refracting substances as a *brightener*, to adjust the lightness of the finished color. Typically brighteners are clear or white particles of a comparable size to that of the pigment. Optical brighteners generally operate by way of absorbing ultraviolet radiation and then immediately re-admitting the energy in the visible blue-white range. Aluminum trihydroxide is the best and most widely used material for brightening and ex-

tending transparent pigments used in glazing and printing inks, while *blanc fixe* (barium sulfate) is used for heavy, opaque pigments [May81]. Precipitated chalk or titanium dioxide is typically used to brighten gouache colors. While used in proper proportions (Mayer states this is around 10%), brighteners may not be considered an adulterant. Yet, an excess of brightener can lead to whitening or sparkling effects on the dried surface. Furthermore, this substance sometimes compromises lightfastness.

Some manufacturing additives extend the shelf life of paints. A *dispersant*, or wetting agent, is sometimes added to improve the milling of a pigment and prevent clumping of pigments after manufacture. Thus, dispersants are common with finely divided synthetic pigments and soft pigments that can compress and cake easily. Ox gall and alcohol are commonly used wetting agents for aqueous and oil-based paints. A painter will notice the presence of such a material as it reduces the time it takes for a paint to dissolve and diffuses aggressively when painted “wet-into-wet”.

Manufacturers also add varying levels of *preservatives* to prevent solutions from decomposing on storage—aqueous media such as casein, gums, glues, and honey are particularly susceptible to these effects. Decomposition may occur from mold, bacteria, or fermentation. Sodium orthophenyl phenate and beta naphthol are both powdered substances that work well as preservatives for aqueous paints [May81]. Mayer recommends the proprietary fungicide Moldex to suppress the growth of mold or bacteria.

While additives increase the marketability of a paint (increased shelf life, decreased costs), at times pigments only comprise of a small portion of the total volume of commercially manufacture paints. Furthermore, the reader is warned

that pigment names used on tubes of artists' colors are not necessarily those of the actual pigments. Johnston and Feller analyzed four tubes of artists' watercolors labeled *Indigo* [JF63]. Natural Indigo (a violet-blue colorant) originally comes from the leaves of the plant *Indigofera tinctoria*, which is cultivated in India.

Spectral curves of the diffuse reflectance of the four indigo paints are shown in Figure 5.1. It was found that of the four manufactured paints, only one tube contained the real pigment Indigo (curve 4). The others contained a diversity of pigments of varying degree, which included Phthalocyanine blue, Iron blue, Ultramarine blue, Phthalocyanine green, Pyrazolone Red, and even black. None of the other three paints (curves 1-3) included true Indigo as an ingredient at all.

The cause could be the result of a number of economic factors, including the use of multiple synthetic pigments. Typically, the practice of combining multiple synthetic pigments to match a more expensive pigment is denoted with the word *hue* at the end of the name of the pigment. A synthetic *hue* pigment is rarely more than a fair approximation of the original's masstone. It is fairly straightforward to match a pigment with multiple colorants. However, the replacements rarely account for other properties of the true pigment, such as the appearance in mixtures with white, tinting strength, opacity, etc.

In an attempt to clarify the components of proprietary mixtures and confusing naming schemes, the standard method of naming pigments worldwide is by means of their *color index* name and number, plus the five-digit constitution number. The general name is based on the most common method to which a colorant is applied (P for pigments). Among pigments, there are nine hue descriptions: blue (B), green (G), violet (V), red (R), orange (O), brown (Br), yellow (Y), white (W) and black (Bk). Following is the general number, referring to the particular type of

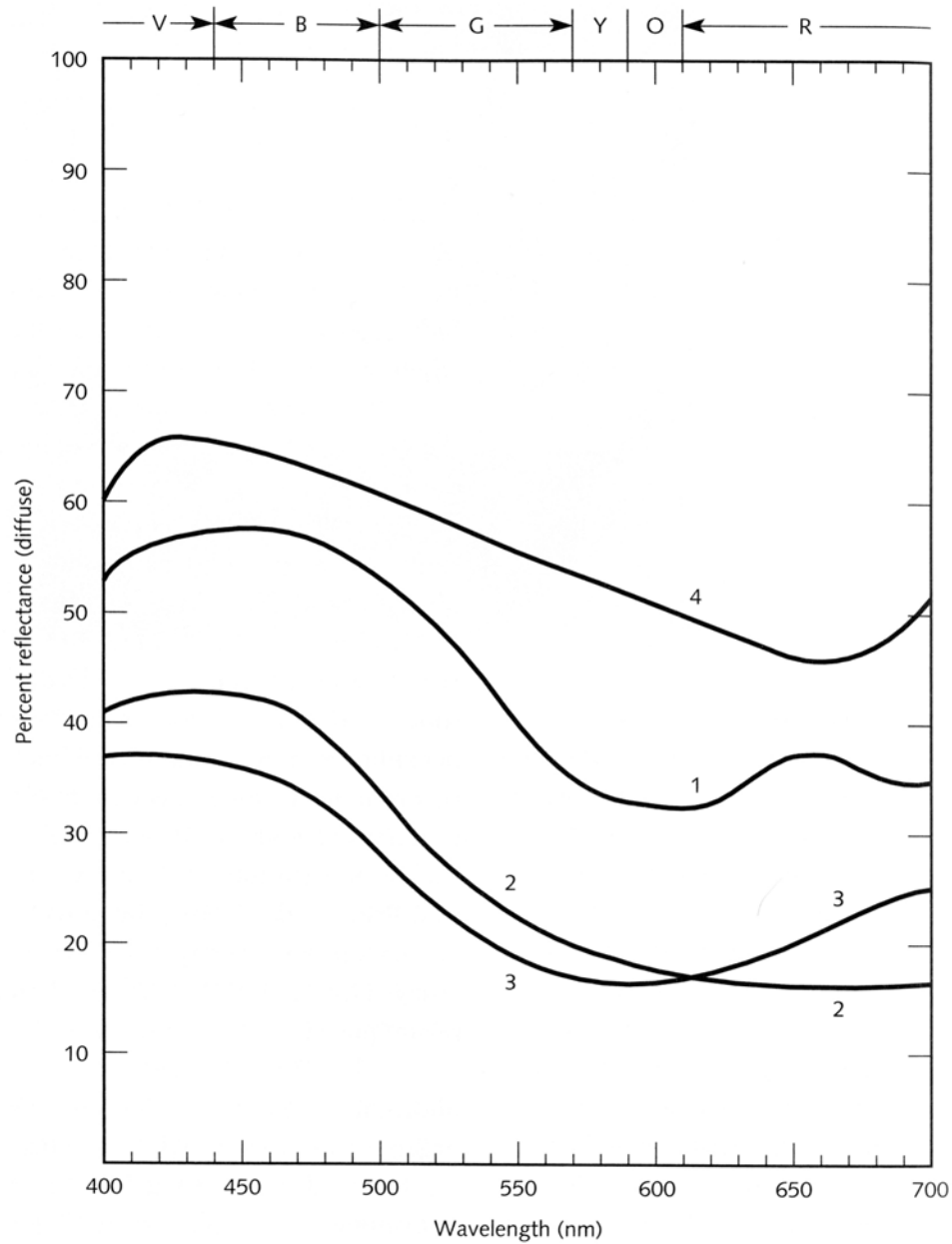


Figure 5.1: Spectral reflectance curves of four tubes of watercolors, all labeled *indigo*. Only curve 4 is real *indigo*. Curve 1 is a mixture of Phthalocyanine blue and black; curve 2 is Iron blue, Ultramarine blue, and black; curve 3 is Ultramarine blue, Phthalocyanine blue, Phthalocyanine green, Pyrazolone red and black. Adapted from [JF01].

pigment. A five-digit number follows the generic name and number, indicating the chemical composition of each colorant, if known (some pigments have no number, as their exact chemical structures are proprietary). As an example, the full color index for Titanium Dioxide white is PW 6 (77891). A more complete discussion of the color index is found in [Ber00].

Ultimately, while many of the major art manufacturers today are honest in their labeling, the practice is not universal, and certainly was not so in the past. Thus, one must still proceed critically even when paint labels list a particular hue or when artists document the palettes they use. As paints are predispersed by suppliers of artists' materials, there is always the possibility of extraneous additives in paint. Mislabeling, synthetic materials, and other substances can all affect the resulting appearance if a pigment in solution. As such, in our research to study the affects of varying binding media over time, we agreed that it was imperative to create all of the paints by hand, rather than purchase premade tube paint. This ensures that only the purest materials went into each paint, eliminating any outside factors. In this manner, the exact same pigments of pure composition are used in the different media. This also ensures that our paints are only made from pigment and binder. There are no inert fillers to dilute pigments, affecting the pigment volume concentration, nor are there materials that affect the chroma or lightness of the hue.

5.1.2 Pigments

With the many colorants available to the modern painter, it is difficult for an artist to choose a finite palette that comprises a sufficient variety to fulfill all of his/her color requirements. The choice typically depends on the artist's preference and

the requirements of the work at hand. A palette that contains less than a dozen colors can be considered a simplified palette, while more than fourteen would be an elaborate palette. Successful painting can be done with a very limited palette, and there are some advantages to doing so. Painters typically receive training with simplified palettes as a matter of discipline; this enforces a sort of color harmony, as hues in a work are derivatives of one another. However, in the majority of cases, it is generally beneficial to have a range of colors available. Single pigment colors are invariably purer than mixtures that imitate them.

The pigments chosen in our work are an attempt to maintain a typical artist's palette, which maximizes the gamut of colors available, while minimizing the amount of pigments that needed to be studied. Neither artists nor scientists wish to perpetuate an excessively large number of unessential items to paint with or study. The author (originally trained as an artist) chose a representable portion that spans Mayer's hue designations in his modern approved list of pigments [May80]. While there may be other (possibly superior) pigments available, each is long established as a useful colorant tool and has its own individual characteristics.

There are many sources of pure pigments available, including *Kremer Pigments (New York)* and *Sinopia Pigments (San Francisco)*. For our research, we decided on *Rublev Pigments* from *Natural Pigments (Willits, CA)*. This line contains a wide variety of naturally occurring earth colors, which were available to historical painters long before the commercial manufacture of artificial pigments. Earth colors also tend to have a very high permanence and lightfastness rating. While synthetic variants have approximated many of these colorants, many still hold a permanent spot in artists' palettes and have done so for thousands of years. The colorants were also chosen such that they were compatible with the many different

binding media in consideration.

A description of the 11 chosen pure pigments follows. *Natural Pigments* provides a great deal of information about the composition and background of each pigment [Fig05]. A much broader analysis of artists' pigments can be found in texts such as [Web23, May81]. Important pigment data is organized in Tables 5.1.2-5.1.2. Magnified images of the pigments are seen in Figure 5.2.

Lapis lazuli. Natural ultramarine (literally, *over the sea*) is the standard blue color in artistic use. The costly rare pigment comes from a semiprecious stone *lazulite* and its manufacture often contains golden specks of iron-pyrites (FeS_2). The mineral has been mined for centuries from Afghanistan, but also comes from Russia and Chile. The rich blue is one of the most chemically complex of pigments. It is a transparent hue that is rarely used full-strength; instead it is utilized in glazes and for tinting other colors.

Cold glauconite. Terre verte (green earth) is a semi-opaque pale green pigment, typically formed on submarine elevations of ancient seabeds and in sedimentary rock formations. The most famous mineral deposit was near Verona, Italy, but is now comes from the Baltic States and near Moscow. Glauconite is not found in large accumulations, and must be processed to obtain the mineral from the clay or sand. Since it contains some clay, it absorbs binder at a moderate to high rate. Terre verte is often used in glazes to produce an cool olive hue, as it is popular in the underpainting values for flesh tones.

Chrome yellow. Yellow oxide occurs naturally as yellow ochre, which is comprised of limonite (hydrated iron oxide) and goethite. Chrome yellow is a bright pigment with good hiding power and a fairly high absorption rate. Both iron hydroxides and iron oxides have been used since prehistoric times, and is perhaps



Figure 5.2: Left: Magnified view of the pigments used in our research. Right: magnified further. (a) Lapis lazuli, (b) Cold glauconite, (c) Chrome yellow, (d) Gold ochre, (e) Raw umber, (f) Burnt sienna, (g) Red ochre, (h) Hematite, (i) Cold hematite, (j) Lampblack, (k) Titanium dioxide.

Table 5.1: Relevant data regarding pigments used in research. Adapted from [Fig05].

Mineral name	Pigment name	Color Index	Chemical name	Chemical Composition
Lapis lazurite	Lapis lazurite	PB 29 (77007)	Sodium Calcium Aluminum Silicate Sulfate	$(Na, Ca)_8Al_6Si_6O_{24}(S, SO_4)$
Cold glauconite	Terre verte,	PG 23 (77009)	Hydrated Iron	$(K, Na)(Fe^3, Al, Mg)_2$
	Green earth		Potassium Silicate	$(Si, Al)_4O_{10}(OH)_2$
Chrome yellow	Chrome yellow,	PY 43 (77492)	Hydrated Iron Oxide	$Fe_2O_3 \cdot H_2O$
	Yellow oxide			
Gold ochre	Gold ochre	PY 43 (42)(77492)	Hydrated Iron Oxide	$Fe_2O_3 \cdot H_2O$
Raw umber	Raw umber	PBr 7 (77491) (77492)(77499)	Hydrated Iron Oxide (partial component)	$FeO^{3+}(OH)$
Burnt sienna	Burnt sienna	PBr 7 (77491)	Iron Oxide (partial)	Fe_2O_3
Red ochre	Red ochre	PR 101 (77491)	Hydrated Iron Oxide	$Fe_2O_3 \cdot H_2O$
Hematite	Indian/Venetian red	PR 101 (77491)	Iron Oxide	Fe_2O_3
Cold hematite	Caput mortem	PR 101 (77491)	Iron Oxide	$Fe_2O_3, Fe_2(SO_4)^3$
Lampblack	Lamp/Carbon black	PBk 6 (77266)	Amorphous Carbon	C
Titanium dioxide	Titanium white	PW 6 (77891)	Titanium Dioxide	TiO_2

Table 5.2: Relevant data regarding pigments used in research. Adapted from [Fig05].

Mineral name	Origin	Density ($\frac{g}{cm^3}$)	Hardness (Mohs)	Refractive index	ASTM rating ^a
Lapis lazurite	Cordillera, Chile	2.38 – 2.9	5.6	1.50	I/I/I
Cold glauconite	Baltic states, Europe	2.2 – 2.9	2.0 – 3.0	1.551 – 1.569	I/I/n.r.
Chrome yellow	(not specified) ^b	2.9 – 4.3	4.0 – 5.5	2.260 – 2.398	I/I/I
Gold ochre	Voronezhskaya, Russia	2.9 – 4.3	4.0 – 5.5	2.260 – 2.398	I/I/I
Raw umber	Khot'kovskaia, Russia	3.3 – 4.3	5.0 – 5.5	2.260 – 2.398	I/I/I
Burnt sienna	Luberon, France	3.3 – 4.3	5.0 – 5.5	2.260 – 2.398	I/I/I
Red ochre	Izyumskyy, Ukraine	2.9 – 4.3	4.0 – 5.5	2.260 – 2.398	I/I/I
Hematite	Kerch, Russia	5.27	5.0 – 6.0	2.78 – 3.01	n.r./I/I
Cold hematite	Novgorod, Russia	5.27	5.0 – 6.0	2.78 – 3.01	n.r./I/I
Lampblack	(not specified)	1.77	(not specified)	2.42	I/I/I
Titanium dioxide	(not specified) ^c	4.00	(not specified)	2.72	I/I/I

^aThe ASTM lightfastness rating is given for the binders (acrylic/oil/watercolor), unless not rated (n.r.)^bNatural yellow oxide comes from South Africa, India, France, Russia and the United States.^cTitanium Dioxide is processed in both the United States and Norway.

the most widely used pigment (many of the pigments on this list are derivatives of similar minerals).

Gold ochre. Similar to yellow oxide, Gold Ochre derives its color from iron hydroxides. The content of iron oxide must not be less than 12% to be considered an ochre. Depending upon the content of hydrated iron oxide, the color of ochre varies from light yellow to golden. While ochres occur all over the world, Mayer states that the best are mined and refined in France [May81]. It is one of the oldest traditional artists' pigments, is typically very opaque and dries to an excellent film.

Raw umber. UMBER (literally *shade*) is one of the most widely used browns. It is a variety of ochre obtaining its color from the presence of iron hydroxides (45-70%) and manganese oxide (5-20%). Historically, the pigment was mined near Umbria, Italy, but now the best umbers are mined primarily in Cyprus. The pigment has a high opacity and tinting strength. Due to its manganese content, umber hastens the drying of media, but forms a good, flexible film.

Burnt sienna. The pigment sienna owes its name to the Tuscan hills surrounding Siena, Italy. Raw sienna is hydrated iron oxide closely resembling yellow ochre (40-70% hydrated iron oxide content). When a limonite, like sienna, is calcined (or roasted) at high temperatures, its water content is eliminated and it becomes a hematite (anhydrous), or burnt sienna. This process changes the pigment to have exceptional translucency (different from most other earths) and a deep rich hue. Burnt sienna is one of the most useful and versatile pigments: its masstone a reddish brown, its glaze a fiery red, its tint with white a salmon pink. This pigment is highly absorbent of binding media.

Red ochre. Natural red ochre has a greater percentage of iron oxide than does its yellow counterparts, to which yields its characteristic red color. French ochre,

historically one of the best grades of limonite, contains about 20% iron oxide and is high in silica. Ochres are among the most permanent hues on the palette and absorb a medium amount of binder.

Hematite. The native mineral hematite (also hæmatite) is essentially ferric oxide, occurring almost chemically pure (approximately 95%) without the presence of water. It has been a source of supply of for natural red pigments since the earliest classical and ancient times—many other pigments are basically hematite with varying degrees of mineral impurities such as clay, chalk and silica. Natural red iron oxides are mostly of dark hue and equally as permanent and dependable as those synthetically prepared. The high purity leads to high tinting strength and opacity. The red iron oxides are among the basic, original pigments usually considered indispensable—one seldom sees a palette that does not contain at least one of them.

Cold hematite. Familiarly known as Caput mortem, this pigment includes small amounts of iron sulfate and other impurities usually associated with hematite, giving the pigment a deep violet hue. It maintains the same qualities as hematite, as the concentration of ferric oxide is comparable.

Lampblack. This pigment is a black of commercially pure carbon. The finer varieties are obtained from wick lamps in which fluid fatty oils rich in carbon are burnt with insufficient air for complete combustion. The soot is collected from plates held in the flame. Lampblack is a very strong color, whose origin dates back to antiquity. It has considerable opacity, and is very stable and permanent. It is very fluffy, of a low specific gravity and absorbs a large portion of binder.

Titanium dioxide. This pigment is a development of the 20th century. It has eclipsed other traditional white pigments due to its high opacity, nontoxic nature

and reasonable cost. It is extremely inert and unaffected by very harsh conditions. Titanium pigments are dense and heavy, and have great hiding power.

5.1.3 Media

In our research we also studied the effects of many various media on the chosen pigments. Each binder imparts its own characteristic optical and textural qualities, as well as maintaining a specific tactile behavior while working. Many different binding media have been discussed in detail in Chapter 2.

To accurately compare different types of binding media, it was necessary that all of the considered media be able to be applied in a similar fashion to a consistent support. Typically, this is not a concern as most media can be applied to the same types of supports—whether it is canvas, panel, or heavy weight paper. Unfortunately, fresco painting does not fit the stereotypical type for binder, as it is applied directly to masonry. Thus, we were unable to study fresco in this work, as creating many small samples of this material would have been too difficult.

Descriptions of the eight binding materials we studied, including more specific details on their composition follow:

Acrylic. The specific acrylic polymer emulsion used was Acrylex Thick Medium #33 from Pearl Paint (New York). The medium is reasonably thick by itself and is considerably opaque while wet. If desired, the medium can be thinned with water to improve handling. One must keep brushes wet as the binder dries to a waterproof film. The translucency increases upon drying.

Casein. Rather than casein powder, premixed borax-hydrolyzing casein from Schmincke (Erkrath-Unterfeldhaus, Germany) was used. For painting, the directions called for the medium be thinned 1:1 with water, though in practice this

created far too strong of a binder, resulting in cracking in many of the paint films. Instead, we settled on a mixture of 2:3 casein to water, with good results. Milk paint dries waterproof, though it must cure for a certain time (usually about a month).

Distemper. Powdered rabbit skin glue can be obtained at any art supply store (Gamblin Artists Colors Co.; Portland, OR). Mix one part dry hide glue with ten parts water and let it sit overnight—the glue will swell and absorb the water. If present, pour off any excess water and warm the glue in a double boiler. The double boiler will dampen the heat to a slow rise, as hide glues should never be heated above 150°F, save risking the integrity of the adhesive. The glue will melt with heat and needs to be kept warm while working. The glue has a thin consistency while warm, but thickens considerably as it cools. The resulting paint dries quickly to a flat and strong film.

Gouache. Most recipes are identical to that of watercolor (a solution of gum arabic), though white pigment and/or chalk is typically added to increase the opacity needed for gouache. We wanted to avoid adding filler to any of the materials. Therefore, we used a synthetic alternative for gouache. The Kremer (New York) gouache recipe calls for 100ml Mowiol and 2g Preventol. Combining the two substances results in a medium thicker in consistency than casein, but thinner than the acrylic polymer. To ease spreading, we added a slight amount of water to the solution. The resulting film displayed the same characteristics of traditional gouache: great hiding and flat color.

Encaustic. Bleached beeswax can be obtained from any art supply store. Chunks of the wax are first heated in a double boiler. After the wax had completely melted, it was mixed 1:1 with mineral spirits to increase fluidity (Gamsol:

Gamblin Artists Colors Co.; Portland, OR). Note that the media congeals quickly without constant heat. The author found that an ideal way of working is to use metal muffin tins on a hot plate for each paint mixture. This keeps the wax molten to work effectively while combining the pigment-media solution.

Oil. There are many oil-painting mediums in use by artists—typically varying combinations of oil, varnish and turpentine. Refined linseed oil is the best for artists' paint. This linseed oil is of a straw color and is obtained from any art supply store (Sunnyside; Wheeling, Illinois). Also, a very small amount of Gamsol mineral spirits is added for consistency.

Tempera. Pure egg yolk, separated from the white is the emulsion for tempera. To separate the contents of an egg, first cleanly break the shell into two halves. Carefully alternate the yolk pouch from one half shell to the other, removing as much of the white as possible. Now, the pouch is rolled dry on a paper towel. Be careful not to dry the pouch too much, as the skin may catch and break open unexpectedly. With one hand, pinch and hold the pouch over a jar. As one punctures the pouch with a sharp tool in the other hand, the yolk will freely run into the jar. Fresh egg yolk must be used in tempera painting. Hence, paints are made fresh daily with yolk and a small amount of water.

Watercolor. Gum arabic provides the adhesion for watercolor paints. Crystals of the substance (Kremer; New York) are combined in a ratio of 1:2 with water. The gum arabic is left to sit in the water for the crystals to dissolve (1-2 days). The solution is heated in a double boiler until the solution is completely dissolved. At this point, the author recommends filtering the solution with cheesecloth to remove any impurities (i.e. small pieces from the accacia tree). A one-half part of glycerin is added as a plasticizer, which keeps the finished paint from becoming

too brittle and cracking. While working with pigments, slightly more water can be added as needed.

5.1.4 Substrate

The magnitude of the number of samples demanded that the substrate to which paint was applied had to be easy to make and provide a consistent surface. The device used to measure the diffuse reflectance governed the size of the sample. The samples needed to be circular with a diameter of 19mm to reasonably fit in the measuring device. In order to provide enough space on each sample for both priming and painting, each sample was made to be approximately 31mm in diameter.

The samples needed to be sturdy and suitable for many drastically different types of binding media. Canvas or paper are too flexible of supports to be used in conjunction with brittle binders (Casein, for instance, would be very susceptible to cracking on such supports). Also, it is important that the support for all of the samples in the research be consistent, as different supports for different media may introduce unwanted errors. Therefore, the work demanded rigid supports.

Mounted canvas was chosen for the surface characteristics of canvas, as well as ease of operation. The canvas selected was the inexpensive, readily available, cotton duct fabric. A template for the desired shape and size was made, and the canvas is easily cut with scissors. The backing also needed to be easy to cut rapidly. Quarter-inch Fome-Cor[®] board was chosen for this purpose. It is a polystyrene core bonded between high-quality papers to provide a lightweight, rigid, smooth surface. It resists warping (though on this scale, this is not much of a concern) and is easily cut with the sharp blade of an X-acto[™] knife on a cutting mat. Each

backing piece is cut to the exact size of the circular canvas pieces.

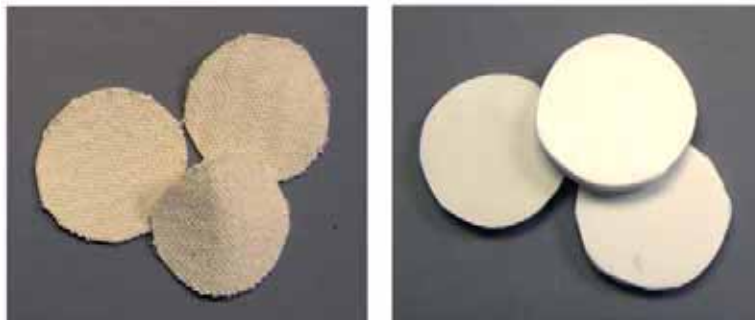


Figure 5.3: Cut canvas and board pieces used to make the sample supports. Each is approximately 31mm in diameter.

21 pigmented mixtures and 8 binding media demanded 168 supports. Two of each were made for a total of 336 pieces of both canvas and board. We used an archival craft glue (Archival Quality Photo-Safe Glue from Delta Technical Coatings) to attach each canvas piece to its respective board. The manufacturer reports independent tests confirming the quality, longevity and non-yellowing formula. It works well for porous surfaces and dries quickly to a clear and permanent surface.

The next stage in preparation of the supports was priming. A synthetic gesso (available at any art supply store) was chosen instead of glue size and traditional gesso. The main reason for this type of gesso was ease of use—it can be used as a primer without the previous application of a glue size. Since there were such a large number of samples that needed to be individually primed, this would allow for the much quicker creation of samples, as one step had been eliminated. As a primer, it provides a sufficient surface for a variety of binding media. The substance dries quickly to a completely waterproof and flexible surface. It does not age, yellow or crack over time. Over a four month period of time, we measured that there was only a 0.0348% change on average in the diffuse reflectance over the visible spectrum for our three-coat gesso ground.

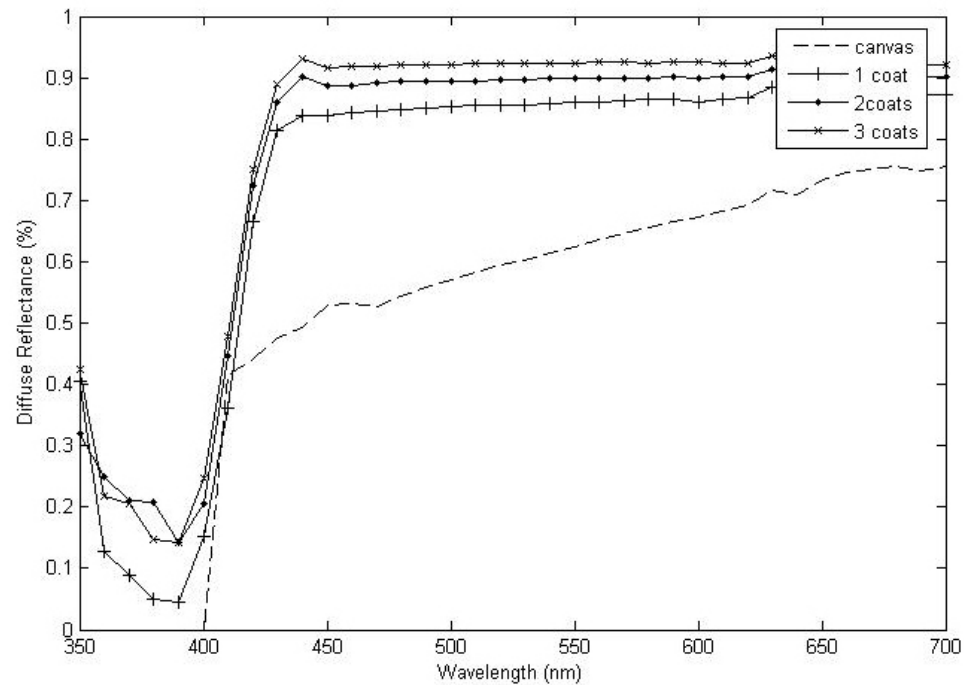


Figure 5.4: Reflectance values for multiple layers of gesso on the canvas board support. Clearly, unprimed canvas does not provide adequate protection or a highly reflecting surface. Increasing layers of gesso serve as much better grounds as they reflect light better over the entire visible spectrum. Corresponding images are seen in Figure 5.5.

Canvas is typically very absorbent. Hence, one coat of gesso typically does not completely hide nor protect the support. As such, the desired optical effects of gesso are not observed unless multiple coats are used. Each additional coat provides a more luminous and reflective surface as seen in Figure 5.4. In the figure, one notices the influence of multiple coats of acrylic gesso. Typical for white paints, there is a high reflectance across all wavelengths of light. The percentage of light reflected increases as more coats of gesso are applied to the support. This is an important trait, as light that enters a paint film and hits the ground will reflect back into the film, creating a more luminous surface. Grounds that are not highly reflective result in paintings that are less vivid in appearance.

In our work, we chose to apply three layers of gesso to each canvas board support. Each layer must be carefully hand painted to ensure a uniform surface. This is done after the preceding layer is completely dry, save risking pulling up previous layers. Too little gesso will result in a poorly reflective surface, while too much will result in an uneven surface. The resulting visual appearance of each layer of gesso can be seen in Figure 5.5.



Figure 5.5: The visual difference between different amounts of acrylic gesso applied to canvas board. From left to right: unprimed canvas, one coat, two coats, and three coats of gesso.

5.1.5 Painting

After the layers of gesso had thoroughly dried, the support was ready to be painted. Many pigment masstones are dark, making it difficult to determine the characteristic absorption bands. As a result, a tint of each pigment was also made with titanium dioxide white. We studied 21 pigment mixtures: 11 pure pigments and 10 tints. The measured ratios in tints had to be very precise to ensure reliability of the data. Tints were made with 50% colored pigment and 50% Titanium Dioxide. We combined each pigment mixture with the eight different binding media. For every pigment-binder mixture, we painted two samples to make sure that we had a sample of sufficient quality. In total there were $21 \times 8 \times 2 = 336$ painted samples. The author notes that this does not include the many samples that were not of adequate quality due to pigment-binder inconsistencies (cracking, clumping, agglomeration, flocculation, inadequate dispersion, etc.).

One binding media was created and measured at a time (for all pigment mixtures). Prior to painting a selection of samples, a specific binding media was made fresh. Some binding media lose adhesive strength if they are stored and reused at a later time. A measured ratio amount of binding media to pigment was combined in a plastic cup.¹ Painstaking care must be taken to prevent any impurities from entering a paint mixture. Contamination can occur at many stages in the painting process.

Kubelka and Munk found in experimentation [KM31] that the steel spatula used to disperse the pigment in the binder left minimal traces of iron in the paint due to the hardness of the pigment. In the particular case, the white paint had

¹Some pigments are toxic and care should be used in handling the dry pigment powder to avoid inhaling the dust.

somewhat reduced reflectance values. The authors found that after replacing the steel spatula with a glass one, the disturbance disappeared and reproducible values of covering power (about half as great) were obtained.

Therefore, we were very aware of every material touching the pigments, binding materials, and paint. Everything needs to be very clean at every stage to minimize any chances of disturbances, as the data is only as good as the measurements. Also, care has to be taken to make sure that the paint film opaquely covers the substrate; otherwise, the underlying gesso will influence the reflectance values of the paint. A painted sample, including the area of which is measured, is shown in Figure 5.6.

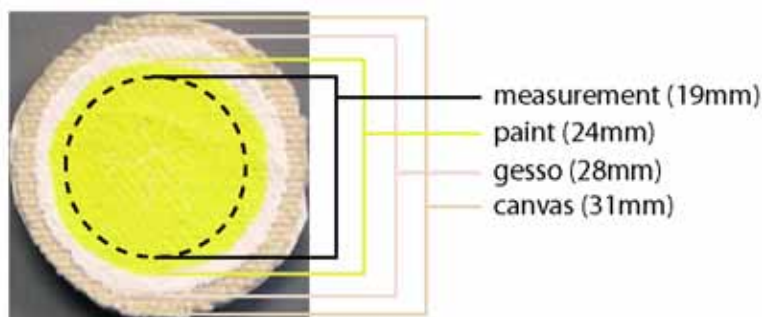


Figure 5.6: A typical painted sample—chrome yellow in gouache after 1 day. Given are the dimensions for an average painted sample. The measurement range is the area in which the diffuse reflectance is measured.

One paint (pigment-binder mixture) was created and applied at a time. This is due to the fact that some binders dry or congeal very quickly. Prior to painting, the back of each sample was labeled with the pigment or tint and media used, and the date painted. The vast amount of data required that the entire procedure be very organized. Immediately after painting a specific sample, it was quickly photographed against a gray card with a digital camera. A *gray card* represents the standard reflectance value which all photo light meters are calibrated against.

The gray card reflected 18% of the light that falls on it and was used to standardize the exposure of an image taken with a camera. Immediately after photographing the sample, it was placed in the sample port to measure its diffuse reflectance.

Distemper and Encaustic must be applied hot, as the consistency of the materials changes completely as the temperature drops. Upon cooling, the materials become very thick and difficult to apply. Hence, for these materials the binder must be kept in a metal container on a hot plate to maintain fluidity. All of the other media were relatively straightforward to apply to their respective substrates.

However, the author notes that problems will inevitably occur while creating one's own binders. One typically tests a binder before its widespread use. Binders with too high a concentration of adhesive will result in a paint film that is too strong, resulting in cracking. Binders that are too dilute will not adequately hold the pigment to the ground, resulting in pigments that rub or flake off. The delicate balance can be determined by brushing out a portion of a pigment-binder mixture. If, upon drying, the former problem occurs, or if it is difficult to brush out a consistent stroke, the solution must be diluted (water, turpentine, etc). If the latter problem occurs, more binder must be added to strengthen the solution. Unwanted issues may result due to inadequate dispersion of the pigments within the binder. In this case, one might experience agglomeration or clumping of pigments, creating an irregular surface. Also, evidence of the differences in pigment size and specific gravity may also show in tinted samples. Pigmented mixtures are susceptible to pigments separating out in solution if they were not adequately dispersed originally. Examples of cracking and inadequate dispersion are shown in Figure 5.7.

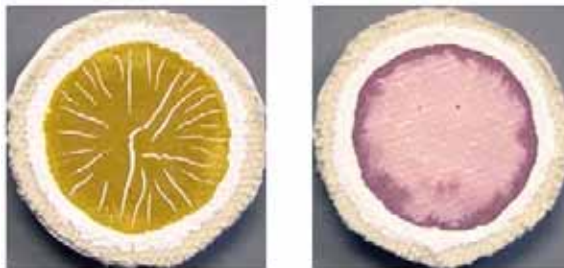


Figure 5.7: Possible problems arising from inadequate pigment-binder mixtures. Left: Too much adhesive in the binder solution leads to cracking in the resulting paint surface; right: pigments separating out of a tinted pigment solution due to poor dispersion.

5.2 Measurement

5.2.1 Spectrophotometer

All measurements were taken using the Optronics Laboratory Single Monochromator (OL 750-M-S). A *monochromator* is an optical device that transmits a selectable narrow band of wavelengths from broad spectrum incident light. Emitted light is provided to the monochromator via the OL 740-20A Source attachment. A sample's diffuse reflectance is measured via the OL 740-70 Integrating Sphere Reflectance attachment. The system is illustrated in Figure 5.8.

The source attachment contains a quartz halogen lamp capable of emitting energy in the electromagnetic spectrum of $250 - 2500nm$. The energy we are interested in (the visible spectrum) is only a subset of this lamp's emitting range (approximately $350 - 700nm$). The light from the lamp is collected via mirrors and directed towards the monochromator.

The monochromator is of the Czerny-Turner design, illustrated in Figure 5.9. Incident light from the source attachment (A) is aimed at the entrance slit (B). The slit is placed at the focus of a curved mirror (C), such that the reflected light

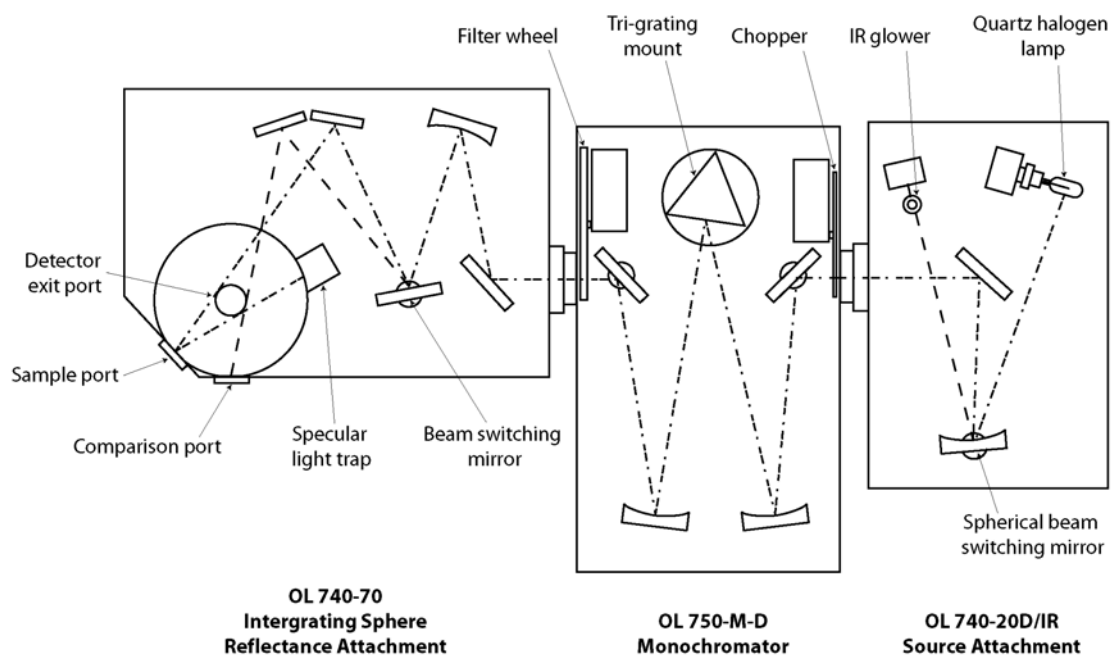


Figure 5.8: The optical setup for diffuse reflectance measurement. Source light is separated into pure wavelength-specific bands by the monochromator. A sample's response to each of these bands (for all of the visible spectrum) is measured and diffuse reflectance is calculated.

from the mirror is collimated (parallel). This light is dispersed into its various components upon striking the *diffraction grating* (D), as different wavelengths of light will reflect at different angles. The dispersed light is collected via another spherical mirror (E) and refocused on the exit slit (F).

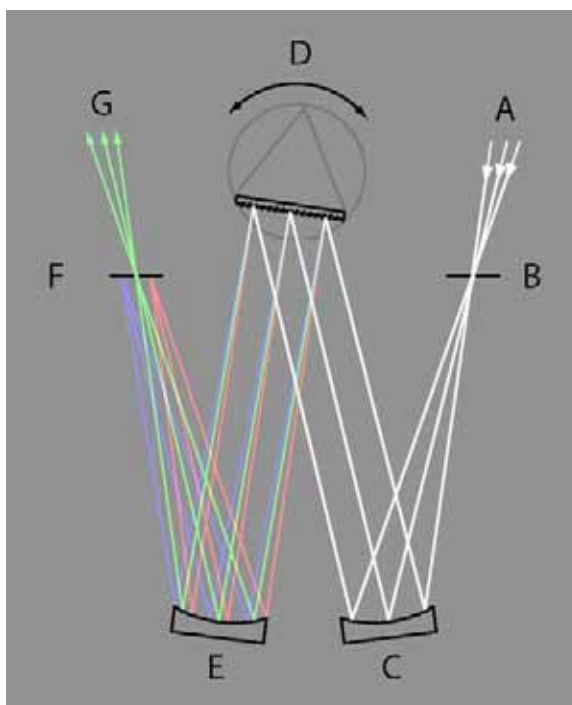


Figure 5.9: Diagram of a Czerny-Turner monochromator.

The desired bandpass of light exiting the monochromator (G) is yielded via rotating the grating (D) to the proper position. Diffraction gratings consist of glass and a layer of deposited aluminum that has been pressure-ruled with a large number of fine equidistant grooves. They are designed to be maximally efficient at specific wavelengths (by varying grooves per distance), hence multiple gratings are required to cover wide wavelength ranges. Also, the range of wavelengths leaving the exit slit (G) is a function of the slit widths (B & F), which are user interchangeable.

Note that harmonics reflect at the same angle (a harmonic is a integer multiple of a frequency $\alpha f \mid \alpha \in \mathbb{Z}$). Hence, to achieve the desired wavelength band, light exiting the monochromator is filtered. For example, light of 400nm reflects off the grating at the same angle as 800nm. If one desires the blue-violet band (400nm) and not light in the infrared (800nm), a filter must be in place to block the extraneous light.

5.2.2 Integrating sphere theory

The desired wavelength band of light is then passed to an integrating sphere in order to calculate the diffuse reflectance of a material. In an integrating sphere, light enters from a small aperture in the sphere and strikes a sample on the opposing surface of the sphere. The light is reflected off the surface of the sample to the entire sphere. The surface of the sphere is covered in a highly reflective diffuse material (typically Polytetrafluoroethylene (PTFE) for measurements in the visible spectrum range). Hence, multiple scattering events occur and the light diffuses over the entire sphere. At another portion of the sphere is a detector to measure the response of light striking that portion.

The basic theory for the integrating sphere has been evaluated analytically by Jacquez and Kuppenhiem [JK55]. In the *comparison method*, the integrating sphere reflectometer has a dual beam design. Incident light enters through an aperture in the sphere at one of two angles. Following these paths of light across the sphere, there are two apertures for samples—the test and comparison samples. A detector is placed at another location on the sphere.

The method requires four separate scans: two calibration scans and two test sample scans. During calibration, a standard reflectance sample of known re-

flectance is placed in the test aperture. The first scan is made with the light beam on the comparison sample, while the detector measures the response. The next scan is done with the beam focused on the standard sample. The calibration factor for the integrating sphere reflectance attachment is calculated at each wavelength [Lab94]:

$$C(\lambda) = R_{st}(\lambda) \left(\frac{S_c(\lambda)}{S_{st}(\lambda)} \right) \quad (5.1)$$

where

C is the spectral calibration factor for the integrating sphere at wavelength λ

$R_{st}(\lambda)$ is the reflectance of the standard reflectance sample

$S_c(\lambda)$ is the signal with the beam focused on the comparison sample

$S_{st}(\lambda)$ is the signal with the beam on the standard reflectance sample

For the test scans, the test sample is then placed in the test aperture. The third and fourth scans are done with the light beam focused on the comparison and test samples, respectively. The reflectance of the test sample is then calculated by [Lab94]:

$$R_{test}(\lambda) = C(\lambda) \left(\frac{S_{test}(\lambda)}{S_c(\lambda)} \right) \quad (5.2)$$

where

$R_{test}(\lambda)$ is the reflectance of the test sample

$C(\lambda)$ is the calibration factor calculated from Equation 5.1

$S_{test}(\lambda)$ is the signal with the beam focused on the test sample

$S_c(\lambda)$ is the signal with the beam focused on the comparison sample

Note that the calibration factors for a set of wavelengths are valid as long as the system setup does not change. Hence, the calibration scans need only to be executed once for multiple test sample scans. However, if for a different set of wavelengths, or more precise measurements are needed, the calibration must be repeated as the data cannot be extrapolated or interpolated. In practice, new calibration factors were calculated daily to ensure precision.

The instrument is designed to measure either the inclusion or exclusion of the specular reflection. The incident light is off the sample perpendicular by about 8-10°. Pure specular reflection will occur at the same angle equal and opposite to the incident angle (-8 to -10°). A light trap placed at the angle of reflectance will absorb the specular reflectance, such that only diffuse reflectance is measured. If a white port is inserted instead, the total reflectance is measured. The difference between the two is a measure of the specular reflectance.

Overall, the comparison method is very accurate in calculating the reflectance of a material. This is due to taking into account the change in efficiencies of the sphere when introducing the test sample. A more detailed account of integrating sphere theory can be found in [JK55].

5.2.3 Measurement

We calculate diffuse reflectance using the comparison method. In our work, standard sample is pressed PTFE (OL 25-RS Diffuse Reflectance Standard). A light trap was used to remove extraneous specular reflection from the measurement. The detector used to measure the radiant energy response was the OL DH-300 Silicon Detector Head, which detects over the range of 300-1000nm. The position of these devices is seen in Figure 5.8.

Measurements were taken for each sample at six different periods of time. The diffuse reflectance of the samples was measured directly after they were freshly painted, after one day, after one week, after one month, after three months, and six months after they were painted. From 21 pigmented mixtures and 8 different binding media, there are 168 different samples. Each sample's reflectance was measured over the visible spectrum (350-700nm) in 10nm increments. Hence, there are 36 wavelength-dependent reflectance values for each sample. Ultimately, each sample was measured six times for a total of 1008 time-dependent reflectance spectra (each of which contains the 36 wavelength-dependent reflectance values).

The samples were subjected to conditions similar to a less-traveled gallery. The atmospheric conditions were fairly constant, as the samples were kept indoors. The room temperature remained constant, at approximately 70°F. Illumination in the room was a combination of General Electric fluorescents Chroma 50 (which has a continuous spectral distribution similar to that of daylight) and Deluxe Specification Series 3500K (a tri-Phosphor lamp with very good color rendering and efficacy). Illuminance on the samples was between 235-560 lux. After creation, the samples remained face-up on a table, unless they were in the process of being measured, and were never touched on the paint surface.

Chapter 6

Experimental Results

6.1 Introduction

The acquired diffuse reflectance data forms a multi-dimensional space, where the desired spectrum is dependent on the pigment, binding media, and time interval. Analyzing the data of such a large hypergraph is difficult and different ways of presenting the data are covered in this section.

6.1.1 Effect of binding media

To study the effect of the binding media on a pigment in a paint solution, a specific time and pigment are held constant. This allows for direct comparison between paint samples of different binders. Given this situation, there are eight spectral reflectance curves for a given pigment-time combination (since there are eight different binders). Plotted against each other, this allows for comparisons of how the binder affects the absorption and scattering of wavelengths of light of a paint sample. These changes of light behavior are important to how we perceive color differences. As seen in Chapter 3, any change in the reflectance spectra will incite

a change in our perception of the color—our eye integrates the surface reflectance with the incident light against our color sensitivity matching functions.

In order to manage the dataset, an interactive viewer was made to browse between the 126 pigment-time combinations. This allowed for easier viewing of the data as one can quickly see the relationships between different samples. The online application was written in JavaScript, allowing for instant feedback from a user-specified pigment and time combination. After selecting the input parameters, the system presents a spectral reflectance plot of the eight different binding media for the chosen input data. The setup for the viewer is seen in Figure 6.1 for Lapis lazuli samples that have been dry for one day. The input data is chosen via drop-down menus in the top-left of the screen. To tint the chosen pigment, the checkbox is selected. Updating the graphics with new selections is done with the display button.

A photograph of the pigment is shown for reference in the top-right (for tints, titanium dioxide white is also shown). Also presented is the corresponding digital photograph for each paint sample, as spectral graphs are not a very intuitive way to analyze subtle color shifts. Yet, it is important to note that the spectral data is what is critical. Displays have significant limitations: monitors approximate colors using only three phosphors (red, green and blue), while printers only use four inks (cyan, magenta, yellow and black) to create images. As a result, many real-world colors cannot be captured by these devices. Therefore, any photographic representation will be an inadequate representation of the actual colors.

The importance of the spectral plots is that they show the behavior of light at *all* wavelengths in the visible spectrum. The spectral data combined with an illuminant and the eye's response curves can be predictive with no loss of information.

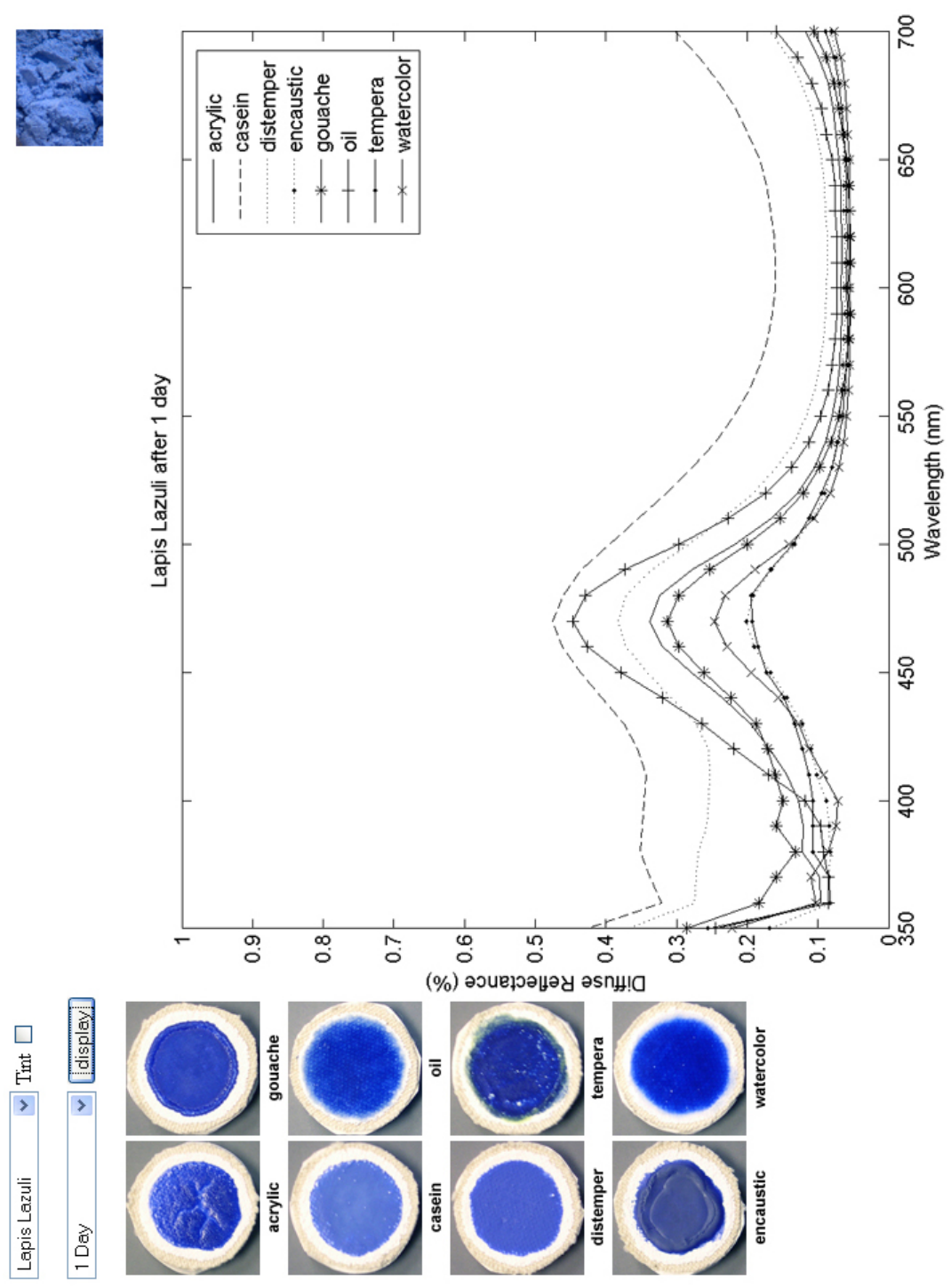


Figure 6.1: Lapis Lazuli in different binding media after one day.

However, while the photographs are not completely physically accurate depictions of the actual color of the samples, they do give the viewer a reasonable subjective comparison.

An important observation occurs when viewing the variation in binding media over the visible spectrum. Typically, the specific pigment determines the general shape of the spectral curve. That is, the intrinsic chemical properties of the material from which the pigment was created determines the central tendency of the material's reflectance, as well as the wavelengths that are primarily absorbed. Yet, the specific binding media determines the exact behavior of how light behaves when striking the material. Each material has its own characteristics that it imparts and one recognizes these differences in a work of art. A painting in one media will invoke a different sensation than that created in a different media. This relationship holds for all of the pigments in the study.

This observation is logical; as one of the criteria for a binding material is that it does not drastically affect the materials that are suspended within it. An artist expects a pigment to maintain a relatively specific hue, whether it is dispersed in oil or watercolor or another media. However, as seen with Lapis Lazuli, while the general color is similar between binding media, there is great variation in the resulting color between the different materials.

A common way to compare colors is to transform them into a perceptually uniform color space and study the results. This allows one to quantify the magnitude of the difference between colors. In our case, this can be used to evaluate how much binding materials affect the color of a pigment.

The basic computation is to first convert the spectral data into CIE tristimulus values XYZ . This is done using the response matching functions, an illuminant

(such as CIE standards C , D_{50} , or D_{65}) and Equation 3.3. Then, XYZ values can be converted into a number of nearly uniform color spaces, such as Munsell, CIE $L^*a^*b^*$ or CIE $L^*u^*v^*$.

Converting XYZ values into the Munsell color space is typically done via a three-dimensional look-up table, as there is no easy way to mathematically transform XYZ values into the Munsell space. Since the Munsell color space is defined by physical samples, the reflectances of the samples which define the space can be measured and converted into XYZ tristimulus values. From this data, one searches the table (such as from [Lab05]) for the nearest XYZ values. The Munsell HVC (hue, value and chroma) coordinates are found by linearly interpolating between adjacent points. Recently, it is of note that there has been a promising attempt to model a general transformation between reflectance spectra and the Munsell color system with good correspondence between the calculated and actual coordinates [LJP06].

Converting XYZ values into the other two spaces is much easier numerically. Tristimulus values XYZ are converted to $L^*a^*b^*$ using Equations 3.9 & 3.11. By design, the distance between any two points in the $L^*a^*b^*$ color system is nearly proportional to the perceptual color difference. Thus, the Euclidean distance (given by Equation 3.12) between any two color coordinates determines approximately the perceptual difference between the two colors. The Munsell color system is also a perceptually uniform space, though it is more difficult to define perceptual differences via a discrete number. Due to the cylindrical nature of the Munsell system, one has to take into account differences in arc length to compare different hues.

Fortunately, there is free software available from GretagMacbeth (the com-

Table 6.1: Color conversions from the spectral reflectances of the samples of Lapis Lazuli in different binding media, dry after one day.

	X	Y	Z	H	V	C	L^*	a^*	b^*
acrylic	10.04	10.50	28.19	2.54PB	3.76	7.06	38.73	0.67	-33.74
casein	21.35	24.01	45.42	8.86B	5.44	5.78	56.10	-6.60	-25.85
distemper	13.28	14.43	35.06	1.29PB	4.35	7.12	44.85	-2.62	-32.83
encaustic	7.75	8.06	17.09	2.54PB	3.32	4.18	34.12	0.96	-22.00
gouache	9.03	9.46	26.48	2.43PB	3.58	7.13	36.85	0.53	-34.33
oil	12.40	13.26	37.67	1.97PB	4.19	8.48	43.15	-1.18	-39.09
tempera	7.53	7.89	17.38	2.25PB	3.29	4.47	33.75	0.46	-23.24
watercolor	7.49	7.58	19.51	3.60PB	3.22	5.66	33.09	2.93	-28.66

pany who currently produces the Munsell Book of Color [Mun]), which computes many conversions from XYZ values (including Munsell HVC , $L^*a^*b^*$, RGB and $CMYK$) [Gre06]. Different color system values computed from the eight differing binding media reflectance spectra in Figure 6.1 are shown in Table 6.1.

We now have a discrete way of evaluating the magnitude of the perceptual differences ΔE between colors. Using the converted $L^*a^*b^*$ colors, one can estimate the perceived difference between colors via the magnitude of its distance from another color in space. Table 6.2 describes the distance between every $L^*a^*b^*$ color in Table 6.1. From this data, we can infer how Lapis Lazuli differs perceptually in the eight binding media. Small values of ΔE indicate that a pair of colors are very similar to each other, while large values show that the two colors are very different.

One can see that paint samples of Lapis lazuli in encaustic and tempera are the most similar colors after one day of drying. While the two samples are very

Table 6.2: Perceptual differences between binding media. Table of perceptual differences ΔE between colors using the $L^*a^*b^*$ color space. The colors are converted from samples of Lapis Lazuli in different binding media, dry after one day.

	acrylic	casein	distemper	encaustic	gouache	oil	tempera
casein	20.416						
distemper	7.008	13.825					
encaustic	12.616	23.561	15.660				
gouache	1.975	22.211	8.728	12.636			
oil	7.182	19.297	6.645	19.447	8.079		
tempera	11.623	23.583	14.989	1.387	11.515	18.501	
watercolor	7.920	25.064	13.656	7.021	7.214	15.063	5.993

similar (as the measure ΔE is small), they are still many times the average human's threshold for detectable differences. Also, by examining the data set from any of the color spaces (XYZ , HVC , or $L^*a^*b^*$), one can readily see the close relation between the two colors—the coordinates of both colors in each space are very similar. Therefore, it is safe to presume that the two samples have comparable spectral reflectance curves. Examining the data from Figure 6.1, one can see that the encaustic and tempera samples are nearly collinear.

In contrast, the colors that differ the most for Lapis Lazuli are the media casein and watercolor. Much of this difference is due to the drastically different values of luminance for the two samples. Using any of the color systems (XYZ , HVC , $L^*a^*b^*$), one notices in each that casein has the highest luminance (Y , V , or L^* , respectively) in each scale, while watercolor has the lowest. In the spectral reflectance plots, this is depicted as casein reflecting the most light over the visible spectrum while watercolor reflects much less light. A comparison of

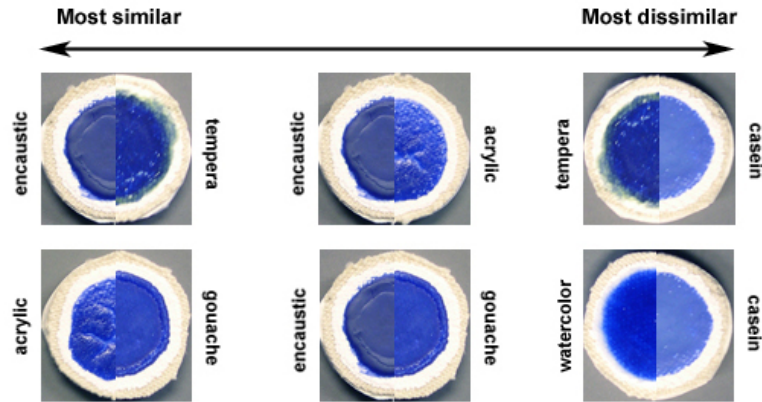


Figure 6.2: Similarity comparison of Lapis Lazuli paint samples. The similarity scale is computed by the Euclidean distance formula of the converted colors in $L^*a^*b^*$ space.

the most similar and least similar colors for Lapis Lazuli after one day are seen in Figure 6.2.

While CIE $L^*a^*b^*$ is useful in determining the relative differences between colors, a visual comparison is much easier in the Munsell color space. This is because it is built on the physical comparison between experimentally proven, perceptually equidistant samples. Figure 6.3 provides a set of Munsell color plots of Lapis Lazuli in the eight binding media. Here, one sees the many factors determining the difference between colors.

The Munsell quasi-cylindrical solid is shown in the top-left of the figure. The solid is comprised of ten leaves rotated around a central axis. Each leaf corresponds to the main hue pages of the Munsell color system (10RP, 10R, 10YR, 10Y, 10GY, 10G, 10BG, 10B, 10PB, and 10P). Note that the hue designations are red R , yellow Y , green G , blue B , and purple P . The ten leaf images (from [Gre06]) are each texture mapped onto a plane at equidistant angles around the center ($\theta = \frac{2\pi}{10}$). The maximum value of one hue (10) is the minimum of the adjacent hue (0). For example, the hue *red* goes from 0 (or 10RP) to 10R (or 0YR).

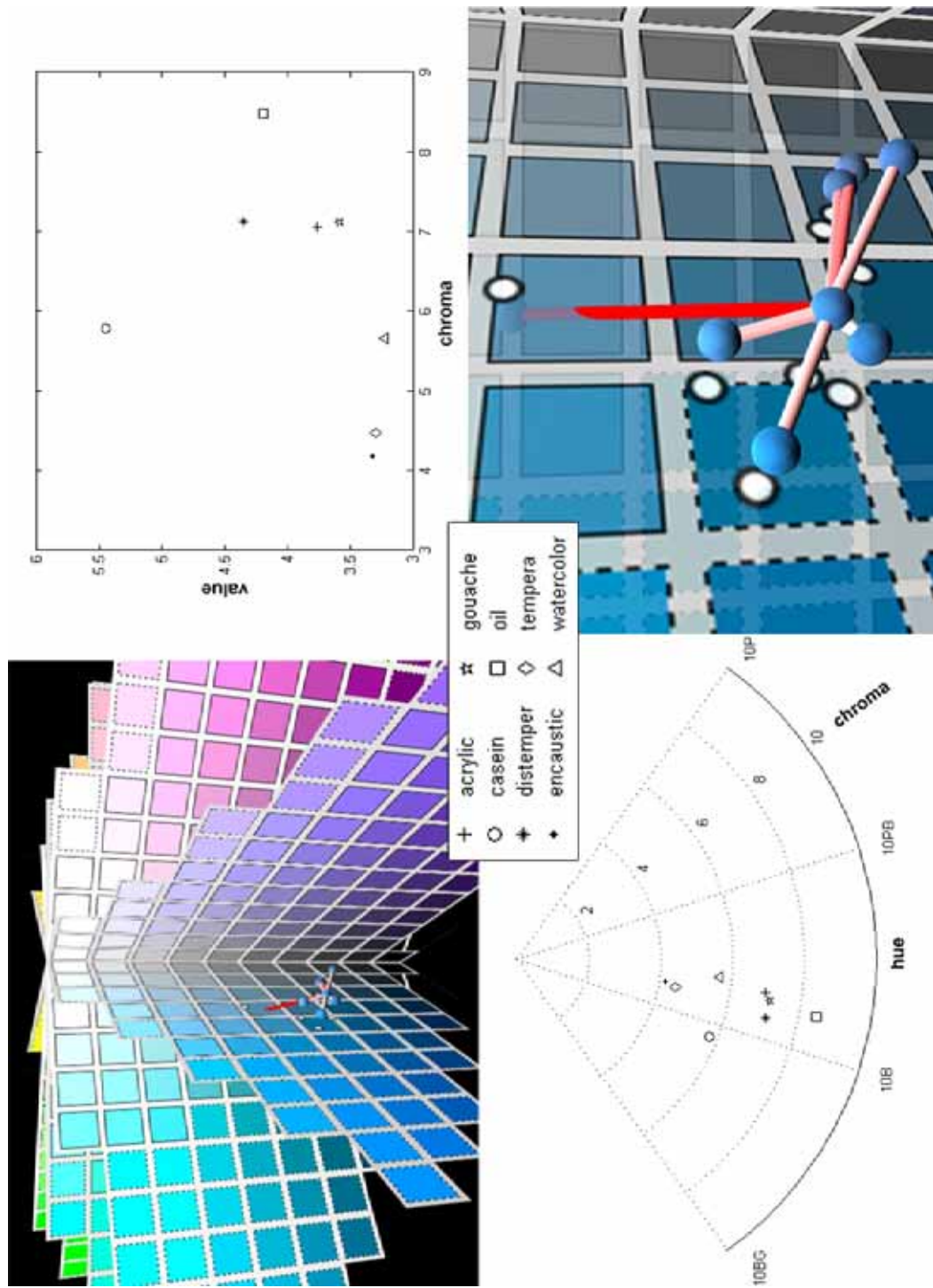


Figure 6.3: Munsell plots of Lapis Lazuli in different binding media after one day.

Looking down the vertical axis of the cylindrical solid yields the polar coordinate plot in the bottom-left of the image. This illustrates the hue versus chroma relationship of the eight samples. For the Lapis Lazuli samples, the central tendency of the hue is around 2-3PB (purple-blue), as most of the colors lie in that range. Note that the most dissimilar colors (casein and watercolor) are the farthest outlying hues in each opposite direction.

The top-right image in the figure can be thought of as a leaf in the solid. It contains the value versus chroma information in a two-dimensional Cartesian plot. In the graph, encaustic and tempera are close in proximity, while casein and watercolor are not.

The bottom-right image of the figure provides a closer view of the relationships between the eight colors in three dimensions. A sphere is placed at the point in space where the hue exists in the Munsell color solid. Each sphere has a diffuse material, colored with *RGB* values converted from the *XYZ* coordinates in Table 6.1 using Equation 3.6. The white dots are value-chroma plots of the points projected onto the nearest leaf. The leaves also define the boundary of the displayable gamut for a typical CRT display monitor. The Munsell color swatches that are surrounded via a dotted line are unable to be realized by a typical CRT monitor (and thus will not appear as they do in real life). Many of the converted colors from the samples fall in or near this range.

The eight spheres are all connected via a series of lines, originating from the acrylic sample. This is to give a sense of the spatial relationship between the points, as there is no easy way to represent the data in only two dimensions. Since a point (casein) lies on the other side of a major hue leaf division, the image is defined to be slightly transparent. A relationship-connecting line between colors i

and j has a saturation of red r_{sat} , such that

$$r_{sat} = r_{maxSat} \left(\frac{\Delta E_{i,j}}{\Delta E_{max}} \right) \quad (6.1)$$

where

r_{maxSat} is red with the maximum saturation

$\Delta E_{i,j}$ is the Euclidean distance between colors i and j in $L^*a^*b^*$ space

ΔE_{max} is the Euclidean distance between the most dissimilar colors in $L^*a^*b^*$

Hence, all of the distances are scaled by the largest distance. The more dissimilar colors will have a more vivid red line, while the more alike colors will have paler line colors.

Ultimately, the images show a vast amount of data in a very concise setting. The resulting conclusion from this information is that the material that adheres the pigment to the support has a great influence on the resulting color, inciting differences in the multi-dimensional space of hue, value and chroma. The differences are many times that of the threshold of the human observer and easily perceptible from many sources. This includes viewing either the spectral data, coordinates from any of the converted color spaces or even direct observation from photographs. More examples of this behavior for different pigment-time combinations can be seen in Appendix B.

6.1.2 Effect of time

In order to study the effect of time on a paint solution, the specific pigment and media are held constant. This allows for comparison of the sample's different stages as time evolves. In our experiment, there are six time intervals, each with its

own spectral reflectance curve for a given pigment-binding media combination. In viewing these plots together, one can translate nonlinear changes in the absorption and scattering of the material into perceptually distinct color changes that the material undergoes over time.

Similarly to the previous section, another interactive JavaScript viewer was created for ease of manipulating the dataset. There are 168 pigment-media combinations in total from which to browse through. After selecting the desired pigment and media input parameters, the application plots the spectral reflectances of the six time intervals. This work studied samples from when they were freshly painted up until six months of aging. The setup for the viewer is seen in Figure 6.4 for the evolution of Lapis Lazuli samples in gouache. The layout for the system is quite similar to the previous one. The input data is selected via the menus in the top-left and the graphics are updated with the display button. Photographs of the current pigments are displayed in the top-right and the six corresponding photographs to the aging samples are seen to the left.

Chapter 4 discusses many of the factors involved with pigmented colorant changes over time in artwork, including photochemical reactions, oxidation and other changes related to varying atmospheric conditions. These physical and chemical changes affect the wavelengths of light that a pigmented material reflects and absorbs. As previously covered, the changes in the spectral reflectance over time are typically nonlinear in both the rate of change as well as the wavelengths affected.

If all of the wavelengths in the visible spectrum increase in the same proportion, the hue remains the same but the color appears lighter. This is because more light is reflected back toward the viewer. Since white light is a combination of all

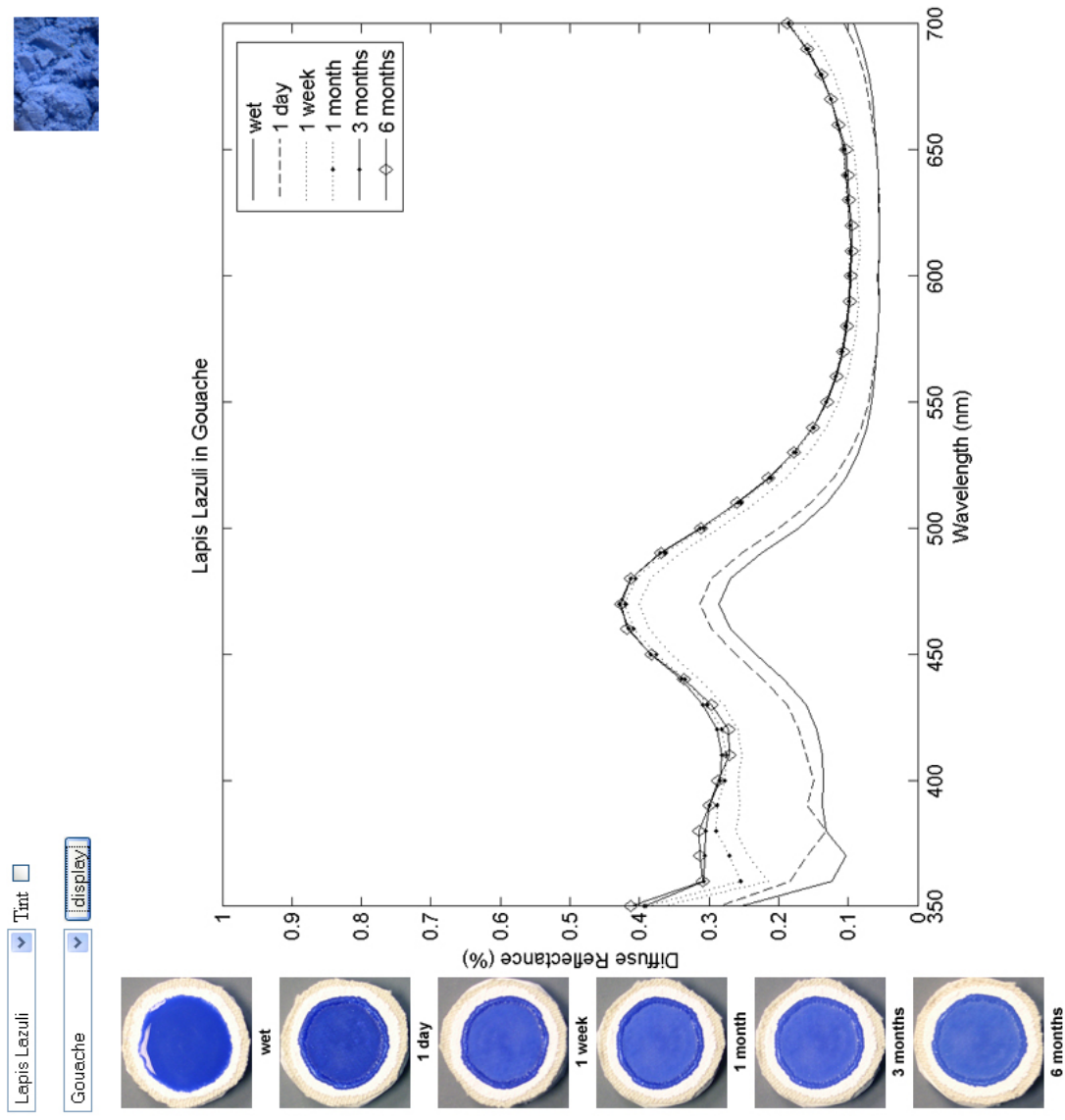


Figure 6.4: Variation of spectral reflectance curves of Lapis Lazuli in Gouache over time.

Table 6.3: Color conversions of Lapis Lazuli in Gouache over time. ΔE is the distance from the previous to current $L^*a^*b^*$ color.

	X	Y	Z	H	V	C	L^*	a^*	b^*	ΔE
wet	8.42	8.63	23.53	3.13PB	3.43	6.56	35.27	2.10	-32.21	
1 day	9.03	9.46	26.48	2.43PB	3.58	7.13	36.85	0.53	-34.33	3.08
1 week	13.23	14.28	36.17	1.61PB	4.33	7.52	44.63	-1.96	-34.66	8.18
1 month	14.78	16.00	38.51	1.48PB	4.55	7.30	46.97	-2.34	-33.55	2.62
3 months	14.86	16.11	39.23	1.46PB	4.57	7.46	47.11	-2.48	-34.20	0.68
6 months	14.67	16.03	38.84	1.16PB	4.56	7.41	47.01	-3.20	-33.88	0.30

wavelengths, an equal additional amount of every wavelength is the perceptual equivalent of the color shifting closer to white. Similarly, if the overall reflectance curve shift is downwards, the material is perceived as getting darker. In both instances, this is not *exactly* the case, since the spectra must be integrated against the eye's response matching functions (which are wavelength-dependent). Hence, luminance changes are wavelength-dependent to some extent.

In Figure 6.4, the spectral curves of Lapis lazuli in Gouache are increasing substantially over time. This is occurring at relatively a uniform rate and one is safe to presume that the overall luminance is increasing (the corresponding images also support this behavior). In the same manner in the previous section, the spectral reflectance data has been converted into the various color systems to aide in further analysis. Viewing any of the luminance indicators (Y , V , or L^*) also supports the behavior that was observed—all of these indicators increase with time.

However, the spectral reflectance curves are not changing entirely uniformly with this material. Reexamining the diffuse reflectance at the six time intervals, it is evident that the reflectance values of the lower and higher regions of the

visible spectrum are increasing at different rates. Yet, understanding the effect on perception of nonuniform changes in the spectral distribution is more complicated than with uniform changes.

Hue shifts occur when spectral distribution reflectance curves change unequally with respect to wavelength. The color of a material depends on both the light that is reflected and light that is absorbed. First, a nonlinear increase in a material's reflectance affects the appearance. For instance, increasing a material's reflectance between $565 - 590nm$ will in turn reflect more yellow light back into the environment. As a result, the viewer will see the material as being yellower.

The second case is slightly less intuitive. For instance, oil paints typically experience a slight yellowing of the binding material due to oxidation. This equates to a drop in the lower regions of the spectral reflectance curve. Then, the material is absorbing more blue light than previously. In other words, the material is thus reflecting less blue light back toward the viewer. Therefore, the material is reflecting relatively more yellow light and hence appears to have yellowed.

In both cases, a hue change is dependent on the relative balance between light reflected and absorbed. A nonuniform change in either can affect the overall perception of a hue.

It is worth mentioning that in paint, what we perceive as hue shifts typically occur when a nonlinear change occurs away from the central tendency of the material's reflectance. For instance, we typically state that a blue has yellowed, or a purple shifted toward red, etc. However, when these changes occur near the central tendency of the reflectance, the perceptual change is not that of hue, but of chroma.

Consider the previous case of Lapis Lazuli in gouache. As the paint evolves,

the rate of which the material reflects light at the lower and middle regions of the visible spectrum is faster than at the higher wavelengths. Thus, relatively more purple, blue and green light is being reflected from the surface than is yellow and red light as the material ages. Since the regions that are increasing the most are in the area of the material's reflectance maxima, this tends to indicate an increase in the material's chroma—the material's hue is becoming more vivid.

Figure 6.5 displays the paint sample as it evolves over time in the Munsell color space. The spectral changes are broken down into individual luminance, hue and chroma changes. In this diagram, the start and end points of the study are labeled as green and red, respectively (corresponding to the reflectance of the sample as it is first painted and again after six months). The intermediate stages (one day, one week, one month, three months) are indicated by coordinates between the two endpoints. In the three-dimensional plot, an interpolating curve connects the intermediate time interval points. The spline is lofted into a ribbon to aid visualization of the curve.

As determined before, Lapis lazuli is getting lighter over time (the value is increasing). Also, due to the relative increase in the rate of the reflectance of blue light, the chroma of the dominant hue is also increasing. However, hue changes are difficult to account for solely based on reflectance spectra.

In the Munsell hue-chroma diagram, one notices that a blue can range from greenish to purplish. Since the relative amount of reflected purple light in the paint sample is increasing at a faster rate than that of the reflected green light, one would presume that the hue is shifting to a more purple state. However, our sensitivity to purple light is very small compared to that of green light (given via the XYZ color matching functions in Figure 3.18). Hence, purple light only contributes a

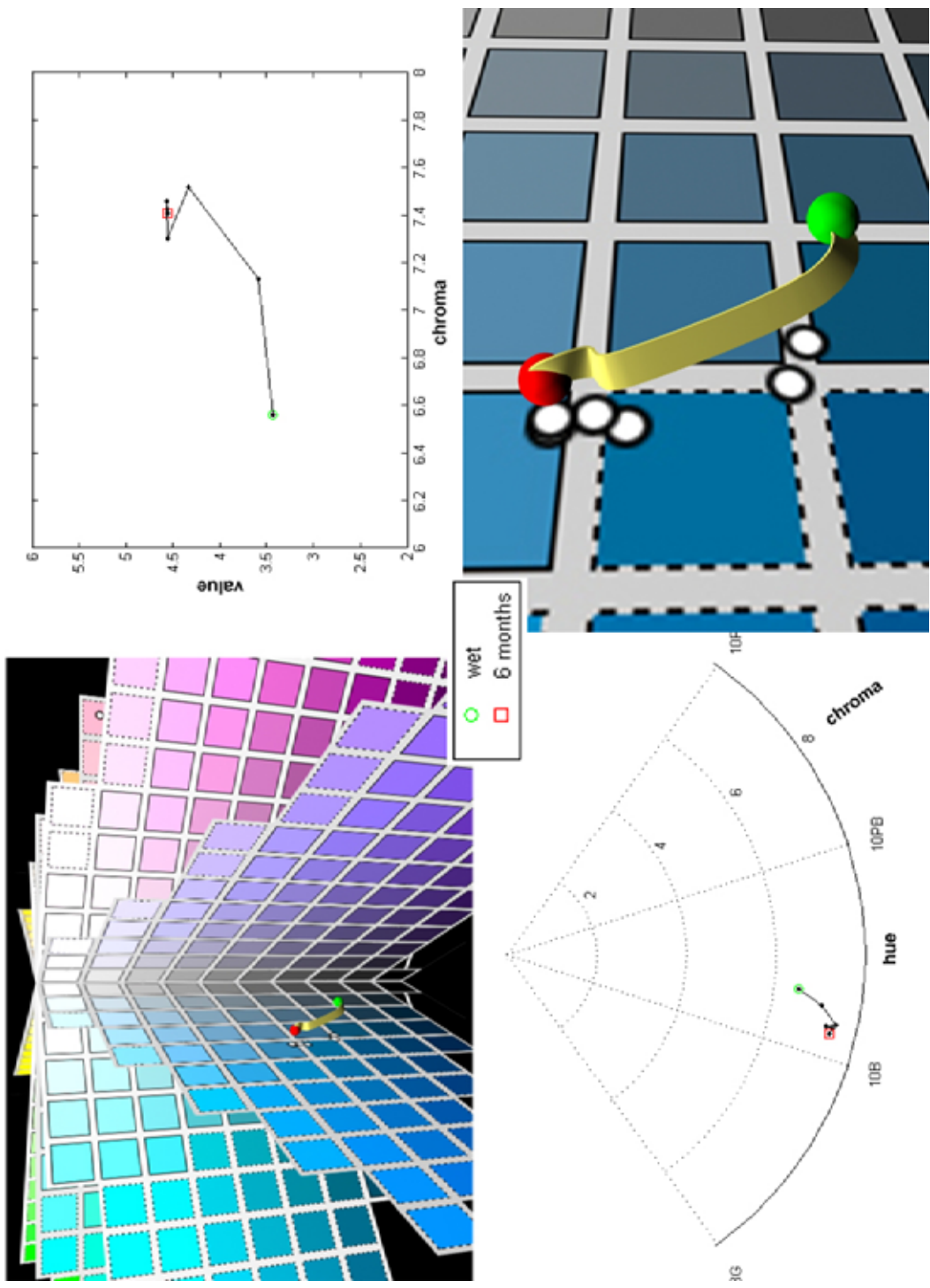


Figure 6.5: Munsell plots of Lapis Lazuli in Gouache over time.

small amount to our perception of a color. Changes in the amount of light in the middle spectral wavelengths have a much larger affect on the resulting color since they are heavily weighted by $\bar{y}(\lambda)$. Therefore, in our example with Lapis lazuli the hue moves slightly closer to green instead of purple.

For the sample of Lapis Lazuli, this behavior is typical of the first stage of fading (a perceived increase in both value and chroma, as well as hue shifts due to changes in the spectra away from the reflectance maxima), which was discussed in the previous chapter. More examples of time-dependent behavior for different pigment-media combinations can be seen in Appendix B.

6.1.3 Applications

None of the research discussed in the previous chapter addresses material changes from the artist's point of view—from the initial fresh mark of paint. As a painter, one only has control over the initial conditions of a color in a painting—one has full control over the combination of pigments, media and other materials. An artist's vision is expressed through the mixing and application of *fresh* paints on a canvas support. Yet, once defined, the appearance of the paint is a function of time. Then, for what time should the artist create a painting for? Is the artist's creative vision only fulfilled upon the immediate completion of a work or is the artwork the living and evolving material object?

A second intrinsic problem in working with paint is color matching. Most creative works are far too complex to be created in a single day. As such, an artist must return to a work for subsequent treatment after some period of time. However, as previously described, many changes (which are often perceptually evident) occur to a paint sample after it has been applied. Assume a painter is

trying to match color c_a from the previous day. If the same exact paint is applied on the second day of work, the color c_b will be one day removed from fading. As seen in Figure 6.6, the colors will not exactly match (as there is some perceptual difference ΔE). The longer the artist waits to match evolving color c_a with wet color c_b on his/her palette, the more dissimilar the colors will be. As a result, a color match will be more difficult, as the fresh color will not have been subjected to the same conditions as the dry color.

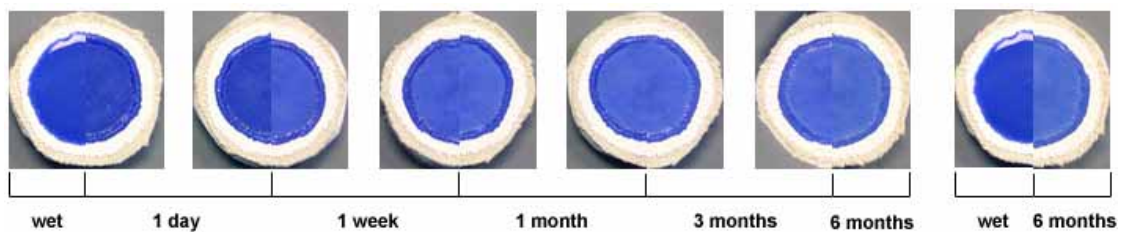


Figure 6.6: Left: Visual comparison of Lapis Lazuli in Gouache changing at each time interval. Right: the overall change.

Hence, in order to match a previously painted brushmark, the artist must alter the pigment mixture of the fresh paint. The logical method would be to save the paint from the previous session and alter the mixture slightly to account for the change. While this may work for some paints (such as oil), many paints have to be made fresh daily (the working properties of different binding media are discussed in previous chapters). This presents a difficult problem, as not only does an artist have to mix a color from scratch to match the previous one, the paint has to be modified (via changes in the concentrations of pigments) in order to account for the color changes that have already taken place. Even if the artist has no idea that the color is changing over time, he/she attempts to match what is seen (and since what is seen changes, the match changes).

For artists, this skill is typically learned based on one's familiarity with the

materials—an artist will know from experience how different pigment-media combinations behave. While this problem is quite difficult, most paint media can be reworked until the desired result is achieved. The inherent problem with fresco is that a dried brushmark is permanent and cannot be reworked. Thus, one needs to understand the time dependencies to correctly match colors between sessions. The color matching problem can readily be seen in the hue discrepancies in Masaccio's giornate in his *Expulsion from the Garden of Eden* (Figure 1.2).

The same problem occurs with the conservator's practice of *in-painting* on losses of paintings. Occasionally, a painting will experience damage to the surface whereas a portion of the work has chipped off. One common technique of is to first disguise the loss with filling to regain the surface topology. The new surface is then retouched to match the current color, which places a large responsibility on correctly identifying the original pigments. Further, the fresh paint must be mixed such that the fresh mixture will age at a similar rate to that of the original surrounding colors. This is difficult as the original artwork will be at a much later stage in fading and will change at a much different rate to that of fresh paint. While a conservator may have carefully matched an in-painting section, the false area may display itself later in its own fading cycle. The difficulty of retouching artworks is further documented in [Sta85].

There is an importance consequence of the artist controlling the initial conditions of a paint. The artist knows the desired color for his or her artistic vision. Then, one can use knowledge of the evolution of a paint in order to modify the fresh paint such that the aged paint will be the desired result. This changes the conception of the term "artwork", as the original is not necessarily the creative vision. Rather, the evolving work moves incrementally closer to the artist's intent

as it ages. This is in direct contrast to the current model of artwork, which must constantly be restored to a previous state to view the artist's original intentions.

In contrast, as an art conservator, one only has knowledge of the current conditions of a color in a painting. To make any assessments about the state of the pigmented colorant, typically one must first identify the pigments and media used in the work. After the composition of the work is known, two directions can be taken. In restoration, one would like to use paint evolution data to travel back in time to view the work in its original brilliance. This knowledge is used in determining the best methods to clean and restore a work of art, as it provides how much a work should be changed to revert to a previous visual state.

In conservation, the goal is to estimate future changes in the materials of the painting and assess what can be done such that the work can still be displayed without much deterioration from the current state. One hopes to minimize the perceptual change from the current state, such that future generations will be able to appreciate the work. In both of these instances, one travels along the same path, defined by the same original initial state.

Chapter 7

Interactive Viewing

7.1 Introduction

In the previous chapter, it has been shown that reflectance data for different samples can be broken down into very intuitive perceptual changes through the use of different color spaces. This data supports that the appearance of paint changes over time, and a specific pigment appears different when dispersed in different materials.

However, the acquired data is limited to a discrete set of measurements, which are from a finite number of paint mixtures at specific times. In this form, one can only study an incomplete view of paint appearance. It is preferable to specify any combination of pigments in any binding media at any time, and see the resulting appearance. Fortunately, using research in subsurface scattering from the graphics literature, our captured reflectance data can be used in order to realistically simulate the appearance of many paints that have not been previously measured.

Therefore, we combine Kubelka Munk theory with our study of naturally occurring material changes to simulate the appearance of paint over time in an in-

teractive viewer. In our application, Kubelka Munk theory is used to effectively predict the appearance of any arbitrary pigmented mixture. Further, with multiple K-M coefficients in time for a given pigment-media mixture, we simulate the reflectance of the arbitrary paint mixture over time.

Recently, it has been demonstrated that paint rendering using K-M theory can be simulated within the gamut of the display in real-time using graphics hardware. This is much more intuitive than analyzing the changes in the spectral reflectance curves or corresponding photographs, as one can view a material at any stage of its evolution.

7.1.1 Conversion to Kubelka Munk

Our conversion to K-M parameters is implemented in a similar manner to the work of William Baxter [BWL04]. We calculate the Kubelka Munk absorption K and scattering S coefficients for each paint sample at each wavelength. Given pigmented mixtures $1 < i < m$ of the pure pigments $1 < j < n$ in a specific binding media, we relate the reflectance of each mixture $R_{\infty,i}$ to the absorption K_j and scattering S_j values for the involved pigments (from Equation 4.10):

$$\begin{aligned} \left(\frac{K}{S}\right)_{mixture,i} &= \frac{\sum_j K_j c_{ij}}{\sum_j S_j c_{ij}} = \frac{(1 - R_{\infty,i})^2}{2R_{\infty,i}} \\ \sum_j S_j c_{ij} &= \sum_j K_j c_{ij} \left(\frac{2R_{\infty,i}}{1 - 2R_{\infty,i} + R_{\infty,i}^2}\right) \end{aligned} \quad (7.1)$$

where

c_{ij} is the relative concentrations of each pigment i in paint mixture j

Pigments not involved in a particular paint mixture are assigned zero concentrations. This method is preferable to [BWL04](6), as small reflectance values do

not interfere with the numerical stability of the equation. From Equation 7.1, we can assemble a linear system for each wavelength of the form

$$A = (-TC \quad C) \begin{pmatrix} K \\ S \end{pmatrix} = 0 \quad (7.2)$$

where $C = \{c_{ij}\}$ is an $m \times n$ matrix containing the pigment concentrations respective to each paint sample in the binding media, and T is an $m \times m$ diagonal matrix, containing the reflectance constant from the right-hand side of Equation 7.1 along the diagonals. The unknowns, K and S , are both $n \times 1$ vectors.

Since, generally the zero vector is the only solution, a nonnegative least squares solution that minimizes $A^T A$ is computed. Since K and S always appear in the form of a ratio, the usual K-M condition is to choose a value for the white pigment. Typically, one sets $S_k = 1$ corresponding to titanium dioxide white as the k th pigment. The K-M values for all of the pigments can be derived from the above procedure, as each pure pigment is related to titanium white via a tint.

7.1.2 Rendering System

The renderer was implemented in Java with NVIDIA'S Cg programming language. The simulated canvas is represented as a rectangular discrete set of points. The simulated canvas is similar to a three dimensional height field, as seen in world space in Figure 7.1. Each point (depicted as a white dot in the figure) has three-dimensional coordinates (x, y, height) and contains the various pigment concentrations and volume of paint deposited at that point. Initially, the heights are given values corresponding to a actual primed canvas by use of a texture map.

The user sees the screen space version of this simulated canvas, which is the

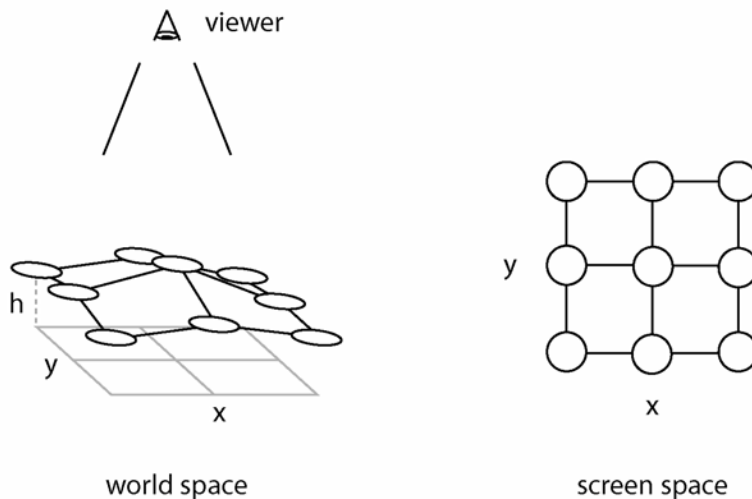


Figure 7.1: Our simulated canvas is discretized similarly to a height field. The user sees the top-down orthographic view of the simulated canvas, whereas every canvas point represents a pixel on the screen. Each point stores its paint volume, pigment concentrations, and normal.

top-down orthographic view of world space. Here, each point in the simulated canvas corresponds to a pixel on the user’s screen. Global canvas parameters are the current binding media used in the simulated painting, the lighting spectra and the current time.

As in previous K-M implementations, it is not feasible to store full-spectrum K and S values per pixel or compute them interactively. For a user-specified light spectrum, time, and binding media, the system chooses eight sample wavelengths to numerically integrate over the spectra and XYZ matching functions. Eight wavelengths is a good fit with graphics hardware, as it can be stored in two floating-point textures.

Fragment shaders calculate the overall RGB reflectance of the painted canvas. Each texture with its four channels represents the concentrations of four pigments simultaneously allowed at any one point. Another texture is designated for the point’s normal and thickness of paint at that point. Upon rendering the canvas,

the normal for every point is calculated, via averaging the results from two cross products. The vectors are made from the current point's three-space coordinates (x, y, height) to the four immediately surrounding points.

Each pixel undergoes the same rendering pipeline. First, $\left(\frac{K}{S}\right)_{mix}$ is calculated as a weighted average of the pigments using their respective concentrations in the mixture from Equation A.16. Reflectance and transmittance of the layer is then calculated:

$$b = \sqrt{\left(\frac{K}{S}\right) \left(\frac{K}{S} + 2\right)} \quad (7.3)$$

$$R = \frac{1}{1 + \frac{K}{S} + b \coth(bSd)} \quad (7.4)$$

$$T = bR \operatorname{csch}(bSd) \quad (7.5)$$

where d represents the thickness of one layer of paint

Compositing multiple layers together (as well as the gesso ground) is done via Equation A.25. If no pigments are present at a given pixel, the reflectance is solely the three-coat gesso. XYZ integrating functions are used to transform the eight wavelength reflectance values for display. Since K-M theory only gives us diffuse reflectance, the lighting computation is completed using Blinn-Phong specular highlights:

$$\begin{aligned} X &= X(n \cdot l) + E \bar{x}(n \cdot h)^k \\ Y &= Y(n \cdot l) + E \bar{y}(n \cdot h)^k \\ Z &= Z(n \cdot l) + E \bar{z}(n \cdot h)^k \end{aligned} \quad (7.6)$$

where

n is the normal at the current point

l is the vector from the current point to the light

$h = \frac{(l + e)}{2}$ is the half-vector, which avoids calculating the reflection vector

e is the vector from the current point to the camera

E is the spectral distribution of the illuminant

$\{\bar{x}, \bar{y}, \bar{z}\}$ are the observer matching functions

k is the specular exponent which controls the shininess of the material

Note that the Blinn-Phong shading model's use of an exponentiated cosine is an ad hoc approximation to specular highlights. A physically accurate model of specular behavior would require a full temporally-varying BRDF for every sample.

The XYZ color is transformed into linear RGB values for display using the transformation matrix M from Equation 3.6. These values are then converted to nonlinear $sRGB$ before outputting to the display:

$$\begin{aligned} R_s &= \begin{cases} 12.92R_l & , R_l \leq .0031308 \\ 1.055R_l^{1/2.4} - 0.055 & , \text{otherwise} \end{cases} \\ G_s &= \begin{cases} 12.92G_l & , G_l \leq .0031308 \\ 1.055G_l^{1/2.4} - 0.055 & , \text{otherwise} \end{cases} \\ B_s &= \begin{cases} 12.92B_l & , B_l \leq .0031308 \\ 1.055B_l^{1/2.4} - 0.055 & , \text{otherwise} \end{cases} \end{aligned} \quad (7.7)$$

where $\{R, G, B\}_l$ are the linear RGB values

The implementation runs interactively on a 3.4GHz Pentium IV machine with a NVIDIA GeForce 6800 GT graphics card. The cost of the rendering is greatly

reduced as the canvas is broken into tiles (each is 64x64 pixels). This drastically improves rendering speed, as only tiles that are modified need to be updated (i.e. only when new paint is applied to a tile). However, the entire canvas is rendered when the user changes global parameters such as lighting, binding media, or time.

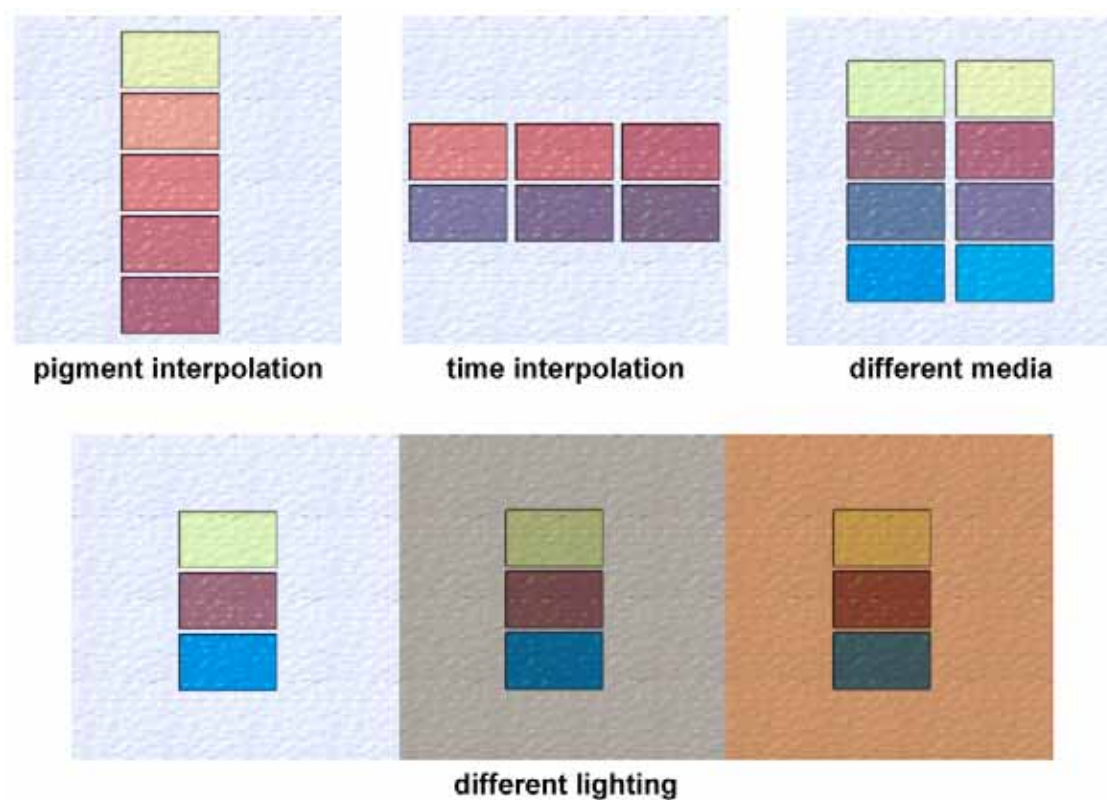


Figure 7.2: Features of our interactive viewer. Top left: K-M theory predicts the three middle paints from the relative concentrations of the other two. Top middle: the center paints are predicted using time as the interpolation weight. Top right: four pigments simulated in different binding media. Bottom: three paints under different illumination.

The system's features are illustrated in Figure 7.2. As in Baxter's work, Kubleka Munk theory predicts the reflectance of any arbitrary pigment mixture (top left) as well as changes in illumination (bottom) in real time. However, in our system, one can also get instant visual feedback from manipulating the time (top middle) and binding media as well (top right).

In summary, our implementation provides a powerful tool in visualization. Provided is a simple method for laying down paint of varying pigment concentrations to see how they react under different conditions—all of the variables can be modified in real time. As computer processing improves, more wavelengths can be used in the lighting computation to better simulate the spectral reflectance. As display technology improves, the gamut of displayable colors will also expand, improving the conditions for which the colors are viewed.

7.1.3 Implementation issues

While this model is effective and can be computed in real time, there are some limitations to this theory of pigment modeling [Fis83, CAS⁺97]. The model assumes the paint is homogeneous. In fact, pigment particles tend to clump into aggregates and often contain inclusions or impurities. Also, the scattering assumptions in the transport theory were based on uniformly sized spherical particles. This is rarely the case for pigment particles as they are often of widely varying shapes and sizes. Further, all colorant layers are immersed in media of the same refractive index. This assumption is violated at the interface between the air and paint and paint to substrate. A fairly simple correction term for reflection and refraction at the paint's surface has been proposed [JW75] that could be used to increase accuracy.

While reasonably accurate, Kubelka Munk theory is only as good as the measurements behind it. Therefore, for more accurate prediction of color mixtures, many more mixtures of multiple pigments of varying concentrations are necessary to obtain better absorption and scattering coefficients.

In our work, only constant volume ratios of pigment-to-media are studied. In paint, artists often manipulate the amount of binder and vehicle (as well as the

addition of other materials) to achieve different tactile behaviors. Similarly, the fluid dynamics of the application of the eight different media are not considered, as this would be a huge undertaking. The study of how a media's tactile behavior changes as it dries or congeals would be an interesting research project.

Also, our work only encompasses a relatively short period of time of the life of a paint film. Remember that most paintings are expected to last indefinitely (at least a hundred years). Longer measurement intervals are needed for a more complete understanding of paint aging behavior. While many known historical samples exist, they were not considered this work, as they may be comprised of different materials or are from different origins.

Chapter 8

Conclusion

We have studied the variation in paint appearance over time in different binding media. We created a vast amount of high quality paint samples from many pure pigments and different binding media. These were made by hand to insure quality of materials, as commercially manufactured paint frequently includes additives that could possibly affect the chroma or lightness of the hue. Therefore, to maintain consistency across multiple binding media, it was imperative that all paints were only made of pigment and binder.

Using sophisticated measuring equipment, we captured the reflectance spectra of the paint samples at different intervals in time to study how paint appearance changes over the course of drying/congealing and the beginning stages of aging. Diffuse reflectance measurements were taken over the visible spectrum after the samples were freshly painted, after one day, one week, one month, three months and six months after they were painted. Converting the spectral data into perceptually uniform color spaces, we determined the differences in appearance were perceptually very significant—paint appearance does vary substantially with time and pigments look drastically different when dispersed in different binding mate-

rials.

In addition, we presented a physically based model to interactively simulate the appearance of pigmented colorants using Kubelka Munk theory and modern graphics hardware. The spectral data is converted into Kubelka Munk absorption and scattering coefficients. As a result, arbitrary mixtures of pigments that we have not measured can be simulated. Further, since our data also spans time, the simulated appearance of these mixtures can be viewed at any point in time.

In our system, other global conditions can also be modified in real time. A user can instantaneously change the binding media in which the pigments are suspended—one can simulate the appearance of a work as if were done in oil or acrylic or another media. Since we compute the lighting calculations from spectra, the simulated painting can be re-lit under a number of different illuminants, such as daylight or fluorescent light.

The previous chapter discusses applications for use of this system for the artist or art historian. Artists that are more aware of their materials will be able to predict how a color will appear after some time and make adjustments that suit their creative vision. Restorationists who understand how a color's underlying materials change can visualize how an artwork looked in its original brilliance. Conservationists can predict how long a work can be displayed under natural conditions before perceptual changes are evident.

Our work has implications in many other industries that utilize pigmented colorants. Currently, digital printing inks use primarily dye based inks. Due to the popularity of digital photography, many individuals are printing on high quality paper and canvas and framing the pieces. However, dye based inks have a longevity of only a few years before serious fading occurs. As a result, pigmented

inks are beginning to find their way into these devices as they have a longevity of 80-100 years or more. Other everyday colored materials contain pigments, such as plastics and non-artists' paints. As such, these materials are also susceptible to natural deterioration, such as the case with many architectural materials. In computer graphics, realistic synthetic material aging is also an increasingly popular research area, enhancing the visual complexity of simulated images.

There are many possible future research areas related to our work. Most importantly, to fully understand the effects of aging, many more time-dependent measurements are needed. Our research only accounts for a very small portion of the life of a painting, which is expected to last indefinitely (at least a hundred years). While this type of study is perhaps impossibly time-expensive, artificial aging accelerators seem to provide a feasible way to simulate some effects. Yet, since natural decay is more than just electromagnetic radiation, a complete system would need to account for other atmospheric effects as well. Another very important factor in the visual appearance of paint is the spectral reflectance component. Not all binding media are completely diffuse materials, as some maintain a characteristic gloss to the surface. This component is also time-dependent, as the specular highlight typically aids in one's perception of a liquid's wetness. Therefore, a full understanding of the appearance of pigmented materials over time would require a complete temporally-varying BRDF. Further, while we have purposefully excluded any additives to our paint, it would be fascinating to study how different materials affect the optical properties of a pigmented colorant.

Due to space considerations, we have presented only a small fraction of the measurements in our study. In this setting, it was impractical to include analysis on all of the 1008 time dependent reflectance spectra (21 pigmented mixtures x 8

binding media x 6 time intervals) from our experiment. However, the entire set of spectral data, converted into different color spaces, is available as a Technical Report [BGM06].

Appendix A

Derivation of K-M theory

The surface of many real world manufactured objects contains pigments, such as paint or painted items, plastic objects and textiles. To accurately describe how these object interact with light and the resulting color appearance, both the pigments and the material that they are dispersed in must be accurately modeled.

A practical model that effectively simulates the appearance of pigmented materials was first introduced by Kubelka and Munk in 1931 [KM31]. The following includes the derivation of the solutions to the differential equations in Kubelka-Munk theory. Also presented are significant improvements to the theory from researchers over the years.

The original paper [KM31], is based on the assumption of a homogeneous pigmented material of a medium that is infinite in extent. By symmetry, all lateral flux can be ignored, since it will be balanced out by an equal and opposite flux. The model describes a material's appearance in terms of only two wavelength-dependent parameters: an absorption constant, $K(\lambda)$, and a scattering constant, $S(\lambda)$.

The model assumes a surface that has been coated by a layer of paint with

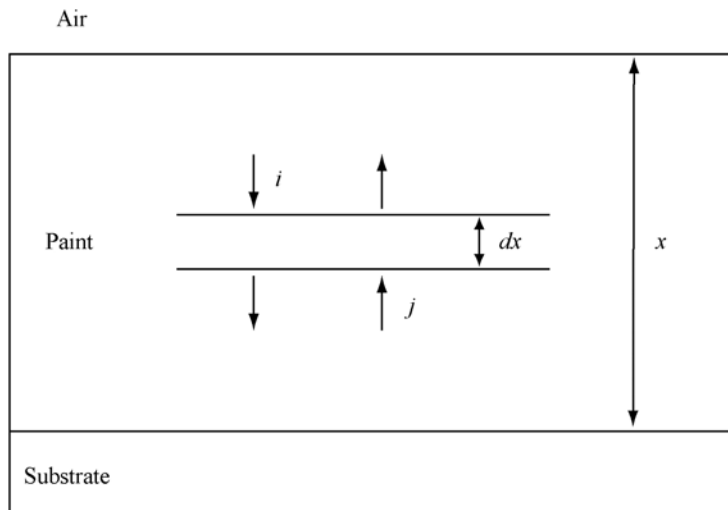


Figure A.1: Coordinate system used to calculate energy scattering and absorption inside a pigmented surface. Adapted from [HM92].

thickness h . We assume we know the reflectance R_0 of the substrate to which the homogeneous layer of paint with uniform thickness x has been applied (typically, the gesso ground in a painting).

Consider some differential horizontal thickness dx within the paint, as in Figure A.1. The net flux that is descending toward the differential surface dx is labeled as i and the upward-moving flux as j (note that these can be the result of multiple scattering events with the paint material). Now, to find the reflectance R_x of a layer of paint of thickness x , we must solve a light transport problem. Note that K , S , and reflectance R are all functions of wavelength. The derivation of this approach taken by Kubelka and Munk follows [HM92, G95b, Kor69].

To begin, the loss in the descending and ascending fluxes due to a single scattering or absorption event is given by:

$$\begin{aligned}\Delta i^- &= (K + S) i dx \\ \Delta j^- &= (K + S) j dx\end{aligned}\tag{A.1}$$

On the other hand, the gains in each flux come from scattering alone. Assuming a single scattering event in the layer dx , the gains are:

$$\begin{aligned}\Delta i^+ &= S j dx \\ \Delta j^+ &= S i dx\end{aligned}\tag{A.2}$$

Then the total loss in each direction is the loss minus the gain. Note that the upward-moving quantity is negated so that we can measure both changes in the same coordinate system.

$$\begin{aligned}di &= \Delta i^- - \Delta i^+ \\ &= (K + S) i dx - S j dx \\ dj &= - [\Delta j^- - \Delta j^+] \\ &= (K + S) j dx - S i dx\end{aligned}\tag{A.3}$$

Letting the constant $a = (1 + \frac{K}{S})$ yields the two differential equations:

$$\begin{aligned}\frac{di}{S dx} &= ai - j \\ -\frac{dj}{S dx} &= aj - i\end{aligned}\tag{A.4}$$

Adding these two equations together and rearranging the terms leads to:

$$\frac{i dj - j di}{i^2 S dx} = -2a \frac{j}{i} + \frac{j^2}{i^2} + 1 \quad (\text{A.5})$$

From the Quotient rule, we observe that

$$\frac{d\left(\frac{j}{i}\right)}{S dx} = -2a \left(\frac{j}{i}\right) + \left(\frac{j}{i}\right)^2 + 1 \quad (\text{A.6})$$

Setting $r = \frac{j}{i}$ then yields

$$\frac{dr}{S dx} = r^2 - 2ar + 1 \quad (\text{A.7})$$

and therefore via rearrangement and integration

$$\int \frac{dr}{r^2 - 2ar + 1} = S \int dx = Sx \quad (\text{A.8})$$

Since we have assumed the paint is homogeneous, the scattering coefficient S is constant throughout the material and can be brought outside the integral on the right hand side. Our goal is to find the value of the change in r as the thickness varies from zero to some thickness x . At a thickness of zero, the reflectance is simply the reflectance of the substrate R_0 . At thickness x , the reflectance is some R_x . Hence, we are interested in evaluating the integral on the left-hand side of Equation A.8 over the range R_0 to R_x . To simplify the integral, we factor the integral by writing $b = \sqrt{a^2 - 1}$ and integrate via partial fractions:

$$\begin{aligned} \int_{R_0}^{R_x} \frac{dr}{r^2 - 2ar + 1} &= \frac{1}{2b} \int_{R_0}^{R_x} \frac{dr}{r - (a + b)} - \frac{1}{2b} \int_{R_0}^{R_x} \frac{dr}{r - (a - b)} \\ &= \frac{1}{2b} \ln \frac{(R_x - a - b)(R_0 - a + b)}{(R_x - a + b)(R_0 - a - b)} \end{aligned} \quad (\text{A.9})$$

Equation A.8 is now:

$$\frac{1}{2b} \ln \frac{(R_x - a - b)(R_0 - a + b)}{(R_x - a + b)(R_0 - a - b)} = Sx \quad (\text{A.10})$$

Rearranging yields:

$$\ln \frac{(R_x - a - b)(R_0 - a + b)}{(R_x - a + b)(R_0 - a - b)} = 2Sxb \quad (\text{A.11})$$

$$\frac{(R_x - a - b)(R_0 - a + b)}{e^{2Sxb}} = (R_x - a + b)(R_0 - a - b) \quad (\text{A.12})$$

Assume that the paint is applied so thickly that the substrate is not visible. Then, $x \rightarrow \infty$ so $R_0 = 0$ and we make the substitution $R_x = R_\infty$. Since $e^\infty \rightarrow \infty$, the left-hand side of A.12 goes to zero. We now have:

$$(R_\infty - a + b)(-a - b) = 0 \quad (\text{A.13})$$

Solving for the reflectance R_∞ , we find

$$R_\infty = a - b = \frac{1}{a + b} \quad (\text{A.14})$$

Recall that $a = 1 + \frac{K}{S}$ and $b = \sqrt{a^2 - 1}$, hence we get

$$\begin{aligned} R_\infty &= \frac{1}{a + \sqrt{a^2 - 1}} \\ &= \frac{1}{1 + \frac{K}{S} + \sqrt{\left(1 + \frac{K}{S}\right)^2 - 1}} \end{aligned} \quad (\text{A.15})$$

Equation A.15 represents the solution to the most basic Kubelka-Munk differential equations as they were originally presented [KM31]. Fishkin describes the evolution of K-M theory through several years of improvements by a series of researchers [Fis83], which we only summarize here.

The Kubelka-Munk equations were generalized to allow arbitrary mixtures of pigments [Dun40]. If there are n multiple materials in the same layer with different scattering and absorption coefficients (ie: multiple pigments within the same layer of paint), they may be combined via linear weighting using their respective concentrations c_i :

$$\begin{aligned} S_{mixture}(\lambda) &= \sum_{i=1}^n c_i S_i(\lambda) \\ K_{mixture}(\lambda) &= \sum_{i=1}^n c_i K_i(\lambda) \end{aligned} \quad (\text{A.16})$$

Kubelka extended the 1931 work in two subsequent articles. He first solved the differential equations of Equation A.4 for a finite thickness of paint (originally, the infinite case was presented) [Kub48]. If the paint film has thickness x , then

$$R_x = \frac{\frac{1}{R_\infty}(R_0 - R_\infty) - R_\infty \left(R_0 - \frac{1}{R_\infty}\right) e^{Sx\left(\frac{1}{R_\infty} - R_\infty\right)}}{(R_0 - R_\infty) - \left(R_0 - \frac{1}{R_\infty}\right) e^{Sx\left(\frac{1}{R_\infty} - R_\infty\right)}} \quad (\text{A.17})$$

Another form of this equation can be found using hyperbolic functions, allowing for simpler computation:

$$R_x = \frac{1 - R_0(a - b \coth bSx)}{a - R_0 + b \coth bSx} \quad (\text{A.18})$$

where $a = 1 + \frac{K}{S}$ and $b = \sqrt{a^2 - 1}$ as earlier. When the paint becomes thick enough to hide the substrate, $R_0 \rightarrow 0$. Thus we have

$$R_x = \frac{1}{a + b \coth bSx} \quad (\text{A.19})$$

and if the paint is infinitely thick, $x \rightarrow \infty$, so $bSx \rightarrow 1$ reducing to

$$R_\infty = \frac{1}{a+b} \quad (\text{A.20})$$

which is exactly Equation A.14, showing that the infinite-thickness solution is just a special case of the more general finite-thickness case. In the same work, Kubelka also found an analogous formula with hyperbolic terms representing transmittance T through a layer:

$$T = \frac{b}{a \sinh bSx + b \cosh bSx} \quad (\text{A.21})$$

Later, Kubelka presented a simple method for computing the reflectance and transmittance of several layers composited on top of each other [Kub54]. Consider two homogeneous layers of different optical properties and possibly different thicknesses.

As seen in Figure A.2, light entering such a material is reflected and transmitted multiple times, forming a tree-like structure for each incident ray. As the light flux from an incident ray hits the top layer, part is reflected (R_1) and part is transmitted (T_1). T_1 reaches the bottom layer and reflects T_1R_2 , while transmitting T_1T_2 . The portion T_1R_2 hits the lower portion of the top layer and transmits $T_1R_2T_1'$ (which exits back into the air), while reflecting $T_1R_2R_1$ back into the lower layer \dots and so on, ad infinitum. Adding up the portions finally transmitted by the combined layered specimen, we have

$$T_{total} = T_1T_2(1 + R_1'R_2 + R_1'^2R_2^2 + \dots) = \frac{T_1T_2}{1 - R_1'R_2} \quad (\text{A.22})$$

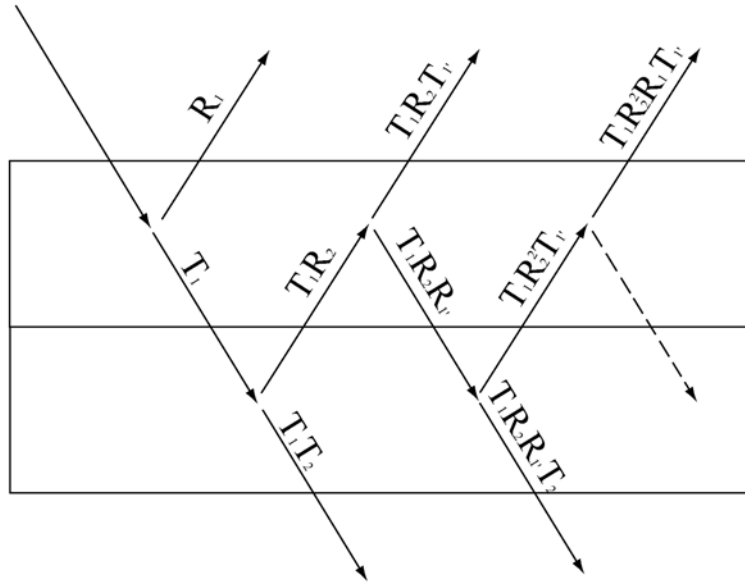


Figure A.2: The path of light between two homogeneous layers.
Adapted from [Kub54]

Summing the portions reflected by the layered specimen, we have

$$R_{total} = R_1 + T_1 T_1' R_2 (1 + R_1' R_2 + R_1'^2 R_2^2 + \dots) = R_1 + \frac{T_1 T_1' R_2}{1 - R_1' R_2} \quad (\text{A.23})$$

For any homogeneous layer, $R_1 = R_1'$, or the material reflects light equally when illuminated from both sides. Also, it can be shown that $T_1 = T_1'$, or the transmittance has the same value, if we illuminate a homogeneous layer from one side or the other. Therefore, the formulas simplify to:

$$T_{total} = \frac{T_1 T_2}{1 - R_1 R_2} \quad (\text{A.24})$$

$$R_{total} = R_1 + \frac{T_1^2 R_2}{1 - R_1 R_2} \quad (\text{A.25})$$

The compositing equations can be used to calculate the reflectance of specimens that contain more than two layers (which is often the case in painting).

One concatenates the layers into a single reflectance value by obtaining R and T from two layers, and using that value for the next compositing operation. For instance, a specimen with three homogeneous layers has reflectance R_1, R_2, R_3 and transmittance T_1, T_2, T_3 :

$$R_{1,2} = \frac{T_1 T_2}{1 - R_1 R_2} \quad (\text{A.26})$$

$$T_{1,2} = R_1 + \frac{T_1^2 R_2}{1 - R_1 R_2} \quad (\text{A.27})$$

$$R_{1,2,3} = \frac{T_{1,2} T_3}{1 - R_{1,2} R_3} \quad (\text{A.28})$$

$$T_{1,2,3} = R_{1,2} + \frac{T_{1,2}^2 R_3}{1 - R_{1,2} R_3} \quad (\text{A.29})$$

Appendix B

Supplemental sample analysis

The following includes supplemental sample analyses from our results [BGM06]. The first section is a group of five pigment-time combinations, showing significant appearance variation across binding media. The second section contains a group of five pigment-media combinations, showing how the appearance of paint changes over time.

For each combination, the following is included: spectral plots and corresponding photographs, three-dimensional Munsell color plots, color space conversions, and the perceptual differences ΔE between colors in the $L^*a^*b^*$ color space.

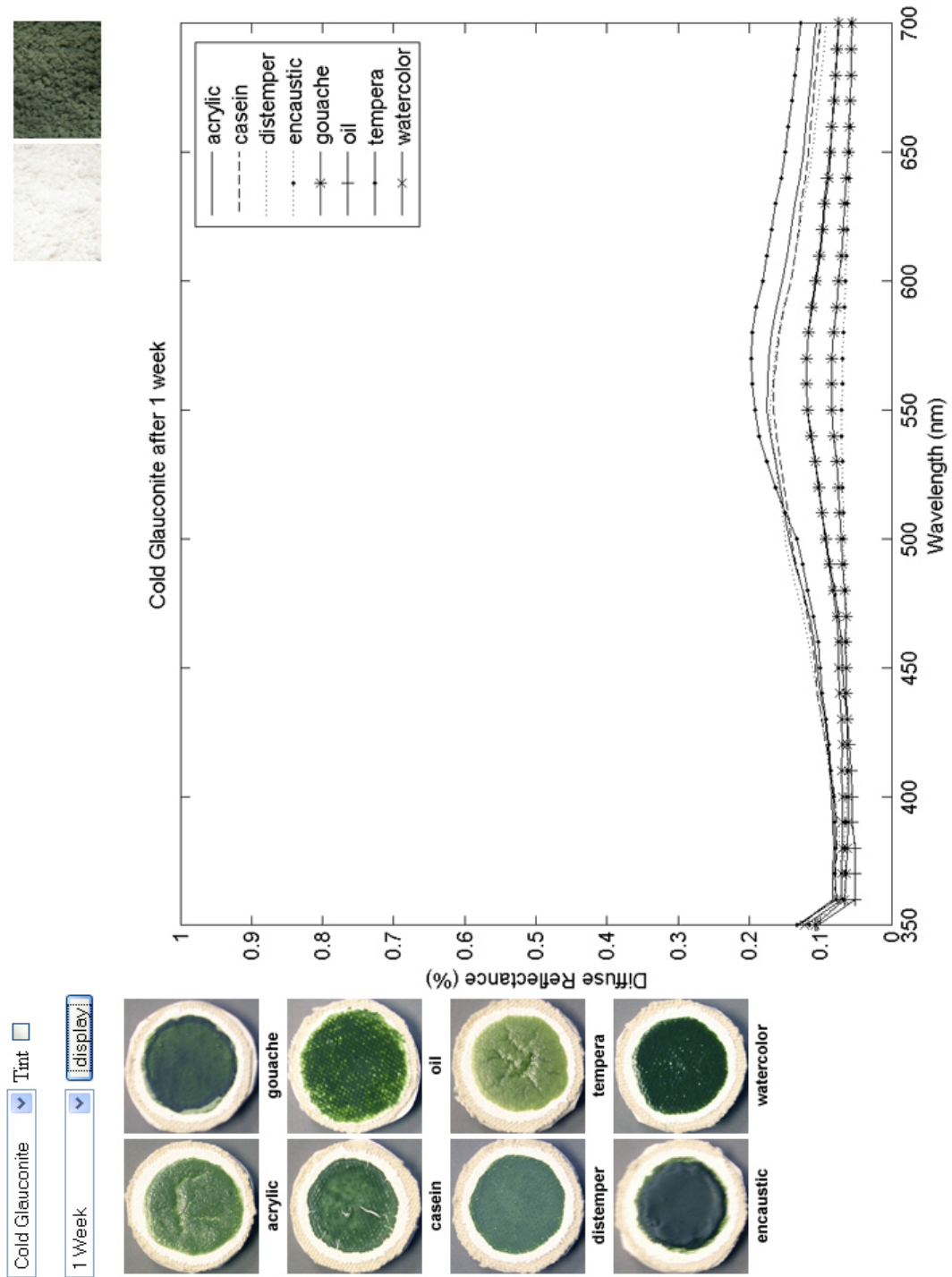


Figure B.1: Cold Glauconite in different binding media after one week.

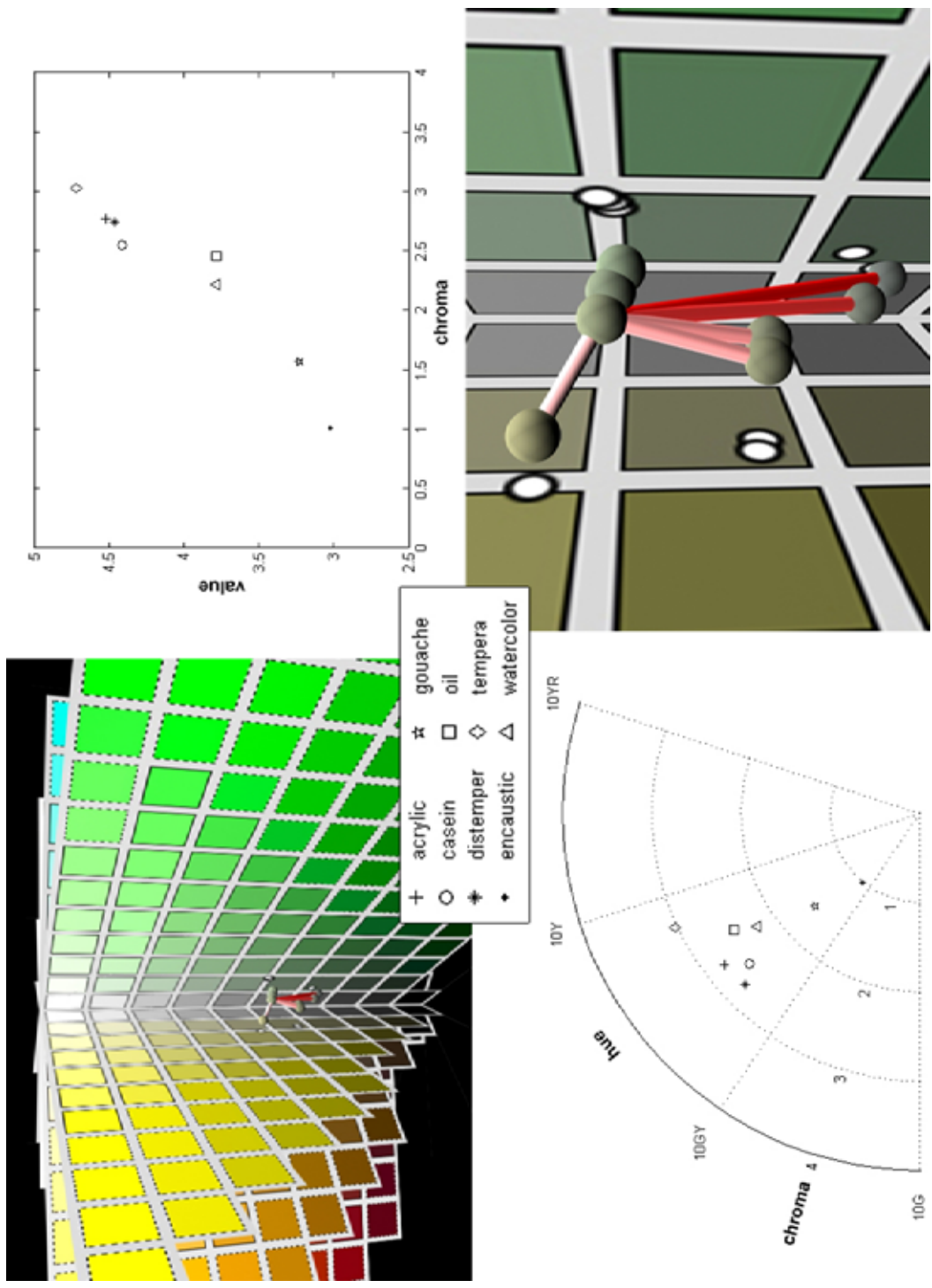


Figure B.2: Munsell plots of Cold Glauconite in different binding media after one week.

Table B.1: Color conversions from the spectral reflectances of the samples of Cold Glauconite in different binding media, after one week.

	X	Y	Z	H	V	C	L^*	a^*	b^*
acrylic	13.75	15.73	15.73	5.52GY	4.52	2.77	46.62	-7.25	2.51
casein	13.00	14.91	11.85	6.52GY	4.41	2.55	45.51	-7.31	10.09
distemper	13.11	15.30	12.21	7.38GY	4.46	2.74	46.04	-8.85	10.04
encaustic	6.13	6.66	6.88	8.95GY	3.02	1.01	31.03	-2.06	1.02
gouache	6.85	7.60	6.91	6.51GY	3.23	1.57	33.13	-3.57	4.56
oil	9.39	10.60	7.57	3.90GY	3.78	2.46	38.89	-5.24	12.02
tempera	15.54	17.31	11.17	1.95GY	4.72	3.03	48.65	-5.03	17.38
watercolor	9.46	10.61	8.15	4.65GY	3.78	2.22	38.92	-4.86	10.00

Table B.2: Table of perceptual differences ΔE between colors using the $L^*a^*b^*$ color space. The colors are converted from samples of Cold Glauconite in different binding media, after one week.

	acrylic	casein	distemper	encaustic	gouache	oil	tempera
casein	7.661						
distemper	7.720	1.629					
encaustic	16.499	17.875	18.782				
gouache	14.132	14.065	14.986	4.384			
oil	12.419	7.200	8.251	13.889	9.572		
tempera	15.171	8.259	8.676	24.227	20.183	11.137	
watercolor	11.005	7.031	8.162	12.277	8.049	2.056	12.213

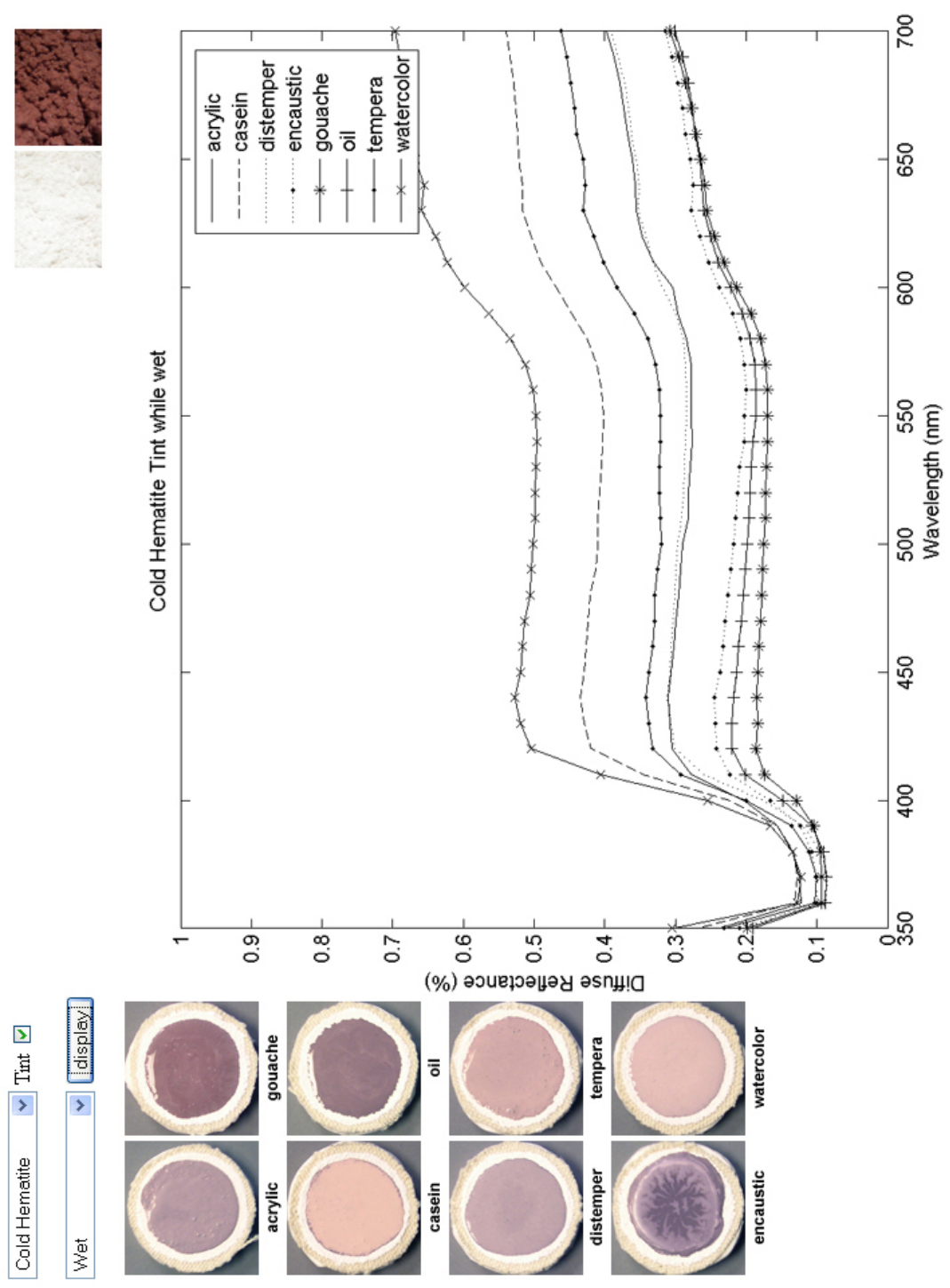


Figure B.3: Cold Hematite Tint in different binding media freshly painted.

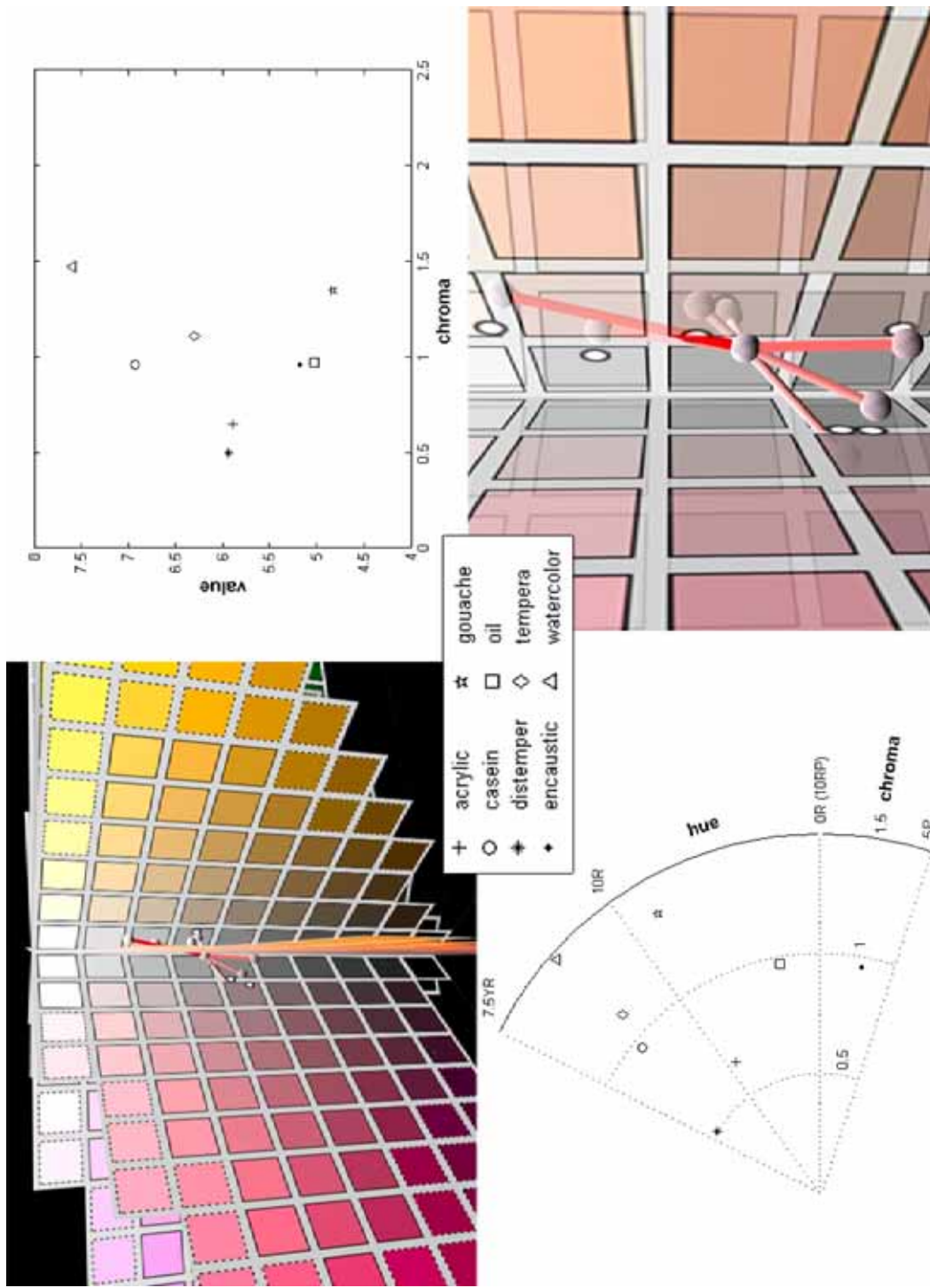


Figure B.4: Munsell plots of Cold Hematite Tint in different binding media freshly painted.

Table B.3: Color conversions from the spectral reflectances of the samples of Cold Hematite Tint in different binding media, freshly painted.

	X	Y	Z	H	V	C	L^*	a^*	b^*
acrylic	28.82	28.75	32.47	9.12R	5.89	0.65	60.56	6.20	-2.28
casein	42.16	42.07	45.44	4.11YR	6.93	0.96	70.92	6.99	-.34
distemper	29.13	29.37	32.64	6.38YR	5.94	0.50	61.11	5.05	-1.56
encaustic	21.85	21.46	25.22	7.12RP	5.18	0.96	53.45	7.20	-3.70
gouache	18.93	18.26	19.51	8.40R	4.83	1.35	49.81	8.58	0.15
oil	20.33	19.92	22.74	2.75R	5.02	0.97	51.75	7.25	-2.44
tempera	34.01	33.67	35.74	3.31YR	6.30	1.11	64.70	7.44	0.50
watercolor	52.75	52.26	54.98	3.47YR	7.60	1.47	77.44	8.50	1.06

Table B.4: Table of perceptual differences ΔE between colors using the $L^*a^*b^*$ color space. The colors are converted from samples of Cold Hematite Tint in different binding media, freshly painted.

	acrylic	casein	distemper	encaustic	gouache	oil	tempera
casein	10.569						
distemper	1.464	10.074					
encaustic	7.319	17.791	8.239				
gouache	11.275	21.176	11.961	5.475			
oil	8.874	19.286	9.655	2.117	3.499		
tempera	5.139	6.293	4.780	12.011	14.938	13.281	
watercolor	17.360	6.837	16.895	24.492	27.645	25.957	12.796

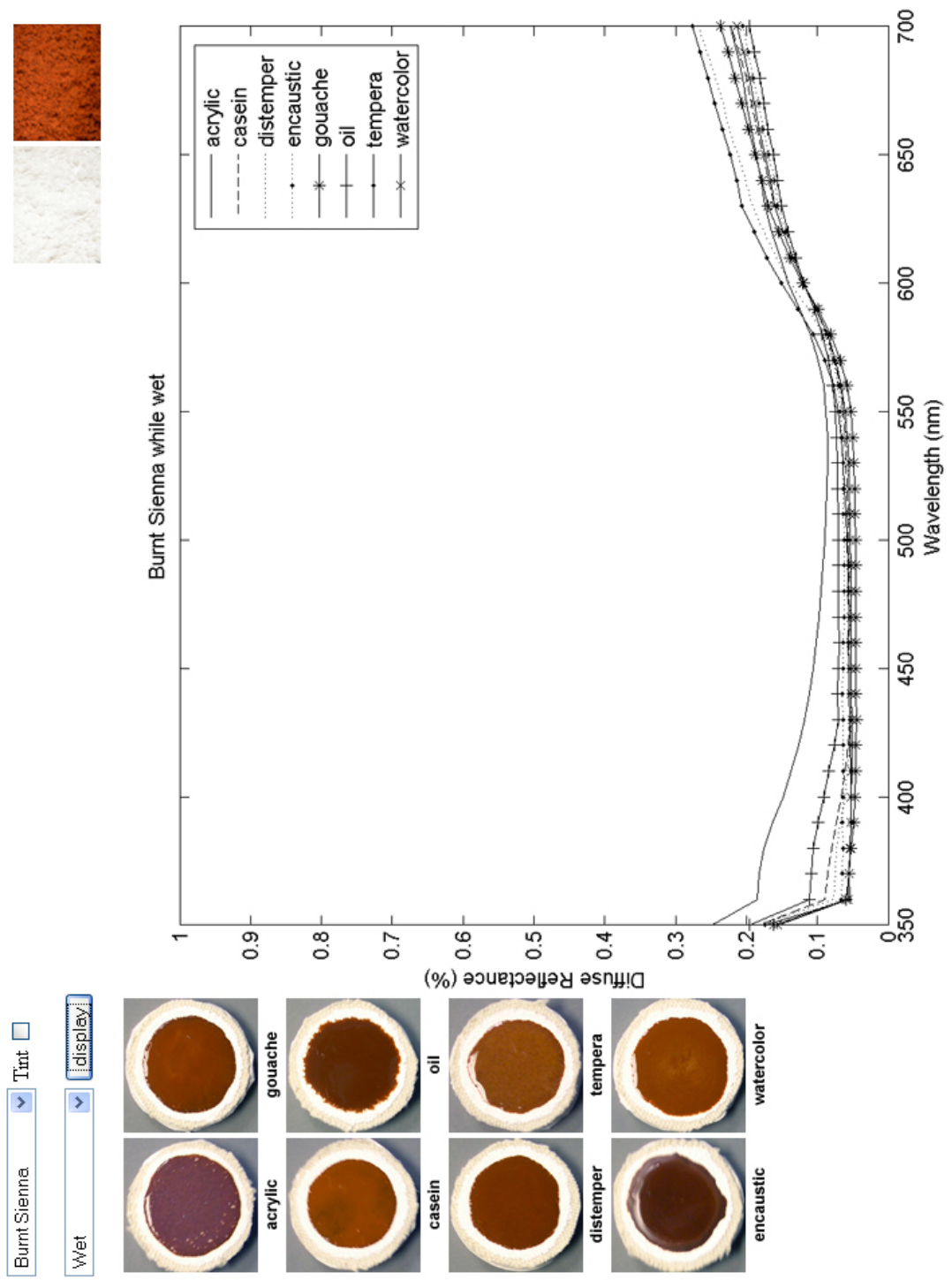


Figure B.5: Burnt Sienna in different binding media freshly painted.

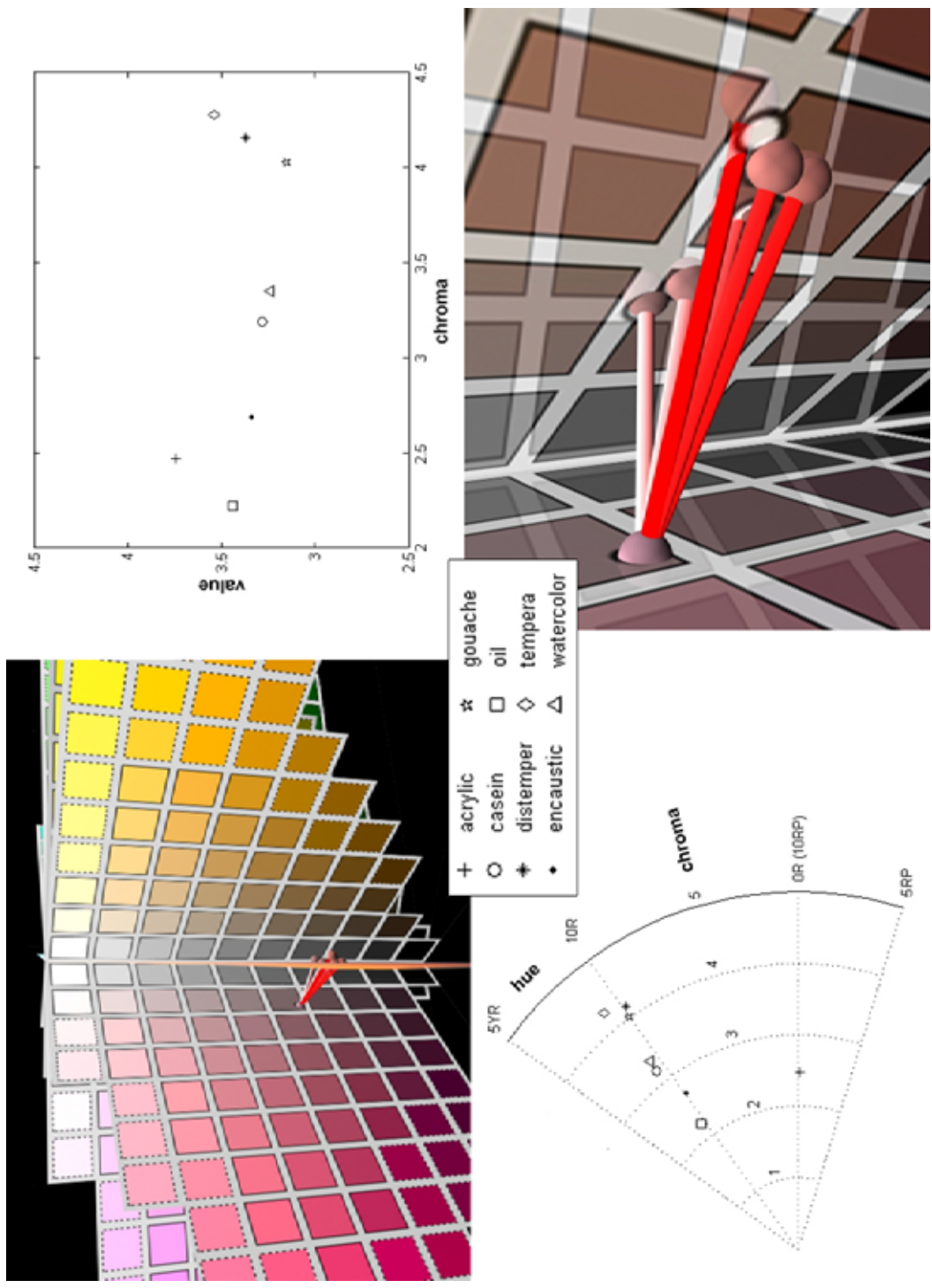


Figure B.6: Munsell plots of Burnt Sienna in different binding media freshly painted.

Table B.5: Color conversions from the spectral reflectances of the samples of Burnt Sienna in different binding media, freshly painted.

	X	Y	Z	H	V	C	L^*	a^*	b^*
acrylic	11.82	10.37	11.49	9.89RP	3.74	2.47	38.50	14.88	-1.00
casein	9.31	7.88	5.96	0.69YR	3.28	3.19	33.73	16.35	9.42
distemper	10.34	8.312	5.72	9.83R	3.37	4.16	34.62	20.68	12.00
encaustic	9.41	8.156	6.83	9.93R	3.34	2.69	34.31	14.68	6.86
gouache	9.06	7.238	4.91	9.99R	3.15	4.03	32.34	20.20	11.80
oil	9.70	8.68	7.67	0.48YR	3.44	2.22	35.36	12.45	5.57
tempera	11.29	9.214	5.99	0.94YR	3.54	4.28	36.39	20.19	13.91
watercolor	9.18	7.684	5.65	0.69YR	3.24	3.35	33.32	16.99	10.05

Table B.6: Table of perceptual differences ΔE between colors using the $L^*a^*b^*$ color space. The colors are converted from samples of Burnt Sienna in different binding media, freshly painted.

	acrylic	casein	distemper	encaustic	gouache	oil	tempera
casein	11.554						
distemper	14.755	5.118					
encaustic	8.909	3.111	7.907				
gouache	15.169	4.735	2.339	7.665			
oil	7.677	5.718	10.470	2.782	10.392		
tempera	15.967	6.479	2.650	9.186	4.567	11.425	
watercolor	12.385	0.987	4.371	4.061	3.785	6.697	5.879

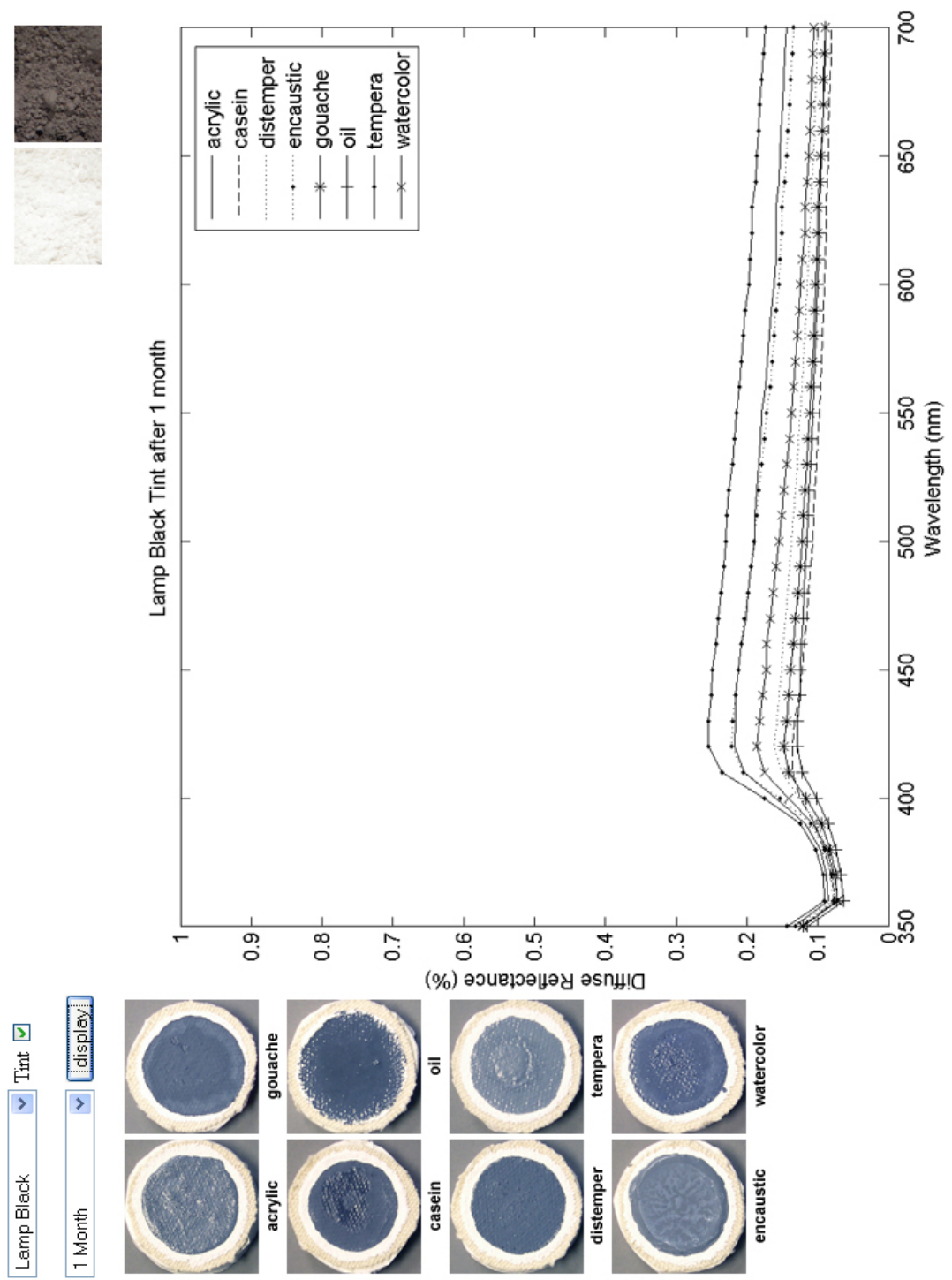


Figure B.7: Lampblack Tint in different binding media after one month.

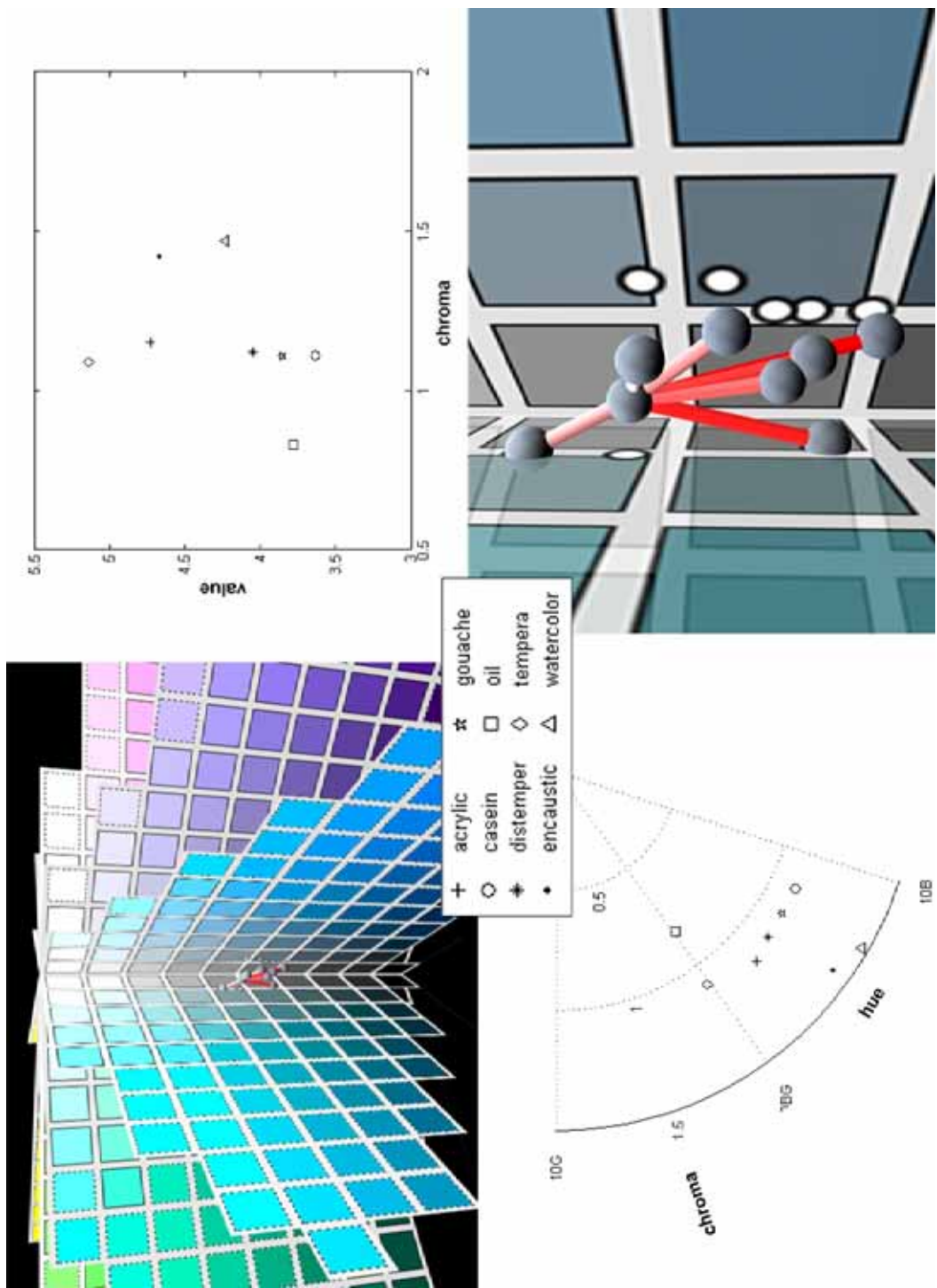


Figure B.8: Munsell plots of Lampblack Tint in different binding media after one month.

Table B.7: Color conversions from the spectral reflectances of the samples of Lampblack Tint in different binding media, after one month.

	X	Y	Z	H	V	C	L^*	a^*	b^*
acrylic	16.39	17.45	22.41	2.89B	4.73	1.15	48.82	-0.85	-6.90
casein	9.25	9.73	13.16	7.69B	3.63	1.11	37.34	0.24	-7.40
distemper	11.58	12.31	16.15	4.43B	4.05	1.12	41.71	-0.65	-6.90
encaustic	15.87	16.94	22.50	5.03B	4.67	1.42	48.18	-1.07	-8.17
gouache	10.42	11.02	14.66	6.07B	3.85	1.11	39.61	-0.20	-7.13
oil	9.96	10.59	13.29	0.11B	3.78	0.83	38.88	-0.60	-5.08
tempera	19.75	21.09	26.36	9.80BG	5.14	1.09	53.05	-1.25	-6.21
watercolor	12.76	13.59	18.55	6.60B	4.23	1.47	43.63	-0.81	-8.60

Table B.8: Table of perceptual differences ΔE between colors using the $L^*a^*b^*$ color space. The colors are converted from samples of Lampblack Tint in different binding media, after one month.

	acrylic	casein	distemper	encaustic	gouache	oil	tempera
casein	11.543						
distemper	7.113	4.488					
encaustic	1.439	10.946	6.607				
gouache	9.236	2.328	2.160	8.677			
oil	10.108	2.909	3.365	9.811	2.213		
tempera	4.305	15.825	11.377	5.253	13.512	14.230	
watercolor	5.462	6.489	2.569	4.578	4.324	5.916	9.728

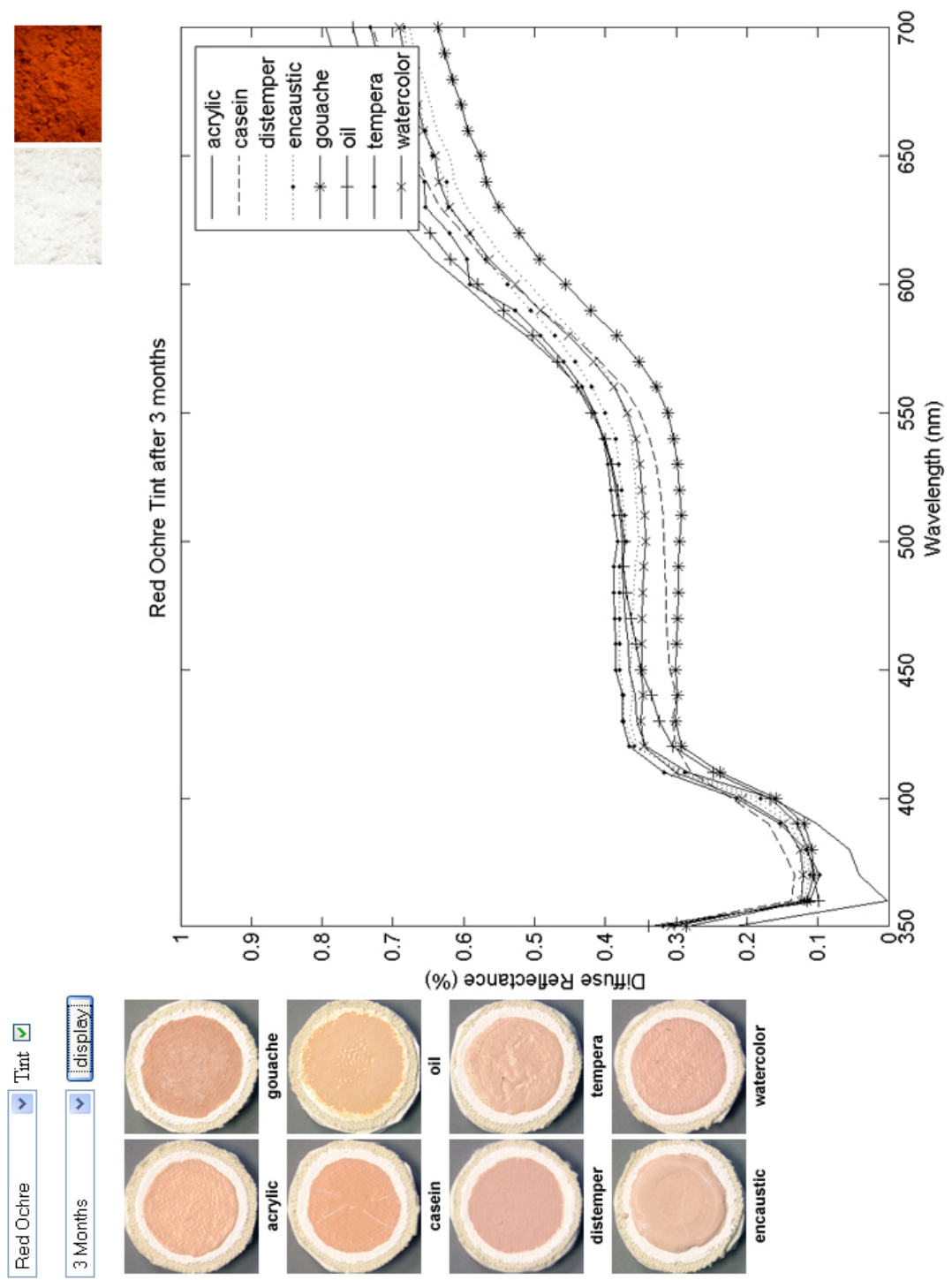


Figure B.9: Red Ochre Tint in different binding media after three months.

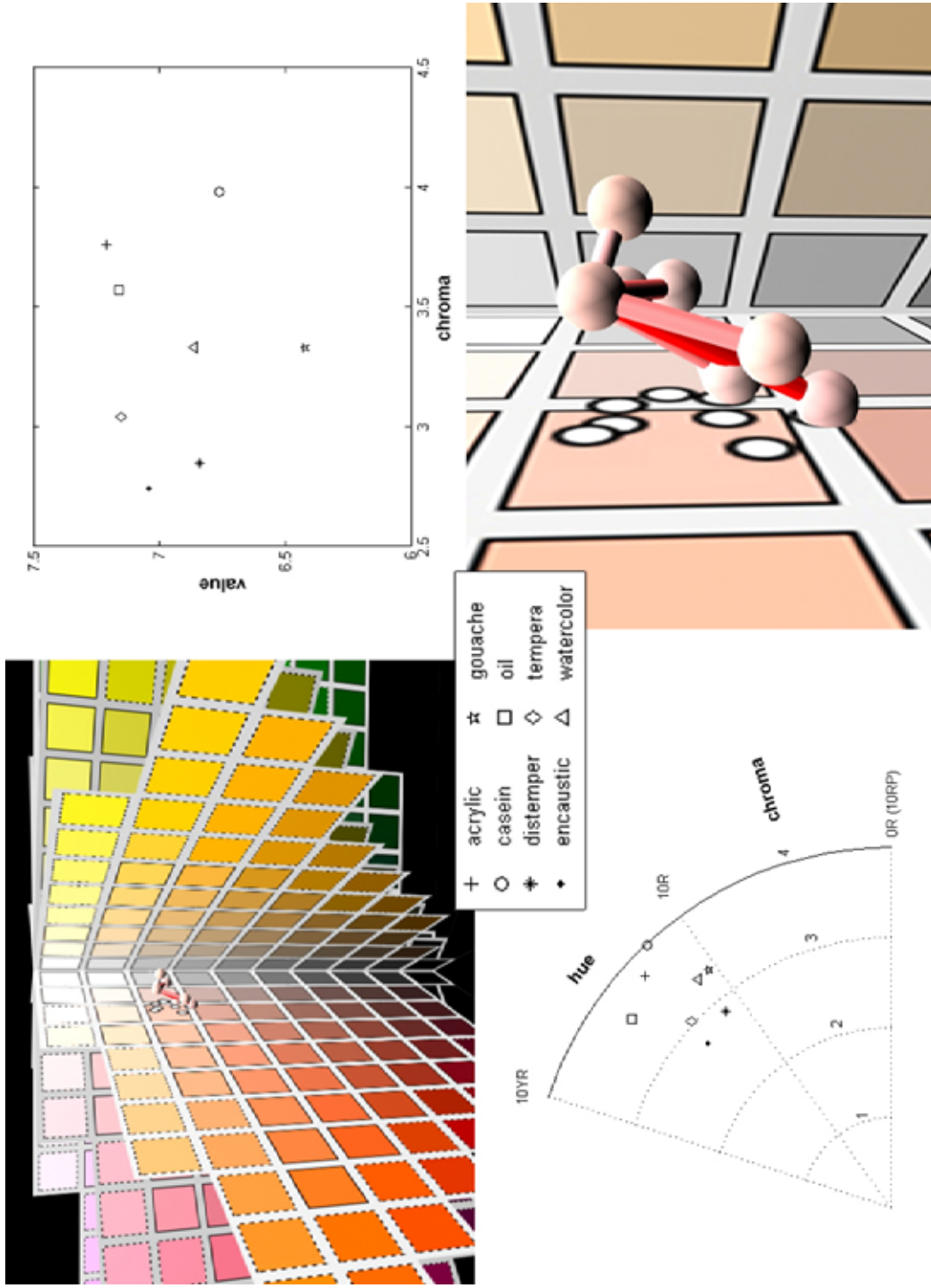


Figure B.10: Munsell plots of Red Ochre Tint in different binding media after three months.

Table B.9: Color conversions from the spectral reflectances of the samples of Red Ochre Tint in different binding media, after three months.

	X	Y	Z	H	V	C	L^*	a^*	b^*
acrylic	49.34	46.17	38.84	2.99YR	7.21	3.76	73.65	15.74	12.04
casein	43.16	39.72	33.08	1.94YR	6.76	3.98	69.27	17.09	11.90
distemper	43.17	40.84	38.62	1.21YR	6.84	2.85	70.06	13.69	6.12
encaustic	45.47	43.36	40.15	3.42YR	7.04	2.74	71.98	12.33	7.55
gouache	38.02	35.17	31.87	0.45YR	6.42	3.33	65.88	15.79	7.73
oil	47.83	45.47	37.02	5.03YR	7.16	3.57	73.20	13.56	13.51
tempera	47.58	45.26	40.79	3.12YR	7.15	3.04	73.06	13.44	8.67
watercolor	43.91	41.02	37.17	1.20YR	6.86	3.33	70.19	15.34	8.14

Table B.10: Table of perceptual differences ΔE between colors using the $L^*a^*b^*$ color space. The colors are converted from samples of Red Ochre Tint in different binding media, after three months.

	acrylic	casein	distemper	encaustic	gouache	oil	tempera
casein	4.586						
distemper	7.221	6.752					
encaustic	5.880	6.995	2.753				
gouache	8.886	5.529	4.947	7.015			
oil	2.668	5.523	8.031	6.207	9.590		
tempera	4.123	6.174	3.945	1.911	7.613	4.844	
watercolor	5.229	4.248	2.612	3.551	4.353	6.408	3.483

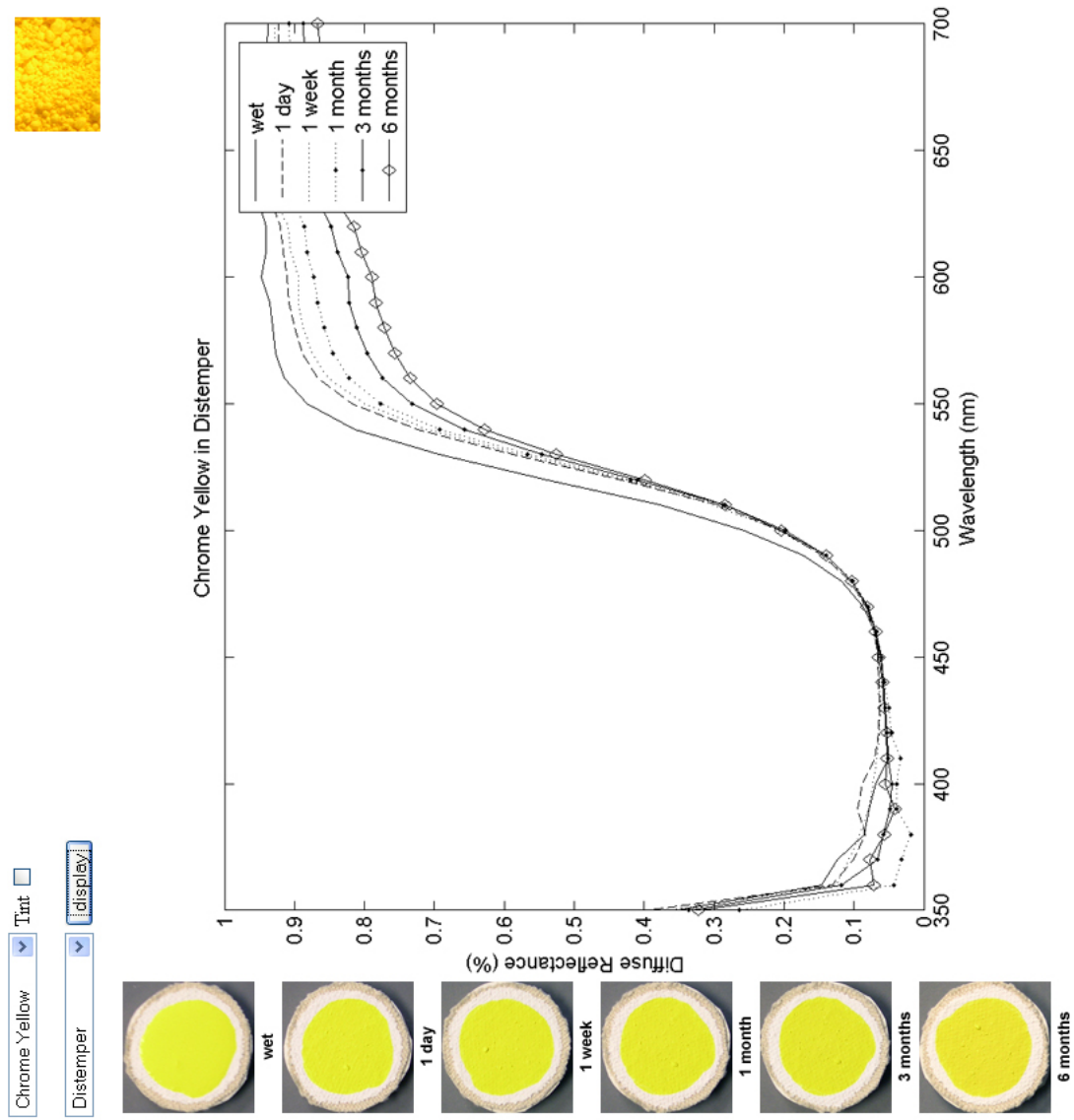


Figure B.11: Variation of spectral reflectance curves of Chrome Yellow in Distemper over time.

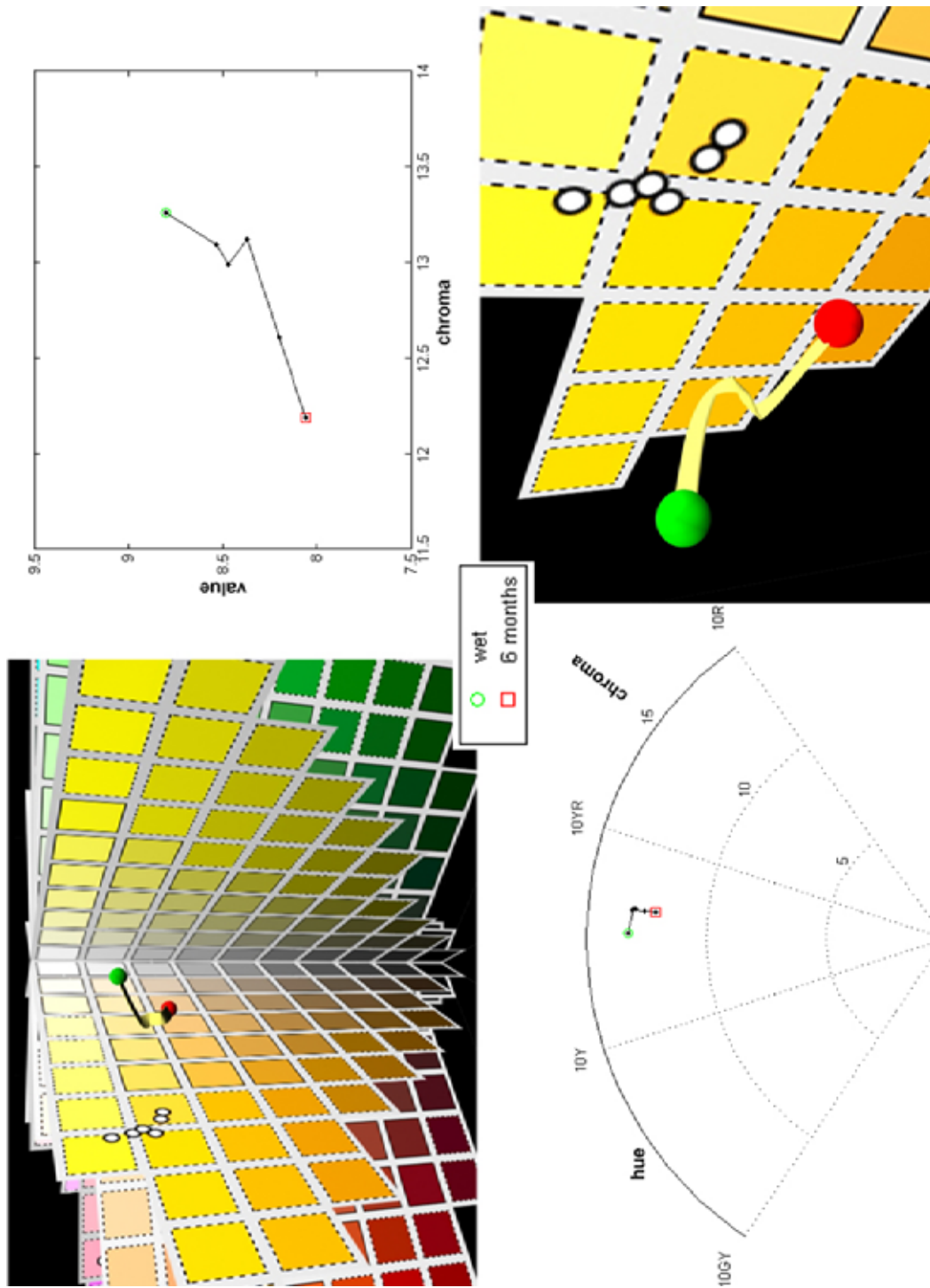


Figure B.12: Munsell plots of Chrome Yellow in Distemper over time.

Table B.11: Color conversions of Chrome Yellow in Distemper over time.
 ΔE is the distance from the previous to current $L^*a^*b^*$ color.

	X	Y	Z	H	V	C	L	a	b	ΔE
wet	70.94	74.41	9.49	4.75Y	8.80	13.26	89.12	0.83	92.11	
1 day	68.26	68.93	9.30	3.49Y	8.53	13.09	86.47	6.46	88.15	7.38
1 week	67.24	67.90	9.25	3.50Y	8.47	12.99	85.96	6.42	87.44	0.88
1 month	65.22	65.93	8.40	3.58Y	8.37	13.12	84.96	6.22	88.50	1.47
3 months	62.10	62.78	8.61	3.60Y	8.20	12.61	83.33	6.10	85.00	3.86
6 months	59.52	60.18	8.74	3.61Y	8.06	12.19	81.94	5.99	82.17	0.44

Table B.12: Color conversions of Hematite Tint in Watercolor over time.
 ΔE is the distance from the previous to current $L^*a^*b^*$ color.

	X	Y	Z	H	V	C	L	a	b	ΔE
wet	34.07	32.44	36.52	0.74R	6.20	2.14	63.70	11.93	-2.22	
1 day	24.53	22.71	27.02	5.78RP	5.31	2.52	54.77	13.52	-4.27	9.30
1 week	23.28	21.50	25.85	5.16RP	5.19	2.53	53.49	13.55	-4.62	1.33
1 month	18.45	16.68	19.70	6.51RP	4.64	2.61	47.85	14.53	-3.59	5.82
3 months	16.93	15.29	17.91	7.02RP	4.46	2.48	46.03	14.20	-3.17	1.90
6 months	16.58	15.01	17.37	7.71RP	4.43	2.39	45.65	13.89	-2.71	0.70

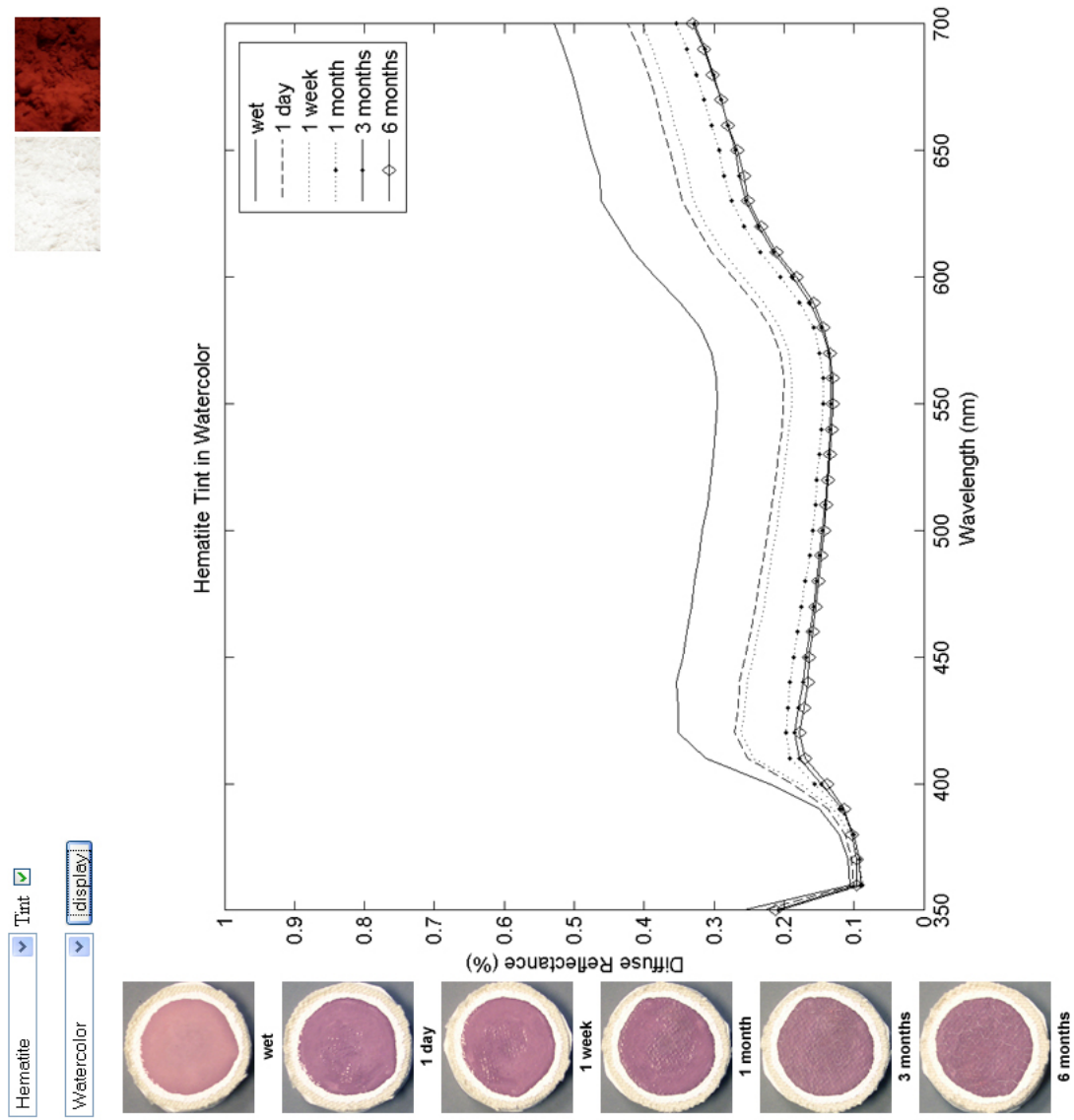


Figure B.13: Variation of spectral reflectance curves of Hematite Tint in Watercolor over time.

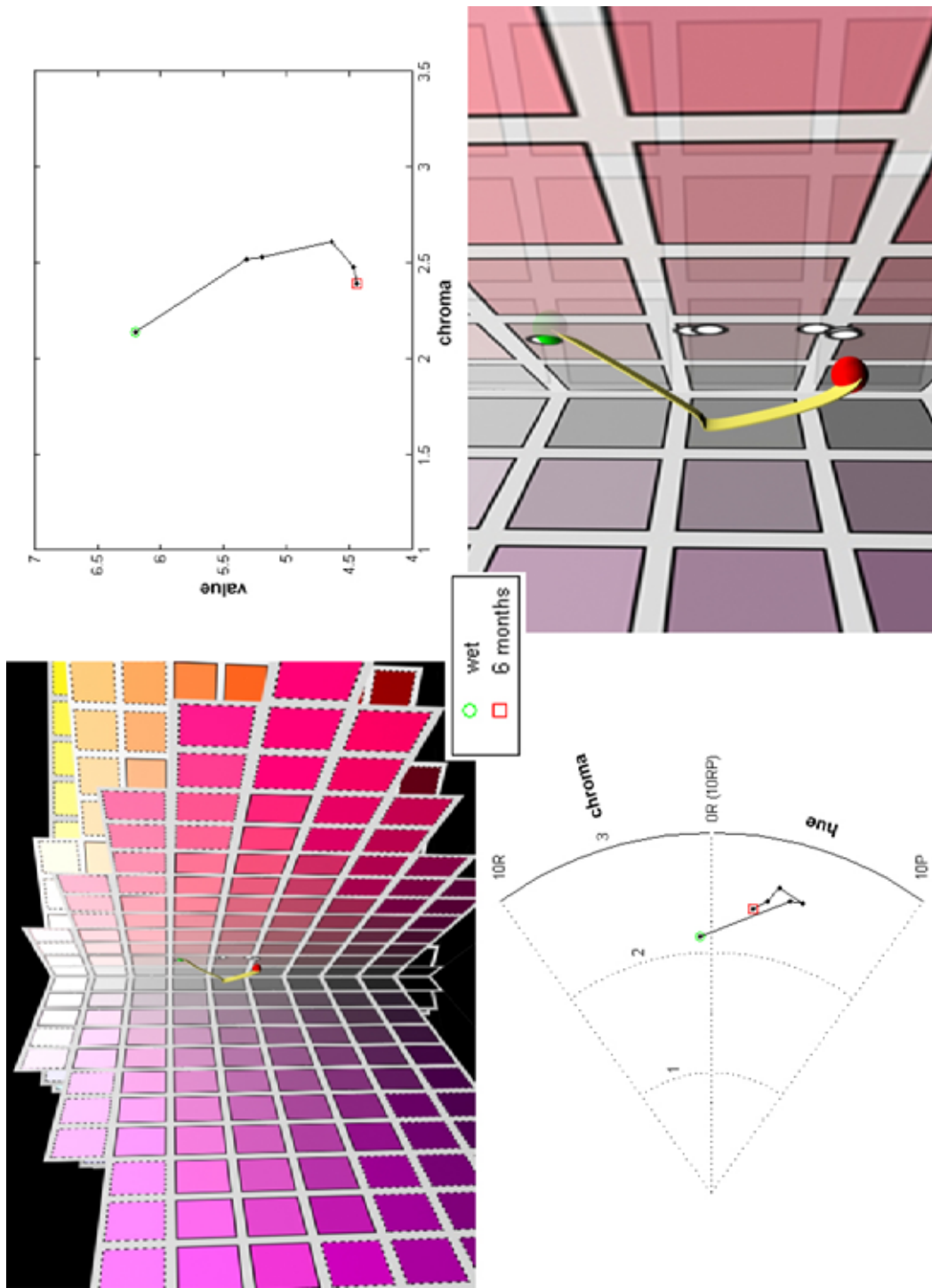


Figure B.14: Munsell plots of Hematite Tint in Watercolor over time.

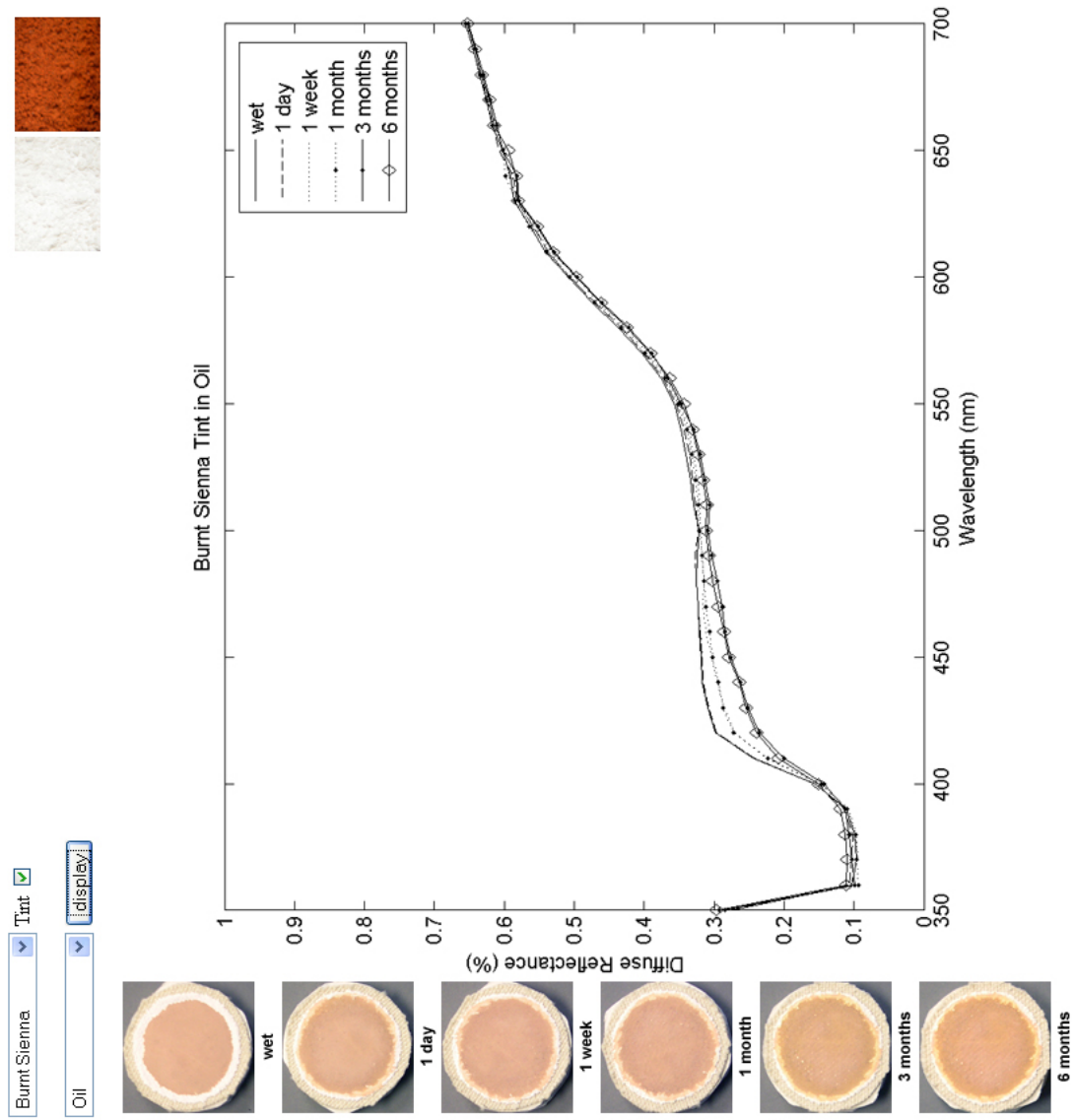


Figure B.15: Variation of spectral reflectance curves of Burnt Sienna Tint in Oil over time.

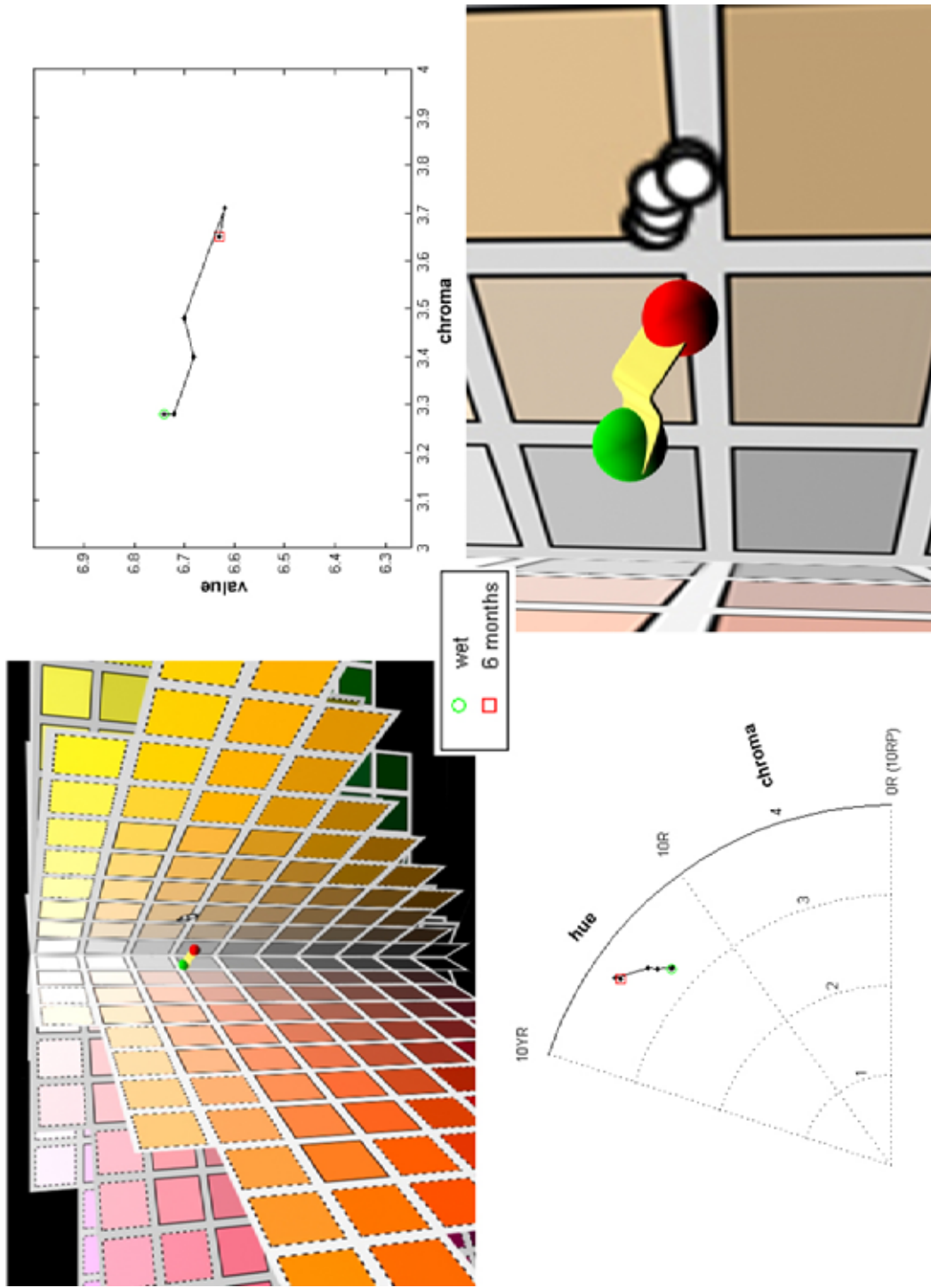


Figure B.16: Munsell plots of Burnt Sienna Tint in Oil over time.

Table B.13: Color conversions of Burnt Sienna Tint in Oil over time. ΔE is the distance from the previous to current $L^*a^*b^*$ color.

	X	Y	Z	H	V	C	L	a	b	ΔE
wet	41.75	39.38	33.88	3.44YR	6.74	3.28	69.02	13.91	10.41	
1 day	41.51	39.11	33.75	3.30YR	6.72	3.28	68.83	14.00	10.25	0.26
1 week	40.93	38.58	32.29	3.94YR	6.68	3.40	68.45	13.89	11.58	1.39
1 month	41.24	38.88	32.08	4.20YR	6.70	3.48	68.66	13.91	12.24	0.69
3 months	40.04	37.84	29.31	5.50YR	6.62	3.71	67.91	13.45	14.90	2.80
6 months	40.14	37.96	29.65	5.43YR	6.63	3.65	67.99	13.39	14.54	0.09

Table B.14: Color conversions of Cold Glaunconite in Watercolor over time. ΔE is the distance from the previous to current $L^*a^*b^*$ color.

	X	Y	Z	H	V	C	L	a	b	ΔE
wet	10.13	11.73	8.69	6.01GY	3.96	2.64	40.78	-7.47	11.38	
1 day	9.17	10.30	7.94	4.76GY	3.73	2.21	38.37	-4.87	9.80	3.88
1 week	9.46	10.61	8.15	4.65GY	3.78	2.22	38.92	-4.86	10.00	0.59
1 month	7.28	8.12	7.44	7.02GY	3.33	1.62	34.24	-3.99	4.43	7.33
3 months	7.29	8.10	7.57	7.20GY	3.33	1.53	34.19	-3.72	3.90	0.60
6 months	7.40	8.22	7.77	7.50GY	3.35	1.50	34.43	-3.73	3.59	0.30

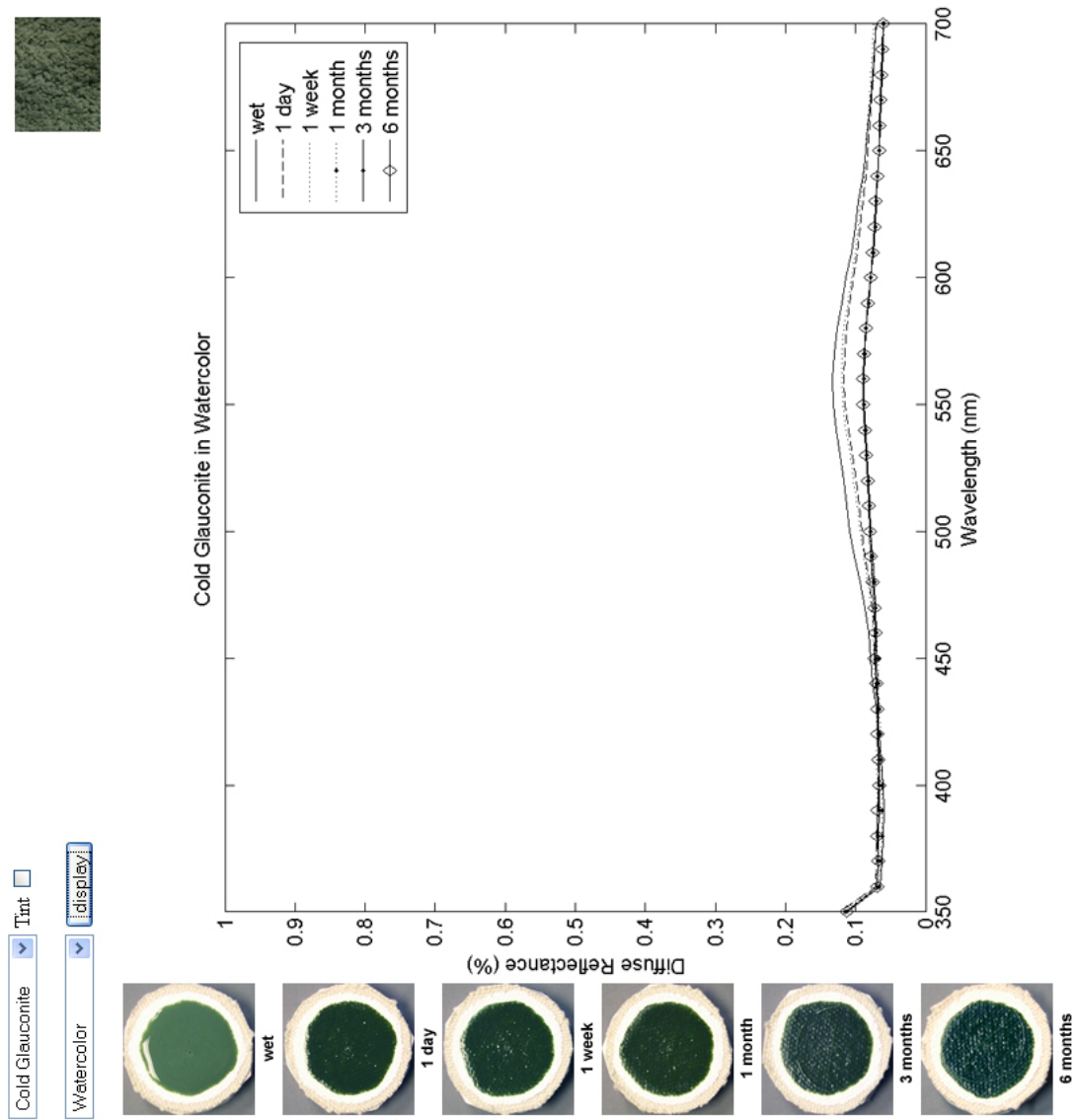


Figure B.17: Variation of spectral reflectance curves of Cold Glaucanite in Watercolor over time.

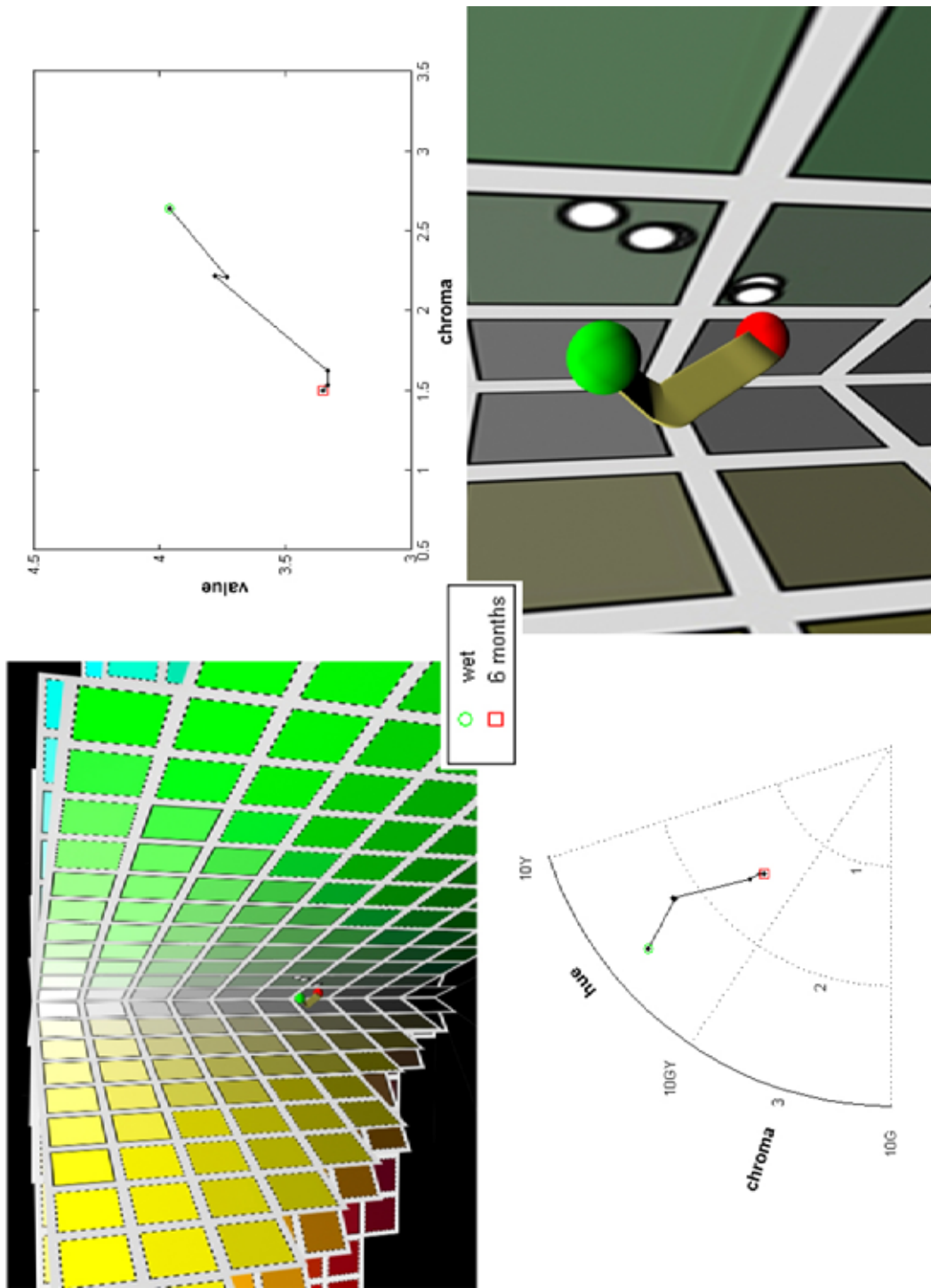


Figure B.18: Munsell plots of Cold Glaunconite in Watercolor over time.

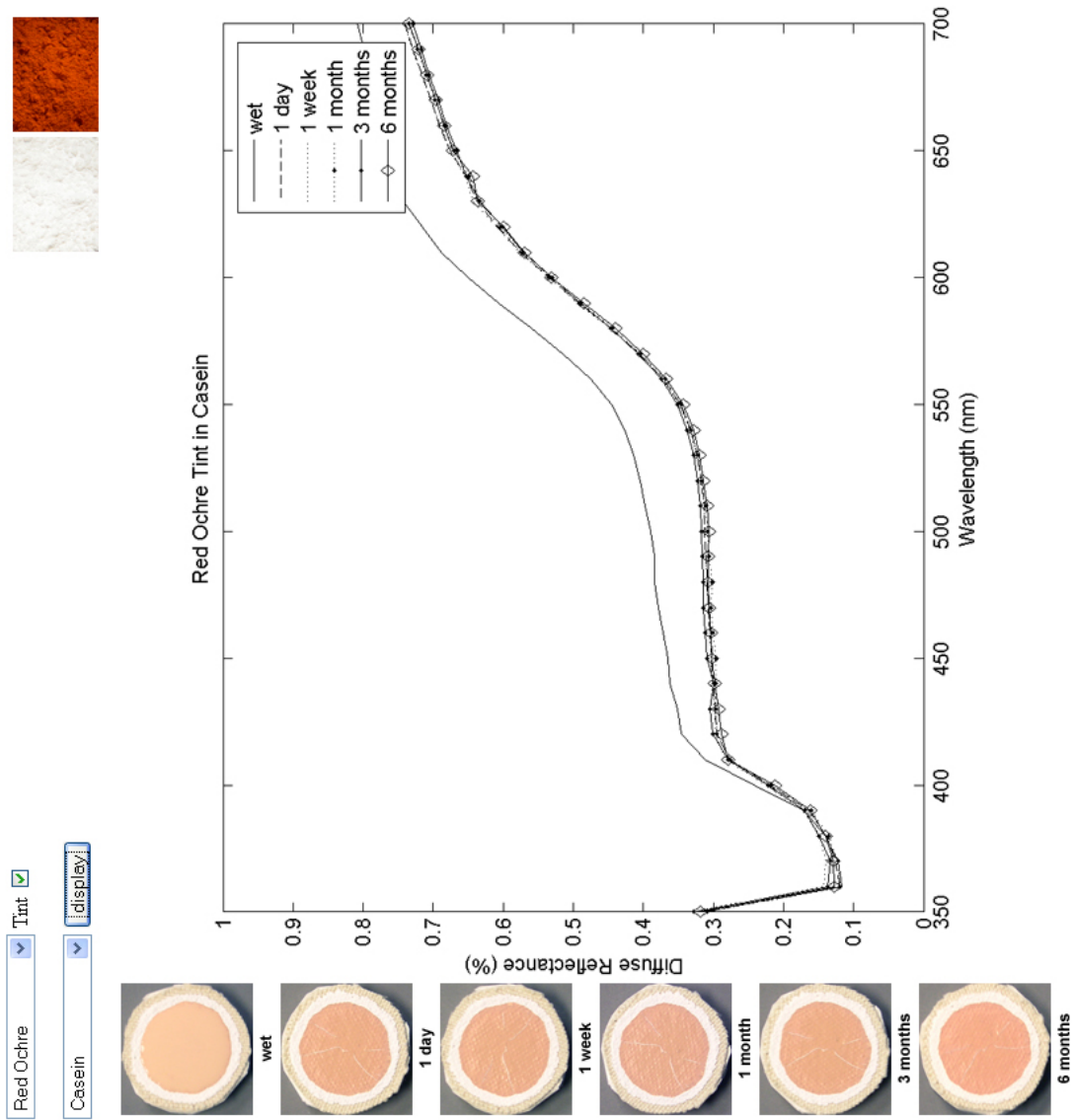


Figure B.19: Variation of spectral reflectance curves of Red Ochre Tint in Casein over time.

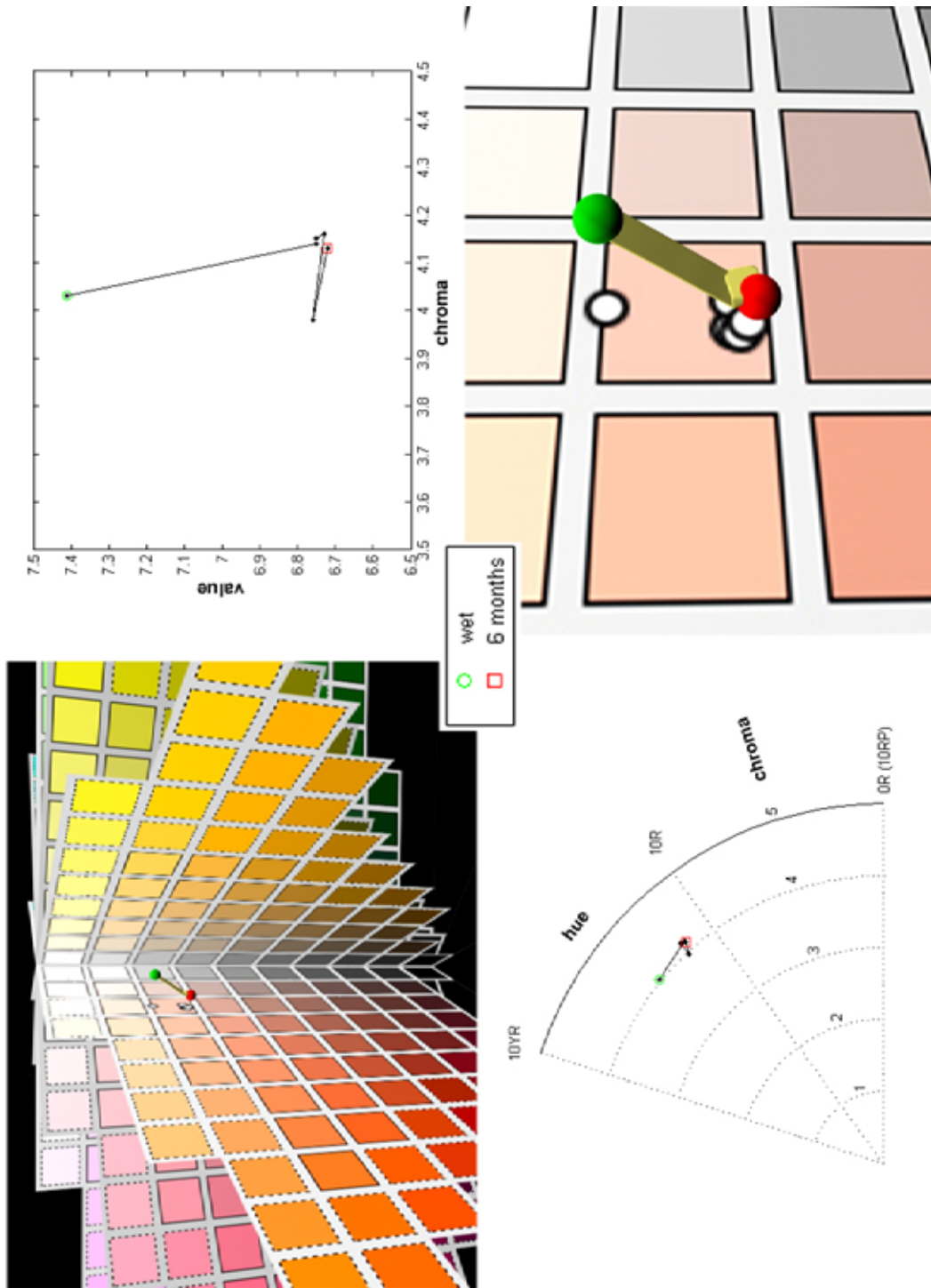


Figure B.20: Munsell plots of Red Ochre Tint in Casein over time.

Table B.15: Color conversions of Red Ochre Tint in Casein over time. ΔE is the distance from the previous to current $L^*a^*b^*$ color.

	X	Y	Z	H	V	C	L	a	b	ΔE
wet	52.41	49.22	39.34	4.09YR	7.41	4.03	75.58	15.59	14.76	
1 day	43.16	39.49	32.54	1.72YR	6.75	4.14	69.11	17.79	12.37	7.24
1 week	43.28	39.58	32.65	1.63YR	6.75	4.15	69.17	17.90	12.32	0.13
1 month	42.95	39.30	32.13	1.89YR	6.73	4.16	68.97	17.76	12.70	0.45
3 months	43.16	39.72	33.08	1.94YR	6.76	3.98	69.27	17.09	11.90	1.09
6 months	42.74	39.07	32.27	1.61YR	6.72	4.13	68.80	17.83	12.21	0.36

References

- [Alb71] Josef Albers. *Interaction of Color*. Yale University Press, New Haven, CT, 1971.
- [Ber00] Roy Berns, editor. *Billmeyer and Saltzman's Principles of Color Technology*. John Wiley & Sons, Inc., New York, NY, 3rd edition, 2000.
- [BGM06] Jeffrey B. Budsberg, Donald P. Greenberg, and Stephen R. Marschner. Reflectance measurements of pigmented colorants. Technical Report PCG-06-02, Cornell University, Ithaca, NY, September 2006.
- [Bli82] James F. Blinn. Light reflection functions for simulation of clouds and dusty surfaces. In *SIGGRAPH '82: Proceedings of the 9th annual conference on Computer graphics and interactive techniques*, pages 21–29, New York, NY, 1982. ACM Press.
- [Box05] The Engineering Tool Box. *Liquids and Fluids - Specific Gravity*, 2005. <http://www.engineeringtoolbox.com/specific-gravity-liquid-fluids-d_294.html>.
- [Bra59] William Bragg. *The Universe of Light*. Dover Publications, New York, NY, 1959.
- [Buo12] Michenagelo Buonarroti. *Sistine Chapel ceiling, Azor-Sadoch lunette*, 1508-1512. Musei Vaticani e Cappella Sistina. Vatican City, Rome. Images Copyright © Nippon Television Network Corporation, Tokyo.
- [BWL04] William V. Baxter, Jeremy Wendt, and Ming C. Lin. IMPaSTo: A realistic, interactive model for paint. In *NPAP '04: Proceedings of the 3rd international symposium on Non-photorealistic animation and rendering*, pages 45–56, New York, NY, June 2004. ACM Press.
- [CAS⁺97] Cassidy J. Curtis, Sean E. Anderson, Joshua E. Seims, Kurt W. Fleischer, and David H. Salesin. Computer-generated watercolor. In *SIGGRAPH '97: Proceedings of the 24th annual conference on Computer graphics and interactive techniques*, pages 421–430, New York, NY, 1997. ACM Press/Addison-Wesley Publishing Co.

- [Col06] Catharine H. Colwell. *Physics Lab: Refraction of light*, 2006. <<http://dev.physicslab.org/Chapter.aspx?cid=15>>.
- [D4384] ASTM D4303-03. *Standard Test Methods for Lightfastness of Colorants Used in Artists' Materials*. ASTM International, 1984. <<http://www.astm.org>>.
- [DEJ+99] Julie Dorsey, Alan Edelman, Henrik Wann Jensen, Justin Legakis, and Hans K ohling Pedersen. Modeling and rendering of weathered stone. In *SIGGRAPH '99: Proceedings of the 26rd annual conference on Computer graphics and interactive techniques*, pages 225–234, New York, NY, 1999. ACM Press.
- [Den05] David Denys. *How to prepare a canvas the safe, traditional way*, 2005. <<http://www.denysart.com/canvasprep.html>>.
- [DH96] Julie Dorsey and Pat Hanrahan. Modeling and rendering of metallic patinas. In *SIGGRAPH '96: Proceedings of the 23rd annual conference on Computer graphics and interactive techniques*, pages 387–396, New York, NY, 1996. ACM Press.
- [Dun40] D. R. Duncan. The colour of pigment mixtures. *Proceedings of the Physical Society*, 52(3):390–401, 1940.
- [Fel68] Robert L. Feller. Problems in spectrophotometry. In *IIC '67: Proceedings of the London Conference for Conservation on Museum Climatology*, pages 196–197, London, 1968. International Institute for Conservation of Historic and Artistic Works.
- [Fel94] Robert L. Feller. *Accelerated Aging: Photochemical and Thermal Aspects*. The Getty Conservation Institute, Los Angeles, CA, 1994. <http://www.getty.edu/conservation/publications/pdf_publications/books.html>.
- [Fis83] Kenneth Paul Fishkin. Applying color science to computer graphics. Master's thesis, University of California, Berkeley, December 1983.
- [G95a] Andrew S. Glassner. *Principles of Digital Image Synthesis*, volume 1. Morgan Kaufmann Publishers, San Francisco, CA, 1995.
- [G95b] Andrew S. Glassner. *Principles of Digital Image Synthesis*, volume 2. Morgan Kaufmann Publishers, San Francisco, CA, 1995.
- [GED64] F. W. Goodhart, M. E. Everhard, and D. A. Dickcius. Stability of certified dyes in tables II. Fading of FD&C Red No. 3 and FD&C Red No. 3 Aluminum Lake in three tablet formulas. *Journal of Pharmaceutical Sciences*, 53:338–340, 1964.

- [GLL⁺04] Michael Goesele, Hendrik P. A. Lensch, Jochen Lang, Christian Fuchs, and Hans-Peter Seidel. DISCO: Acquisition of translucent objects. *ACM Transactions in Graphics*, 23(3):835–844, 2004.
- [GM97] Edward J. Giorgianni and Thomas E. Madden. *Digital Color Management Encoding Solutions*. Addison-Wesley Publishing Co., Reading, MA, 1997.
- [Goh05] Alexandra Goho. Venetian grinds: The secret behind italian renaissance painters’ brilliant palettes. *Science News Online*, 167(11):168, March 2005. <<http://www.sciencenews.org/articles/20050312/bob8.asp>>.
- [Got87] Mark D. Gottsegen. *A Manual of Painting Materials and Techniques*. Harper and Row Publishers, Inc., New York, NY, 1987.
- [Gra53] H. G. Grassman. Zur theorie der farbenmischung (On the theory of compound colors). *Annalen der Physik und Chemie*, 89:69–84, 1853. Translation in *Philosophical Magazine*, 4(7):254–264, 1854.
- [Gre06] GretagMacbeth. *Munsell Color Conversion Freeware 6.5.5*, 2006. <http://www.gretagmacbeth.com/home/products/products_color-standards/products_books-for-designers/products_munsell-freeware.htm?>>.
- [GSC92] D. Grosjean, L. Salmon, and G. R. Cass. Fading of artists’ colorants by atmospheric nitric acid: Reaction products and mechanisms. *Environmental Science and Technology*, 26:952–959, 1992.
- [GTR⁺06] Jinwei Gu, Chien-I Tu, Ravi Ramamoorthi, Peter Belhumeur, Wojciech Matusik, and Shree Nayar. Time-varying Surface Appearance: Acquisition, Modeling and Rendering. *ACM Transactions in Graphics*, 25(3):762–771, July 2006.
- [GW77] Rafael C. Gonzalez and Paul Wintz. *Digital Image Processing*. Addison-Wesley Publishing Co., Reading, MA, 1977.
- [Her78] K. E. K. Hering. Zur lehre vom lichtsinn (On the theory of sensibility to light). *Sitzungsberichte der kaiserlichen Akademie der Wissenschaften*, 66:5–24, 1978. Translated by L.M. Hurvich and D. Jameson. Harvard University Press, Cambridge, MA, 1964.
- [HM92] Chet S. Haase and Gary W. Meyer. Modeling pigmented materials for realistic image synthesis. *ACM Transactions in Graphics*, 11(4):305–335, 1992.

- [IGG92] E. L. Williams II., E. Grosjean, and D. Grosjean. Exposure of artists' colorants to airborne formaldehyde. *Studies in Conservation*, 37:201–210, 1992.
- [IGG93a] E. L. Williams II., E. Grosjean, and D. Grosjean. Exposure of artists' colorants to peroxyacetyl nitrate. *Journal of the American Institute for Conservation*, 32:59–79, 1993.
- [IGG93b] E. L. Williams II., E. Grosjean, and D. Grosjean. Exposure of artists' colorants to sulphur dioxide. *Journal of the American Institute for Conservation*, 32(3):291–310, 1993.
- [JF63] Ruth M. Johnston and Robert L. Feller. The use of differential spectral curve analysis in the study of museum objects. *Dyestuffs*, 44(9):1–10, 1963.
- [JF99] Garrett M. Johnson and Mark D. Fairchild. Full-spectral color calculations in realistic image synthesis. *IEEE Computer Graphics Applications*, 19(4):47–53, 1999.
- [JF01] Ruth Johnston-Feller. *Color Science in the Examination of Museum Objects*. The Getty Conservation Institute, Los Angeles, CA, 2001.
- [JFFBC84] Ruth Johnston-Feller, Robert L. Feller, Catherine W. Bailie, and Mary Curran. The kinetics of fading: Opaque paint films pigmented with alizarin lake and titanium dioxide. *Journal of the American Institute of Conservation*, 23:114–129, 1984.
- [JK55] John A. Jacquez and Hans F. Kuppenheim. Theory of the integrating sphere. *Journal of the Optical Society of America*, 45(6):460–470, June 1955.
- [JMLH01] H. W. Jensen, S. R. Marschner, M. Levoy, and P. Hanrahan. A practical model for subsurface light transport. In *SIGGRAPH '01: Proceedings of the 28th annual conference on Computer graphics and interactive techniques*, pages 511–518, New York, NY, 2001. ACM Press.
- [Joh67] Ruth M. Johnston. Spectrophotometry for the analysis and description of color. *Journal of Paint Technology*, 39(509):346–354, 1967.
- [Joh86] Ruth M. Johnston. Reflections on the phenomenon of fading. *Journal of Coatings Technology*, 58(736):32–50, 1986.
- [JW75] D. B. Judd and G. Wyszecki. *Color in Business, Science and Industry*. John Wiley & Sons, Inc., New York, NY, third edition, 1975.

- [KM31] Paul Kubelka and Franz Munk. Ein beitrag zur optik der farbastriche (An article on optics of paint layers). *Zeitschrift fr Technischen Physik*, 12(112):47–53, August 1931. Translated by Stephen Westin <<http://www.graphics.cornell.edu/~westin/pubs/kubelka.pdf>>.
- [Kor69] Gustav Kortüm. *Reflectance Spectroscopy: Principles, Methods, Applications*. Penguin Books, New York, NY, 1969. Translated by James E. Lohr.
- [Koz04] O. N. Kozakov. Computer simulation of integral and differential optical characteristics of paints. *Optics and Spectroscopy*, 96(1):122–127, 2004. Original text in *Optika i Spektroskopya*, 96(1):133–138, 2004.
- [Kub48] Paul Kubelka. New contributions to the optics of intensely light-scattering materials. part i. *Journal of the Optical Society of America*, 38(5):448–457, May 1948.
- [Kub54] Paul Kubelka. New contributions to the optics of intensely light-scattering materials. part ii: Nonhomogeneous layers. *Journal of the Optical Society of America*, 44(4):330–335, April 1954.
- [Lab94] Optronics Laboratories. *OL Series 750 Automated Spectroradiometric Measurement System Manual*, 1994.
- [Lab05] Munsell Color Science Laboratory. *Munsell Renotation Data*, 2005. <<http://www.cis.rit.edu/mcsl/online/munsell.php>>.
- [LaF86] R. H. LaFontaine. Seeing through a yellow varnish: A compensating illumination system. *Studies of Conservation*, 31:97–102, 1986.
- [Lan77] Edwin Land. The retinex theory of color vision. *Scientific American*, 238(6):108–128, December 1977.
- [Lau26] Arthur P. Laurie. *The Painter's Methods and Materials*. Seeley, Service & Co., London, 1926.
- [LGB⁺03] Hendrik P. A. Lensch, Michael Goesele, Philippe Bekaert, Jan Kautz, Marcus Magnor, Jochen Lang, and Hans-Peter Seidel. Interactive rendering of translucent objects. *Computer Graphics Forum*, 22(2):195–205, June 2003.
- [LJP06] H. Laamanen, T. Jääskeläinen, and J. Parkkinen. Conversion between reflectance spectra and the Munsell notations. *Color Research and Application*, 31(1):57–66, February 2006.
- [LKG⁺01] Hendrik P. A. Lensch, Jan Kautz, Michael Goesele, Wolfgang Heidrich, and Hans-Peter Seidel. Image-based reconstruction of spatially

- varying materials. In Steven Gortler and Karol Myszkowski, editors, *Rendering Techniques 2001: Proceedings of the 12th Eurographics Workshop on Rendering*, pages 104–115, London, 2001. Springer.
- [Mac05] Bruce MacEvoy. *The Material Attributes of Paints*, 2005. <<http://www.handprint.com/HP/WCL/pigmt3.html#attributes>>.
- [Mas27] Masaccio. *The Expulsion from the Garden of Eden*, 1427. Brancacci Chapel, Santa Maria del Carmine. Florence, Italy.
- [May80] Ralph Mayer. *The Painter's Craft: An Introduction to Artists' Methods and Materials*. Penguin Books, New York, NY, 1980.
- [May81] Ralph Mayer. *The Artist's Handbook of Materials and Techniques*. The Viking Press, New York, NY, 1981.
- [Mey88] Gary W. Meyer. Wavelength selection for synthetic image generation. *Computer Vision, Graphics, and Image Processing*, 41(1):57–79, 1988.
- [Mun] *Munsell Book of Color*. Gretag MacBeth, Inc., Munsell Color Dept., 617 Little Britain Road, New Winsor, NY 12553-6148.
- [NMN87] Tomoyuki Nishita, Yasuhiro Miyawaki, and Eihachiro Nakamae. A shading model for atmospheric scattering considering luminous intensity distribution of light sources. In *SIGGRAPH '87: Proceedings of the 14th annual conference on Computer graphics and interactive techniques*, pages 303–310, New York, NY, 1987. ACM Press.
- [NRH⁺77] F. E. Nicodemus, J. C. Richmond, J. J. Hsia, I. W. Ginsberg, and T. Limperis. *Geometrical considerations and nomenclature for reflectance*. U.S. Department of Commerce, National Bureau of Standards, NBS Monograph No. 160, Washington, D.C., 1977.
- [O'H04] George O'Hanlon. *Why Some Paints are Transparent and Others Opaque*, 2004. <<http://www.naturalpigments.com/education/article.asp?ArticleID=8>>.
- [PA98] M.R. Pointer and G.G. Atridge. The number of discernable colors. *Color Research and Application*, 23:52–54, 1998.
- [Pig05] Natural Pigments. *Rare Artists Colors and Materials*, 2005. <<http://www.naturalpigments.com>>.
- [PvBM⁺06] Pieter Peers, Karl vom Berge, Wojciech Matusik, Ravi Ramamoorthi, Jason Lawrence, Szymon Rusinkiewicz, and Philip Dutré. A compact factored representation of heterogeneous subsurface scattering. *ACM Transactions in Graphics*, 25(3):746–753, 2006.

- [Rat72] Floyd Ratliff. Contour and contrast. *Scientific American*, 226(6):90–101, June 1972.
- [RMN03] D. Rudolf, D. Mould, and E. Neuffeld. Simulating wax crayons. In *Proceedings of 11th Pacific Conference on Computer Graphics and Applications*, pages 163–172, October 2003.
- [Saa01] Bob Saar. *The Hawk Eye: Egg Science*, 2001. <<http://www.thehawkeye.com/columns/saar/2001/csa21801.html>>.
- [SB02] Robert Sekuler and Robert Blake. *Perception*. McGraw Hill, New York, NY, 4th edition, 2002.
- [SC83] Cynthia L. Shaver and Glen R. Cass. Ozone and the deterioration of works of art. *Environmental Science and Technology*, 17(12):748–752, 1983.
- [SCG⁺92] L. G. Salmon, G. R. Cass, D. Grosjean, M. C. Jones, M. P. Ligocki, and W. W. Nazaroff. Protection of works of art from atmospheric nitric acid. Final Report to the Getty Conservation Institute, Environmental Quality Laboratory Report R-35, California Institute of Technology, Pasadena, CA, May 1992.
- [Seu86] Georges Seurat. *Un dimanche aprs-midi l’Ile de la Grande Jatte*, 1884-86. Art Institute of Chicago, Helen Birch Bartlett Collection. Chicago, IL.
- [Sta85] Sarah Standiforth. Retouching and colour matching: The restorer and metamerism. *Studies in Conservation*, 30(3):101–111, August 1985.
- [TM00] W. Stanley Taft and James W. Mayer. *The Science of Paintings*. Springer-Verlag New York, Inc., New York, NY, 2000.
- [TWL⁺05] Xin Tong, Jiaping Wang, Stephen Lin, Baining Guo, and Heung-Yeung Shum. Modeling and rendering of quasi-homogeneous materials. *ACM Transactions in Graphics*, 24(3):1054–1061, 2005.
- [WB97] Paul M. Whitmore and Catherine Bailie. Further studies on transparent glaze fading: Chemical and appearance kinetics. *Journal of the American Institute for Conservation*, 36(3):207–230, 1997.
- [WC89] Paul M. Whitmore and Glen R. Cass. The fading of artists’ colorants by exposure to atmospheric nitrogen dioxide. *Studies in Conservation*, 34(2):85–97, 1989.
- [WCD87] Paul M. Whitmore, Glen R. Cass, and J. R. Druzik. The ozone fading of traditional natural organic colorants on paper. *Journal of the American Institute for Conservation*, 26:45–58, 1987.

- [Web23] F. W. Weber. *Artist's Pigments: Their Chemical and Physical Properties*. D. Van Nostand Company, Inc., New York, NY, 1923.
- [Weh75] Kurt Wehlte. *Werkstoffe und Techniken der Malerei (The Materials and Techniques of Painting)*. Van Nostrand Reinhold Co., New York, NY, 1975. Translated by Ursus Dix.
- [WPB99] Paul M. Whitmore, Xun Pan, and Catherine Bailie. Predicting the fading of objects: Identification of fugitive colorants through direct nondestructive lightfast measurements. *Journal of the American Institute for Conservation*, 38(3):395–409, 1999.